Université du Québec
Institut National de la Recherche Scientifique
Centre Énergie, Matériaux et Télécommunications

Génération et traitement du signal optique basés sur le filtrage linéaire de phase-seule dans les domaines temporel et spectral

Par

Reza Maram Qartavol

Thèse présentée pour l'obtention du grade de
Doctorat en Télécommunication, Ph.D.

Jury d'évaluation

Examinateur externe	Carlos R. Fernandez-Pousa Universidad Miguel Hernández de Elche, Spain
Examinateur externe	Shulabh Gupta Carleton University, Canada
Examinateur interne	Luca Razzari INRS-EMT, Canada
Directeur de recherche	José Azaña INRS-EMT, Canada

Pour mes parents et Samané

To my parents and Samane

Acknowledgements

"If I have seen further it is only by standing on the shoulders of giants."

Isaac Newton

To begin, I would like to acknowledge the whole Canadian continent and, in particular, Montréal for being such an amazing place. A combination of a tech-savvy society, world-class scientific community, down-to-earth people and a vibrant ecosystem make it doubtlessly the best location on the globe for accomplishing a PhD in optical telecom.

As part of this scientific community, José Azaña is the person who gave me the opportunity to join the UOP family. Living 30 milliseconds of fiber optic latency away from home — or around 18 hours by plane — is an everyday challenge that can only be taken up with the support of an adoptive family which I partly found in the friendly UOP team at INRS-EMT. Among them, José Azaña, my supervisor, is the one who guided me at light speed through this scientific journey. His guidance, counsel and attitude pushed me to do my best on my current projects while keeping a place for imagination and new ideas. He taught me valuable lessons not only to become a better researcher and scientific professional, but also a better person in life. It has been an honor to work with him and learn so much from him. José, thanks so much for everything you have done for me.

I would like to deeply thank my lovely wife Samaneh for her constant support, help, care, encouragement, laughter and her mere company. She is my best friend and my companion in life. I thank her for her sacrifice as I pursued my goals and dreams in graduation levels. No amount of words is enough to express my true gratitude for her patience and for always being there. Samaneh, I cannot imagine what my life would look like without you. I love you very much and I thank you with all my heart for being such a great part of my life.

I also thank my parents, Ali and Fatemeh, for their unconditional love, support throughout my life and your encouragement for pursuing my education. They have walked with me along good and difficult times, and during this path, they have taught me to always think big and work hard to achieve my goals. Their precious advice for life will always accompany me. They continue to inspire me in every way of life and with all their love they have shown me how to succeed in all

of life's challenges. My deep thanks and lots of appreciation must go to my brothers, Hamed, Mohammad, and Amir and my little sister, Zeinab, whose love and support from thousands of kilometers away have always given me the energy to work and follow my dreams. Special gratitude must also go to the members of my family-in-law, Hassan, Roghayeh, Hamid, Elahe, Saeede, Alireza for their love and support. Thank you all.

I would like to give my special and sincere thanks to Prof. James Van Howe, from Augustana College, IL, US, for being an excellent mentor entire my PhD studies and for the fruitful discussions and collaborations on several of my projects. At the beginning of my PhD, Prof. Van Howe joined our group for two months as a visiting professor. During this period, he taught me valuable experimental techniques and theoretical analyses that will always be with me in my professional career and I greatly appreciate his time and effort. He has a wonderful grasp on math and physics, matched by an ability to explain them. Since then, we have been working together in many common projects. It is always a pleasure to work, and share time and ideas with such excellent and reputable professionals.

Prof. Leif Katsuo Oxenløwe and his group members, Deming Kong, Michael Galili, Francesco Da Ros, Pengyu Guan, and Kasper Meldgaard Røge, from the Technical University of Denmark (DTU), deserves special thanks for hosting me and the great collaboration during my two visits, in total of 40days, to DTU. Their priceless assistance and suggestions and supplying state-of-the-art lab equipment have helped me to successfully carry out several of my projects presented in this Thesis.

I am indebted to all past, present and honouree members of the UOP Lab: Dr. Reza Ashrafi, Dr. Maurizio Burla, Dr. Hossein Asghari, Dr. Hugues Guillet de Chatellus, Dr. Ming Li, Dr. Mohamed Seghilani, Dr. Bo Li, Dr. Lei Lei, Dr. Alejandro Carballar, Dr. Antonio Malacarne, Dr. María del Rosario Fernández Ruiz, Dr. Hamed Pishvai Bazargani, Luis Romero Cortés, Jeonh Hyun Huh, Jinwoo Jeon, and Sai krishna reddy. Thank you so much for your help but most importantly for your friendship. In particular, I would like to thank Luis Romero Cortés who helped a great deal in several of project conducted in this Thesis. Also, special thanks to Dr. Reza Ashrafi, for great times and discussions we had at Park-Milton Presse Café for learning new things on weekends. Additionally, I would like to thank the staff from the INRS-EMT.

My sincere gratitude goes to the core committee for my Ph.D Thesis: Prof. Luca Razzari, Prof. Carlos R. Fernandez-Pousa and Prof. Shulabh Gupta. Thank you for your time and efforts in reviewing my Thesis.

Finally, I thank le Fonds Québécois de la Recherche sur la Nature et les Technologies (FQRNT), and Institut National de la Recherche Scientifique – Énergie, Matériaux et Télécommunications (INRS-EMT), for providing the funding which allowed me to undertake this PhD research.

Reza Maram

Résumé

Les exigences sans cesse croissantes du trafic de données dans les services de télécommunication conduisent à un besoin continu de capacités de réseau plus élevés. Dans ce scénario, le débit binaire dans un canal de longueur d'onde ainsi que le nombre de canaux ne cessent d'augmenter dans les réseaux de télécommunication grâce aux progrès des technologies de transmission optiques. Aujourd'hui, les systèmes de multiplexage en longueur d'onde (WDM pour wavelength division multiplexing en anglais) supportent des capacités de transmission d'environ 14 Tbit/s, des milliers de fois plus élevé que la capacité de toute autre liaison de transmission (par exemple ondes radio et téléphonie), ce débit est réalisé par le multiplexage de plusieurs centaines de longueurs d'onde avec un débit binaire de ~ 40 Gbit /s par canal. Cependant, le signal lumineux porteur d'information doit être converti à un signal électronique compatible avec les routeurs/commutateurs dans les réseaux de télécommunication. Dans cette conversion, le débit d'information est considérablement ralenti en raison du déséquilibre de bande passante entre la transmission optique et les routeurs électroniques. Le traitement du signal optique est une solution alternative potentielle très prometteuse aux problèmes liés à l'électronique. Récemment, un effort considérable a été investi dans le développement des méthodes optiques ultrarapides de traitement du signal pour les applications dans les réseaux de fibre optique, les plateformes de traitement de l'information et d'informatique optique à haute vitesse. Cependant, en pratique, la vitesse de traitement est seulement une des plusieurs questions importantes à prendre en considération lors du déploiement de nouvelles technologies de traitement. L'une des principales raisons pour lesquelles le traitement électronique du signal est préféré actuellement sur d'autres alternatives, en particulier sur le traitement du signal optique, est que les appareils électroniques consomment relativement moins d'énergie. Contrairement à l'électronique, la plupart des processeurs optiques proposés à ce jour, typiquement basés sur des effets "non linéaires", nécessiteraient une consommation d'énergie peu pratique, plus élevée de plusieurs ordres de grandeur que celle des processeurs électroniques lorsqu'ils sont utilisés dans des situations réelles et à pleine échelle. En effet, la performance énergétique médiocre des méthodes de traitement du signal optique entrave considérablement leur capacité à offrir une solution pratique et compétitive pour le traitement du signal.

Afin de maintenir une pénétration accrue de l'optique dans les futurs systèmes de traitement et aider à réaliser la transition de technologie de l'électronique à l'optique dans les plateformes de traitement de l'information et de calcul, des processeurs optiques écoénergétiques innovants doivent être conçus et développés pour effectuer les tâches nécessaires, idéalement avec une perte minimale de l'énergie du signal d'entrée et une utilisation réduite de l'alimentation externe supplémentaire. Dans cet objectif, il faut étudier la possibilité d'utiliser des techniques linéaires purement passives pour le traitement du signal optique, en évitant l'utilisation de mécanismes actifs et /ou non linéaires conventionnels dans les dispositifs de traitement du signal. Ces mécanismes nécessitent une alimentation externe suffisamment élevée et/ou consomment/dissipent une partie importante de l'énergie du signal entrant. En revanche, le traitement du signal basé uniquement sur des composants optiques linéaires passifs, offre la possibilité de mettre en œuvre des circuits de traitement qui permettent fondamentalement une consommation nulle de l'énergie du signal tout en évitant l'utilisation d'une source supplémentaire de lumière.

Dans cette thèse, je considère l'utilisation des procédés purement linéaires pour manipuler les profils temporel et spectrale du signal sous test, à savoir la modulation temporelle linéaire et le filtrage spectral linéaire, respectivement. La manipulation désirée peut être produite sur le profil amplitude du signal sous test par modulation temporelle d'intensité ou filtrage spectral d'amplitude. Si aucun gain supplémentaire n'est utilisé dans le système ciblé (régime passive), la modulation d'intensité ou le filtrage d'amplitude produit nécessairement une perte d'une partie de l'énergie du signal d'entrée. En fonction de la fonctionnalité ciblée, les pertes de modulation/filtrage peuvent être considérables. En revanche, l'énergie du signal peut être entièrement préservée si seule la phase du signal est manipulée dans le domaine temporel, c.-à-d. par filtrage spectrale de phase.

Dans l'ensemble, les nouveaux systèmes de traitement optique des signaux proposés dans ma thèse sont basés sur une combinaison appropriée de la modulation temporelle linéaire de phase-seule et les processus de filtrage spectral, conduisant à la mise en œuvre de la fonctionnalité souhaitée avec un rendement énergétique optimisé. Ce résultat est obtenu sans compromis sur les avantages de traitement du signal intrinsèque à l'optique. Dans les processeurs proposés dans cette thèse, l'énergie du signal entrant est efficacement redistribuée pour construire le signal de sortie

ciblé sans l'utilisation d'aucune puissance optique externe supplémentaire. J'utilise cette approche pour la mise en œuvre d'une série d'importantes fonctionnalités de traitement du signal. En particulier, dans le chapitre 2, nous utilisons la combinaison des effets Talbot temporel et spectral, impliquant la modulation de phase temporelle et le filtrage de phase spectrale, pour contrôler et programmer le taux de répétition et l'énergie par impulsion associée d'une source laser impulsionnelle à faible taux de répétition d'impulsions. Dans le chapitre 3, nous démontrons une nouvelle approche tout-optique efficace énergétiquement pour la conversion de format de données de télécommunication optique: retour-à-zéro (RZ) au non-retour-à-zéro (NRZ). Cette approche a été mise en œuvre expérimentalement avec un débit binaire de 640 Gbit/s. Nous démontrons également d'autres nouvelles approches de récupération des signaux d'horloge de base et sous-harmonique à partir de signaux de données de type tout-ou-rien (OOK pour on-off-keying en anglais). Ce travail de recherche peut ouvrir de nouvelles perspectives importantes pour la mise en œuvre d'autres processeurs optiques critiques avec une efficacité énergétique sans précédent, dépassant les limites de consommation d'énergie des technologies optiques actuelles sans perdre leur avantage en matière de vitesse de traitement.

Abstract

The ever-increasing data traffic requirements in telecommunication services lead to a continuous need for higher network capabilities. In this scenario, the bit rate of one wavelength channel and the number of channels keep increasing in telecommunication networks thanks to the advancement of optical transmission technologies. Nowadays, wavelength division multiplexing (WDM) systems support transmission capabilities of about 14 Tbit/s, through multiplexing of several hundred wavelengths with a single channel bit rate of ~ 40 Gbit/s, thousands of times higher than any other transmission link (e.g. direct radio and telephone links) capacity. However, light information has to be converted to electrons when accessed by electronic routers/switches in the telecommunication networks. In that conversion, information is significantly slowed down due to the bandwidth imbalance between the optical transmissions and electronic routers. Optical signal processing is a very promising potential alternative solution to the problems associated with electronics. Recently, there has been a significant effort toward the realization of ultrafast optical signal processing methods for applications in next-generation fiber-optic networks and high-speed information processing and optical computing platforms. However, in practice, processing speed is only one of the several important issues to be considered when deploying new processing technology. One of the main reasons why electronic signal processing is preferred presently over other alternatives, particularly over optical signal processing, is that electronic devices consume a relatively smaller amount of energy. Unlike electronics, most optical processors proposed to date, typically realized using "nonlinear" effects, would require unpractical power consumption, orders-of-magnitude higher than that of their electronic counterparts, when used at a real-world scale. Indeed, the poor energy performance of optical signal processing methods greatly hinders their capability to offer a practical, competitive solution for signal processing.

In order to keep optics penetration deeper into future processing systems and help to realize the technology shift from electronics to optics in information processing and computing platforms, innovative energy-efficient optical signal processors should be designed and developed to perform the needed tasks ideally with minimal loss of the input signal's energy and reducing the use of supplementary external power. To this end, one needs to explore the possibility of using purely passive and linear techniques for optical signal processing, avoiding the use of conventional active

and/or nonlinear mechanisms in the signal-processing engines. These mechanisms require a sufficiently high external power and/or consume/dissipate significant energy from the incoming signal. In sharp contrast, signal processing based on only linear, passive optical components offers the possibility of implementing processing circuits that fundamentally enable no signal power consumption while avoiding the use of any additional optical light source.

In this Thesis, I consider the use of purely linear processes to manipulate the temporal and spectral profiles of a signal under test, namely linear temporal modulation and linear spectral filtering, respectively. The desired manipulation can be produced on the amplitude profile of the signal under test through temporal intensity modulation or amplitude spectral filtering. If no additional active gain is employed in the target system (passive scheme), intensity modulation or amplitude filtering necessarily wastes some of the input signal's energy. Depending on the target functionality, modulation/filtering losses can be considerable. In sharp contrast, the signal energy can be fully preserved if only the signal phase is manipulated in the time domain, i.e., by temporal phase modulation, and/or in the frequency domain, i.e., by spectral phase filtering.

Generally, the novel optical signal-processing schemes proposed in my Thesis are based on a suitable combination of phase-only linear temporal modulation and spectral filtering processes, leading to the implementation of the desired functionality with an optimized energy performance. This is achieved without trading the signal processing advantage intrinsic to optics. In my newly proposed processors, the incoming signal's energy is effectively redistributed to build up the target output signal without using any additional external optical power. I am using this approach for implementation of a range of important signal processing functionalities. In particular, in **Chapter 2**, we use the combination of the temporal and spectral Talbot effect, involving temporal phase modulation and spectral phase filtering, to control and program the repetition-rate and associated energy per pulse of a low-rate laser source. In **Chapter 3**, we demonstrate a novel energy-efficient approach for all optical return-to-zero (RZ)-to-non-RZ (NRZ) telecommunication data format conversion, experimentally implemented at a bit rate of 640 Gbit/s, and novel approaches for base-rate and sub-harmonic clock recovery of on-off-keying (OOK) data signals. This research may open new, important perspectives for implementing other critical optical signal processors with unprecedented energy efficiency, overcoming the energy-consumption limitations of present optical technologies without trading their processing speed advantage.

Table des matières

Liste des figures

Publications associées

Articles de journaux

[1] R. Maram, L. Romero Cortés and J. Azaña, "Programmable Fiber-Optics Pulse Repetition-Rate Multiplier," *IEEE, J. Lightwave Technol.*, vol. 34, pp. 5403-5406, 2016. [INVITED].

[2] R. Maram, D. Kong, M. Galili, L. K. Oxenløwe and J. Azaña, "640 Gbit/s return-to-zero to non-return-to-zero format conversion based on optical linear spectral phase filtering," *Opt. Lett.*, vol. 41, pp. 64-67, 2016.

[3] R. Maram, L. Romero Cortés and J. Azaña, "Sub-harmonic periodic pulse train recovery from aperiodic pulse trains through dispersion-induced temporal self-imaging," *Opt. Express*, vol. 23, pp. 3602-3613, 2015.

[4] R. Maram, J. Van Howe, M. Li, and J. Azaña, "Lossless fractional pulse repetition-rate multiplication of optical pulse trains," *Opt. Lett.*, vol. 40, pp. 375-378, 2015.

[5] R. Maram, J. Van Howe, M. Li and J. Azaña, "Noiseless intensity amplification of repetitive signals by coherent addition using the temporal Talbot effect" *Nat. Commun.*, vol. 5, pp. 4827(1-10), (doi: 10.1038/ncomms6163), 2014.

[6] R. Maram, D. Kong, M. Galili, L. K. Oxenløwe and J. Azaña, "All-optical clock recovery based on spectral phase-only optical filtering" *Opt. Lett.*, vol. 39, pp. 2815-2818, 2014.

Articles de conférences internationales

[7] R. Maram, L. Remero Cortes, and J. Azaña "Versitaile pulse repetition rate multiplier based on temporal self-imaging," Optical Fiber Communication Conference (OFC 2016), March 20-24, 2016, Anaheim, CA, USA. Paper: W3E.4. [INVITED]

[8] R. Maram, J. Van Howe, and J. Azaña, "Demonstration of input-to-output gain in a Talbot Amplifier," IEEE Photonics Conference (IPC 2015), October 04 – 08, 2015, Reston, Virginia, USA. Paper: TuB2.5.

[9] R. Maram, L. R. Cortés and J. Azaña, "Programmable fibre-optics pulse repetition rate multiplier for high-Speed optical communication systems," 41st European Conference on Optical Communications (ECOC 2015), September 27 - October 1, 2015, Valencia, Spain. Paper: P.1.17.

[10] J. Azaña, R. Maram, J. Van Howe, and M. Li, "Passive amplification and real-time averaging of repetitive waveforms by Talbot effect," Lasers and Electro-Optics Europe (CLEO EUROPE 2015), June 21-25, 2015, Munich, Germany. Paper: CI-4.1. [INVITED]

[11] R. Maram, L. R. Cortés and J. Azaña, "Electrically-tunable fiber-optics pulse repetition-rate multiplier," Optical Fiber Communication Conference (OFC 2015), March 21-26, 2015, Los Angeles, CA, USA. Paper: W1K.5. [Featured as a TOP SCORED paper in the conference].

[12] R. Maram, D. Kong, M. Galili, L. K. Oxenløwe, and J. Azaña, "Passive linear-optics 640 Gbit/s logic NOT gate," Optical Fiber Communication Conference (OFC 2015), March 21-26, 2015, Los Angeles, CA, USA. Paper: W2A.48.

[13] R. Maram, J. Van Howe, and J. Azaña, "Noise-eating amplifier for repetitive signals," IEEE Photonics Conference (IPC 2014), October 12 – 16, 2014, San Diego, CA, USA. Paper: WE2.2.

[14] R. Maram, D. Kong, M. Galili, L. K. Oxenløwe, and J. Azaña, "640 Gbit/s RZ-to-NRZ format conversion based on optical phase filtering," IEEE Photonics Conference (IPC 2014), October 12 – 16, 2014, San Diego, CA, USA. Paper: TuG3.5.

[15] R. Maram, J. Van Howe, M. Li and J. Azaña, "Passive waveform amplification by self-imaging," Conference on Lasers and Electro-optics (CLEO 2014), June 8-13, 2014, San Jose, CA, USA. Paper: SM1O.8.

[16] R. Maram, L. R. Cortes and J. Azana, "Reconfigurable optical sub-harmonic clock recovery based on inverse temporal self-imaging," Conference on Lasers and Electro-optics (CLEO 2014), June 8-13, 2014, San Jose, CA, USA. Paper: SW3J.3.

[17] R. Maram and J. Azaña, "Fractional pulse repetition-rate multiplication based on temporal self-imaging," Optical Fiber Communication Conference (OFC 2014), March 9-13, 2014, San Francisco, CA, USA. Paper: Th2A.32.

[18] R. Maram, D. Kong, M. Galili, L. K. Oxenløwe and J. Azaña, "Ultrafast all-optical clock recovery based on phase-only linear optical filtering," Optical Fiber Communication Conference (OFC 2014), March 9-13, 2014, San Francisco, CA, USA. Paper: W3F.2.

[19] R. Maram, M. R. Fernández-Ruiz, J. Azana "Design of an FBG-based phase-only (all-pass) filter for energy-efficient all-optical clock recovery," OSA Topical Meeting on Bragg Gratings, Photosensitivity and Poling in Glass Waveguides (BGPP 2014), July 27-31, 2014, Barcelona, Spain. Paper: BM4D.7.

[20] R. Maram and J. Azaña, "Energy-efficient all-optical clock recovery based on spectral phase-only optical filtering," Asian Symposium on Electromagnetics and Photonics Engineering (ASEPE 2013), August 28-30, Tabriz, Iran. Paper: OThA4.

[21] R. Maram, M. Li and J. Azaña, "High-speed all-optical NOT gate based on spectral phase-only linear optical filtering," Optical Fiber Communication Conference (OFC 2013), March 17-21, 2013, Anaheim, CA, USA. Paper: JW2A.62.

Autres publications qui ne sont pas directement en rapport avec la thèse

[22] R. Maram, J. Van Howe, L. Romero Cortés, and J. Azaña, "Energy-preserving arbitrary repetition-rate control of periodic pulse trains using temporal Talbot effects," *IEEE, J. Lightwave Technol.*, Submitted. [INVITED]

[23] L. Romero Cortés, R. Maram and José Azaña, "Energy-preserving arbitrary repetition rate control of waveform trains," International Conference on Optical, Optoelectronic and Photonic Materials and Applications (ICOOPMA), June13–17, 2016, Montreal, Canada. Paper: Mo-C1-I11. [INVITED]

[24] R. Maram, and J. Azaña, "Spectral self-imaging of time-periodic coherent frequency combs by parabolic cross-phase modulation" *Opt. Express*, vol. 21, pp. 28824-28835, 2013.

[25] L. Romero Cortés, R. Maram, H. Guillet de Chatellus, and J. Azaña "Arbitrary control of the free spectral range of periodic optical frequency combs through linear energy-preserving time-frequency Talbot effects," IEEE Photonics Conference (IPC 2016), October 02– 06, 2016, Waikoloa, Hawaii, USA. Paper: MF2.2.

[26] L. Romero Cortés, R. Maram, and J. Azaña "Full-field broadband invisibility cloaking,," IEEE Photonics Conference (IPC 2016), October 02– 06, 2016, Waikoloa, Hawaii, USA. Paper: MF3.5.

[27] L. Lei, J. Huh, L. Romero Cortés, R. Maram, B. Wetzel, D. Duchesne, R. Morandotti and J. Azaña, "Observation of spectral self-imaging induced on a frequency comb by nonlinear parabolic cross-phase modulation," *Optics Letters*, vol. 40, no. 22, pp. 5403-5406, (2015).

[28] L. Romero Cortés, R. Maram and J. Azaña, "Fractional averaging of repetitive waveforms induced by self-imaging effects," *Physical Review A*, vol. 92 no. 4, pp. 041804(1-5), (2015).

[29] L. R. Cortés, R. Maram and J. Azaña, "Spectral compression of complex-modulated signals without loss of information by joint temporal-spectral self-Imaging," 41st European Conference on Optical Communications (ECOC 2015), September 27 - October 1, 2015, Valencia, Spain. Paper: P.3.5.

[30] L. R. Cortés, R. Maram, L. Lei and J. Azaña, "Robust RZ to NRZ format converter based on linear joint temporal-spectral self-imaging and band-pass filtering," 41st European Conference on Optical Communications (ECOC 2015), September 27 - October 1, 2015, Valencia, Spain. Paper: P.4.5.

[31] R. Maram and J. Azaña, "Intensity amplification by Talbot-based coherent addition of repetitive waveforms using fiber-optics XPM" OSA Topical Meeting on Nonlinear Optics: Materials, Fundamentals and Applications (NLO 2015), June 26-31, 2015, Kauai, Hawaii, USA. Paper: Tu2A.2.

[32] L. R. Cortés, R. Maram and J. Azaña, "Real-time averaging of repetitive optical waveforms by non-integer factors based on temporal self-Imaging," Conference on Lasers and Electro-optics (CLEO 2015), May 10-15, 2015, San Jose, CA, USA. Paper: STu4N.7.

[33] L. R. Cortés, R. Maram, J. Azana, "Photonic integrator based on a distributed feedback semiconductor optical amplifier," OSA Topical Meeting on Bragg Gratings, Photosensitivity and Poling in Glass Waveguides (BGPP 2014), July 27-31, 2014, Barcelona, Spain. Paper: BW3D.5.

[34] R. Maram and J. Azaña, "Spectral self-imaging of time-periodic coherent frequency combs by parabolic cross-phase modulation" OSA Topical Meeting on Nonlinear Optics: Materials, Fundamentals and Applications (NLO 2013), June 21-26, 2013, Kohala Coast, Hawaii, USA. Paper: NW4A.10.

Chapitre 1

Introduction (en français)

Le passage du traitement du signal de l'électronique à l'optique dans les réseaux de télécommunications optiques est décrit. Des problèmes pratiques primordiaux des processeurs optiques existants sont identifiés, ainsi que des solutions potentielles. Ensuite, grâce à une vue d'ensemble des technologies optiques de traitement du signal, les fondements de cette thèse sont établies. Les différentes contributions décrites dans la thèse sont présentés et la structure de la thèse est décrite.

1.1 Traitement du signal Transition de l'électronique à l'optique?

Depuis l'invention des ''guides d'ondes diélectriques'' en 1966 par Charles Kao et George Hockham de la compagnie ''Standard Telephone Cables (STC) Ltd.'' à Harlow en Angleterre [1], les systèmes de communication à fibres optiques ont utilisé des ondes lumineuses en tant que porteuse pour transmettre l'information d'un endroit à un autre. La distance de quelques mètres en laboratoire a été portée à quelques kilomètres, à des centaines de kilomètres, puis à des milliers de kilomètres dans la première décennie de ce siècle, avec des débits allant de quelques dizaines de Mbit/s en fin des années 1960 à 100 Gbit/s et des dizaines de Tbit/s à l'heure actuelle [2]. D'énormes progrès ont été réalisés pendant les 55 dernières années grâce à des progressions significatives dans (i) Les techniques de modulation et de détection, de sorte que le débit de données des premiers systèmes de communication optiques, soit 100 Mb/s (1980), a été progressivement augmenté à 40Gbit/s avec une seule longueur d'onde; (ii) Les technologies de transmission et de composants matériels, y compris des techniques de multiplexage tels que multiplexage dense en longueur d'onde (DWDM) [1], de multiplexage optique dans le domaine

[1] DWDM est une technologie de multiplexage optique pour combiner et transmettre des signaux optiques multiples simultanément à différentes longueurs d'onde sur la même fibre optique monomode.

temporel (OTDM)[2], de multiplexage optique par répartition en fréquences orthogonales (OFDM)[3], rendus possible, à terme, grâce au développement des amplificateurs à fibres dopée à l'erbium (EDFA, pour erbium-doped fiber amplifier, en anglais), des amplificateurs à effet Raman (ROA pour Raman optical amplifier, en anglais), des amplificateurs paramétriques à fibre, etc.

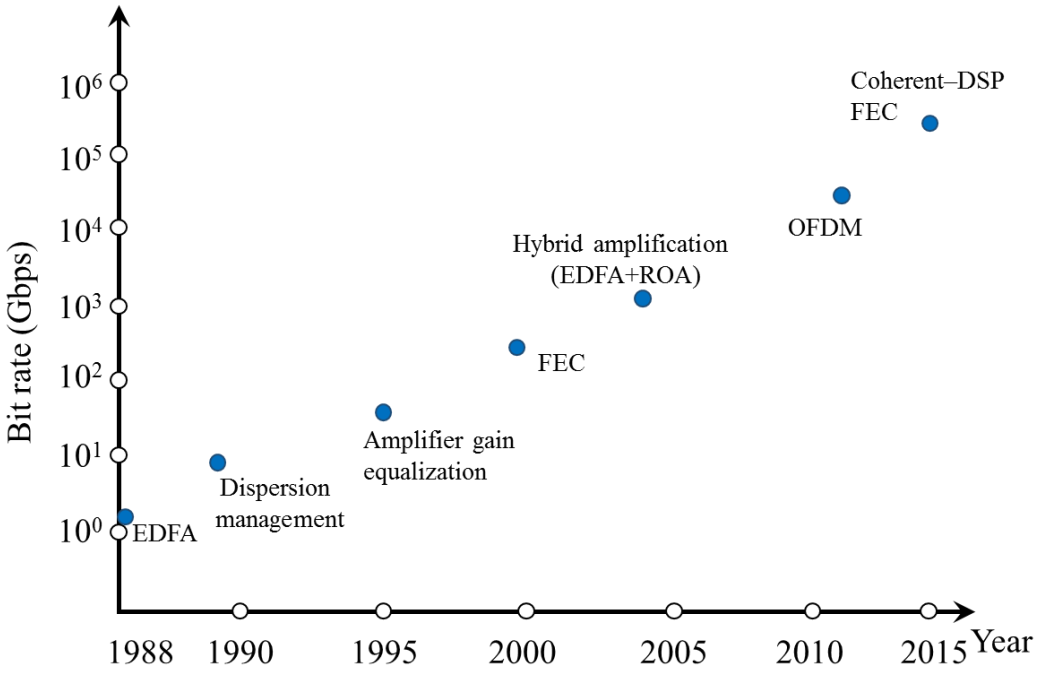

Figure 1.1 – Capacités de transmission démontrées expérimentalement d'une fibre monomode. Les données ont été compilées à partir de [2].

Le progrès de la capacité de transmission longue distance en fonction du temps est représenté dans la Figure 1.1, avec une distance de transmission atteignant plusieurs milliers de kilomètres le long d'une fibre monomode (SMF). Après l'invention des EDFA et des techniques de gestion de la dispersion, pour de surmonter l'atténuation optique et la dispersion dans les supports de transmission, la capacité de transmission a atteint 10 Gbits/s en 1990. Ensuite, la capacité de transmission a encore augmenté avec le multiplexage de plusieurs canaux de longueur d'onde de

[2] OTDM est une technologie de multiplexage optique pour combiner et transmettre des signaux optiques multiples à la même longueur d'onde sur la même fibre monomode. Les signaux sont multiplexés temporellement, et chaque signal apparaît sur la ligne de transmission, une fraction du temps seulement dans un motif alterné.
[3] OFDM optique est une technologie de multiplexage par répartition en fréquence. Contrairement à WDM, les sous - porteuses OFDM optiques se chevauchent significativement et ont donc une efficacité spectrale plus élevée.

la bande C ainsi que des bandes L- et S-. Avec l'égalisation du gain, la capacité totale a pu atteindre 40-100 Gbit/s en 1995 [2]. L'exploitation de l'efficacité spectrale serait alors améliorée avec d'autres travaux de R&D et des démonstrations expérimentales en déployant des canaux sur l'ensemble de la bande C, puis sur les bandes L et S en utilisant des amplificateurs hybrides (EDFA + ROA) pour atteindre 2 Tbit/s au tournant de ce siècle.

Au cours des quinze premières années de ce siècle, nous avons assisté à d'autres progrès ayant pour put de pousser la limite de capacité de transmission avec les techniques DWDM, OTDM et OFDM. Cela a été démontré par les réalisations de transmissions de données de 10,2 Tbit/s sur une seule longueur d'onde [3], en utilisant l'OFDM optique [4] et de 14 Tbit/s (111 Gbit/s × 140 canal de longueur d'onde) de 26 Tbit/s dans une liaison WDM [5]. En raison de cette énorme capacité de transmission, depuis le début de vingt-et-unième siècle, les systèmes à base de fibre-fibre ont largement remplacé les systèmes de transmission radio pour les transmissions longue-distance de données de télécommunication. Ils ont révolutionné les appels téléphoniques longue distance, la télévision par câble et, plus important encore, l'Internet. La mise en place de l'Internet à base de fibres optiques a permis d'établir une plateforme de communication à l'échelle mondiale pour l'ensemble des modes de communication, à savoir les données, la voix et la vidéo, à la fois pour le contenu temps réel et non-temps réel. L'internet est composé de grandes mailles des routeurs et des commutateurs électroniques interconnectés à travers des réseaux de fibres optiques à haute capacité.

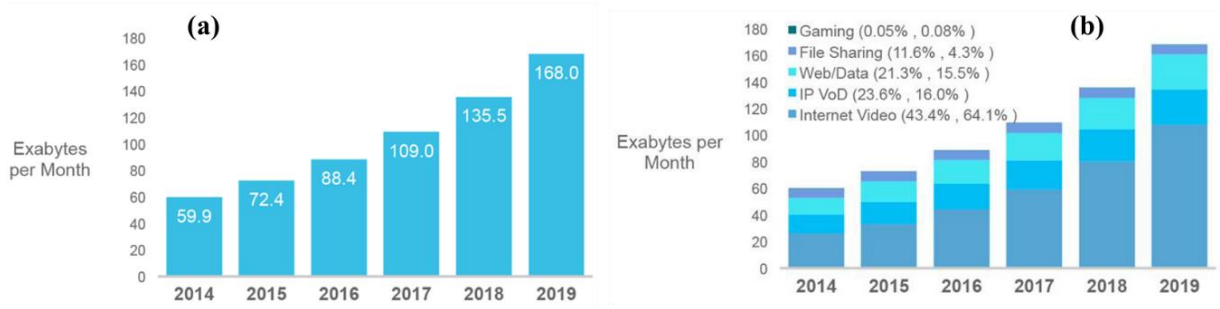

Figure 1.2 – (a) La croissance prévue du trafic Internet mensuel 2014-2019, (b) Distribution de services prévue pour la période 2014-2019 (exaoctets/mois) [6].

L'infrastructure de l'Internet a augmentée considérablement pour accueillir un nombre croissant d'utilisateurs, ainsi que les exigences de bande passante plus élevée découlant de nouveaux services et applications Internet, plus exigeants. En particulier, la popularité croissante

des services gourmands en bande passante tels que la diffusion vidéo (Netflix, YouTube, télévision sur protocole Internet (IPTV)), la vidéophonie (Skype, FaceTime, Google Hangouts), les jeux en ligne en haute définition (League of legends, Counter-strike, Fallout) et de services de d'informatique hébergés (cloud computing) ont conduit à une augmentation incessante du trafic Internet au cours de la dernière décennie - une tendance qui devrait se poursuivre pendant des années à venir. Selon le Cisco Visual Networking Index (Cisco CVNI), le trafic Internet mondial a augmenté de plus de quatre fois au cours des cinq dernières années et devrait tripler au cours des cinq prochaines années (voir la Figure 1.2 (a)) [6]. Parmi les autres services, les services de vidéo vont dominer la croissance du trafic Internet prédit par le CVNI (Figure 1.2 (b)). Le trafic Internet devrait croître à 168 exaoctets par mois en 2019, contre 59,9 exaoctets par mois en 2014, voir Figure 1.2 (a). Pour apprécier l'ampleur des volumes de trafic Internet, mettons les chiffres en termes plus familiers: en 2019, le trafic Internet va globalement atteindre 518 térabits par seconde (Tbit/s). Ceci est l'équivalent de 191 millions de personnes visionnant sur internet une vidéo haute définition (HD) en même temps, toute la journée, chaque jour, ou l'équivalent de 42 milliards de DVD par mois.

La capacité susmentionnée fournie par les technologies de transport optique ont toujours été en avance sur la demande de trafic Internet, et l'accès à la capacité de transmission nécessaire pour les prochaines années est non loin de la réalisation. Toutefois, la capacité de transmission ne constitue pas l'ensemble du tableau, mais une partie de celui-ci, comme mentionné précédemment, l'Internet et, en général, un réseau de communication a essentiellement deux fonctions: la transmission et le routage/commutation [7]. L'information sous forme de bits binaires est envoyée à partir d'une origine à une destination finale à travers les canaux de transmission via de nombreux nœuds de réseau intermédiaires. À ces nœuds, la commutation a lieu de manière à acheminer les bits à partir de l'origine à la destination le long d'un chemin prédéfinie. L'acheminement (ou le routage) et la commutation peuvent être réalisés soit dans le domaine électrique ou optique.

La technologie de commutation dans le domaine électrique est mature et très efficace. À ce jour, la combinaison de transmission optique et de routage électrique fonctionne très bien, comme en témoigne le fait que jusqu'à présent, dans la plupart des réseaux commerciaux, les informations sont transmises dans le domaine optique et acheminés dans le domaine électrique. Cependant, le routage/commutation dans le domaine électrique connaît une pression en constante augmentation

à cause de l'augmentation continue des capacités de transmission dans les fibres optiques discutée ci-dessus.

Par conséquent, une des sérieuse préoccupations est que la capacité réalisable ultime des réseaux sera finalement limitée par ce que l'on appelle ‘‘goulots d'étranglement de bande passante’’ dans les routeurs électroniques, c.-à-d. le déséquilibre de bande passante entre les transmissions optiques et les routeurs électroniques [8, 9]. Un routeur est composé de plusieurs unités de traitement du signal, et la capacité globale du routeur dépend de la vitesse des unités individuelles [10]. Bien que la vitesse d'horloge des unités électroniques de traitement du signal pour le traitement de l'information ait augmenté linéairement jusqu'à il y a quelques années, elle semble maintenant arriver à saturation, comme le montre la Figure 1.3. La grande consommation d'énergie et la dissipation de chaleur associée est également un sujet de préoccupation dans les processeurs électroniques des routeurs, cela est susceptible de devenir encore plus problématique que les routeurs requière plus de capacité de traitement. La situation devient encore pire quand il y a beaucoup de canaux de longueur d'onde dans une fibre optique, comme cela est courant dans les réseaux DWDM d'aujourd'hui, car un grand nombre de récepteurs optiques pour la conversion optique-électronique (O/E), de modulateurs et de lasers pour la conversion électronique-optique (EO) sera nécessaire à chaque nœud du réseau pour interfacer les circuits électroniques de traitement au support de transmission optique, ce qui engendre des coûts de réseau prohibitifs. Le routeur Cisco CRS-1 avec une capacité de commutation maximale de 92 Tbit/s (72 étages, avec une carte de 400 Gbit/s dans chaque étage) occupe 100m^2 d'espace, consomme 1 MW de puissance et pèse 60 Tonne [4] .

Actuellement, les technologies électroniques suivent les exigences de bande passante en utilisant un parallélisme intensif [11, 12], où le nombre de composants et de leur consommation combinée de puissance, augmentent tout simplement avec la bande passante. À l'heure actuelle, dans les pays développés, l'énergie totale consommée par l'infrastructure Internet représente 2-3% de la consommation totale d'énergie dans le monde entier [13] et la contribution associée aux émissions mondiales de CO_2 [14, 15]. Cette part ne cesse d'augmenter avec de graves conséquences pour l'économie et l'environnement. Cela soulève la question de savoir si la

[4] http://www.cisco.com/en/US/products/ps5763/index.html

croissance de l'Internet pourrait être finalement limitée par la consommation d'énergie plutôt que par la bande passante! [16].

Plusieurs solutions ont été proposées pour répondre aux problèmes de bande passante et de la consommation d'énergie liés au traitement de signaux électroniques dans les routeurs, et dans tout dispositif de calcul numérique en général. En particulier, il y a trois décennies, les chercheurs et les développeurs ont suggéré que le passage à des technologies optiques de traitement du signal va grandement atténuer le déséquilibre de bande passante, dans ces technologies les signaux optiques sont traités et acheminés dans le domaine optique [17]. Les avantages revendiqués comprennent (i) des bandes passantes plus larges en raison de la nature large-bande intrinsèque de l'optique, au-delà des capacités de l'électronique, et (ii) la compatibilité avec l'idée générale du réseau tout-optique, dans lequel les données passent de façon transparente à travers le réseau de la source à destination sous forme optique sans subir des conversions O/E ou E/S, ce qui permet une faible consommation électrique, réduisant éventuellement le coût [18].

Pendant ces débuts le traitement du signal optique a nourri de grands espoirs comme une plate-forme de traitement plus rapide que l'électronique. Cependant, aujourd'hui, une certaine désillusion a remplacé l'enthousiasme du début et au cours des dix dernières années, cette proposition a eu de plus en plus de sceptiques à l'intérieur de la communauté optique même. En effet, la vitesse disponible des composants optiques surpasse largement l'état de l'art de l'électronique, avec des vitesses de traitement potentielles au-dessus du régime THz. Dans la Figure 1.3, la fréquence d'horloge des dispositifs de traitement de signaux optiques est comparée à la fréquence de processeurs électroniques. Cependant, dans la quête de vitesses de traitement de plus en plus élevées, de nombreux chercheurs ont ignoré le problème fondamental de la consommation d'énergie des processeurs optiques.

Bien que la technologie optique permette des vitesses de traitement beaucoup plus rapide que les meilleures dispositifs électroniques, la puissance requise pour la plus parts des processeurs optiques proposés est d'environ trois ordres de grandeur plus élevé que celle de leurs homologues électroniques [8], voir Figure 1.4. Telle qu'elles sont, les solutions proposées pour les plateformes optiques sont beaucoup moins pratiques du point de vue consommation d'énergie que l'électronique actuelle. Cet inconvénient est en partie responsable de ce qu'on appelle maintenant le «goulot d'étranglement photonique» [20].

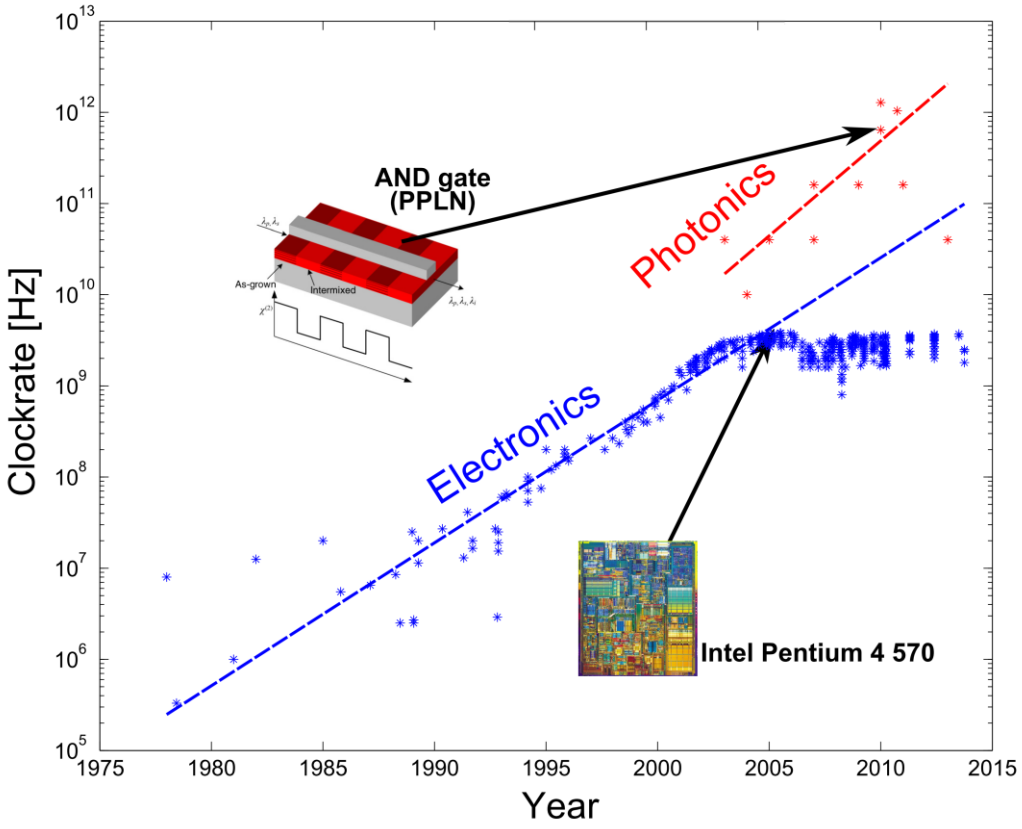

Figure 1.3 – Evolution électronique et photonique traitement du signal technologies capacité [19].

La forte consommation d'énergie est en grande partie imputable au fait que les processeurs de signaux optiques utilisent généralement des effets non linéaires pour effectuer une opération [8]. Mais, l'optique est tout au contraire, un domaine au comportement très linéaire. En raison de leur nature bosonique, les photons ont une extrêmement faible interaction avec la matière, cette force est de l'ordre de 137 (pour $\chi^{(2)}$, non-linéarité du second ordre) et 137^2 (pour $\chi^{(3)}$, non-linéarité du troisième ordre) plus faible que l'interaction des signaux électroniques [20], en conséquence une forte puissance est consommée pour exciter les interactions non linéaires [21]. La majeure partie de cette puissance est alors perdue après l'opération de traitement du signal; la question de la consommation d'énergie dans les interactions non linéaires sera décrite en détail plus loin dans ce chapitre, à la section 1.2.1. Par conséquent, la faiblesse inhérente des interactions optiques et la difficulté de mettre des nœuds optiques non linéaires en cascade, nécessitant une amplification optique après chaque nœud, rendent la plus part des architectures complexes non pratiques. La

Figure 1.4 compare la consommation d'énergie des transistors électroniques et des dispositifs optiques basés sur des mécanismes non linéaires classiques au fil des décennies [8]. La courbe supérieure (traits discontinus) représente les données calculées pour plusieurs types de dispositifs optiques.

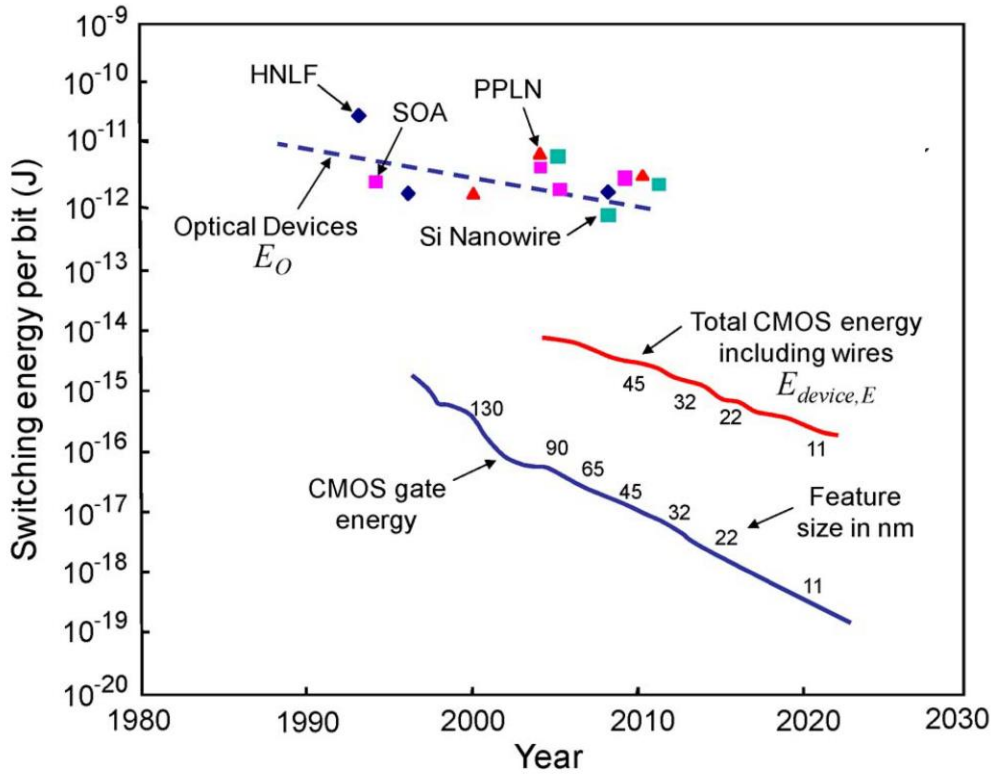

Figure 1.4 – Énergies par bit d'un appareil en fonction du temps [8]. AOS : amplificateur optique à semi-conducteur, FHNL: fibre hautement non linéaire, NLPP: niobate de lithium périodiquement polarisé, COMS: pour complementary metal-oxyde-semiconducteur, en anglais.

La question: comment le traitement du signal optique pourrait devenir compétitif face à l'électronique reste alors ouverte à l'exploration par les chercheurs au court et au moyen terme. Il y a six ans, David Miller et Rod Tucker ont présenté séparément des discussions bien argumentées sur les exigences pour les processeurs numériques optiques afin qu'ils puissent concurrencer et surpasser les processeurs électroniques [22, 23]. À moins que, des processeurs de signaux optiques au moins aussi rapides que et plus économes en énergie que leurs homologues électroniques, au niveau de 10 fJ/bit, soient mis au point, les technologies électroniques sont susceptibles de rester

la technologie de choix pour la grande majorité de processeurs de signaux [23]. Cela peut suggérer qu'au moins dans un avenir proche, l'optique ne deviendra pas une alternative viable à l'électronique dans le traitement des signaux et dans l'informatique.

Cependant, malgré ces perspectives moins optimistes pour l'optique dans le traitement du signal, certains chercheurs sont restés optimistes. Ils font valoir que de nombreux avantages de l'optique dans le traitement du signal ne peuvent pas être négligés et au lieu de l'abandonner, de nouvelles recherches devraient être menées pour résoudre les problèmes. Par conséquent, afin que les technologies optiques de traitement du signal deviennent une alternative solide à l'électronique dans le traitement de l'information, la commutation, et les plateformes informatiques, il y a un fort besoin de développements révolutionnaires dans la science de l'optique, qui permettront de nouvelles technologies de pointe et mèneront vers l'accroissement de la capacité de traitement avec une consommation d'énergie fortement réduite. En effet, le traitement du signal optique a été revu au cours des dernières années en abordant les limitations restantes et (ré) introduisant de (anciennes) nouvelles techniques de traitement des signaux optiques [24, 25, 26, 11, 27, 28, 29]. A cette fin, de nombreuses approches sont actuellement étudiées pour la possibilité de développer des processeurs du signal optique efficaces énergétiquement. En particulier, certains groupes de recherche exploitent de nouveaux guides d'ondes optiques avec des non-linéarités plus forts pour réaliser une opération souhaitée avec une plus faible consommation d'énergie [11, 30, 31, 32, 33]. De nombreux chercheurs croient également que tous les processeurs optiques ne seraient pas l'objectif le plus prudent [24, 34, 35, 36]. Au lieu de cela, une approche hybride devrait être utilisée, elle profiterait des avantages de l'électronique et de l'optique en même temps, en tirant bénéfice de ce qui est possible avec l'électronique et ce qui est possible avec l'optique. En outre, les chercheurs étudient la possibilité d'utiliser des techniques linéaires et purement passives de traitement du signal optique [26, 25, 37, 38, 39, 40, 41], en évitant l'utilisation de mécanismes actifs et/ou non linéaires conventionnels dans les blocs de traitement du signal, réduisant ainsi potentiellement la consommation d'énergie de façon significative. Conformément à ces dernières tentatives, cette thèse traite de nouvelles conceptions pour le traitement des signaux optiques capables de réaliser une ultra-faible consommation d'énergie. Nous avons démontré des systèmes à haute efficacité énergitique, comprenant la manipulation de phase temporelle et/ou spectrale des signaux optiques, pour effectuer plusieurs opérations élémentaires de traitement du signal dans le contexte des communications optiques.

Dans ce chapitre, nous allons d'abord examiner les principes de base des technologies optiques de traitement du signal en mettant l'accent sur leur performance en matière de consommation d'énergie. Enfin, nous concluons ce chapitre d'introduction avec un aperçu de l'état de l'art d'un ensemble particulier de fonctionnalités optiques de traitement du signal de haute importance pour cette thèse.

1.2 Traitement du signal optique et consommation d'énergie

Le traitement du signal optique est une technologie habilitante qui englobe la théorie fondamentale, les applications, les algorithmes et les implémentations de traitement ou de transfert de l'information codée dans une onde lumineuse - le signal optique- dans le domaine temporel et/ou domaine spatial. L'objectif principal de cette thèse est le traitement du signal optique dans le domaine temporel, qui est d'un grand intérêt et largement utilisé dans les systèmes de communication et d'informatique.

Le traitement du signal optique temporel a été le champ d'investigations actives depuis de nombreuses années, réunissant divers domaines de l'optique et du traitement du signal -à savoir, les dispositifs et processus linéaires/non-linéaires, l'optique, les signaux analogiques et numériques- pour réaliser des fonctions de traitement du signal à haute vitesse qui peut potentiellement fonctionner aux vitesses des signaux à la sortie des fibres optiques de communications. En particulier, le traitement du signal optique dans le domaine temporel peut généralement être classés en deux catégories principales: traitement linéaire et non linéaire du signal, selon les effets optiques (linéaires/ non-linéaire) qu'ils utilisent pour effectuer le traitement du signal.

Dans le cadre du traitement du signal optique, le traitement linéaire utilise un cadre théorique riche basé sur la théorie des systèmes linéaires et des transformées de Fourier, largement utilisées en optique pour la description de la diffraction et du filtrage spatial. Les processeurs de signaux linéaires exécutent la fonctionnalité ciblée sur le signal optique d'entrée en le déviant, le retardant, et le filtrant, mais la fréquence reste inchangée et le principe fondamental de superposition est toujours maintenu. En revanche, l'optique non linéaire, connue comme l'optique de la lumière intense, est utilisée dans les processeurs optiques qui nécessitent un ou plusieurs faisceaux optiques pour interagir les uns avec les autres sans interférence [42]. Les faisceaux optiques s'affectent

mutuellement et modifient l'amplitude, la phase, la longueur d'onde et polarisation caractéristiques de chacun d'eux en se propageant à travers le milieu non linéaire et, en conséquence, le principe de superposition n'est plus valide.

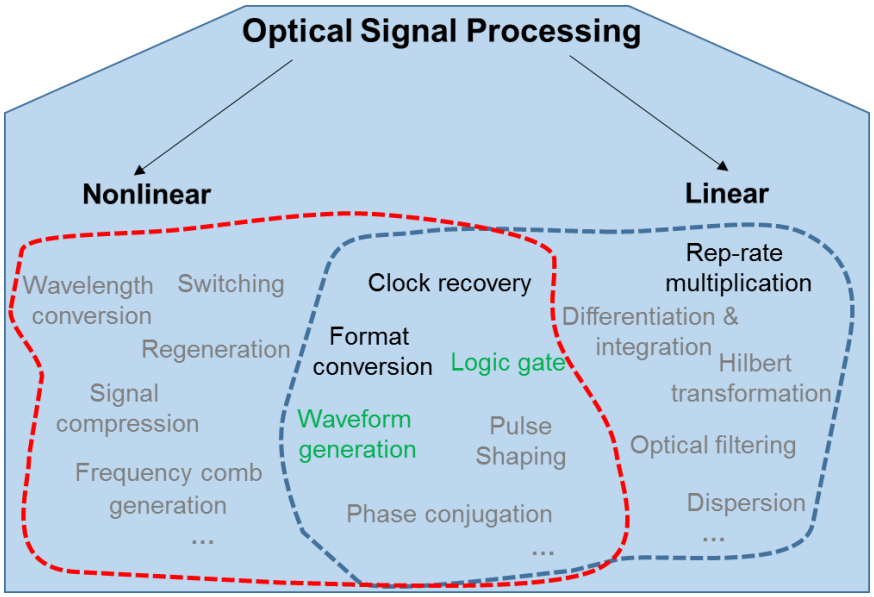

Figure 1.5 – Les applications de traitement de signaux optiques linéaires et non linéaires [43, 44, 45, 46, 47, 48, 49]. Les sujets en noir uni sont abordés dans ce travail et ceux en vert sont dans les perspectives pour les travaux futurs.

Il existe de nombreuses fonctionnalités qui sont intrinsèquement non linéaires et nous avons besoin d'un mécanisme non linéaire pour effectuer le traitement du signal associé, telles que la conversion de la longueur d'onde et la régénération. Cependant, il existe un grand nombre de fonctionnalités qui sont soit intrinsèquement linéaires, comme la différenciation et l'intégration, soit nous nous pouvons trouver des façons de les réaliser avec des mécanismes linéaires, tels que la récupération d'horloge, la conversion de format et les portes logiques, comme représenté dans l'arborescence dans la Figure 1.5.

Une brève étude des deux types de processeurs de signaux optiques non-linéaires et linéaires est présentée dans les sections suivantes en mettant l'accent sur leur performance en matière de consommation d'énergie. Nous concluons que, dans le but de réduire le coût énergétique global d'un système optique, il est nécessaire d'éviter l'utilisation des mécanismes non linéaires gourmands en énergie; autant que possible, la fonctionnalité spécifique ciblée doit être réalisée par des mécanismes linéaires économes en énergie.

1.2.1 Traitement non-linéaire du signal optique

La plupart des phénomènes optiques observés dans la vie quotidienne entrent dans la catégorie de l'optique linéaire qui explique des effets comme la diffraction, la réfraction et les interférences. Cependant, à des intensités élevées, des interactions complexes peuvent se produire, ces derniers sont décrits par la théorie de l'optique non linéaire [50, 49, 51]. Plus concrètement, l'optique non linéaire est l'étude des interactions complexes qui se produisent suite à la modification des propriétés optiques d'un système de matériaux par la présence d'une lumière intense. Les niveaux d'intensité lumineuse qui sont nécessaires pour observer des effets optiques non linéaires sont si élevés qu'ils ne peuvent généralement pas être observés dans les phénomènes de la vie quotidienne, et ne peuvent être obtenus qu'en utilisant des lasers à ondes continues (CW) intenses et des lasers pulsés.

Dans un milieu de propagation diélectrique, les interactions linéaires et non linéaires avec la lumière peuvent être comprises comme une interaction du champ électrique de la lumière avec les atomes et les molécules constituant le milieu. Les matériaux sont constitués d'atomes comprenant des particules chargées (par exemple des ions positifs et des électrons) qui sont affectés par les champs électriques et magnétiques. Les matériaux diélectriques ont une distribution de charge neutre à l'échelle macroscopique, ils comprennent un nombre égal de charges positives et négatives à l'échelle atomique (des ions positifs et des électrons). Un champ électrique oscillant $E(t)$ déplace les charges et exerce une action de séparation entre les charges positives et négatives (moment dipolaire), modifiant ainsi le moment dipolaire par unité de volume ou la polarisation $P(t)$ du matériau (t est la variable du temps). À noter qu'aux fréquences visibles / proche infrarouge, le champ électrique $E(t)$ interagit avec les matériaux diélectriques principalement par le biais des charges négatives (électrons). Tant que la perturbation de la trajectoire initiale des charges est faible, le déplacement induit est linéairement proportionnelle à l'amplitude du champ d'excitation $E(t)$ décrite par

$$P(t) = \epsilon_0 \chi^{(1)} E(t) \tag{1.1}$$

où la constante de proportionnalité $\chi^{(1)}$ est la susceptibilité linéaire et ε_0 est la permittivité de l'espace libre. Des déformations plus fortes des distributions de charge peuvent conduire à rompre

cette relation proportionnelle et la réponse optique, la polarisation *P(t)*, est alors exprimée par une série de puissance de la force du champ *E(t)* comme suit

$$P(t) = \epsilon_0 [\chi^{(1)} E(t) + \chi^{(2)} E^2(t) + \chi^{(3)} E^3(t) + \ldots] \quad (1.2)$$

Les quantités $\chi^{(2)}$ et $\chi^{(3)}$ sont connus comme les susceptibilités optiques non linéaires de deuxième et de troisième ordre, respectivement. Pour plus de simplicité, nous avons pris les champs *P(t)* et *E(t)* comme des grandeurs scalaires. Nous avons également supposé que la polarisation à l' instant *t* ne dépendrait que de la valeur instantanée de la force du champ électrique, ce qui implique (à travers les relations de Kramers-Kronig) que le milieu doit être sans perte et sans dispersion. Nous appelons $P^{(2)}(t) = \epsilon_0 \chi^{(2)} E^2(t)$ la polarisation non linéaire de second ordre et $P^{(3)}(t) = \epsilon_0 \chi^{(3)} E^3(t)$ la polarisation non linéaire de troisième ordre. Les interactions optiques non linéaires de deuxième ordre ne peuvent se produire que dans des cristaux non-centrosymétrique tels que le Quartz et le Niobate de lithium ($LiNbO_3$), c.-à-d., dans les cristaux qui ne présentent pas une symétrie d'inversion. Dans des matériaux comme les liquides, les gaz, les solides amorphes (comme le verre), et même un grand nombre de cristaux présentent une symétrie d'inversion, $\chi^{(2)}$ est nul, et par conséquent de tels matériaux ne peuvent pas produire des interactions optiques non linéaires de deuxième ordre. Cependant, les interactions optiques non linéaires de troisième ordre (c.-à-d., ceux qui sont décrits par la susceptibilité $\chi^{(3)}$) peuvent se produire dans de tels milieux centrosymétriques.

De nos jours, l'application de l'optique non linéaire dans le cadre des sciences de l'information a deux motivations principales. Les effets non linéaires sont nécessaires pour la création d'une base pour le traitement des signaux optiques, tandis que d'autre part, ils provoquent des déformations préjudiciables aux signaux de communication dans les fibres optiques longue distance. Par conséquent, les applications de traitement du signal, nécessitent un milieu de propagation avec des effets non linéaires plus élevés pour faciliter le traitement de signal optique à moindre coût en énergie. À l'opposé, pour la transmission de signaux optiques, on cherche à minimiser l'effet des non-linéarités du milieu de propagation pour augmenter la capacité de transmission. Dans le contexte du traitement des signaux optiques, les techniques optiques utilisent une large gamme de dispositifs non-linéaires avec différents mécanismes pour réaliser de multiples

fonctionnalités de réseau. Parmi les technologies de traitement tout-optique nous citons celles présentant un intérêt significatif pour ce trvail

- Les amplificateurs optiques à semiconducteurs (AOS) utilisant $\chi^{(3)}$ pour exciter les effets non-linéaires suivant: la modulation croisée du gain (XGM), l'auto-modulation de phase (SPM pour self-phase modulation), la modulation croisée de phase (XPM), et le mélange à quatre ondes (FWM pour four-wave-mixing) [52, 53].
- Les fibres fortement non linéaires (HNLF pour Highly Nonlinear Fibers) [54, 55, 56, 57] ou d'autres guides d'ondes (de verre de chalcogénure [58], le silicium sur isolant (SOI) [59], et semiconducteurs III-V [60, 61]) utilisant $\chi^{(3)}$ pour exciter effets non linéaires SPM, XPM, FWM.
- Niobate de lithium polarisé périodiquement (PPLN pour Periodically Poled Lithium Niobate, en anglais) en utilisant $\chi^{(2)}$ pour exciter l'effet non linéaire de mélange à trois ondes (TWM pour three wave mixing en anglais) [62, 63, 64].

Toutes ces plates-formes ont été largement exploitées, permettant de mettre en œuvre des portes logiques toutes-optiques [55], la conversion de longueur d'onde [43], la régénération [44], la génération de peigne de fréquence [45], etc. Elles présentent des réponses optiques picoseconde et sous-picoseconde et par conséquent, peut potentiellement mener à la réalisation des dispositifs optiques avec une dynamique beaucoup plus rapide que celle des appareils électroniques actuels. Mais une vitesse de traitement élevé ne suffit pas à elle seule pour obtenir des systèmes optiques fiables de haute capacité. La consommation d'énergie du dispositif est au moins aussi importante [8]. Comme de fortes intensités de lumière sont nécessaires pour stimuler les effets non linéaires, les dispositifs à base de matériaux non linéaires consomment beaucoup d'énergie. Pour mieux comprendre les mécanismes de base derrière la consommation d'énergie dans les dispositifs optiques non linéaires, nous devons tenir compte des processus de transformation de l'énergie au niveau de l'appareil ou du circuit. La Figure 1.6 montre un schéma bloc d'un dispositif (ou circuit) de traitement du signal optique basé sur des mécanismes non linéaires. Le circuit est constitué d'un milieu non linéaire, tel que les SOA, HNLFs ou PPLNs. Typiquement, le dispositif ou le circuit aura deux ou plusieurs entrées de signal (la Figure 1.6 montre toutes les entrées considérés comme entrées de l'informations) et une ou plusieurs sorties de signal (la Figure 1.6 montre toutes les sorties considérées comme sortie de L'informations). La Figure 1.6 représente également une

entrée d'alimentation, une condition essentielle dans tous les circuits non-linéaires, la source d'alimentation peut être un courant électrique ou une pompe optique en fonction du milieu non-linéaire utilisé. Une puissance relativement élevée est fournie au circuit pour exciter une interaction non linéaire, c.-à-d., pour activer et désactiver le milieu non linéaire pour une opération de traitement. La puissance totale P_T consommée par un dispositif ou un circuit pour traiter les informations d'entrée est la somme des puissances P_{in} à l'entrée et la puissance d'alimentation P_s moins la puissance du signal de sortie, P_{out} [65]:

$$P_T = P_{in} + P_s - P_{out} \tag{1.3}$$

L'énergie totale consommée par le circuit non linéaire, E_T , est tout simplement la puissance totale multipliée par la période de bit τ_b (le temps entre deux opérations consécutives) $E_T = P_T \tau_b = (P_{in} + P_s - P_{out}) \tau_b$.

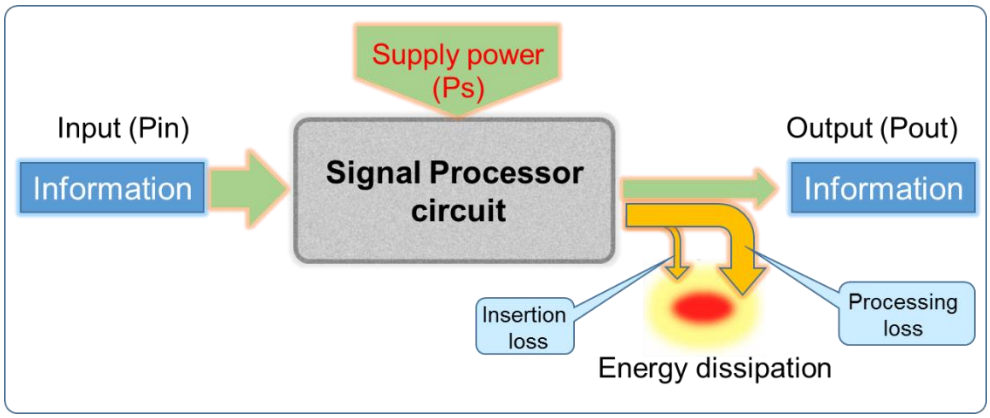

Figure 1.6 – Schéma du flux d'énergie dans un circuit de traitement de signaux optiques basé sur des mécanismes non linéaires.

Comme les photons ont relativement une faible interaction avec la matière, une forte énergie doit être fournie ($P_{in} + P_s$) à un processeur non linéaire afin d'exciter une interaction non linéaire pour le traitement [8]. En plus de cette dépense d'énergie importante nécessaire pour traiter les informations, il y a également des pertes d'énergie sous forme de dissipation de chaleur. Ce sont les pertes de traitement et d'insertion [8]. Les pertes de traitement proviennent de la faible conversion des champs d'entrée et d'alimentation, $P_{in} + P_s$, dans les informations de sortie P_{out}. À cause de la faible interaction de la lumière avec la matière, une grande partie de la puissance dans les deux champs P_{in} et P_s, passe à travers le circuit sans être utilisée, et convertie en chaleur, ce

qui résulte en une faible P_{out} (P_{in} +P_s >> P_{out} signifie un grand E_T). Les pertes d'insertion proviennent de l'absorption et la diffraction de la lumière quand elle se propage à travers le circuit, car un dispositif optique ne peut pas passer 100% d'une onde lumineuse. En outre, le traitement du signal optique utilisant des interactions non linéaires nécessite, en général, un approvisionnement continu d'énergie, indépendamment du fait que ce dispositif exécute ou non une opération de traitement [8].

En plus des problèmes d'énergie, le degré élevé de contrôle requis sur les caractéristiques des signaux d'entrée (par exemple, la puissance, la fréquence centrale, état de polarisation, etc.) impliqués dans une opération non linéaire de traitement a empêché l'application du traitement du signal optique non linéaire au-delà de l'environnement bien contrôlé de laboratoire. Un inconvénient supplémentaire des techniques d'optiques non linéaires est que des fibres fortement non linéaires ou des guides d'ondes à profils de dispersion personnalisés sont nécessaires pour un traitement efficace, rendant le système coûteux. En outre, la mise en œuvre de systèmes plus complexes reposant sur la concaténation de deux ou plusieurs processeurs non linéaires du signal optique pourrait dégrader sensiblement la qualité du signal. Cette dégradation peut être provoquée par la réduction du rapport signal sur bruit (associée à la faible efficacité énergétique de ces processeurs, et l'exigence d'amplification supplémentaire), et/ou par l'introduction de composantes de fréquence parasites dans la bande passante du signal d'information.

1.2.2 Traitement linéaire du signal optique

Les systèmes linéaires peuvent être utilisés pour modéliser et analyser un large éventail de problèmes dans les domaines de la science et de l'ingénierie. En particulier, les filtres optiques linéaires ont été largement étudiés, ces dispositifs occupent une position d'une importance fondamentale dans l'optique spatiale et temporelle [41, 66, 67]. Le traitement linéaire du signal optique est basé sur la riche théorie des systèmes linéaires et dans de nombreuses applications, les méthodes de traitement linéaires se révèlent optimales; deux exemples seront présentés dans la section 1.3. En outre, les méthodes linéaires sont intrinsèquement simples à mettre en œuvre, ce qui est probablement la raison de leur utilisation généralisée dans la pratique.

Un processeur est dit linéaire si la fonction de transfert, à savoir $y = f(x)$, la fonction définissant la relation entre les signaux d'entrée et de sortie (x et y respectivement), satisfait au principe de

superposition, de telle sorte que $f(x_1+x_2)=f(x_1) + f(x_2)$ and $f(n\ x) = n\ f(x)$ [68]. Autrement dit, si le signal d'entrée est une somme pondérée de plusieurs signaux, la sortie du system est aussi une somme pondérée (ou superposition) des réponses à chacun des signaux. La propriété superposition rend les systèmes linéaires faciles à analyser, car il est possible de décomposer tout signaler linéaire en composantes simples et les analyser séparément.

Si les paramètres de la fonction de transfert du système linéaire sont constants au cours du temps, l'opération de traitement du signal est dite invariante dans le temps [68]. Un décalage temporel dans le signal d'entrée provoque le même décalage temporel dans le signal de sortie. Parfois, une telle opération est appelée processeur linéaire invariant dans le temps (LTI pour linear time invariant en anglais). Très souvent, ces processeurs sont supposés être causaux, soit le signal de sortie dans le présent dépend des signaux présents et passés, mais pas sur ceux à venir[5].

L'analyse de Fourier fournit un ensemble d'outils puissants et de perceptions pour la conception et la compréhension des systèmes LTI. La réponse impulsionnelle et la réponse fréquentielle (fonction de transfert spectrale) sont deux caractéristiques qui très utiles pour la caractérisation des systèmes LTI. Ils fournissent deux façons complètes et différentes de calculer la sortie d'un système LTI pour un signal d'entrée donné. La réponse impulsionnelle temporelle d'un système LTI, souvent notée $h(t)$ avec t la variable de temps, est définie comme étant le signal de sortie qui est obtenu quand une impulsion est appliquée à l'entrée du système. En connaissant la réponse impulsionnelle, la sortie du système LTI peut être facilement calculée pour chaque signal d'entrée arbitraire par convolution du signal d'entrée avec la fonction de la réponse impulsionnelle. Alternativement, le système LTI peut être caractérisée par une fonction de transfert spectrale $H(\omega) = V(\omega)/U(\omega)$ dans le domaine de fréquences où $U(\omega)$ et $V(\omega)$ sont les transformées de Fourier spectrales des signaux du système d'entrée et de sortie, respectivement, et ω est la variable de fréquence angulaire (pulsation). Il y a une myriade de fonctionnalités optiques de

[5] Un système causal (également connu comme un système physique ou non-anticipative) est un système dans lequel la sortie dépend des entrées dans le passé et le présent, mais pas des entrées à venir, à savoir, la sortie $u(t_0)$ dépend seulement de l'entrée $v(t)$ pour valeurs de $t \leq t_0$. En général, les systèmes LTI opérant sur des signaux dépendant du temps sont toujours causaux et ne peuvent pas répondre aux événements futurs. Cependant, tous les systèmes n'ont pas le temps comme variable indépendante. Si la variable indépendante est l'espace, le système n'est pas forcément causal, à savoir la sortie $u(x_0)$ peut dépendre de l'entrée $v(x)$ pour toutes les valeurs de x, $x \leq x_0$ ou $x \geq x_0$; par exemple, pour un système de traitement d'images.

traitement de signaux qui peuvent être décrites par la réponse d'un système LTI, voir Figure 1.5, telles que les techniques optiques de récupération d'horloge, la mise en forme d'impulsions optiques, différentiateurs/intégrateurs optiques, et les transformateurs d'impulsions tels que les transformateurs de Hilbert, entre plusieurs autres applications.

En général, il existe deux procédures principales pour mettre en œuvre des processeurs de signaux optiques, (i) la conception des filtres spectrales linéaires, tels que résonateurs en anneau, interféromètres ou des réseaux à fibre, où l'opération de filtrage est réalisée en modifiant directement le spectre du signal d'entrée (Figure 1.7, à gauche); (ii) le développement des filtres temporels équivalents aux filtres spatiaux[6]. Dans les filtres temporels l'opération de filtrage est réalisée dans le domaine temporel via des processus de modulation (Figure 1.7, à droite). Il convient de noter que développement des filtres optiques temporels équivalents aux filtres optiques spatiaux ont été réalisés grâce à ce qui est appelé la dualité espace-temps dans l'optique, qui sera défini en détail dans le Chapitre 2. L'utilisation de cette dualité, permet d'appliques des techniques spatiales très efficaces de traitement de l'information optiques sur des signaux temporels, ce qui rend au final des approches plus sophistiquées et puissantes accessible aux applications de transformation et de caractérisation de l'information temporelle [69]. Plus particulièrement, une telle approche a permis le développement de la notion de la lentille-temporelle [69], l'imagerie temporelle / systèmes d'auto-imagerie [41], le filtrage et la transformation de Fourier optiques en temps réel [69], etc.

La modulation temporelle linéaire et les processus de filtrage spectral, à leur tour peuvent être scindés en deux catégories: modulation/filtrage de phase et d'amplitude. La manipulation désirée du signal peut être produite sur le profil temporel (ou spectrale) d'amplitude ou de phase du signal sous test par la modulation (filtrage) temporelle (ou spectrale) d'intensité ou de phase, comme le montre la Figure 1.7.

Un filtre optique d'amplitude spectrale ayant une fonction de transfert $H(\omega) = A(\omega) \exp[j\phi(\omega)]$, où $A(\omega)$ et $\phi(\omega)$ désignent les profils d'amplitude et de phase du filtre, respectivement, modifie le

[6] Dans le traitement en domaine spatial, l'information est codée dans la distribution spatiale de la lumière, qui se propage dans l'espace libre. Le traitement de l'information optique spatiale est effectué en utilisant des optiques en espace libre [67], ce qui implique l'utilisation de lentilles optiques, des réseaux de diffraction, des modulateurs spatiaux de lumière, etc.

contenu spectral du signal d'entrée, et le traitement du signal est typiquement effectuée en atténuant et/ou en supprimant une partie des composantes spectrales du signal d'entrée (Figure 1.7 , à gauche, en haut). On notera que dans ce type de filtres, si $\phi(\omega) = 0$, le filtre est dit filtre idéal d'amplitude-seule, ayant une réponse impulsionnelle pair et non-causale. Dans la pratique cependant, une phase spectrale linéaire $\phi(\omega) = \omega\ t_0$ est typiquement introduite pour satisfaire la causalité. Cette variation de phase correspond seulement à un retard temporel de $t_{0,}$ elle n'a donc pas d'incidence sur la définition du filtre d'amplitude et ne réalise aucune autre transformation sur le signal d'entrée. Un exemple de filtres d'amplitude typiques comprennent les résonateurs en anneau [70, 48, 71], les interféromètres [72, 47] ou les structures périodiques comme les réseaux de fibre ou de guide d'ondes [73, 74]. D'autre part, un filtre optique spectrale de phase-seule (passe-tout) est caractérisé par une réponse en fréquence $H(\omega) = A$ exp $[j\phi(\omega)]$, où A est une amplitude constante, indépendamment de la variable de fréquence. Par conséquent, le filtre spectral de phase-seule fait passer toutes les composantes spectrales avec une amplitude égale; alors, si la fonction de transfert d'amplitude spectrale uniforme est conçue pour une transmission de 100%, fondamentalement aucune énergie de signal n'est perdue dans le procédé (Figure 1.7 , à gauche, en bas). Au lieu de cela, le filtre de phase décale les composantes spectrales pour effectuer le traitement du signal voulu. En règle générale, l'intuition des effets temporels induits par l'amplitude de la réponse en fréquence d'un filtre sur un signal entrant est assez bien développée, mais en revanche, la visualisation de l'effet de la phase de la réponse en fréquence du signal est plus subtile, mais tout aussi importante. Un milieu dispersif, tel qu'une fibre optique monomode classique, est un exemple d'un filtre de phase-seule [41].

De même, les modulateurs d'intensité optique temporelle avec une fonction de modulation $p(t) = A(t)$ atténuent ou éliminent certaines composantes temporelles du signal d'entrée pour produire le signal de sortie ciblé, voir Figure 1.7, droite, haut. En revanche, comme le montre la Figure 1.7, à droite, en bas, un modulateur de phase temporelle avec fonction de modulation de $p(t) = \exp[\ j\phi(t)]$ ne modifie que la phase de l'onde lumineuse qui le traverse et, en substance, aucune énergie n'est perdue dans le processus.

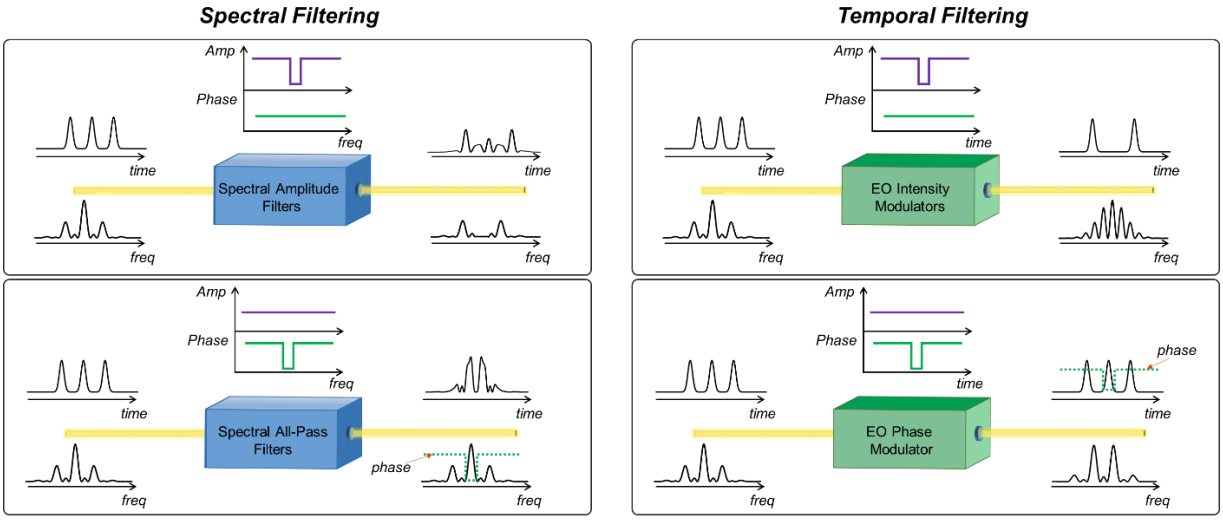

Figure 1.7 – Procédures de mise en œuvre de la modulation temporelle et du filtrage spectral linéaires.

Il convient de noter que les filtres spectraux sont des composants passifs, c.-à-d., ils ne nécessitent pas une source externe d'énergie pour accomplir leurs fonctionnalités. Cependant, les modulateurs temporels sont des composants actifs, qui nécessitent une source d'énergie externe pour fonctionner et remplir les fonctions ciblées. Dans cette thèse, chaque fois que possible, nous utilisons des techniques de filtrage spectral linéaires passives et économes en énergie pour réaliser une fonctionnalité spécifique. Néanmoins, toutes les fonctionnalités ne peuvent être mises en œuvre en utilisant uniquement des systèmes passifs et dans de nombreux cas, nous avons besoin d'incorporer des techniques linéaires de modulation temporelles actives. Les mécanismes de modulation temporelle d'un signal optique les plus simples et les plus économes en énergie peuvent être réalisés grâce aux systèmes de modulation électro-optique. Dans ces systèmes, le signal de modulation est un signal électronique, qui a intrinsèquement une énergie inférieure à celle du signal optique. Plus important encore, l'effet de modulation électro-optique est induit en utilisant une non-linéarité du second ordre, ce qui nécessite typiquement beaucoup moins d'énergie provenant de la source de modulation comparé à la modulation tout-optique qui utilise la non-linéarité de troisième ordre.

La Figure 1.8 illustre la transformation de l'énergie qui a lieu dans les méthodes de modulation/filtrage linéaires d'amplitude et de phase. L'énergie de l'information de sortie provient entièrement de l'énergie de l'information d'entrée dans tous les procédés.

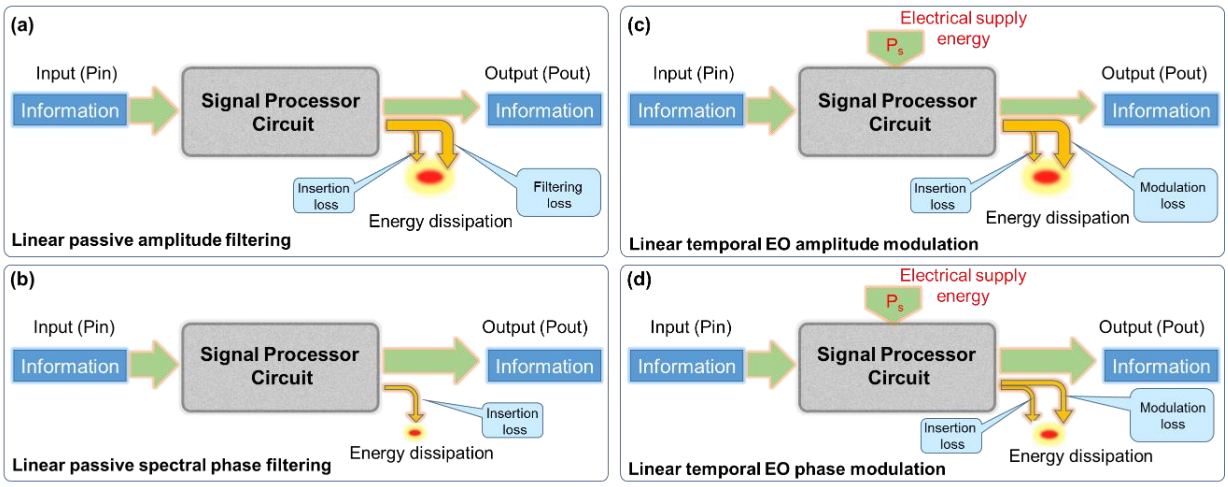

Figure 1.8 – Schéma bloc d'un circuit de traitement de signaux optiques basé sur des mécanismes linéaires. (a) filtrage linéaire d'amplitude spectrale, (b) filtrage spectral linéaire de phase-seule, (c) Filtrage optique linéaire de modulation temporelle, (d) Modulation temporelle linéaire de phase-seule.

La Figure 1.8 (a) et (b) montre le flux d'énergie dans les approches linéaires de filtrage spectral d'amplitude et de phase-seule. Dans ces approches, aucune énergie d'alimentation n'est nécessaire (dispositif passif), de sorte que l'énergie totale consommée par le circuit est simplement $E_T = (P_{in} - P_{out})\ \tau_b$. Le filtrage linéaire passif supprime complètement la contribution la plus significative à la perte d'énergie, P_s, dans l'équation de consommation d'énergie; en outre, l'utilisation d'un filtre optique linéaire passif permet un P_{out} beaucoup plus grand que dans le cas utilisant un milieu non linéaires, ce qui rend E_T plus petit. Cependant, comme le montre la Figure 1.8 (a) et la Figure 1.7 (à gauche, en haut), le filtrage d'amplitude cause nécessairement la perte d'une partie de l'énergie du signal d'entrée; on appelle cette perte comme la perte de filtrage. En fonction de la fonctionnalité ciblée, les pertes de filtrage, $P_{in} - P_{out}$, peuvent être considérable dans les filtres d'amplitude. Alors que dans des procédés de filtrage de phase-seule, si la fonction spectrale de transfert d'amplitude uniforme est conçue pour réaliser 100%e transmission, fondamentalement toute l'énergie du signaler est conservée et pertes de filtrage sont réduites à près de 0, autrement dit, en excluant la perte d'insertion, $P_{in} \approx P_{out}$, entrainant une consommation d'énergie totale $E_T \approx 0$.

D'autre part, dans les mécanismes linéaire actifs de modulation d'intensité et de phase, comme le montre la Figure 1.8 (c) et (d), les modulateurs ont besoin d'être alimentés en énergie électrique

(P_s) afin d'exciter l'interaction non linéaire du second ordre, l'énergie totale consommée par les modulateurs est alors $E_T = (P_{in} + P_s - P_{out})\ \tau_b$. Dans ces mécanismes, l'énergie d'alimentation ne contribue pas directement à l'énergie de sortie porteuse d'informations, c.-à-d., l'énergie du signal d'information de sortie, P_{out}, provient entièrement de l'énergie de l'information d'entrée, P_{in}, (i.e., $P_{out} \leq P_{in}$). Par conséquent, l'énergie d'alimentation P_s est entièrement dissipée dans le dispositif, après avoir permis de réaliser la modification désirée dans les caractéristiques de phase du signal d'entrée. Cependant, la quantité d'énergie d'alimentation électrique, P_s, est nettement inférieure à celle des dispositifs optiques non linéaires, où un signal optique est utilisé comme l'énergie d'alimentation pour exciter un effet non linéaire dans le milieu non linéaire représentés sur la Figure 1.6, ce qui rend l'énergie consommée ET plus faible dans les mécanismes de modulation électro-optique. Il importe de mentionner que dans la modulation EO d'amplitude temporel, en plus de l'alimentation en tension de modulation, nous avons également besoin d' une alimentation en tension de polarisation qui rend la puissance d'alimentation totale, P_s, dans ce procédé plus grande que celle de la modulation de phase EO.

D'une manière générale, les pertes de modulation désignent la quantité d'énergie qui est perdue à partir de la puissance d'entrée dans le processus de modulation, $P_{in} - P_{out}$. Les pertes de modulation excluent la contribution des pertes d'insertion. Comme mentionné plus haut, comme dans le filtrage d'amplitude, la modulation d'intensité cause également une perte d'une partie de l'énergie du signal d'entrée, cela est montré dans la Figure 1.8 (c) et la Figure 1.7 (gauche, bas). Par conséquent, l'énergie perdue de la puissance d'entrée, $P_{in} - P_{out}$, peut être considérable dans un procédé de modulation d'intensité. À l'inverse de cela, l'énergie du signal peut être entièrement préservée si seule la phase du signal est manipulée dans le domaine temporel par la modulation de phase temporelle. Par conséquent, la majeure partie de la lumière passe à travers les dispositifs de modulation de phase, assurant ainsi une plus faible consommation d'énergie, pratiquement $P_{in} \approx P_{out}$ et la consommation totale d'énergie sera alors déterminée par l'énergie d'alimentation externe, $E_T = P_s\ \tau_b$.

Afin de fournir un exemple quantitatif de consommation d'énergie dans la modulation de phase temporelle d'un signal d'entrée, nous estimons la consommation d'énergie dans le processus de modulation de phase électro-optique et le procédé de modulation en phase croisée (XPM) pour induire un effet d'auto-imagerie spectrale [75] (qui sera adressé dans le chapitre suivant) sur un

train d'impulsions optiques périodiques (avec une période temporelle de 100ps), comme le montre la Figure 1.9 . Dans notre estimation, nous prenons en compte un HNLF avec un coefficient non-linéaire (d'effet Kerr) $\gamma = 11\ W^{-1}Km^{-1}$ et un modulateur de phase électro-optique avec $V_\pi = 3.0$ V. Ces spécifications correspondent aux valeurs conventionnelles pour les deux processus évalués, selon l'état actuel de la technologique. La consommation d'énergie estimée est de $E_T = P_s\ \tau_b$ = 125mW× 100ps = 12.5 pJ/période pour le processus de modulation de phase en utilisant la XPM [76], et il est de $E_T = P_s\ \tau_b = \frac{V_\pi^2}{8\,R}\ \tau_b$ = 22.5mW× 100ps = 2.25 pJ/période, où R = 50Ω est la résistance du modulateur, pour la modulation électro-optique [77]. En plus de l'amélioration de la performance énergétique par un facteur cinq, la modulation électro-optique fournit également le mécanisme le plus simple de modulation de phase temporelle.

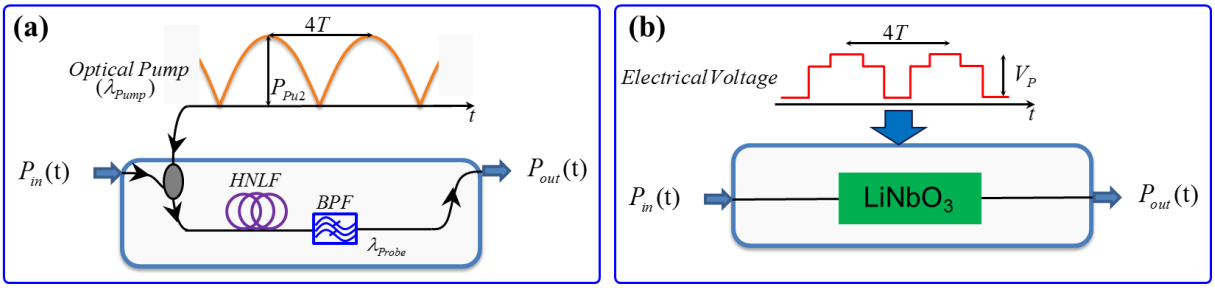

Figure 1.9 – Traitement d'un train périodique d'impulsions optiques d'entrée ($P_{in}(t)$) en utilisant (a) la modulation non linéaire de phase croisée (XPM) et (b) l'effet électro-optique.

L'utilisation de l'optique linéaire permet une consommation d'énergie beaucoup plus faible que dans le cas utilisant les mécanismes non-linéaires. Par conséquent, afin de réduire le budget énergétique global d'un système de traitement du signal optique, il est nécessaire d'éviter l'utilisation des mécanismes non linéaires gourmands en énergie, et de mettre en œuvre les fonctionnalités spécifiques souhaitées à l'aide des mécanismes linéaires économes en énergie.

1.3 Revu des processeurs de signaux optiques pertinents étudiés dans cette thèse

Parmi les fonctions de traitement du signal d'importance critique étudiées dans cette thèse nous citons: la récupération d'horloge (RH) tout-optique, la conversion de format optique et le contrôle du taux de répétition des lasers impulsionnels pour des applications de télécommunications. Dans cette section, nous passons en revue de manière courte et non-exhaustive les quelques-unes des méthodes démontrées précédemment. Le but de cette discussion est de mettre notre travail en contexte.

1.3.1 Récupération de l'horloge optique

Au cours des 20 dernières années, une grande variété de méthodes optiques de récupération des signaux d'horloge "de base" et "sous-harmonique" basées sur différents principes physiques ont été proposées et démontrées [78, 79, 46, 80, 81, 82, 83, 84, 85]. La RH est une opération fondamentale effectuée dans tous les appareils numériques de communication allant des téléphones mobiles ordinaires à des récepteurs optiques à grande vitesse. Dans les télécommunications optiques, l'horloge est traditionnellement récupérée par des circuits électroniques. Pour un récepteur classique qui convertit le signal optique en un signal électrique, le RH électronique est un choix naturel. Il existe, cependant, des emplacements et des dispositifs dans l'architecture des réseaux optiques, où la conversion optique-électrique n'est pas nécessaire. Le choix préféré serait alors de maintenir le signal dans le domaine optique. Des exemples de tels dispositifs sont, les régénérateurs de signaux tout-optique [44], les(dé)multiplexeurs par division temporelle [17], les portes logiques optiques [55], ou, en général, les points dans le réseau où le signal transmis doit être (re)synchronisé mais pas terminé. Tous les systèmes de télécommunications numériques se composent de trois principaux éléments: un émetteur, un chemin de transmission, et un récepteur. L'émetteur et le récepteur sont généralement séparés par une distance considérable, donc le récepteur n'a aucun moyen d'obtenir des informations directes sur l'horloge de l'émetteur. Naturellement, les informations d'horloge pourraient être envoyées à travers un canal de communication séparé menant à la réduction de la bande passante nette et

l'augmentation des coûts du système. C'est pourquoi, le récepteur récupère généralement l'horloge à partir de bits entrant.

Les méthodes de RH optiques peuvent être scindées en deux grandes catégories: des techniques de filtrage actives (non-linéaire) et passives (linéaires). Dans cette section, Nous présentons deux méthodes de RH optiques, une de chaque catégorie.

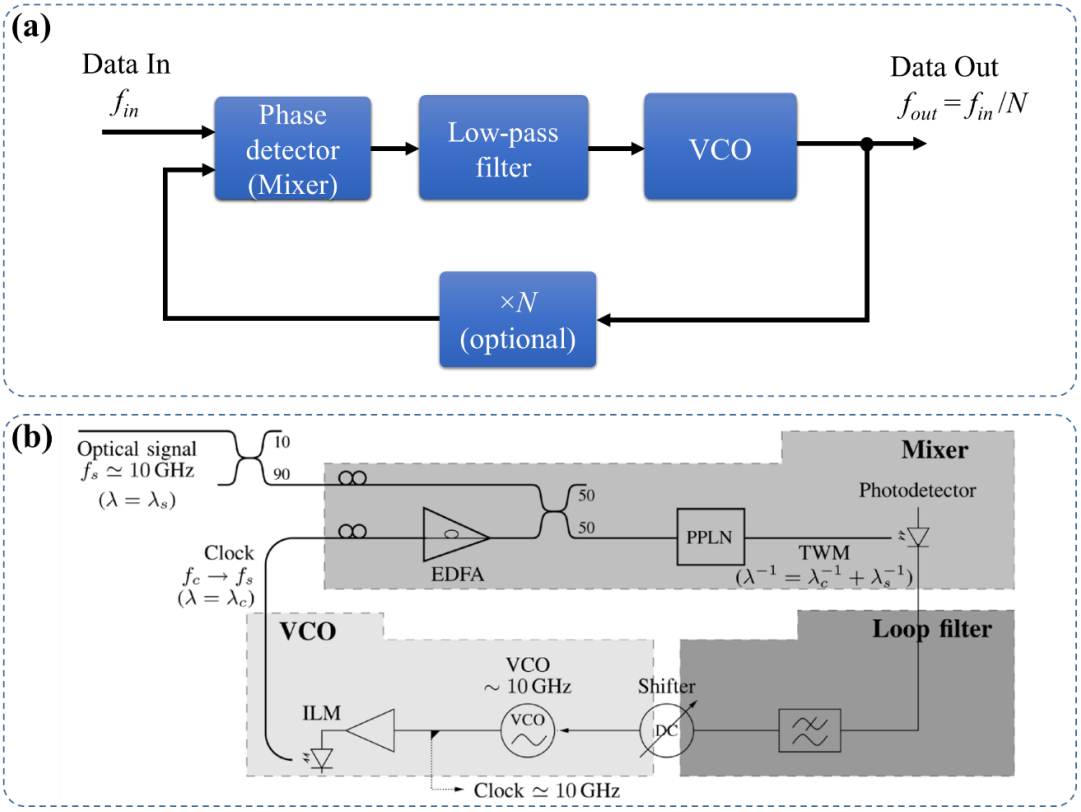

Figure 1.10 – (a) Représentation schématique des composants d'une PLL. (b) Configuration d'une PLL; le «mélangeur» est basé sur le mélange à trois ondes dans le NLPP [92].

Une des techniques actives répandues de récupération d'horloge optique est d'utiliser une boucle à verrouillage de phase (Phase-locked loop- PLL) optique [86, 87]. La fonction de la PLL optique imite étroitement une PLL électrique conventionnelle qui est largement utilisée dans des applications de radiofréquence (RF) et la technologie des télécommunications. La PLL synchronise un oscillateur interne avec un signal de données externe. Grâce au processus de synchronisation la PLL obtient des informations sur la fréquence et la phase du signal de données, qui peuvent par ailleurs être enterrés sous la modulation des données. La Figure 1.9 (a) montre la PLL électrique classique qui se compose de quatre éléments de base: une détecteur phase

(mélangeur), un filtre passe-bas, un oscillateur commandé en tension (voltage-controlled oscillator - VCO) et une boucle de réaction [85, 86, 87]. En outre, la boucle de réaction peut consister en un compteur de multiplication, lorsque l'oscillation déterminée est une sous-harmonique du signal de données.

La synchronisation est réalisée en ajustant le VCO de sorte que la valeur de corrélation croisée des données et des signaux locaux est maximisée. Dans une PLL électrique classique, le signal optique d'entrée est converti en un signal électronique à l'entrée du détecteur de phase et mélangé avec le signal local, afin de réaliser la synchronisation. Toutefois, dans cette configuration, le débit binaire d'entrée maximum est limité par le temps de réponse du détecteur de phase [91, 46]. Des techniques optoélectroniques alternatives ont été proposées pour effectuer la corrélation croisée nécessaire dans le détecteur de phase en utilisant des interactions optiques non linéaires pour construire une PLL optique. La Figure 1.9 (b) montre un exemple d'une PLL optique [92]. La corrélation croisée requise de l'horloge optique locale et des signaux de données est effectuée par mélange à quatre ondes (FWM) dans un milieu optique non linéaire, tel qu'un SOA [93], ou le mélange à trois ondes (TWM) dans le niobate de lithium périodiquement polarisé (PPLN) [78]. Les impulsions, en fonction du degré de chevauchement, interagissent par FWM ou TWM et fournissent la corrélation croisée des signaux. Cette opération réalise un filtrage passe-bande sur la longueur d'onde générée, et l'information sur la moyenne temporelle de la puissance optique mesurée est renvoyée au VCO.

En utilisant cette technique la récupération d'horloge optique à des débits élevés, ainsi que le démultiplexage d'un flux de donnée OTDM à 320 Gbit/s ont été démontrés [78, 94]. Récemment, une autre méthode de corrélation croisée non linéaire a été introduite, elle est basée sur l'absorption à deux photons dans une photodiode à avalanche en silicium [95]. La moyenne temporelle de la réponse de la photodiode est fonction du chevauchement temporel des impulsions optiques et peut donc être incorporé dans la synchronisation de la PLL. En plus des structures PLL, les effets non linéaires sont également utilisés pour la récupération d'horloge optique employant le verrouillage de mode d'un laser à fibre et à semi-conducteur (semiconductor fiber laser SFL) basée sur l'utilisation d'un miroir à boucle optique non linéaire et une rotation de polarisation non-linéaire [85] .

Comparée à d'autres méthodes de RH optique, les configurations optiques non-linéaires/actives souffrent souvent de complexité et des coûts de fabrication considérables. Cependant, la qualité de l'horloge récupérée en matière de gigue et de stabilité est généralement élevée et la PLL fournit la possibilité de RH subharmonique, qui ne peut être réalisé par d'autres méthodes.

En fait, la récupération d'horloge ne requiert pas nécessairement un système actif/non-linéaire. Elle peut également être réalisée par des techniques de filtrage linéaire passif [46, 96, 97]. Ces méthodes enlèvent une partie ou la totalité de l'information contenue dans le signal reçu et de ne conserver que la fréquence de base associée au débit binaire du signal de données. Ces techniques présentent généralement une construction simple et un faible coût de fabrication, leur défi étant la qualité du signal d'horloge récupéré.

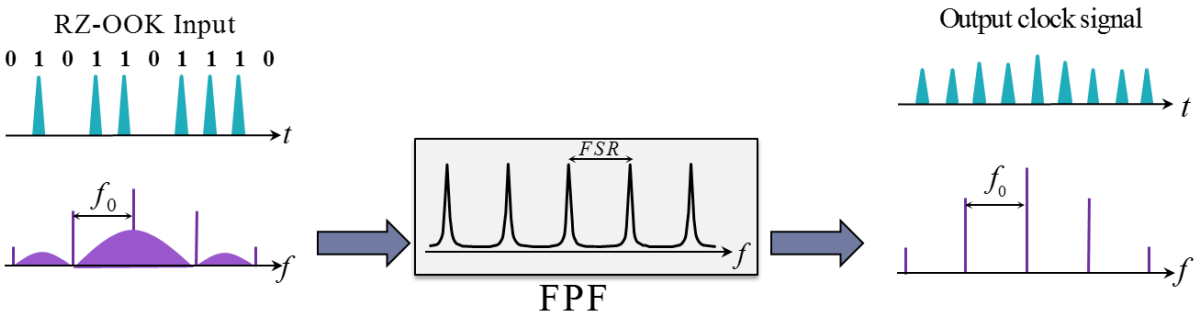

Figure 1.11 – Principe de récupération d'horloge optique basé sur le filtrage d'amplitude spectrale en utilisant un FFP.

La récupération d'horloge optique basée sur un filtre Fabry-Perot (FFP) est une des techniques passives les plus étudiés pour récupérer le signal d'horloge à partir d'un signal optique de données de type retour à zéro tout-ou-rien (RZ-OOK). Un FFP est un filtre d'amplitude dont les pics de transmission spectraux sont périodiques et les bandes de transmission sont généralement étroite, voir Figure 1.10. Ce filtre, avec un intervalle spectrale libre (ISL) accordé sur le débit binaire du signal de données optiques entrant, préserve les composantes spectrales discrètes du signal l'horloge et supprime le reste du contenu spectral du signal de données, qui contient typiquement environ 50% de l'énergie globale du signal de données entrant.

Étant donné qu'un FFP est un dispositif entièrement passif, la vitesse de fonctionnement des techniques basées sue un FFP est théoriquement illimitée. Toutefois, pour obtenir un signal

d'horloge de haute qualité, un FFP de haute finesse est nécessaire pour moyenner le profil temporel de données entrantes. La haute finesse nécessaire impose une tolérance très réduite pour le désaccord entre les spécifications du filtre (fréquence de résonance et ISL) et les spécifications de signaux de données entrants (longueur d'onde centrale et le débit binaire, respectivement). D'autre part, une finesse réduite du FFP conduit à une modulation d'amplitude (AM) dans le signal d'horloge. Pour minimiser cette modulation, la FFP devrait être suivie d'un sous-système non linéaire [96], par exemple, un amplificateur optique à semiconducteur (AOS), un interféromètre non linéaire ultrarapide, ou d'un interféromètre de Mach-Zehnder, agissant en tant qu'égaliseur de puissance optique. L'ajout de tels sous-circuits augmente de la complexité des circuits de récupération d'horloge, de plus, ces sous-systèmes peuvent limiter le débit de données du système, par exemple, à quelques dizaines de Gbit/s lors de l'utilisation d'un AOS. En outre, malgré toutes les techniques de RH passives publiées à ce jour, la possibilité de la RH sous-harmonique utilisant un système de RH à base FFP n'a pas été démontrée en [46].

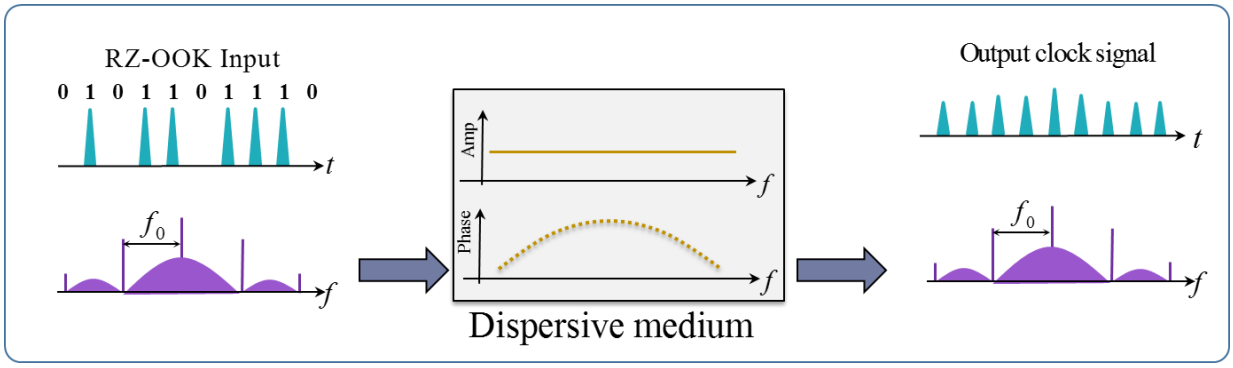

Figure 1.12 – Technique de récupération d'horloge en utilisant l'effet Talbot temporel induit par la dispersion [96].

Fernández-Pousa et al [98] ont proposé un autre régime de RH passive linéaire en utilisant un segment de milieu dispersif, dont la dispersion est accordée sur une valeur correspondant à l'effet Talbot temporel. Cette proposition a été démontrée expérimentalement plus tard par Pudo et al [99, 100] et Oiwa et al [101]. L'effet Talbot temporel avait déjà été utilisé pour traiter des signaux d'entrée périodiques et générer des signaux de sortie périodiques. Cependant, Fernández-Pousa et al, ont montré que l'effet Talbot temporel a une capacité tampon intrinsèque de générer un signal de sortie périodique, même à partir d'un train d'impulsions d'entrée apériodique, c.-à-d., signal de données. La technique proposée offre des avantages similaires à ceux des processeurs de signaux

à base de l'effet Talbot, à savoir la simplicité, le potentiel d'atténuation de la gigue temporelle et un rendement énergétique élevé. Cette dernière est due au fait que, fondamentalement, aucune énergie n'est perdue dans le processus de récupération, car cette technique n'implique que les manipulations de l'information de phase spectral du signal. Cette technique sera décrite en détail plus loin dans la section 3.3.

1.3.2 Conversion de formats RZ à NRZ optiques

Les réseaux optiques du futur seraient probablement des hybrides de différentes technologies en raison de la grande variété d'applications et de leur structure hiérarchique, ce qui implique diverses spécifications pour les différents segments de réseau. Dans ce contexte, un segment de réseau utilise le format de modulation adéquat qui répond à ses exigences [102, 103]. Par conséquent, les convertisseurs de format tout-optique sont d'une grande importance pour interconnecter de façon transparente les différentes parties des réseaux, ce qui évite le recours aux convertisseurs optique-électrique (O/E) et électrique-optique (E/O), et éviter ainsi les limitations imposées par l'électronique en matière de débit et de bande passante de fréquence [103]. En particulier, la conversion entre les formats de signaux retour-à-zéro (RZ)[7] et non-retour-à zéro (NRZ)[8] est particulièrement intéressante: les deux formats sont matures et largement utilisés dans les différentes parties des réseaux, par exemple, le format RZ est adopté dans les systèmes de multiplexage dans le domaine temporel (OTDM) pour être en mesure d'effectuer le multiplexage d'impulsions, tandis que le format NRZ est préféré dans les systèmes de multiplexage en longueur d'onde (WDM) en raison de sa plus grande efficacité spectrale [71]. En outre, la conversion de format d'un signal RZ à son équivalent NRZ est également souhaitable dans de multiplexage des signaux OTDM car les signaux NRZ améliorent la tolérance des processus de multiplexage à la gigue temporelle grâce à leur forme temporelle à sommet plat [104].

---

[7] Le retour à zéro (RZ) est un code de ligne utilisé dans les signaux de télécommunications dans lequel chaque impulsion représentant 1 bit est choisie pour être plus courte que la durée de bits, et son amplitude retourne à zéro avant que la durée de bit ne soit terminée.

[8] Le non-retour à zéro (NRZ) est un code de ligne utilisé dans les signaux de télécommunications dans lequel chaque impulsion représentant 1 bit occupe entièrement la durée de bit et ne tombe pas à zéro entre deux ou plusieurs bits successifs.

Jusqu'à présent, divers systèmes ont été développés pour réaliser la conversion de format RZ-à-NRZ en utilisant principalement des techniques non-linéaires ou linéaires de traitement de signaux optiques [104, 56, 105, 106, 107, 108, 109, 110].

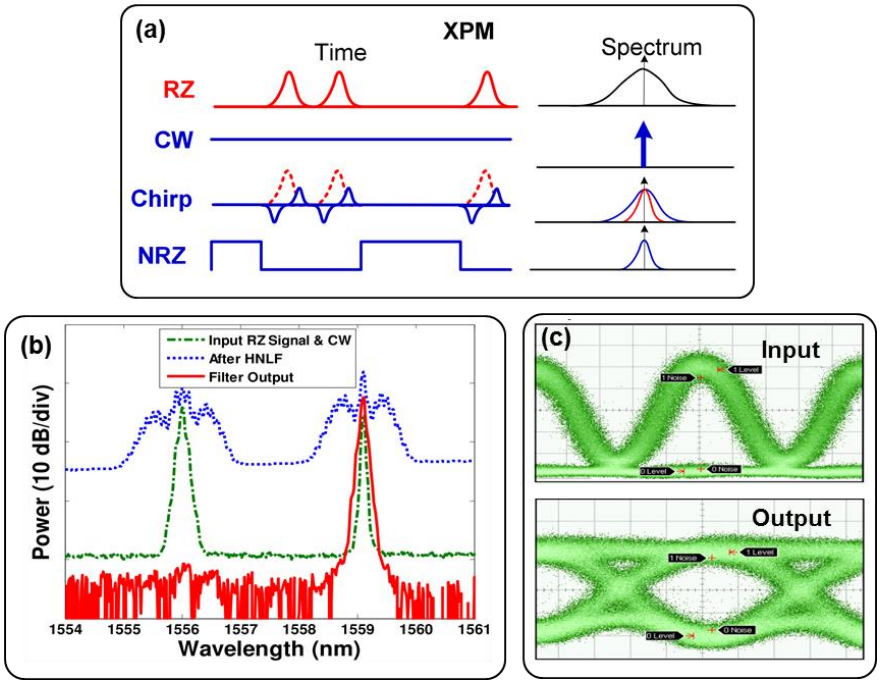

Figure 1.13 – (a) Schéma de conversion de format à base de XPM, (b) les spectres de la sonde de lumière CW, du signal RZ d'entrée avant et après la HNLF, et du signal NRZ converti, (c) diagrammes de l'œil du signal RZ d'entrée et du NRZ converti [56].

Les systèmes basés sur les effets non linéaires, tels que XPM, XGM et FWM, emploient différents milieux non linéaires pour réaliser la conversion de format ciblé, y compris les HNLFs [56], AOS [105] et les guides d'ondes PPLN [106]. Par exemple, la référence [56], présente une conversion de format RZ-à-NRZ utilisant l'XPM avec un faisceau à onde continue, comme le montre la Figure 1.12 (a). Quand un signal d'entrée RZ et une lumière sonde à onde continue sont lancés dans un milieu non linéaire, la XPM produit une modulation de phase non-linéaire. Pour la lumière sonde, la modulation de phase est régie par le taux de variation de puissance du signal RZ d'entrée. Un décalage (pépiement) ver le rouge est provoqué par le front montant du signal RZ, tandis qu'un décalage ver le bleu est généré par front descendant du signal RZ. En outre, la longueur d'onde instantanée reste inchangée lorsque le taux de variation de puissance est égal à zéro, conduisant à une composante fréquentielle sans pépiement. Par conséquent, un signal NRZ

inversé peut être obtenu en filtrant les composantes fréquentielles contenant un pépiement de la lumière sonde d'entrée. La Figure 1.12 (b) montre les spectres de la lumière sonde à onde continue, du signal RZ avant et après la HNLF, et le signal NRZ converti. Il est clair que le spectre d'entrée de la lumière sonde est considérablement élargie à cause de l'effet de la XPM dans de la boucle. Les diagrammes de l'œil mesurés du signal RZ original de 40 Gbit/s et du signal NRZ converti sont représentés sur la Figure 1.12 (c). Cette technique, et plus généralement les systèmes non-linéaires de conversion de format nécessitent un faisceau optique supplémentaire pour réaliser la conversion, en plus des signaux d'entrée de haute puissance.

D'autre part, les convertisseurs de format basé sur le traitement linéaire des signaux optiques sont généralement basés sur le filtrage d'amplitude spectrale linéaire pour changer le spectre d'un signal d'entrée RZ vers le spectre du signal NRZ ciblé, cette approche est appelée 'transformation du spectre optique' [104, 107, 108, 109], voir Figure 1.13 . En particulier, les convertisseurs linéaires de formats RZ-à NRZ reposent sur la suppression des composantes harmoniques de premier ordre dans le spectre d'un signal RZ en utilisant un filtre d'amplitude coupe-bande périodique dont l'ISL est égale à deux fois le débit binaire du signal. Le signal NRZ converti après le filtre coupe-bande, présente cependant des ondulations d'amplitude relativement assez importantes en raison des composantes haute fréquence résiduelle dans spectre. Un filtre optique passe-bande étroit est généralement utilisé pour éliminer les composantes résiduels, ce qui conduit à une réduction des ondulations d'amplitude et l'amélioration de la qualité du signal NRZ converti. Les filtres d'amplitude coupe-bande nécessaires peuvent être mises en œuvre en utilisant une variété de technologies, tels que les micro-résonateurs photoniques en anneau [104, 107, 108], les interféromètres [109], et les réseaux de Bragg à fibre (FBG, pour fiber Bragg grating, en englais) [110].

Les plates-formes linéaires de conversion de format sont d'un plus grand intérêt en raison de leur simplicité intrinsèque, leur capacité à opérer à grande vitesse et leurs performances stables. En outre, à la différence des systèmes non-linéaires, les convertisseurs linéaires ne nécessitent aucun faisceau optique supplémentaire pour réaliser la conversion de format, tout en évitant le besoin de signaux d'entrée de haute puissance, comme l'exige les effets non linéaires optiques.

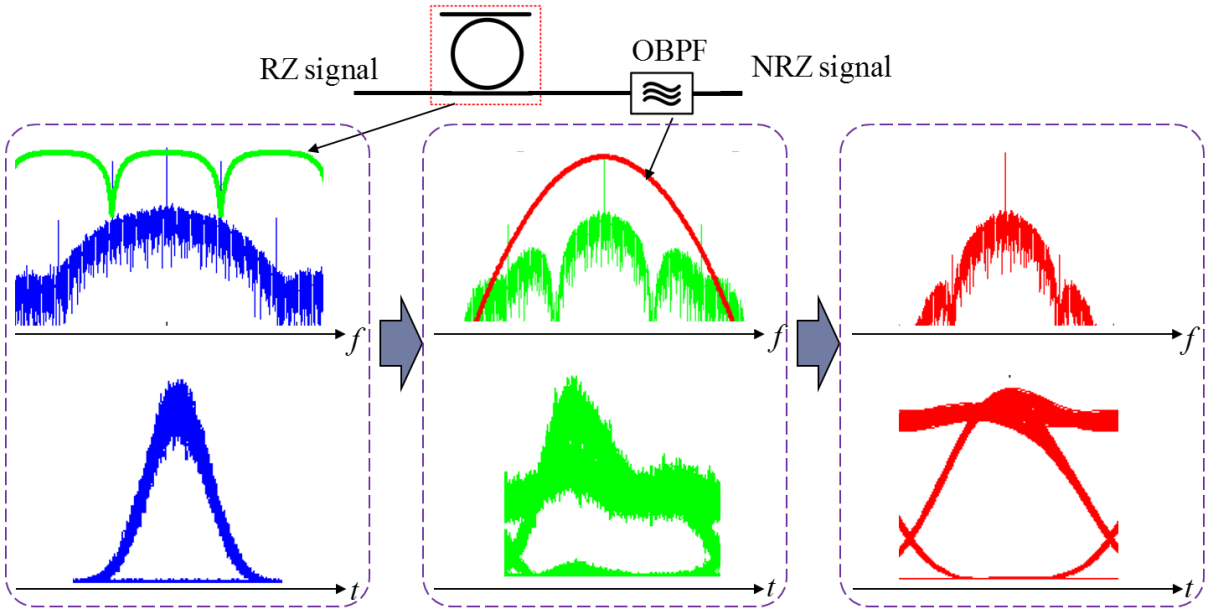

Figure 1.14 – Évolution des spectres (rangée du haut) et des formes d'onde temporelles (rangée du bas) pour la conversion de format de RZ à NRZ basé sur la transformation de spectre optique. *f* : fréquence, *t* : temps.

1.3.3 Méthodes de génération des impulsions optiques picoseconde pour les systèmes optiques à haute vitesse

Les trains d'impulsions optiques picoseconde dans le régime gigahertz (GHz) et au-delà sont d'un intérêt fondamental pour une très large gamme d'applications dans les domaines de communications par fibre optique [111], l'informatique optique [112], la photonique micro-ondes [113], le traitement des matériaux [114], les peignes de fréquences [115], l'optique non linéaire [116] etc. En particulier, dans le cadre des communications optiques, les systèmes OTDM nécessitent des sources optiques impulsionnels stables à taux de répétition élevé qui peuvent agir à la fois, comme une source de données de transmission, et comme une horloge optique utilisée pour synchroniser le signal et en extraire l'information transmise. La synchronisation temporelle est également d'une grande importance dans les processeurs de signaux optiques, y compris les régénérateurs et les circuits logiques [112, 44]. Afin d'assurer la synchronisation dans un circuit optique de traitement du signal, une horloge optique de référence unique, à savoir, un train d'impulsion à taux de répétition élevé, peut être utilisée. Les circuits optiques sont souvent

constitués d'un certain nombre d'opérations rapides, synchronisées les unes aux autres, mais fonctionnant à des vitesses différentes selon la fonction qu'ils remplissent. Les unités de traitement optiques centrales fonctionnent souvent à un taux de référence, tandis que les unités de traitement optique dans les circuits périphériques peuvent fonctionner à des taux sensiblement supérieurs ou inférieurs. Par conséquent, une source d'impulsion optique fiable à haut taux de répétition avec la possibilité de programmer le taux de répétition de quelques GHz à plusieurs centaines de GHz est nécessaire.

Un autre champ d'application potentiel des sources d'impulsions à haute vitesse réside à l'interface entre l'optique et des dispositifs dont le spectre opérationnel se situe dans et au-dessus de la plage des micro-ondes [113]. Pour commencer, certains systèmes électroniques peuvent exiger des taux d'échantillonnage hyperfréquences dans les convertisseurs analogique-numérique [117]. Dans ce cas, les impulsions optiques peuvent être utilisées pour générer une courte rafale d'électrons, qui agissent ensuite comme un train d'impulsions d'échantillonnage dans la gamme sous-THz. L'interface des technologies d'ondes optiques et millimétrique est suffisamment importante pour être considérée comme un domaine séparé, à savoir la photonique micro-onde, pour lequel les trains d'impulsions optiques à taux de répétition élevé sont particulièrement importants.

Parmi un grand nombre de caractéristiques souhaitables d'une source d'impulsions optique à haut taux de répétition utilisée dans les applications mentionnées ci-dessus, on peut inclure la stabilité d'impulsions, la faible gigue temporelle, et les faibles fluctuations d'amplitude, en particulier pour les applications utilisant le train d'impulsions comme référence ou comme signal horloge d'échantillonnage.

Un grand nombre de sources laser d'impulsions courtes à taux de répétition élevé a été démontré à ce jour. Les lasers à fibre ultrarapides offrent une plate-forme immédiate et attractive pour la génération de trains d'impulsions à haut taux de répétition [118]. Dans les premières démonstrations visant à réaliser de sources d'impulsions à taux de répétition élevés, les systèmes laser à verrouillage actif de modes ont été utilisés, avec des taux de répétition démontrés allant jusqu'à ~ 40 GHz. Toutefois, la bande passante des modulateurs et de leurs circuits électroniques de contrôle empêche d'augmenter plus le taux de répétition de ces sources.

Auparavant, diverses approches ont été explorées pour générer des impulsions à haut taux répétition en utilisant des mécanismes qui permettent de surmonter les limitations de bande passante électrique dans lasers à fibres à verrouillage de modes passif et actif [118]. Cependant, bien que des résultats impressionnants aient été démontrés à l'aide de ces approches, elles nécessitent généralement un contrôle précis des propriétés optiques de la cavité laser et elles offrent une flexibilité très limitée de programme ou régler le taux de répétition de sortie. Ceci empêche l'utilisation potentielle de ces systèmes dans une large gamme d'applications qui nécessitent la programmabilité et le contrôle du taux de répétition.

Une méthode alternative d'obtention des impulsions à haut taux de répétition est de multiplier ce dernier de manière toute-optique, en dehors de la cavité laser, en utilisant les techniques de multiplication du taux de répétition d'impulsions (MTRI) [41, 119, 120, 121, 122, 123, 124], comme le montre la Figure 1.14. Dans ces techniques, le facteur de multiplication, *m* est un nombre entier et la forme et la largeur d'impulsion des impulsions individuelles sont conservées dans le processus de multiplication.

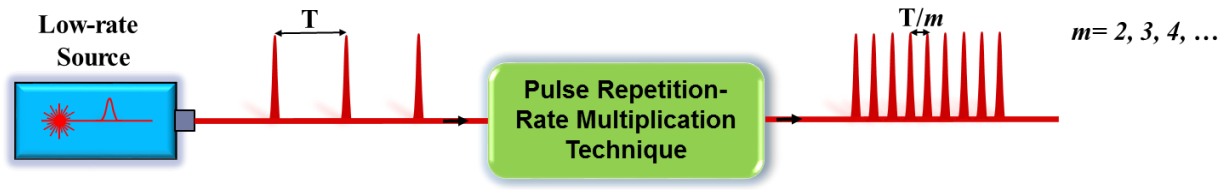

Figure 1.15 – Technique de multiplication du taux de répétition d'impulsions pour augmenter le taux de répétition d'une source laser à faible taux.

En général, les techniques de multiplication du taux de répétition précédemment démontrées peuvent se diviser en deux catégories: Les techniques basées sur le filtrage linéaire d'amplitude spectrale et filtrage linéaire de phase spectrale. Dans cette section, nous présentons les techniques de MTRI les plus pertinentes.

Une technique simple pour multiplier le taux de répétition d'une source à faible taux est l'utilisation des filtres d'amplitude spectrale [119, 125], par découpage du contenu spectral du train d'impulsions d'entrée. Il convient de noter que le train d'impulsions d'entrée est constitué d'impulsions périodiques temporelles avec une période *T*. Dans le domaine de fréquence, il présente des modes spectraux avec un espacement de *F*, où *F* et *T* sont inversement proportionnels

F=1/T. La Figure 1.15(a) montre le spectre de transmission d'un filtre d'amplitude périodique utilisé pour la multiplication du taux de répétition d'impulsions. L'intervalle spectrale libre (ISL) du filtre est réglé sur un multiple entier de l'espacement de modes spectraux du train d'impulsions d'entrée, c.-à-d., T_{out}= T/ m.

Différentes mises en œuvre de cette approche ont été envisagées, comme celle basée sur un étalon de Fabry-Pérot [119], des réseaux de guides d'ondes [126, 121], des interféromètres [127], des réseaux de Bragg à fibre superposés [120], etc. Cependant, ces systèmes exigent un alignement très strict entre les modes spectraux du filtre et ceux de la source d'entrée. Par conséquent, une mise en œuvre très précise d'un tel filtrage doit être effectuée afin d'assurer un train régulier d'impulsions de sortie. Toute erreur dans le trajet optique des longueurs - ou de manière équivalente, dans l'alignement de la période spectrale du filtre par rapport aux modes de source - introduit une gigue temporelle et des fluctuations d'amplitude d'impulsion à impulsion dans le train de sortie. Cette déficience peut représenter une limitation très sérieuse pour les applications utilisant un train d'impulsions comme un signal de référence, étant donné qu'il est en principe beaucoup plus facile de corriger les fluctuations d'amplitude que pour une incertitude temporelle. Par ailleurs, l'un des principaux inconvénients de cette méthode est la perte intrinsèque d'énergie, car seule une fraction du spectre incident reste dans le signal de sortie. L'augmentation du facteur de multiplication conduit à l'élimination de plus de composantes spectrales et, par conséquent, une plus grande perte d'énergie.

D'autre part, les techniques de multiplication du taux de répétition basées sur le filtrage de phase spectrale affectent toutes les composantes spectrales de l'entrée de manière égale en amplitude et aucune des composantes n'est éliminée [41, 120], comme le montre la Figure 1.15 (b); donc, idéalement aucune énergie d'entrée n'est perdue dans ce processus. En particulier, la propagation d'un train d'impulsions à travers un milieu dispersif, caractérisé par une réponse quadratique en phase spectrale, avec une valeur de dispersion bien définie conduit à une multiplication du taux de répétition par effet Talbot temporel. En résumé, une multiplication de m fois du taux de répétition d'un train d'impulsions incident se produit dans un milieu dispersif à condition que la dispersion (ϕ_2, défini comme la pente du retard de groupe en fonction de la fréquence angulaire) et la période d'impulsion temporelle, T, satisfassent la condition suivante [41, 120] :

$$\phi_2 = = \frac{s}{m}\frac{T^2}{2\pi} \tag{1.4}$$

où m et s sont des nombres entiers tels que s/m est un nombre rationnel irréductible. Une explication plus détaillée de cette technique sera fournie dans le Chapitre 2.

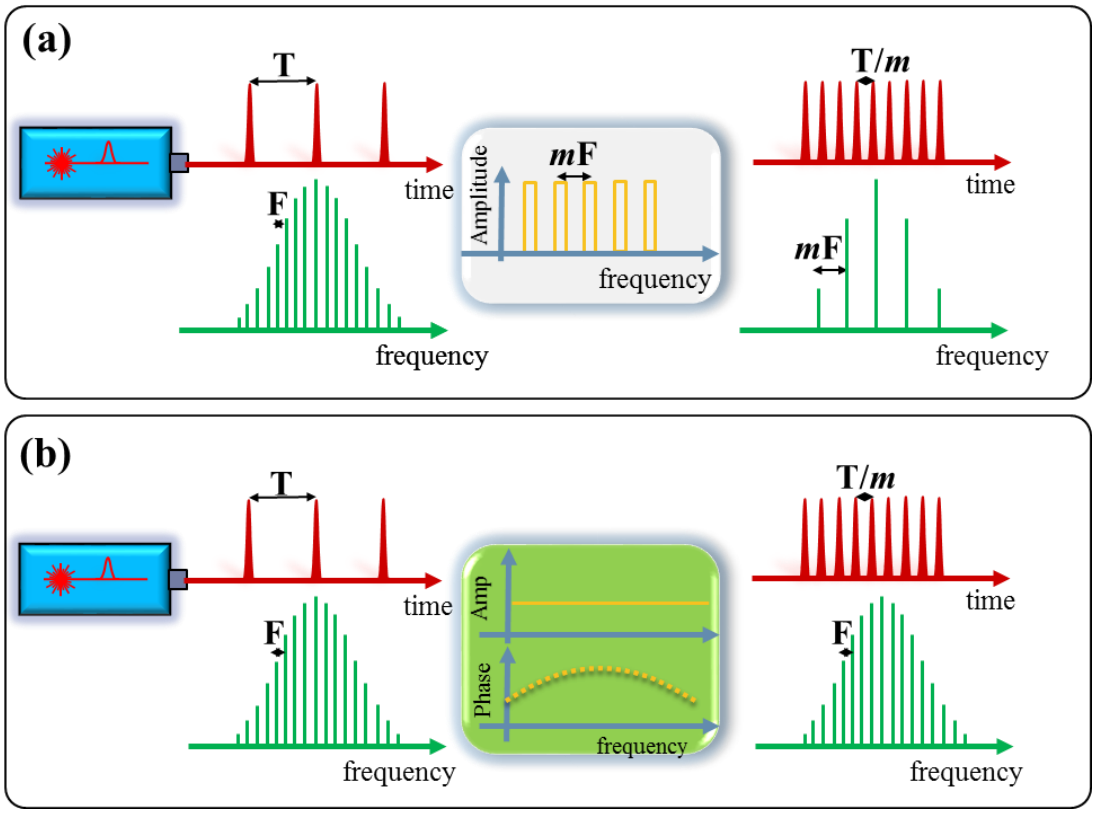

Figure 1.16 – Techniques de multiplication du taux de répétition d'impulsions basé sur le filtrage linéaire (a) d'amplitude spectrale et (b) de phase spectrale.

La multiplication du taux de répétition d'impulsions basée sur l'effet Talbot temporel a attiré beaucoup d'attention au cours des années grâce à sa mise en œuvre simple, avec une complexité sensiblement réduite en comparaison avec les méthodes de filtrage d'amplitude spectrale. Cette approche fournit la copie d'un train d'impulsions optiques entrant avec le taux de répétition multiplié tel que désiré, simplement par un procédé de filtrage de phase spectrale-seule induit par une dispersion appropriée. En outre, cette méthode (i) offre une meilleure efficacité énergétique, car fondamentalement l'énergie est conservée dans le filtrage de phase-seule, (ii) offre des

capacités d'atténuation du bruit de phase et d'amplitude, et (iii) elle est robuste contre les désalignements possibles entre le filtre et la source d'entrée.

Cependant, malgré son ensemble attrayant d'avantages, la technique de MTRI à base d'effet Talbot nécessite l'utilisation d'une quantité dispersion adéquate fixée, pour réaliser un facteur de multiplication donné; une fois que la dispersion est fixé, généralement en utilisant une section d'une fibre dispersive ou un réseau de Bragg à fibre (FBG, pour fiber Bragg grating) à pas variable, il est difficile de régler ou de programmer le facteur de multiplication du taux sans changement importants de la configuration du système (par exemple, en changeant le milieu dispersif). En outre, le procédé est limité à des taux de répétition de sortie qui ne sont que des multiples entiers du taux de répétition initial, c.-à-d., *m* est un nombre entier. Cette même restriction fondamentale s'applique à toutes les méthodes de MTRI publiées à ce jour.

1.4 Objectif et Organisation de la Thèse

La consommation d'énergie, et les problèmes thermiques associés, ont été une préoccupation principale et qui a motivé la plupart des progrès réalisés par l'industrie électronique au cours du dernier demi-siècle. En comparaison, la communauté de recherche de traitement du signal optique a prêté peu d'attention à la question de la consommation d'énergie. Il est souvent avancé que le traitement du signal optique remplacera le traitement du signal numérique en raison de ses capacités de haute vitesse. Toutefois, les arguments simplistes basés sur la vitesse seule manquent souvent le point d'importance critique que les dispositifs optiques sont généralement très gourmands en énergie. À moins qu'il n'y ait une amélioration de plusieurs ordres de grandeur dans l'efficacité énergétique des processeurs optiques, l'électronique est susceptible de rester la technologie de choix pour la grande majorité d'applications de traitement du signal et de commutation dans les réseaux de télécommunication.

Un des objectifs clés de cette thèse est de mettre en évidence l'importance de la consommation d'énergie en tant que mesure de la performance dans le traitement du signal optique et d'essayer de fournir une solution technologique au problème de la consommation d'énergie dans les processeurs optiques pertinents. En particulier, dans cette thèse, nous explorons la possibilité d'utiliser des techniques linéaires passives/actives pour le traitement du signal optique économe en énergie, en évitant l'utilisation de mécanismes optiques classiques actifs et/ou non-linéaires gourmands en énergie; nous choisissons un système de modulation temporelle linéaire actif, à savoir, la modulation électro-optique, qui fournit le mécanisme de modulation temporelle d'un signal optique le plus simple et le plus efficace en énergie (c.-à-d., ayant la plus faible consommation d'énergie). En particulier, nous introduisons de nouveaux concepts et des approches novatrices pour la mise en œuvre des opérations importantes de traitement du signal optique en utilisant une modulation de phase temporelle et/ou le filtrage de phase spectrale qui conservent intrinsèquement toute l'énergie du signal d'entrée sans nécessiter de sources de lumière supplémentaires. Grâce à ces concepts, l'énergie du signal entrant est redistribuée efficacement pour construire le signal de sortie visé, sans perte d'énergie et sans utiliser une puissance optique externe supplémentaire.

Cette dissertation est principalement axée sur le traitement optique de signaux optiques périodiques et apériodiques (données). La Figure 1.17 présente un résumé des fonctionnalités proposées dans ces deux catégories dans mon programme de recherche doctoral.

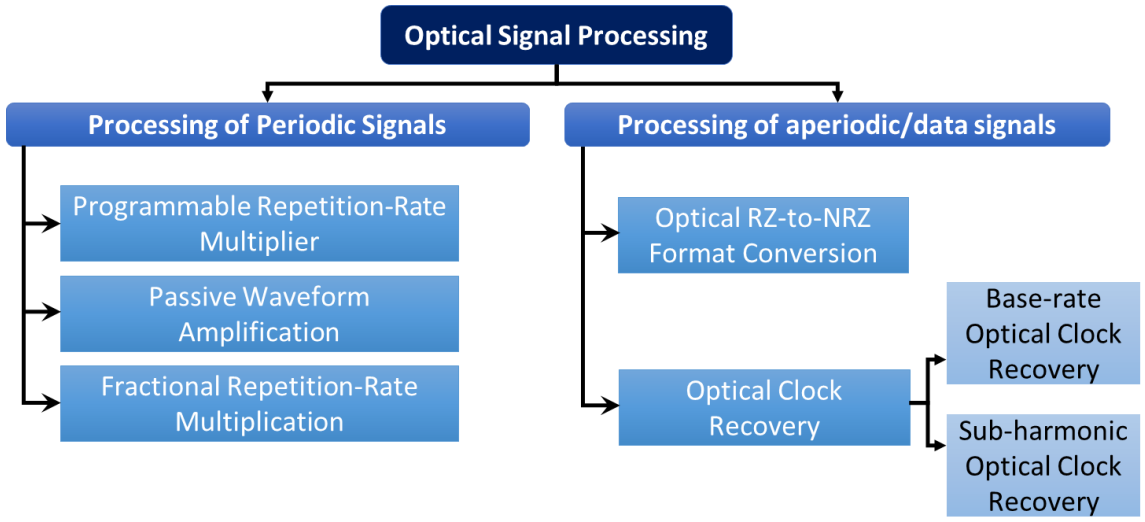

Figure 1.17 – Schéma général des objectifs poursuivis au cours de ce programme de doctorat.

La figure 1.18 montre un exemple d'application des fonctionnalités étudiées dans le contexte d'un routeur optique. Le paquet de données d'entrée, constitué des données réelles (charge utile) et des informations de destination du paquet (en-tête), est la première horloge récupérée; L'en-tête est ensuite extrait à l'aide de l'horloge récupérée. L'en-tête extrait est traité dans l'unité de traitement optique pour trouver l'itinéraire de destination et aussi pour créer un nouvel en-tête. Ensuite, le nouveau paquet généré, y compris la charge utile et le nouvel en-tête, est dirigé vers la destination appropriée par un commutateur optique. Les trois fonctionnalités étudiées dans cette dissertation sont (i) une source d'impulsions optiques polyvalente et économe en énergie, utilisée dans les unités de traitement optique et de génération d'en-tête, (ii) l'unité de récupération d'horloge optique et (iii) l'unité de conversion de format.

Donc, tout d’ abord, nous démontrons un système fiable et économe en énergie pour générer des impulsions picosecondes avec une programmabilité et un degré de contrôle du taux de répétition sans précédents. Ce système emploie une combinaison de modulation temporelle phase-seule et les processus de filtrage spectral (par exemple, la dispersion de vitesse de groupe). En outre, cette thèse propose des méthodes de filtrage de phase spectrale pour effectuer deux

opérations de base de traitement du signal dans le contexte des communications optiques: la récupération des signaux d'horloge sous-harmonique et de base à partir des signaux de données, et la conversion de format optique RZ à NRZ.

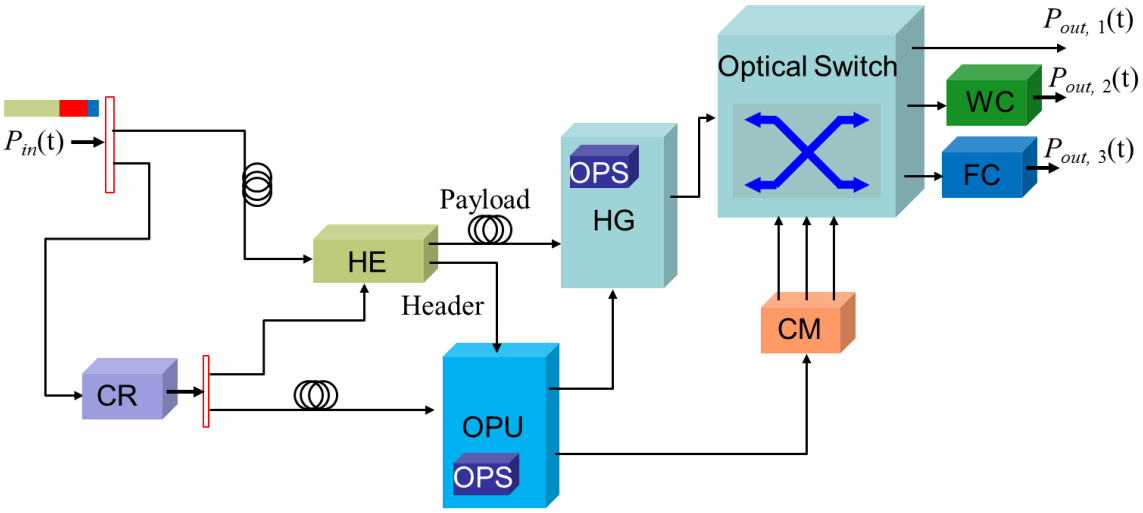

Figure 1.18 – Exemple d'architecture d'un routeur optique []. CR: Récupération d'horloge, HE: Extraction d'en-tête, OPS: Source d'impulsions optiques, OPU: Unité de traitement optique, HG: Génération d'en-tête, CM: Module de commande, FC: Conversion de format. Extrait de [128, 129, 130, 105].

Chaque chapitre de cette thèse est centré sur une réalisation différente de ce travail de recherche doctorale. Le **Chapitre 2** fournit une introduction complète à l'effet Talbot temporel, où la description analytique de la méthode et de ses propriétés fondamentales sont discutées. La combinaison de la modulation de phase temporelle avec l'effet d'auto-imagerie temporelle (effet Talbot) c.-à-d., filtrage de phase spectrale, est employée pour la mise en œuvre de nouvelles fonctionnalités de traitement des trains de formes d'onde arbitraires et périodique (par exemple, des impulsions). L' application d'un profil de phase prédéterminé de modulation temporelle à un train d'entrée d'impulsions périodiques produit de nouvelles composantes de fréquence, ensuite l'effet d'auto-imagerie temporelle induite par dispersion redistribue temporellement le nouveau spectre pour produire le signal de sortie ciblé. En fonction de la modulation de phase prédéterminée et la quantité de dispersion utilisée, plusieurs types de manipulations de signaux peuvent être réalisés à la sortie du système, pour répondre aux exigences de différentes applications. En particulier, en utilisant des combinaisons appropriées de filtrage temporel et spectral linéaires,

nous allons montrer (i) une technique ***programmable*** de multiplication de taux répétition, où le taux de répétition de sortie peut être programmée électriquement pour être un multiple entier du taux de répétition d'entrée; (ii) une technique ***fractionnaire*** de multiplication de taux de répétition, où le taux de répétition du signal de sortie peut être ajusté pour être un multiple fractionnaire du taux de répétition du signal d'entrée; (iii) des mécanismes de ***division*** de taux de répétition avec conservation de l'énergie d'entrée, et produisant donc, une amplification passive de chaque forme d'onde individuelle sans distorsions, c.-à-d., un amplificateur de forme d'onde passive sans utilisation de gain actif.

Le **Chapitre 3** introduit de nouveaux concepts et technologies de traitement de signaux économes en énergie pour les signaux de données optiques. A cette fin, nous définissons, concevons et développons deux ensembles pertinents de processeurs: (i) Une nouvelle approche toute-optique de conversion de format de données de télécommunication retour-à-zéro (RZ) -à-non-RZ (NRZ), qui a été expérimentalement mise en œuvre avec un débit de 640 Gbit/s. Dans cette approche, nous montrons comment une manipulation adéquate de phase-seule des composantes fréquentielles d'un signal de données RZ peut être utilisée pour réaliser la conversion vers le signal NRZ équivalent. (ii) de nouvelles approches pour la récupération des signaux d'horloge de base et sous-harmonique à partir de signaux de données tout ou rien (OOK). Le premier de ces deux processeurs est réalisé en utilisant le filtrage optique linéaire de phase-seule du signal RZ d'entrée, alors que le deuxième exploite l'effet appelé 'auto-imagerie inverse '.

Le **Chapitre 4** résume les travaux présentés dans cette thèse et propose des perspectives potentielles pour les travaux futurs.

Chapter 1

Introduction

The transition of signal processing from electronics to optics in optical telecommunication networks is described. Paramount practical concerns of present optical signal processors and potential solutions are identified. Next, through an overview of optical signal processing technologies, the foundation for this Thesis is established. The various contributions described in the Thesis are presented and the structure of the Thesis is outlined.

1.1 Signal processing: Transition from electronics to optics?

Since the invention of "dielectric waveguides" in 1966 by Charles Kao and George Hockham of Standard Telephone Cables (STC) Ltd. in Harlow of England [1], optical fiber communication systems have used lightwaves as carriers to transmit information from one place to the other. The distance of a few meters in laboratory was increased to a few kilometers, to hundreds of kilometers, and now thousands of kilometers in the first decade of this century with bit rates reaching from few tens of Mbit/s in late 1960s to 100 Gbit/s and tens of Tbit/s at present [2]. Tremendous progress has been made through nearly the last 55 years due to significant advancements in (i) modulation and detection techniques, so that the data bit rate of the early-stage communication systems, i.e. 100 Mb/s (1980), has been gradually increased to 40Gbit/s at a single wavelength, (ii) the transmission technologies and hardware components, including multiplexing techniques such as dense wavelength division multiplexing (DWDM)[9], optical time-division multiplexing (OTDM)[10], optical orthogonal frequency-division multiplexing (OFDM)[11], ultimately enabled by the

[9] DWDM is an optical multiplexing technology for combining and transmitting multiple optical signals simultaneously at different wavelengths on the same optical single-mode fiber.
[10] OTDM is an optical multiplexing technology for combining and transmitting multiple optical signals at the same wavelength on the same single-mode fiber. The signals are temporally multiplexed, and each signal appears on the transmission line only a fraction of time in an alternating pattern.
[11] Optical OFDM is a frequency division multiplexing technology. In contrast to WDM, optical OFDM subcarriers overlap each other significantly and therefore has a higher spectral efficiency.

development of the erbium-doped fiber amplifier (EDFA), fiber Raman optical amplifier (ROA), optical parametric amplifier, etc. The progress of long-haul transmission capacity versus time is depicted in Figure 1.1, with transmission distance reaching several thousands of kilometers along a single mode fiber (SMF). After the invention of EDFAs and dispersion management techniques, to overcome the optical attenuation and dispersion of the transmission media, the transmission capacity reached to 10 Gbits/s in 1990. Thereafter, the transmission capacity has been further increased with multiplexing of several wavelength channels in the C-band as well as L- and S-bands. With gain equalization, the total capacity was able to reach 40–100 Gbit/s in 1995 [2]. The exploitation of spectral efficiency would then be enhanced with further R&D and experimental demonstrations by deploying channels over the entire C-band and then over the L- and S-bands using hybrid amplifiers (EDFA+ROA) to reach 2 Tbit/s at the turn of this century.

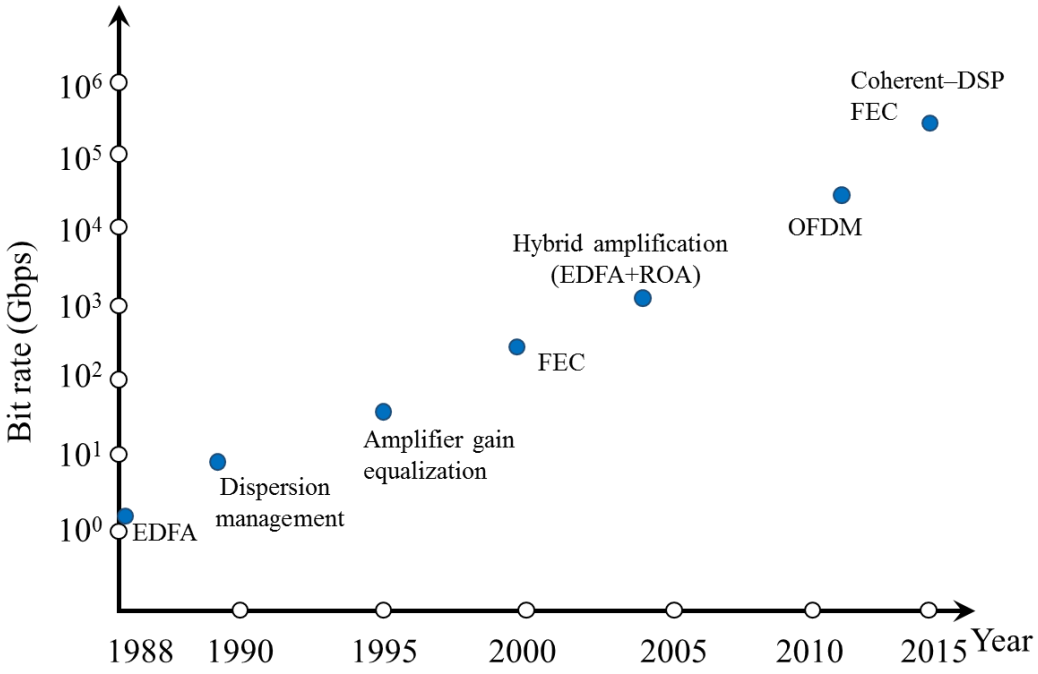

Figure 1.1 – Experimentally demonstrated single-mode, single-fiber transmission capacity. Data has been compiled from [2].

Over the first fifteen years of this century, we have witnessed further progresses to push the transmission capacity limit with DWDM, OTDM and OFDM. This is demonstrated by reports of 10.2 Tbit/s data transmission on a single wavelength [3], 26 Tbit/s using optical OFDM [4] and 14 Tbit/s (111 Gbit/s × 140 wavelength channel) in a WDM link [5]. Due to such enormous

transmission capacity, since the turn of the twenty first century, fiber optic-based systems have largely replaced radio transmitter systems for long-haul telecommunication data transmission. They have revolutionized long-distance phone calls, cable TV and, more importantly, the Internet. The establishment of the fiber-optic based Internet has led to a worldwide communications' medium for the entire spectrum of communication modes, namely data, voice and video, both real-time and non real-time content. The net is made up of large mesh of electronic routers and switches interconnected through high capacity optical fiber networks.

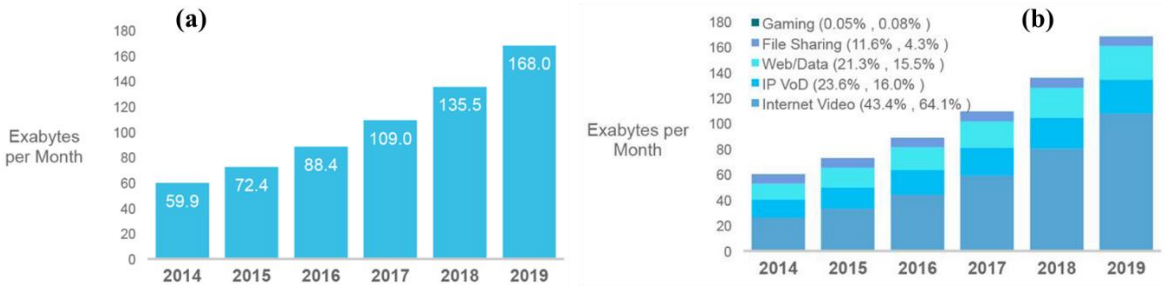

Figure 1.2 – (a) Projected growth in monthly Internet traffic 2014-2019, (b) projected service distribution 2014-2019 (Exabytes/month) [6].

The Internet infrastructure has been growing substantially to accommodate an increasing number of users, and higher bandwidth requirements arising from new, more demanding Internet services and applications. In particular, the increasing popularity of bandwidth intensive (high-bandwidth-consuming) services such as Internet-based video streaming (Netflix, YouTube, Internet protocol television (IPTV)), video telephony (Skype, FaceTime, Google Hangouts), high-quality online gaming (League of legends, Counter-strike, Fallout) and Cloud-based services have led to a relentless rise in Internet traffic over the past decade - a trend which is likely to continue for years to come. According to the Cisco Visual Networking Index (CVNI), global Internet traffic has increased more than four-fold in the past five years and is expected to increase threefold over the next five years (see Figure 1.2(a)) [6]. Among other services, video services will dominate the growth in Internet traffic, predicted by CVNI (Figure 1.2(b)). The Internet traffic is expected to grow to 168 exabytes per month by 2019, up from 59.9 exabytes per month in 2014, Figure 1.2(a). To appreciate the magnitude of Internet traffic volumes, it helps to put the numbers in more familiar terms: by 2019, Internet traffic globally will reach 518 terabits per second (Tbit/s) in 2019.

This is the equivalent of 191 million people streaming Internet high-definition (HD) video simultaneously, all day, every day, or equivalent to 42 billion DVDs per month.

The aforementioned capacity provided by optical transport technologies has continued to keep ahead of the Internet traffic demand, and access to the required transmission capacity for the next coming years is not far from realization. However, transmission capacity does not form the whole picture in the communication networks. As mentioned above, the Internet and, in general, a communication network basically has two functionalities: transmission and routing/switching [7]. Information in the form of bits is sent from an origin to a final destination through transmission channels via many intermediate network nodes. At these nodes, the switching takes place so as to route the bits from the origin to the destination along a prescribed pathway. The routing and switching itself can be implemented in either the electrical or the optical domain. Switching in the electrical domain is very efficient and the technology is mature. To date, the combination of optical transmission and electrical routing works very well, as evidenced by the fact that so far in most of the commercial networks, the information is transmitted in the optical domain and routed in the electrical domain. However, the routing/switching in the electrical domain is experiencing greatly increased pressure from the above-mentioned ever-increasing transmission capacity in optical fibers.

Therefore, there is serious concern that the ultimate achievable capacity of the networks will eventually be limited by so-called "bandwidth bottlenecks" in electronic routers, i.e. the bandwidth imbalance between the optical transmissions and electronic routers [8, 9]. A router is composed by many signal processing units and the overall capacity of the router depends on the speed of the individual signal processing units [10]. Although the clock speed of the electronic signal processing units for information processing increased linearly until a couple of years ago, it now seems to be running out of steam, as shown in Figure 1.3. Also of concern is the large power consumption and heat dissipation associated with the processing of data in electronic processors in the routers, which is likely to become even more problematic as routers become even larger. The situation becomes even worse when there are many wavelength channels in one optical fiber, as is common in today's DWDM networks, because a large number of optical receivers for optical to electronic conversion (O/E conversion), modulators and lasers for electronic to optical conversion (E/O conversion) will be required at each network nodes to interface electronic

processing circuits to the optical transmission medium, resulting in a prohibitively expensive network. The Cisco CRS-1 router with up to 92 Tbit/s switch capacity (72 line card shelves, 400 Gbit/s line cards in one shelf) occupies 100m^2 space, consumes 1 MW of power and weighs 60 Ton[12].

Currently, electronic technologies are keeping up with the bandwidth demands using extensive parallelism [11, 12], where the number of components and their combined power consumption, simply scale with the bandwidth. Presently, in the developed countries, the total energy consumed by the Internet's infrastructure accounts for 2-3% of the overall worldwide energy consumption [13] and the associated contribution to the global CO_2 emissions [14, 15]. This share will only keep increasing with serious consequences for the economy and the environment. This raises the issue of whether Internet growth may ultimately be constrained by energy consumption rather than by bandwidth! [16].

A number of solutions have been proposed to address bandwidth and power consumption problems in electronic signal processing in routers, and in general, in any digital computing device. In particular, three decades ago, researchers and developers suggested that a move to optical signal processing technologies will greatly alleviate the bandwidth imbalance, in which optical signals are processed and routed in the optical domain [17]. The claimed advantages include (i) higher bandwidths due to the inherent broadband nature of optics beyond the capabilities of electronics, and (ii) compatibility with the general idea of all-optical networking, in which data pass transparently through the network from source to destination in optical form without undergoing any O/E or E/O conversions, allowing lower power consumption, eventually reducing the cost [18].

Optical signal processing primary nurtured big hopes as a platform faster than electronics to carry out operations. However, today, some disillusion has replaced the early enthusiasm and in the last ten years, this proposition has had increasing sceptics inside the optical community itself. Indeed, the available speed of optical components massively outperforms the state of the art in electronics, with potential processing speeds well above the THz regime. In Figure 1.3, the clock rate of optical signal processing devices is compared with the rate of electronic processors.

[12] http://www.cisco.com/en/US/products/ps5763/index.html

However, in the quest for blazing processing speeds, many optical researchers have ignored the fundamental problem of energy consumption of optical processors.

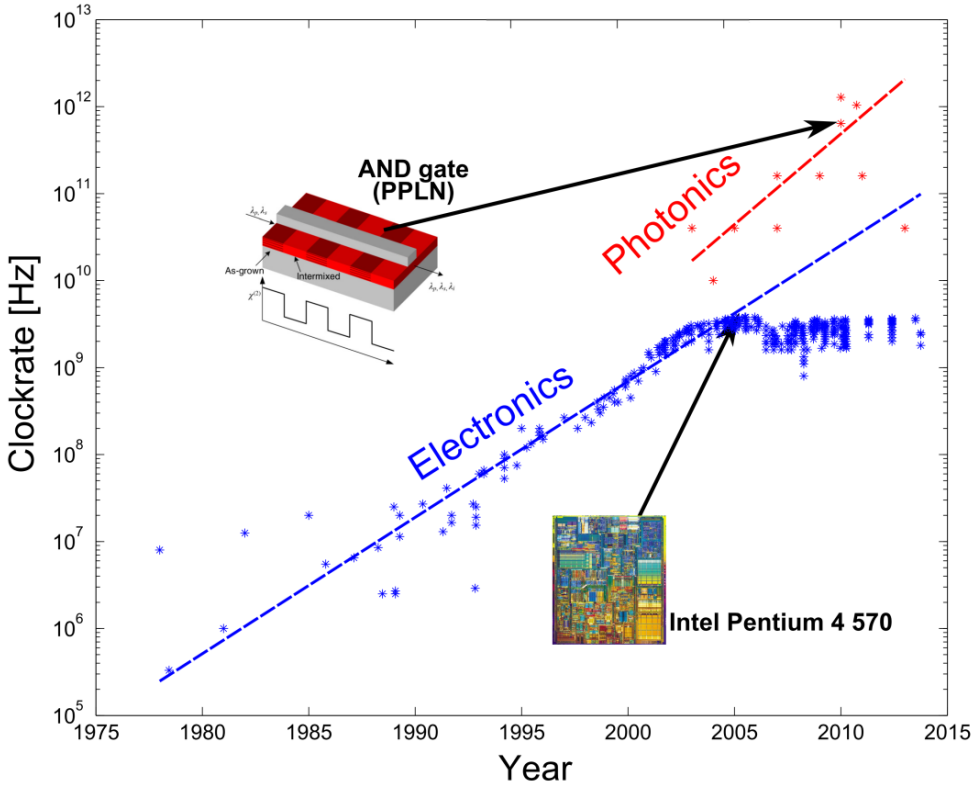

Figure 1.3 – Evolution of electronic and photonic signal processing technologies capacity [19].

Though optical technology allows for speeds much faster than the best electronics, the power required for most proposed optical processors is approximately three orders of magnitude higher than their electronic counterparts [8], see Figure 1.4. As it is, the solutions proposed for optical platforms are much more impractical from an energy-consumption viewpoint than current state-of-the-art electronics. This drawback is partly responsible for what is now referred to as the "photonic bottleneck" [20].

High energy consumption is largely attributed to the fact that optical signal processors typically use nonlinear effects to perform an operation [8]. But, optics is just the opposite, it is a field of very linear behaviour. Due to their bosonic nature, photons have extremely low interaction with matter, their strength is of order 137 (for $\chi^{(2)}$, second-order nonlinearity) and 137^2 (for $\chi^{(3)}$, third-order nonlinearity) weaker than the electronic interaction [20], and therefore high power signals are consumed to excite the nonlinear interactions [21].

The majority of this power is then wasted after the signal processing operation; the power consumption issue in nonlinear interactions will be described in detail later in this Chapter, in Section 1.2.1. Therefore, the inherent weakness of optical interactions and the difficulty of cascading nonlinear optical nodes, requiring optical amplification after each node, make most complex architectures impractical. Figure 1.4 shows the energy-consumption comparison of electronic transistors and optical devices based on conventional nonlinear mechanisms over the decades [8]. The upper curve (broken lines) shows the data calculated for a variety of optical devices.

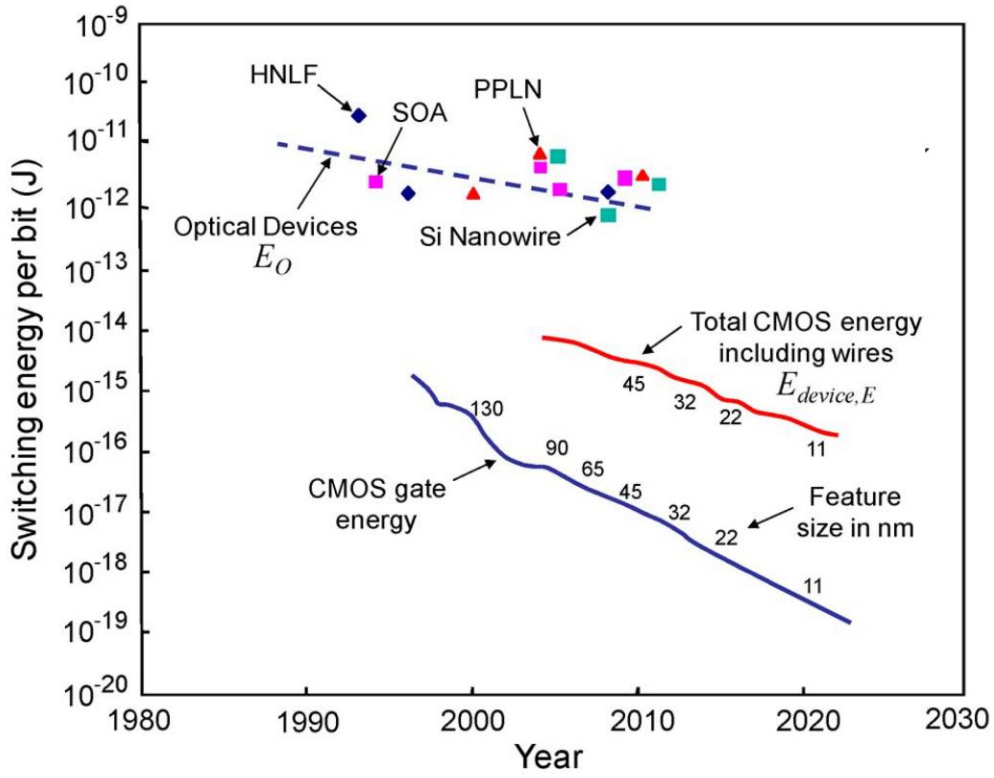

Figure 1.4 – Device energies per bit against time [8]. SOA: semiconductor optical amplifier, HNLF: highly nonlinear fiber, PPLN: periodically poled lithium niobate, COMS: complementary metal–oxide–semiconductor.

It is then still an open question for research to explore, from the present and the medium term evolution of the state-of-art in photonics, how optical signal processing might become competitive with electronics. Six years ago, David Miller and Rod Tucker presented separately well-argued discussions on the requirements for practical optical digital processors that could compete with

and surpass electronic devices [22, 23]. Unless, optical signal processors being at least as fast as and more energy-efficient than their electronic counterparts, to the 10 fJ/bit level, are developed, electronic technologies are likely to remain the technology of choice for the vast majority of signal processors [23]. This may suggest that at least in the near future, optics will not become an alternative to electronics in processing and computing.

However, despite this less hopeful outlook for optics in signal processing, some researchers have remained optimistic. They argue that many advantages of optics in signal processing cannot be overlooked and instead of abandoning it, new research should be conducted to resolve the problems. Hence, for optical signal processing technologies to become a solid alternative to electronics in information processing, switching and computing platforms, there is a strong need for ground-breaking developments in optical science enabling novel breakthrough technologies that will allow for increased capacity with a greatly reduced energy consumption. Indeed, optical signal processing has been revisited during the last several years by addressing the remaining limitations and (re)introducing (old)new optical signal processing techniques [24, 25, 26, 11, 27, 28, 29]. To this purpose, many approaches are being currently investigated for the possibility of developing energy-efficienct optical signal processors. In particular, some research groups are exploiting new optical waveguides with stronger nonlinearities to achieve a desired operation with lower energy consumption [11, 30, 31, 32, 33]. Many researchers also believe that all-optical processors may not be the most prudent goal [24, 34, 35, 36]. Instead, a hybrid approach, which harvest the benefits from both electronics and optics to globally benefit from what is possible with electronics and what is possible with optics, should be utilized. In addition, researchers are now exploring the possibility of using purely passive and linear techniques for optical signal processing [26, 25, 37, 38, 39, 40, 41], avoiding the use of conventional active and/or nonlinear mechanisms in the signal-processing engines, potentially reducing the energy consumption significantly. In line with these latest attempts, this Thesis deals with novel optical signal processing designs capable of providing ultra-low-energy consumption. We have demonstrated energy efficient schemes, comprising temporal and/or spectral phase manipulation of optical signals, for performing several basic signal processing operations in the context of optical communications.

In this Chapter, we will first review the basis of optical signal processing technologies with an emphasis on their energy-consumption performance. Finally, we conclude this introductory

Chapter with an outline of the state-of-the-art of a particular set of optical signal processing functionalities of high relevance for this dissertation.

1.2 Optical signal processing and energy consumption

Optical signal processing is an enabling technology that encompasses the fundamental theory, applications, algorithms, and implementations of processing or transferring information encoded in a traveling light wave across the time and/or space domains — the optical signal. The main focus of this Thesis is on time-domain optical signal processing, which is of great interest and use in communication and computing systems.

Temporal optical signal processing has been under active investigation for many years, bringing together various fields of optics and signal processing—namely, linear/nonlinear devices and processes, the analog and digital signals—to achieve high-speed signal processing functions that can potentially operate at the line rate of fiber optic communications. In particular, temporal optical signal processing can generally be classified into two main categories: linear and nonlinear signal processing, depending on whether they make use of optical nonlinear effects to perform signal processing.

Within the context of optical signal processing, linear optical signal processing uses a rich theoretical framework based on the early linear system theory and Fourier transforms, used extensively in optics for the description of diffraction and spatial filtering. Linear signal processors perform the target functionality on the input optical signal by deflecting, delaying and filtering the signal but the frequency is unchanged and the fundamental principle of superposition holds. Practice has shown that linear systems/processes emerge in a broad range of applications. In contrast, nonlinear optics, known as the optics of intense light, is employed in optical processors that require one or several optical beams to interact with each other without interference [42]. The optical beams affect amplitude, phase, wavelength and polarization features of themselves or each other's as they propagate through the nonlinear medium and correspondingly, the superposition principle is not valid.

There are many functionalities that are intrinsically nonlinear and we need a nonlinear mechanisms to perform the related signal processing, such as wavelength conversion and regeneration. However, there is a large number of functionalities that are either intrinsically linear,

such as differentiation and integration, or we can find ways to do them with linear mechanisms, such as clock recovery, format conversion and logic gates, as depicted in the tree view in Figure 1.5.

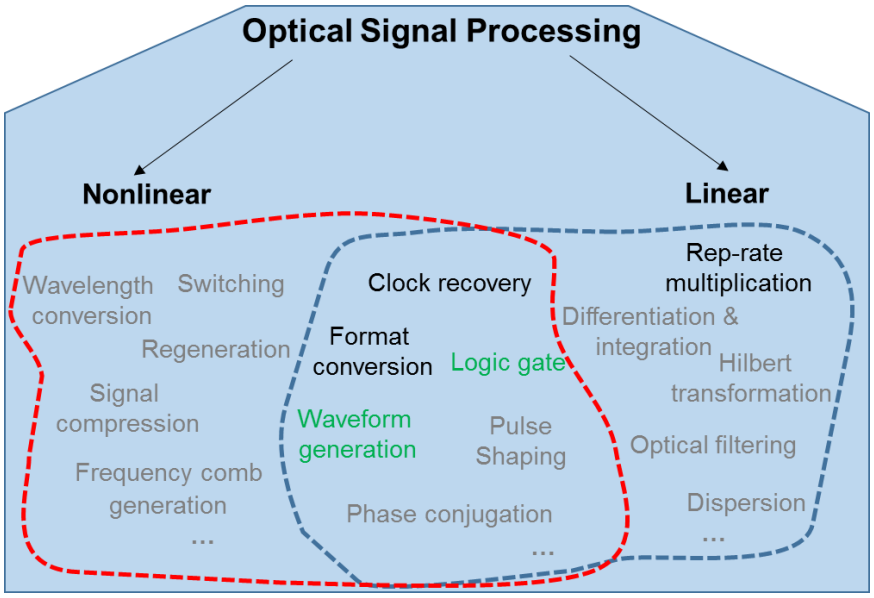

Figure 1.5 – Linear and nonlinear optical signal processing applications [43, 44, 45, 46, 47, 48, 49]. Topics in solid black are addressed in this work and the topics in solid green are the plan for future work.

A brief review of both nonlinear and linear optical signal processors is presented in the following Sections with an emphasis on their energy-consumption performance. We conclude that in order to reduce the overall energy cost of an optical system, it is required to avoid using energy-hungry nonlinear mechanisms; whenever possible, the specific target functionality should be carried out by energy-efficient linear mechanisms.

1.2.1 Nonlinear optical signal processing

Most optical phenomena observed in everyday life fall under the category of linear optics which explains common effects such as diffraction, refraction and, interference. However, at high intensities, complex interactions can occur which are described by the theory of nonlinear optics [50, 42, 51]. To be more concrete, nonlinear optics is the study of complex interactions that occur as a consequence of the modification of the optical properties of a material system by the presence

of an intense light. The light intensity levels that are required to observe optical nonlinear effects are so high that they can usually not be observed in everyday life phenomena, and only can be provided when using intense continuous-wave and pulsed lasers.

In a dielectric propagation medium, linear and nonlinear interactions with light can be understood as an interaction between the light field and the atoms and molecules constituting the medium. Materials are made up of atoms comprising charged particles (i.e. positive ions and electrons) that are affected by the electric and magnetic fields. Dielectric materials have a neutral charge distribution at a macroscopic scale and comprise an equal number of positive and negative charges (positive ions and electrons) at the atomic scale. An incoming oscillating electric field $E(t)$ displaces the charges and exerts a separating action between the positive and negative charges (dipole moment), changing the dipole moment per unit volume, or polarization $P(t)$, of the material (t is time variable). Notice that at visible/near-infrared frequencies, the electric field $E(t)$ interacts with dielectric materials mainly through negative charges (electrons). As long as the perturbation of the initial trajectory of the charges is small, the displacement induced is linearly proportional to the amplitude of the excitation field, $E(t)$, described by

$$P(t) = \epsilon_0 \chi^{(1)} E(t) \tag{1.1}$$

where the constant of proportionality $\chi^{(1)}$ is known as the linear susceptibility and ε_0 is the permittivity of free space. Stronger deformations of the charge distributions may lead to break this proportional relationship and the optical response, polarization $P(t)$, is then expressed by a power series in the field strength $E(t)$ as

$$P(t) = \epsilon_0 [\chi^{(1)} E(t) + \chi^{(2)} E^2(t) + \chi^{(3)} E^3(t) + \ldots] \tag{1.2}$$

The quantities $\chi^{(2)}$ and $\chi^{(3)}$ are known as the second- and third-order nonlinear optical susceptibilities, respectively. For simplicity, we have taken the fields $P(t)$ and $E(t)$ to be scalar quantities. We have also assumed that the polarization at time t depends only on the instantaneous value of the electric field strength, implying (through the Kramers–Kronig relations) that the medium must be lossless and dispersionless. We refer to $P^{(2)}(t) = \epsilon_0 \chi^{(2)} E^2(t)$ as the second-order nonlinear polarization and to $P^{(3)}(t) = \epsilon_0 \chi^{(3)} E^3(t)$ as the third-order nonlinear polarization. Second-order nonlinear optical interactions can occur only in noncentrosymmetric crystals such as Quartz

and lithium niobate ($LiNbO_3$) —that is, in crystals that do not display inversion symmetry. Since liquids, gases, amorphous solids (such as glass), and even many crystals display inversion symmetry, $\chi^{(2)}$ vanishes identically for such media, and consequently such materials cannot produce second-order nonlinear optical interactions. On the other hand, third-order nonlinear optical interactions (i.e., those described by a $\chi^{(3)}$ susceptibility) can occur in centrosymmetric media.

Nowadays, the application of nonlinear optics in the framework of information science has two main motivations. Nonlinear effects are required for creating a substrate for processing optical signals, whereas on the other hand, they cause detrimental distortions to long haul fibre optic communication signals. Therefore, for signal processing applications, we require a propagation medium with higher nonlinear effects to facilitate optical signal processing with lower cost in energy. In sharp contrast, for optical signal transmission, one is interested in minimizing the effect of nonlinearities of the propagation medium to increase transmission capacity. In the context of optical signal processing, optical techniques employ a wide range of devices with various nonlinear mechanisms to achieve multiple network functionalities. Several all-optical processing technologies of significant interest are

- Semiconductor Optical Amplifiers (SOA) using $\chi^{(3)}$ to excite cross-gain modulation (XGM), self-phase modulation (SPM), cross phase modulation (XPM), and four-wave-mixing (FWM) nonlinear effects [52, 53].
- Highly Nonlinear Fibers (HNLF) [54, 55, 56, 57] or other waveguides (Chalcogenide glass [58], silicon-on-insulator (SOI) [59], and III-V semiconductor [60, 61]) using $\chi^{(3)}$ to excite SPM, XPM, FWM nonlinear effects.
- Periodically Poled Lithium Niobate (PPLN) using $\chi^{(2)}$ to excite three wave mixing (TWM) nonlinear effect [62, 63, 64].

All these platforms have been largely exploited, allowing to implement all-optical logic gates [55], wavelength conversion [43], regeneration [44], frequency comb generation [45], etc. They exhibit picosecond and sub-picosecond optical responses and therefore, potentially can construct optical devices with a much faster dynamic than current electronic devices. But there is much more to obtaining reliable high capacity optical systems than just high speed devices. The energy consumption of the device is at least as important [8]. Because high intensity lights are required to

stimulate the nonlinear effects, the devices constructed by nonlinear media consume significant amount of energy. To reach a better understanding of the basic mechanisms behind energy consumption in the nonlinear optical devices, we need to consider energy transformation processes at the device or circuit level. Figure 1.6 shows a simple block diagram of an optical signal processing device or circuit based on nonlinear mechanisms. The circuit is composed of a nonlinear medium, such as SOAs, HNLFs or PPLNs. Typically, the device or the circuit will have two or more signal inputs (Figure 1.6 shows all inputs as the input information) and one or more signal outputs (Figure 1.6 shows all outputs as the output information). Also shown in Figure 1.6 is a power supply input, a key requirement in all nonlinear circuits, which can be an electrical current or an optical pump depending on the used nonlinear medium. Relatively high power is supplied to the circuit to excite a nonlinear interaction, i.e., to activate and deactivate the nonlinear medium for a processing operation. The total power P_T consumed by a device or a circuit to process the input information is the sum of the input powers P_{in} at the input and the supply power P_s minus the output signal power, P_{out} [65]:

$$P_T = P_{in} + P_s - P_{out} \tag{1.3}$$

The total energy consumed by the nonlinear circuit, E_T, is simply the total power multiplied by the bit period τ_b (the time between two consecutive operations) $E_T = P_T \tau_b = (P_{in} + P_s - P_{out}) \tau_b$.

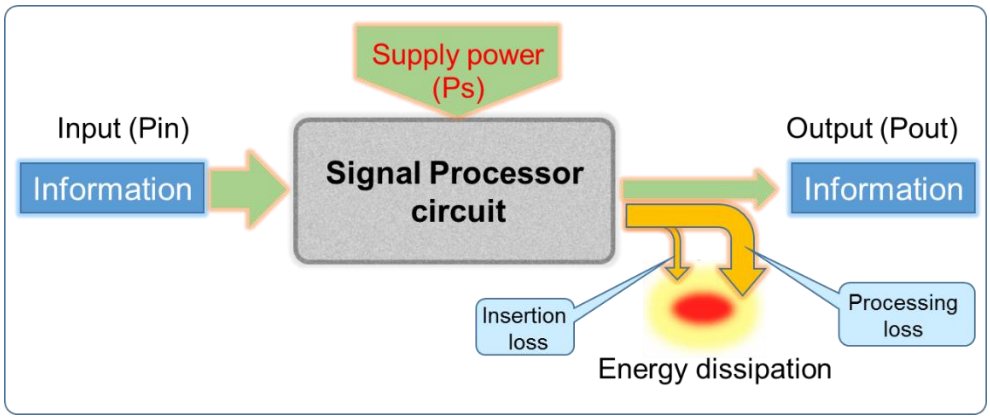

Figure 1.6 – Block diagram of the flow of energy in an optical signal processing circuit based on nonlinear mechanisms.

Because photons have relatively low interaction with matter, high energy needs to be supplied (large P_{in}+ P_s) to a nonlinear processor to excite a nonlinear interaction for processing [8]. In

addition to this large energy cost required to process the information, there are energy losses, leading typically to heat generation. These are processing-energy loss and insertion loss [8]. Processing-energy loss comes from weak conversion of the input and supplied fields, $P_{in} + P_s$, into the correct output information P_{out}. Because of light's low interaction with matter, most of the power in both the input and supplied fields, $P_{in} + P_s$, actually passes through the circuit unused, and converted into heat, resulting in a small P_{out} ($P_{in} + P_s >> P_{out}$ means large E_T). Insertion loss comes from the absorption and diffraction (spreading) of light when it propagates through the circuit, just as any optical device cannot pass 100 percent of a lightwave. Additionally, optical signal processing, in general, based on nonlinear interactions require continuous supply of energy, regardless of whether that device is performing a processing operation or not [8].

In addition to energy concerns, the high degree of control required on the characteristics of the input signals (e.g., power, central frequency, state of polarization, etc.) involved in a nonlinear processing operation has hindered application of nonlinear optical signal processing beyond a well-controlled laboratory environment. An additional drawback of nonlinear optical techniques is that highly nonlinear fibers or waveguides with customized dispersion profiles are needed for an efficient processing, making the system costly. Moreover, the implementation of more complex systems relying on the concatenation of two or more nonlinear optical signal processors may notably degrade the information signal's quality. This degradation might be caused by the reduction of the signal-to-noise ratio (associated to the low energy efficiency of these processors and the requirement of amplification stages), and/or by the inclusion of spurious frequency components in the bandwidth of the information signal.

1.2.2 Linear optical signal processing

Linear systems can be used to model and analyze a wide range of problems in science and engineering. In particular, linear optical filters, which occupy a position of fundamental importance in spatial and temporal optics have been studied extensively [41, 66, 67]. Linear optical signal processing is founded in the rich theory of linear systems and in many applications, linear processing methods prove to be optimal; two examples will be shown in Section 1.3. Moreover, linear methods are inherently simple to implement, perhaps the dominant reason for their widespread use in practice.

A processor is said to be linear if the transfer function, i.e. $y = f(x)$, the function defining the relationship between the input and output signals (x and y respectively), satisfies the principle of superposition, such that $f(x_1+x_2)=f(x_1)+f(x_2)$ and $f(n\,x) = n\,f(x)$ [68]. That is, if an input to the system consists of a weighted sum of several signals, the output of the system is the weighted sum (or superposition) of the responses for each of the signals. The superposition property makes linear systems easy to analyse, as it is possible to break down any linear signal into simple components and analyse these separately.

If the parameters of the transfer function of the linear system are constant over the time of interest, the signal processing operation is said to be time invariant [68]. A time shift in the input signal causes the same time shift in the output signal. Sometimes such an operation is referred to as a linear time invariant (LTI) processor. Quite often, such processors are assumed to be casual, i.e. the present output signal depends on present and past signals, but not on future ones[13].

Fourier analysis provides a set of powerful tools and insights for the design and understanding of LTI systems. The impulse response and frequency response (spectral transfer function) are two attributes that are useful for characterizing LTI systems. They provide two different complete ways of calculating what an LTI system's output will be for a given input signal. An LTI system's temporal impulse response, often annotated as $h(t)$ with t being the time variable, is defined as the output signal that results when an impulse is applied to the system input. By knowing the impulse response, the output of the LTI system can be easily computed for any arbitrary input signal by convolving the input signal with the impulse response function. Alternatively, the LTI system can be characterized by a spectral transfer function $H(\omega) = V(\omega)/U(\omega)$ in the frequency domain where $U(\omega)$ and $V(\omega)$ are the spectral Fourier transforms of the input and output signals of the system, respectively, and ω is the angular frequency variable. There is a myriad of optical signal processing functionalities that can be described by an LTI system response, see Figure 1.5, such as optical

[13] A causal system (also known as a physical or nonanticipative system) is a system where the output depends on past and current inputs but not future inputs, i.e., the output $u(t_0)$ only depends on the input $v(t)$ for values of $t \leq t_0$. In general, the LTI systems operating on time-dependant signals are always casual and they cannot respond to the future events. However, not all systems have time as an independent variable. If the independent variable is space, the system does not need to be causal, i.e. the output $u(x_0)$ can depend on the input $v(x)$ for all values of x, $x \leq x_0$ or $x \geq x_0$; for example, a system that processes images.

clock recovery techniques, optical pulse shapers, optical differentiators/integrators, and pulse processors such as Hilbert transformers, among many others.

In general, there exist two main procedures to implement linear optical signal processors, (i) design of linear spectral filters, such as ring resonators, interferometers or fiber gratings, where the filtering operation is realized by directly tailoring the input signal's spectrum (Figure 1.7, left), (ii) development of time-domain analogs of well-known spatial-domain filters in which the filtering operation is carried out in the time domain via modulation processes (Figure 1.7, right). It is worth mentioning that time-domain equivalents of spatial-domain optical filters have been identified and created owing to the so-called space-time duality, which will be defined in detail in Chapter 2. Using this duality, highly effective spatial-domain optical information processing techniques[14] can be applied on temporal domain signals, which ultimately enables more sophisticated and powerful approaches to temporal processing and characterization of information [69]. Most notably, such an approach has enabled development of the time-lens concept [69], temporal imaging/self-imaging systems [41], real-time Fourier transformation and filtering [69], etc.

Linear temporal modulation and spectral filtering processes in turn can be divided in two categories: amplitude and phase modulation/filtering. A desired signal manipulation can be produced on the temporal (or spectral) amplitude or phase profile of the signal under test through temporal (or spectral) intensity or phase modulation (filtering), as depicted in Figure 1.7.

An optical spectral amplitude filter with a transfer function of $H(\omega) = A(\omega) \exp[j\phi(\omega)]$, where $A(\omega)$ and $\phi(\omega)$ denote the amplitude and phase profiles of filter, respectively, modify the spectral content of the input signal, and signal processing is typically carried out by attenuating and/or removing some of the spectral components of the input signal, (Figure 1.7, left, top). Note that in this type of filters, if $\phi(\omega) = 0$, the filter is called as an ideal amplitude-only filter, having an even and non-casual impulse response. In practice, however, a spectral linear phase of $\phi(\omega) = \omega\ t_0$ is typically introduced to satisfy the causality. This phase variation corresponds just to a temporal delay of t_0, so it does not affect the definition of the amplitude filter and it does not perform any

[14] In spatial-domain processing, information is encoded in the spatial distribution of light, which propagates in free-space. Processing of the spatial optical information is performed using free space optics [68], which involves the use of optical lenses, diffraction gratings, spatial light modulators, etc.

other transformation on the input signal. Example of typical amplitude filters include ring resonators [70, 49, 71], interferometers [72, 48] or periodic structures such as fiber or waveguide gratings [73, 74]. On the other hand, an optical spectral phase-only (all-pass) filter is characterized by a frequency response of $H(\omega) = A \exp [\, j\phi(\omega)]$, where A is a constant amplitude, independent of the frequency variable. Therefore, the spectral phase-only filter passes all spectral components equally in amplitude; therefore, if the uniform spectral amplitude transfer function is designed for 100% transmission, fundamentally no signal energy is lost in the process (Figure 1.7, left, bottom). Instead, the filter phase shifts the spectral components to carry out the target signal processing. Typically, our intuition for the time-domain effects induced by a filter's frequency response amplitude on an incoming signal is rather well-developed, but in contrast, visualizing the effect of the phase of the frequency response on the signal is subtler, but equally important. A dispersive medium, such as a conventional single-mode optical fiber, is an example of a phase-only filter [41].

Similarly, optical temporal intensity modulators with a modulation function of $p(t) = A(t)$ attenuates or eliminate some temporal components of the input signal to produce the target output signal, see Figure 1.7, right, top. In contrast, as shown in Figure 1.7, right, bottom, a temporal phase modulator with modulation function of $p(t) = \exp[\, j\phi(t)]$ only modifies the phase of the light-wave traversing it and, in essence, no signal energy is then lost in the process.

It should be noted that spectral filters are *passive* components, i.e., they do not require an external source of energy to perform their intended functions. However, temporal modulators are *active* components, which require an external energy source to operate and perform the target functions. In this Thesis, whenever possible, we use energy-efficient passive linear spectral filtering techniques to carry out a specific functionality. Nevertheless, not all functionalities can be implemented using only passive systems and in many cases, we need to incorporate linear active temporal modulation techniques. The simplest and most energy-efficient (i.e., the lowest consuming energy) mechanism for temporal modulation of an optical signal can be achieved through an electro-optic modulation scheme. In this scheme, the modulating signal is an electronic signal, which intrinsically have lower energy than an optical signal. More importantly, electro-optic modulation effect is induced using a second-order nonlinearity, which typically requires

much less energy from the modulating source than that of the third-order nonlinearity used for all-optical modulation.

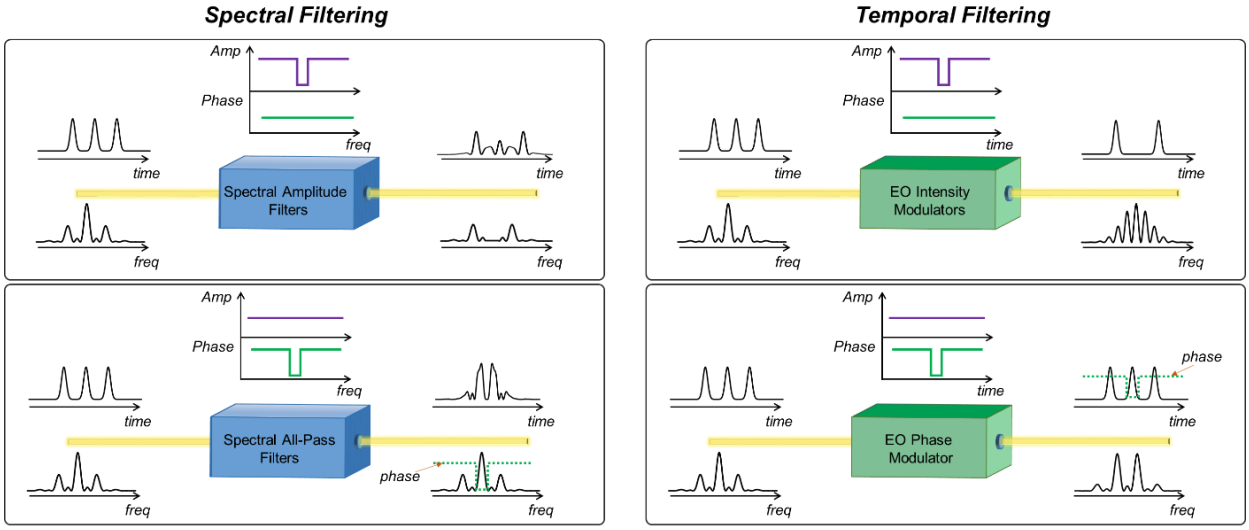

Figure 1.7 – Procedures for implementing linear temporal modulation and spectral filtering.

Figure 1.8 illustrates the energy transformation that takes places in linear amplitude and phase modulation/filtering approaches. The energy of the output information comes entirely from energy of the input information in all the processes.

Figure 1.8(a) and (b) shows the energy flow in the linear spectral amplitude and phase-only filtering approaches. In these approaches, no supply energy is needed (the device is passive) so that the total energy consumed by the circuit is simply $E_T = (P_{in} - P_{out})\,\tau_b$. Linear passive filtering completely removes the most significant contribution to energy loss, $P_s \times \tau_b$, from the energy-consumption equation; additionally, the use of a linear passive optical filter allows P_{out} to be much bigger than the case using nonlinear media, making E_T smaller. Still, as depicted in Figure 1.8(a) and Figure 1.7(left, top), amplitude filters necessarily wastes some of the input signal's energy; we refer to this loss as filtering loss. Depending on the target functionality, the filtering loss, $P_{in} - P_{out}$, can be considerable in amplitude filters. However, in phase-only filtering processes, if the uniform spectral amplitude transfer function is designed for 100% transmission, fundamentally no signal energy is lost so that the filtering loss is reduced to nearly 0, i.e., excluding the insertion loss, $P_{in} \approx P_{out}$, resulting in a total energy consumption $E_T \approx 0$.

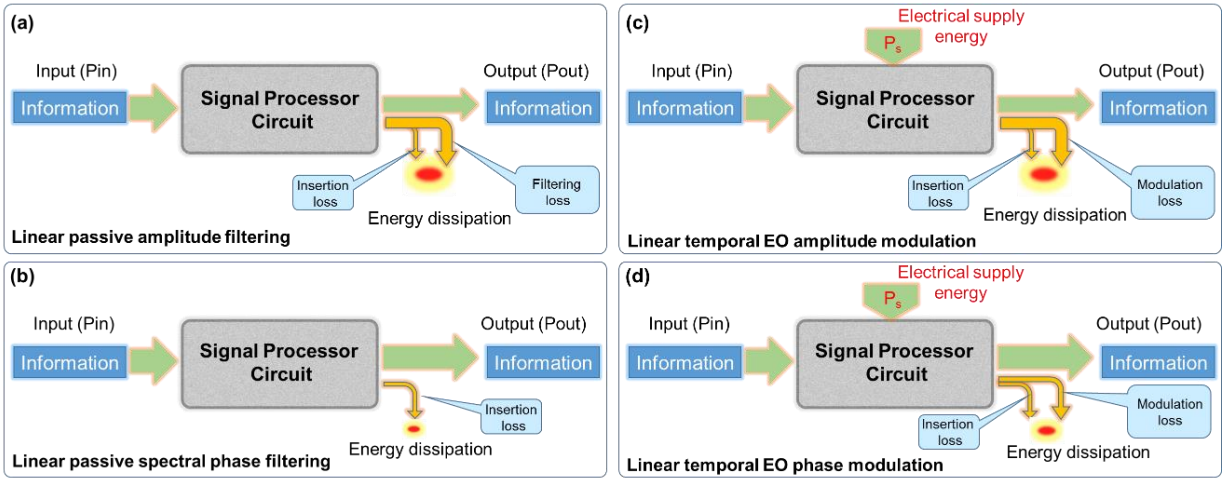

Figure 1.8 – Block diagram of optical signal processing circuit based on linear mechanisms. (a) Linear optical amplitude spectral filtering, (b) Linear optical phase-only spectral filtering, (c) Linear optical amplitude temporal modulation, (d) Linear optical phase-only temporal modulation.

On the other hand, in linear active intensity and phase modulation mechanisms, as shown in Figure 1.8(c) and (d), electrical power needs to be supplied (P_s) to the modulators to excite a second-order nonlinear interaction so that the total energy consumed by the modulators is $E_T = (P_{in} + P_s - P_{out})\ \tau_b$. In these mechanisms, the supply energy does not directly contribute to the output information energy, i.e., the energy of the output information signal, $P_{out} \times \tau_b$, comes entirely from energy of the input information, $P_{in} \times \tau_b$, (i.e., $P_{out} \leq P_{in}$). Therefore, the supply energy, $P_s \times \tau_b$, is entirely dissipated through the device, after enabling to implement the desired modification in the input signal's phase characteristics. However, the amount of electrical supply energy, P_s, is significantly lower than that of the optical nonlinear mechanisms, where an optical signal is used as the supply energy to excite a nonlinear effect in the nonlinear medium as shown in Figure 1.6, making the consumed energy E_T smaller in the electro-optic (EO) modulation mechanisms. It is worth mention that in the temporal EO amplitude modulation, in addition to the modulating voltage supply, we also require a bias voltage supply which makes the total supply power, P_s, in this process larger than that of the temporal EO phase modulation.

In general, the modulation loss refers to the amount of energy that is lost from the input power in the modulation process, $P_{in} - P_{out}$. The modulation loss excludes the contribution of the insertion loss. As mentioned above, similar to amplitude filtering mechanism, intensity modulation also wastes some of the input signal's energy, as shown in Figure 1.8 (c) and Figure 1.7(left, bottom).

Therefore, the wasted energy from the input power, P_{in} - P_{out}, typically can be considerable in an intensity modulation process. In sharp contrast, the signal energy can be fully preserved if only the signal phase is manipulated in the time domain by temporal phase modulation. Therefore, most of the light passes through the phase modulator devices, ensuring that the energy consumption is lower, i.e., essentially $P_{in} \approx P_{out}$ and the total energy consumption then will only be determined by the external supply energy, $E_T = P_s\, \tau_b$.

In order to provide a quantitative example of energy consumption in temporal phase modulation of an input signal, we estimate the energy consumption in the electro-optic phase modulation process and the cross-phase modulation (XPM) process to induce a spectral self-imaging effect [75] (which will be mentioned in the next Chapter) over a periodic optical pulse train (with a temporal period of 100ps), as shown Figure 1.9. In our estimation, we take into account a HNLF with a Kerr effect coefficient of γ= 11 $W^{-1}Km^{-1}$ and an electro-optic phase modulator with $V_\pi = 3.0V$. These specifications correspond to standard values for the two evaluated processes, as per present technology status. The estimated energy consumption is $E_T = P_s\, \tau_b$ = 125mW× 100ps = 12.5 pJ/period for the phase modulation process using XPM [76] and it is $E_T = P_s\, \tau_b = \frac{V_\pi^2}{8\,R}\, \tau_b$ = 22.5mW× 100ps = 2.25 pJ/period, where R = 50Ω is the modulator resistor, for the electro-optic modulation [77]. In addition to around five-fold energy performance improvement, the electro-optic modulation also provides the simplest mechanism for temporal phase modulation.

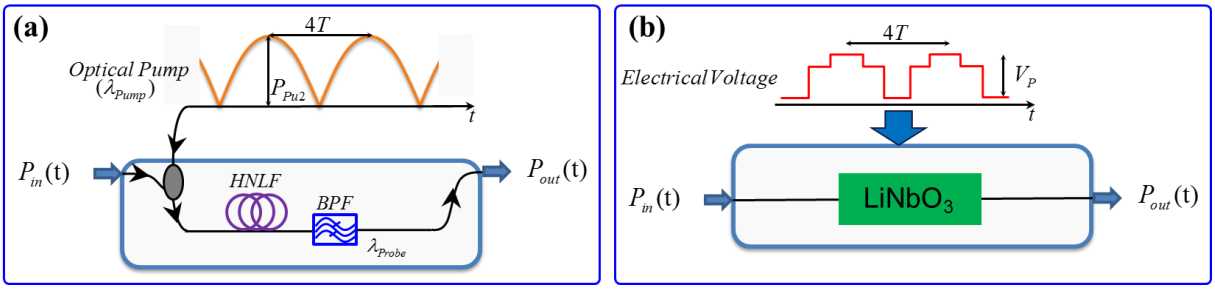

Figure 1.9 – Processing a periodic optical input pulse train ($P_{in}(t)$) based on (a) nonlinear cross phase modulation (XPM) and (b) electro-optic effect.

The use of linear optics allows energy consumption to be much lower than the case using nonlinear mechanism. Therefore, in order to reduce the overall energy budget of an optical signal

processing system, it is required to avoid the use of energy-hungry nonlinear mechanisms and to implement the desired specific functionality using energy-efficient linear mechanisms.

1.3 Review of relevant optical signal processors studied in this dissertation

Signal processing functions of importance studied in this dissertation are all-optical clock recovery, optical format conversion and repetition-rate control of pulse lasers for telecom applications. In this Section, we do a short and non-exhaustive review of some of the previously demonstrated methods. The purpose of this discussion is to put our work into context.

1.3.1 Optical Clock Recovery

During the last 20 years a wide variety of optical "base-rate" and "sub-harmonic" clock recovery (CR) methods based on different physical principles have been proposed and demonstrated [78, 79, 46, 80, 81, 82, 83, 84, 85]. CR is a fundamental operation performed in all digital communications devices ranging from ordinary mobile phones to high-speed optical receivers. In optical telecommunications, the clock has traditionally been recovered with electrical circuitry. For a conventional receiver converting the optical signal to an electrical one, the electronic CR is the obvious choice. There are, however, locations and devices in the optical network architecture, where the optical-to-electrical conversion is unnecessary. The preferred choice would then be to preserve the signal in the optical domain. Such devices are, for example, all-optical signal regenerators [44], time-division (de-) multiplexers [17], logical optical gates [55], or, in general, locations where the transmitted signal needs to be (re-) timed but not terminated. All digital telecommunications systems consist of three main building blocks: a transmitter, a transmission path, and a receiver. The transmitter and the receiver are typically separated by a considerable distance, therefore the receiver has no means to obtain direct information about the transmitter clock. Naturally, the clock information could be sent through a separate communication channel leading to reduced net bandwidth and increased costs of the system. Therefore, the receiver typically recovers the clock from the incoming flow of bits.

Optical CR methods may be divided into two main categories: active/nonlinear and passive/linear filtering techniques. In this Section, I provide a review of two optical CR methods, one from each category.

A common active optical clock recovery technique is to use an optical phase-locked loop (PLL) [86, 87]. The function of the optical PLL closely imitates a conventional electrical PLL that is extensively used in applications of radio frequency (RF) and telecommunications technology. The PLL synchronizes an internal oscillator with an external data signal. Through the synchronization process the PLL obtains information about the frequency and the phase of the data signal, which otherwise may be buried under the data modulation. Figure 1.10(a) shows the conventional electrical PLL that is composed of four basic components: a phase detector (mixer), a low-pass filter, a voltage-controlled oscillator (VCO), and a feedback loop [88, 89, 90]. Additionally, the feedback loop may consist of a multiplication counter, when the resolved oscillation is a sub-harmonic of the data signal.

The synchronization is made by adjusting the VCO such that the cross-correlation value of the data and local signals is maximized. In a conventional electrical PLL, the input optical signal is converted to the electronic signal in the input of the phase detector and mixed with the local signal in order to realize the synchronization. However, in this configuration, the ultimate input bit rate is limited by the phase detector response time [91, 46]. Alternative opto-electronic techniques have been suggested to perform the required cross-correlation in the phase detector based on optical nonlinear interactions to build an optical PLL. Figure 1.10(b) shows an example of an optical PLL [92]. The required cross-correlation of the local optical clock and the data signals is performed through four-wave mixing (FWM) in a nonlinear optical medium, such as an SOA [93], and three-wave mixing (TWM) in periodically poled lithium niobate (PPLN) [78]. The pulses, depending on the degree of overlap, interact through the FWM or TWM process and provide the cross-correlation of the signals. The generated wavelength is bandpass filtered and the information about the time averaged measured optical power is fed back to the VCO. Using this technique optical clock recovery have been demonstrated at high data rates and de-multiplexing from a 320-Gbit/s and a 640-Gbit/s OTDM stream [78, 94]. Recently, another nonlinear cross-correlation method was introduced that is based on two-photon absorption in silicon avalanche photodiode [95]. The time averaged photodiode response is dependent on the temporal overlap of the optical pulses and

can thus be incorporated in PLL synchronization. In addition to the PLL structures, nonlinear effects are also employed for optical clock recovery involving mode-locking a semiconductor fiber laser (SFL) based on the use of a nonlinear optical loop mirror (NOLM) and nonlinear polarization rotation (NPR) [85].

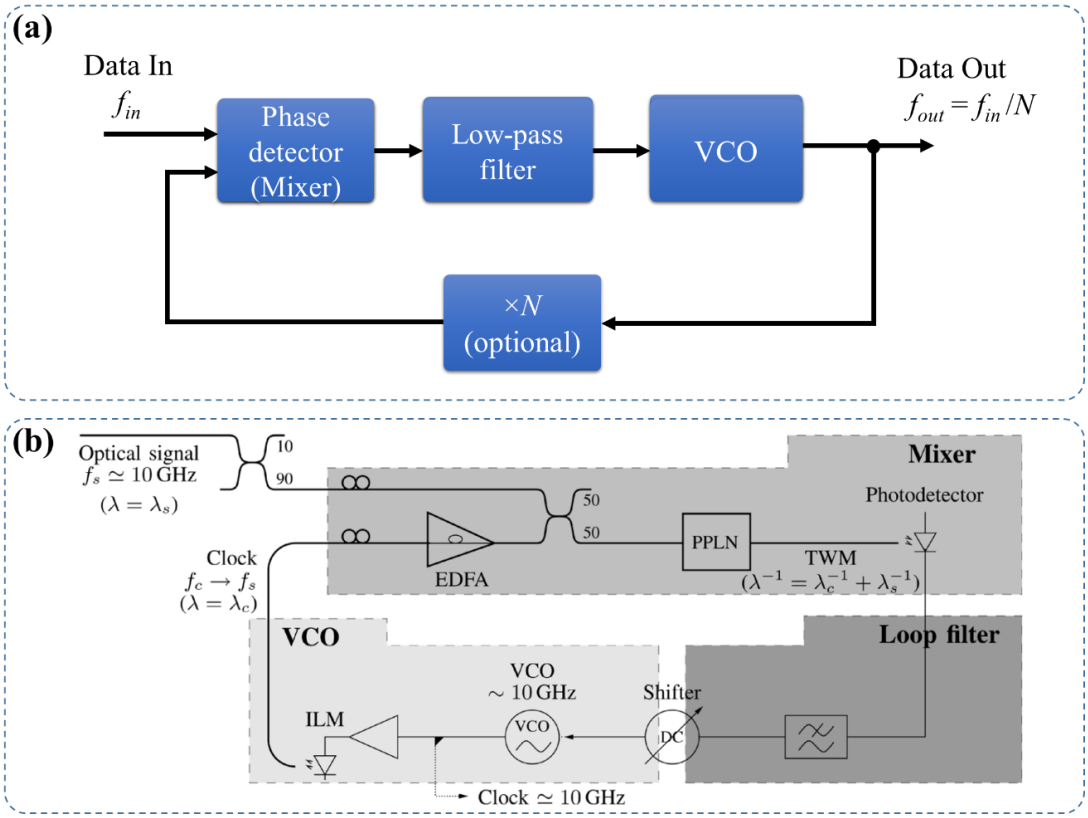

Figure 1.10 – (a) Schematic illustration of components of a PLL. (b) Optical PLL setup; the "mixer" is based on three-wave mixing in the PPLN [92].

Compared to other optical CR methods, the optical active/nonlinear setups often suffer considerable complexity manufacturing costs. However, the recovered clock quality in terms of jitter and stability is typically high and PLLs provide the possibility for subharmonic CR, which may not be attainable by other methods.

As a matter of fact, clock recovery does not necessarily require an active/nonlinear arrangement. It can also be performed by linear passive filtering techniques [46, 96, 97]. These methods simply remove a part or all of the information from the received signal and preserve only the base frequency associated with the bit rate of the data signal. These techniques typically have

simple construction and low manufacturing cost, their challenge being the quality of the recovered clock signal.

Optical clock recovery based on a Fabry – Perot filter (FPF) is among the most studied passive techniques to recover the clock signal from a return-to-zero on – off-keying (RZ-OOK) incoming optical data signal. A FPF is an amplitude filter whose spectral transmission peaks are periodic and the transmission bands are typically narrow, see Figure 1.11. This filter, with a free spectral range (FSR) tuned to the bit rate of the incoming optical data signal, preserves the discrete clock spectral components from the incoming optical data signal and removes the rest of the signal's continuous spectral content, which typically contains about 50% of the overall energy of the incoming data signal.

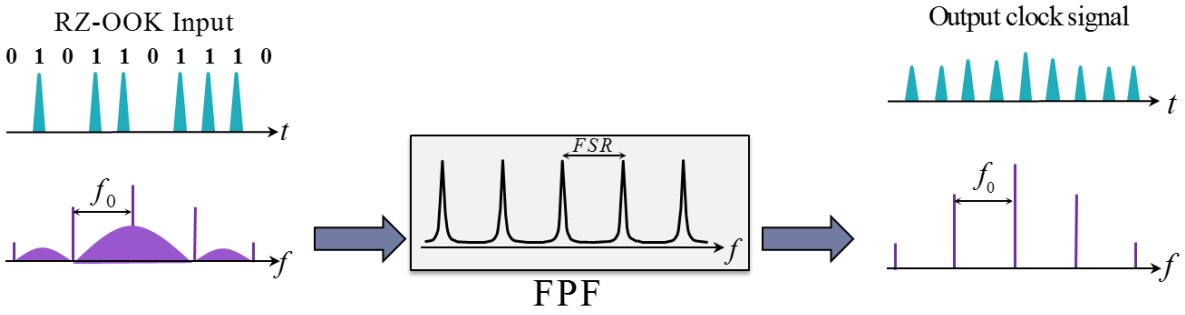

Figure 1.11 – Principle of optical clock recovery based on spectral amplitude filtering using a FPF.

Since a FPF is a fully passive device, the operation speed of techniques based on a FPF is ideally unlimited. However, to achieve a high-quality clock signal, a high-finesse FPF is required to average out the incoming data pattern. The needed high finesse imposes a very stringent tolerance for mismatching between the filter specifications (resonant frequency and FSR) and the incoming data signal specifications (central wavelength and bit rate, respectively). On the other hand, a lower FPF finesse leads to amplitude modulation (AM) in the clock signal. To minimize this AM, the FPF should be followed by a nonlinear subsystem [96], e.g., a semiconductor optical amplifier (SOA), an ultrafast nonlinear interferometer, or a Mach – Zehnder interferometer, acting as an optical power equalizer. Not only does this increase the clock-recovery circuit complexity, but additionally, these subsystems may limit the system operating data rate, e.g., to tens of Gbit/s when using SOAs. In addition, along with all the passive CR techniques reported to date, the possibility of sub-harmonic CR has not been demonstrated using a FPF-based CR system [46].

Fernández-Pousa et al [98] have proposed another linear passive CR scheme using a piece of dispersive medium, whose dispersion is tuned to a value according to the temporal Talbot effect. This proposal has been demonstrated experimentally later by Pudo et al [99, 100] and Oiwa et al [101]. Temporal Talbot effect had already been used to process periodic input signals to generate periodic output signals. However, Fernández-Pousa et al, showed that the temporal Talbot effect has an inherent buffering ability to generate a periodic output, even from an aperiodic input pulse train, i.e. data signal. The proposed technique offers similar advantages to those of the conventional Talbot-based signal processors, namely simplicity, the potential for timing-jitter mitigation and high energy efficiency. The latest is associated with the fact that fundamentally, no energy is lost in the recovery process, since this involves only manipulations of the signal's phase information in the frequency domains. This technique will be described in deeper detail in Section 3.3.

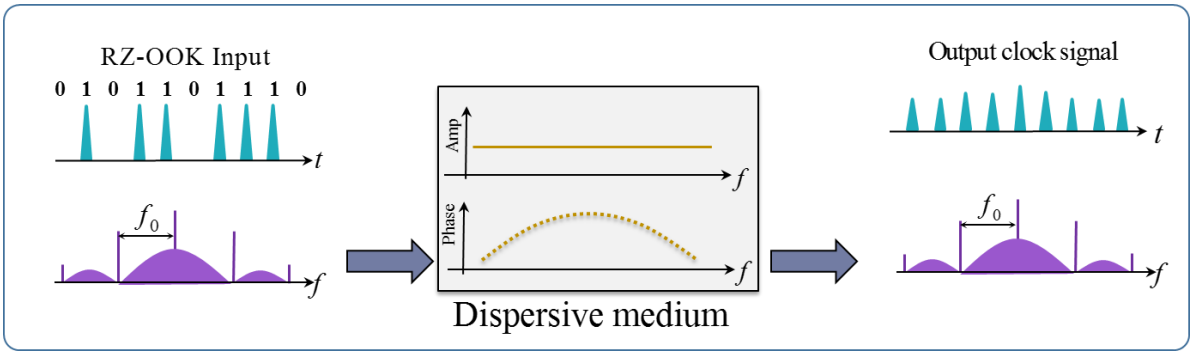

Figure 1.12 – Optical clock recovery technique through dispersion-induced temporal Talbot effect [100].

1.3.2 Optical RZ to NRZ format conversion

Future optical networks are likely a hybrid scenario of various technologies owing to the large variety of applications and to their hierarchical structure, which implies diverse specifications for different networks' segments. In this context, a specific network segment employs an adequate modulation format that meets its requirements [102, 103]. Therefore, all-optical format converters are of great importance to transparently and seamlessly interconnect different parts of the networks, avoiding the use of optical-to-electrical (O/E) and electrical-to-optical (E/O) converters,

as well as overcoming limitations imposed by electronics in terms of bit rate and frequency bandwidth [103] .

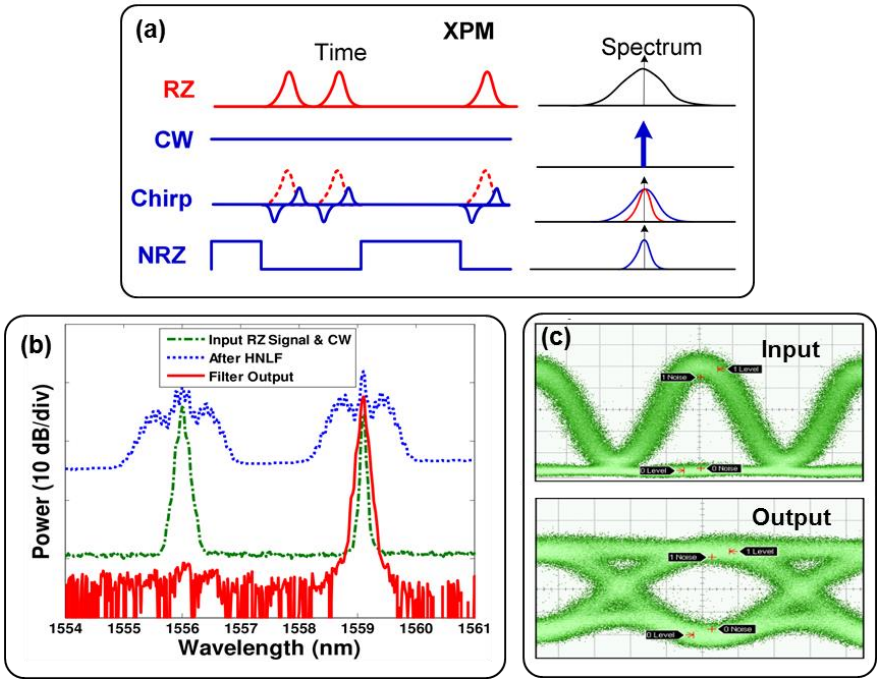

Figure 1.13 – (a) Schematic diagram of XPM-based format conversion, (b) spectra of the CW probe light, the input RZ signal before and after the HNLF, and converted NRZ signal, (c) corresponding eye diagrams of input RZ and converted NRZ signals [56].

In particular, format conversion between return-to-zero (RZ)[15] and nonreturn-to-zero (NRZ)[16] signals is particularly interesting: both formats are mature and widely used in different parts of the networks, e.g., the RZ format is adopted in time division-multiplexing (OTDM) systems to be able to perform pulse multiplexing, while the NRZ format is preferred in wavelength-division-multiplexing (WDM) systems due to its higher spectral efficiency [71]. In addition, format conversion of an RZ signal to its equivalent NRZ is also desired in de-multiplexing of OTDM signals as NRZ signals improve timing-jitter tolerance in the de-multiplexing process thanks to their flat-top temporal shape [104]. So far, a variety of schemes have been developed to realize

[15] Return-to-zero (RZ) describes a line code used in telecommunications signals in which each pulse representing 1 bit is chosen to be shorter than the bit slot, and its amplitude returns to zero before the bit duration is over.
[16] Non-return-to-zero (NRZ) describes a line code used in telecommunications signals in which the pulse representing each 1 bit occupies the entire bit slot and does not drop to zero between two or more successive 1 bits.

RZ-to-NRZ format conversion, mainly using either nonlinear or linear optical signal processing techniques [104, 56, 105, 106, 107, 108, 109, 110].

Schemes based on nonlinear effects, such as XPM, XGM, and FWM, employ different nonlinear media to realize the target format conversion, including HNLFs [56], SOAs [105] and PPLN waveguides [106]. For example, in [56], a RZ-to-NRZ format conversion is presented based on XPM of a CW beam, as shown in Figure 1.13(a). When an RZ input signal and continuous-wave (CW) probe light are launched into a nonlinear medium, nonlinear phase modulation between them occurs due to XPM. For the CW probe light, the XPM induced phase modulation is governed by the rate of power change of the input RZ signal. A red chirp is caused by the rising edge of the RZ signal, while a blue chirp is generated due to the falling edge of the RZ signal. In addition, the instantaneous wavelength remains unchanged when the rate of power change is zero, leading to chirp-free wavelength components. Therefore, an inverted NRZ signal can be obtained by filtering out the chirped components of the input CW probe light. Figure 1.13(b) shows the spectra of the CW probe light, the RZ signal before and after the HNLF, and the converted NRZ signal. It is clear that the spectrum of the input CW probe light is significantly broadened due to the XPM effect inside the loop. The measured eye diagrams of the original 40-Gbit/s RZ signal and converted NRZ signal is shown in Figure 1.13(c). This technique, and in general, nonlinear-based format conversion schemes require an additional optical beam to perform the format conversion, while also requiring high power input signals.

On the other hand, format converters based on linear optical signal processing are typically based on linear spectral amplitude filtering to tailor the spectrum of an RZ input signal into the target NRZ signal spectrum, that is the so-called optical spectrum transformation [104, 107, 108, 109], see Figure 1.14. In particular, linear RZ-to-NRZ format converters rely on the suppression of the first-order harmonic components in the spectrum of an RZ signal using a periodic amplitude notch filter whose FSR is matched to twice the signal bit rate. The resulting converted NRZ signal after the notch filter yet exhibits relatively large amplitude ripples due to the residual high-frequency components of the spectrum. Therefore, a narrow optical bandpass filter (OBPF) is typically used to eliminate these residual components, leading to a reduction of the amplitude ripples and the associated improvement in the quality of the converted NRZ signal. The required amplitude notch filters can be implemented using a variety of technologies, such as photonic

microring resonators [104, 107, 108], interferometers [109], and fiber Bragg gratings (FBGs) [110].

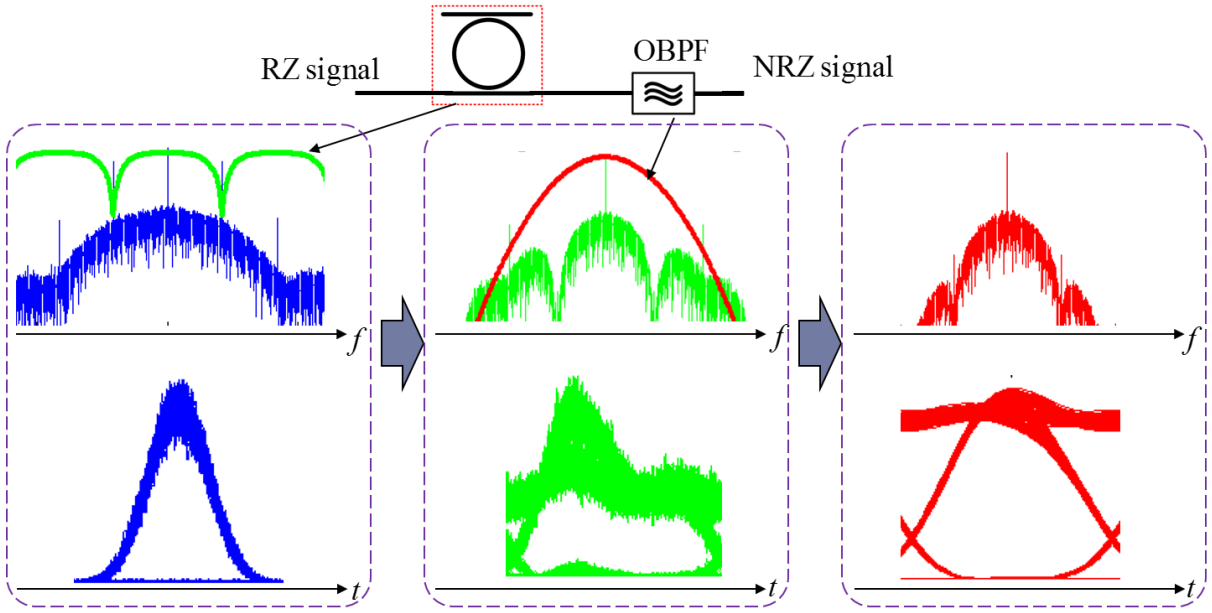

Figure 1.14 – Spectra (top row) and temporal waveforms (bottom row) evolution of format conversion from RZ to NRZ based on optical spectrum transformation. *f*: frequency, *t*: time.

Linear format conversion platforms are of greater interest due to their intrinsic simplicity, suitability for high speed operation and stable performance. In addition, unlike nonlinear-based schemes, linear converters do not require any additional optical beam to perform the format conversion while also avoiding the need for high power input signals, as required otherwise to excite optical nonlinear effects.

1.3.3 Optical picosecond pulse generation methods for high-speed optical systems

Picosecond optical pulse trains in the gigahertz (GHz) regime and beyond are of fundamental interest for a very wide range of applications in the fields of fiber optics communications [111], optical computing [112], microwave photonics [113], material processing [114], frequency combs [115], nonlinear optics [116] and so on. In particular, in the context of optical communications, OTDM systems require stable high repetition-rate optical pulse sources which can act both as a data transmission source, and as an optical clock used to synchronize the signal and extract the transmitted information. Temporal synchronization is also of great importance in optical signal

processors including regenerators and logic circuits [112, 44] . In order to ensure synchronization in an optical signal processing circuit, a single reference optical clock, i.e., a high repetition-rate pulse train, may be used throughout the circuit. Optical circuits are likely to consist of a number of fast operations, synchronized to each other, but running at different rates depending on the function that they perform. The central optical processing units may be expected to run at a reference rate, while optical processing units in the periphery of the optical circuit may be run at significantly higher or lower rates. Therefore, a reliable high repetition-rate optical pulse source with the possibility of programming the repetition-rate from several GHz to hundreds of GHz is required.

Another potential field of application for high speed optical pulse source is the microwave photonics— the interface between optical components and devices whose operating spectrum (frequency) resides well within and above the microwave range. [113]. Certain electronic systems may require ultrahigh sampling rates in analog-to-digital converters [117]. In this context, optical pulses can be used to generate short burst of electrons, which subsequently act as a sampling pulse train in the sub-THz range.

Amongst many desirable characteristic of a high repetition-rate optical source used at the aforementioned applications, one can include pulse stability, low timing jitter, and low amplitude fluctuations, especially for applications using a pulse train as a reference or sampling clock signal.

A large number of short pulse, high repetition-rate laser sources have been demonstrated so far. Ultrafast fiber lasers offer an immediate and attractive platform for generation of high repetitive pulse trains [118]. In early demonstrations aimed at achieving high repetition-rate pulse sources, actively mode-locking schemes have been used, with demonstrated repetition-rates up to ~40GHz. However, a further increase of the repetition-rate is limited by the available electrical bandwidth of the modulator and its driving electronics. Previously, various approaches have been explored to generate high repetition-rate pulses both from passively and actively mode-locked fiber lasers, using mechanisms that enable overcoming electrical bandwidth limitations [118]. However, though impressive results have been demonstrated using these approaches, they typically require a precise control of the optical properties of the laser cavity and they offer very limited flexibility to program or tune the output repetition-rates. This precludes the potential use

of these systems for the broad range of applications that require repetition-rate programmability and control.

An alternative methodology to achieve high repetition-rate pulses is to multiply the repetition-rate of a stable low-rate laser source all-optically, outside the laser cavity, using pulse repetition-rate multiplication (PRRM) techniques [41, 119, 120, 121, 122, 123, 124], as shown in Figure 1.15. In these techniques, the multiplication factor, *m*, is an integer value and the shape and pulsewidth of individual pulse are preserved in the multiplication process.

Figure 1.15 – Pulse repetition-rate multiplication technique to increase the repetition-rate of a low-rate laser source.

In general, previously demonstrated rate multiplication techniques can fall into two categories: techniques based on linear spectral amplitude filtering and spectral phase filtering. In this Section, a review of the most relevant rate multiplication techniques is presented.

A straightforward technique for multiplying the repetition-rate of a low-rate source involves the use of spectral amplitude filters [119, 125], through slicing the spectral content of the incoming pulse train. It should be noted that the input pulse train is composed of temporal periodic pulses repeating with temporal period of *T*. In the frequency domain, it exhibits spectral modes with spacing of *F*, where *F* and *T* are inversely related through $F=1/T$. Figure 1.16(a) shows the transmission spectrum of a periodic amplitude filter used for pulse repetition-rate multiplication. The free spectral range (FSR) of the filter is set to an integer multiple of the spectral mode spacing of the input pulse train, i.e FSR= $m\,F$. The filter selects specific spectral modes of the input, and eliminates the others, with a separation in frequency equal to the target output repetition-rate, i.e. $T_{out}= T/\,m$.

Different implementations of this approach were considered, such as one based upon a Fabry-Pérot etalon [119], arrayed waveguide gratings [126, 121], interferometers [127], superimposed fiber Bragg gratings [120], etc. However, these schemes require very strict alignment in between

the filter and the spectral modes of the input source. Therefore, a very precise implementation of such a filtering must be performed in order to ensure a regular output pulse train. Any error in the optical path lengths - or equivalently, in the alignment of the comb filter spectral period with respect to the source modes - introduces temporal jitter and pulse-to-pulse amplitude fluctuations in the output pulses. Such impairment can be a very serious issue for applications using a pulse train as a reference signal, given that it is in principle much easier to correct for amplitude fluctuations than for a temporal uncertainty. Moreover, one of the main drawbacks of this method is the inherent energy loss, as only a fraction of the incident spectrum remains in the output signal. Increase of the multiplication factor leads to elimination of more spectral components, and consequently, a larger amount of energy is lost.

On the other hand, rate multiplication techniques based on spectral phase filtering passes all the spectral components of the input equally in amplitude and none of the spectral components are eliminated [41, 120], as shown in Figure 1.16(b); therefore, ideally no input energy is lost in this process. In particular, propagation of a pulse train through a dispersive medium, characterized by a quadratic spectral phase response, with a well-defined amount of dispersion results in an intensity repetition-rate multiplication through the temporal Talbot effect. In short, an m times repetition-rate multiplication of an incident pulse train occurs in a dispersive medium provided that the dispersion (ϕ_2, defined as the slope of group delay as a function of radial frequency) and the temporal pulse period, T, satisfy the following condition [41, 120]:

$$\phi_2 = = \frac{s}{m}\frac{T^2}{2\pi} \tag{1.4}$$

where m and s are integers such that s/m is an irreducible rational number. A more detailed explanation of this technique will be provided in Chapter 2.

Pulse repetition-rate multiplication based on temporal Talbot effect has attracted a great deal of attention over the years due to its simple implementation, with a substantially reduced complexity in comparison with spectral amplitude filtering methods. This approach provides the desired multiplied-rate copy of an incoming optical pulse train simply through a proper dispersion-induced spectral phase-only filtering process. Additionally, this method (i) offers increased energy efficiency, since fundamentally no energy is lost by phase-only filtering, (ii) has amplitude and

phase noise mitigation capabilities, and (iii) is robust against possible misalignments between the filter and the input source.

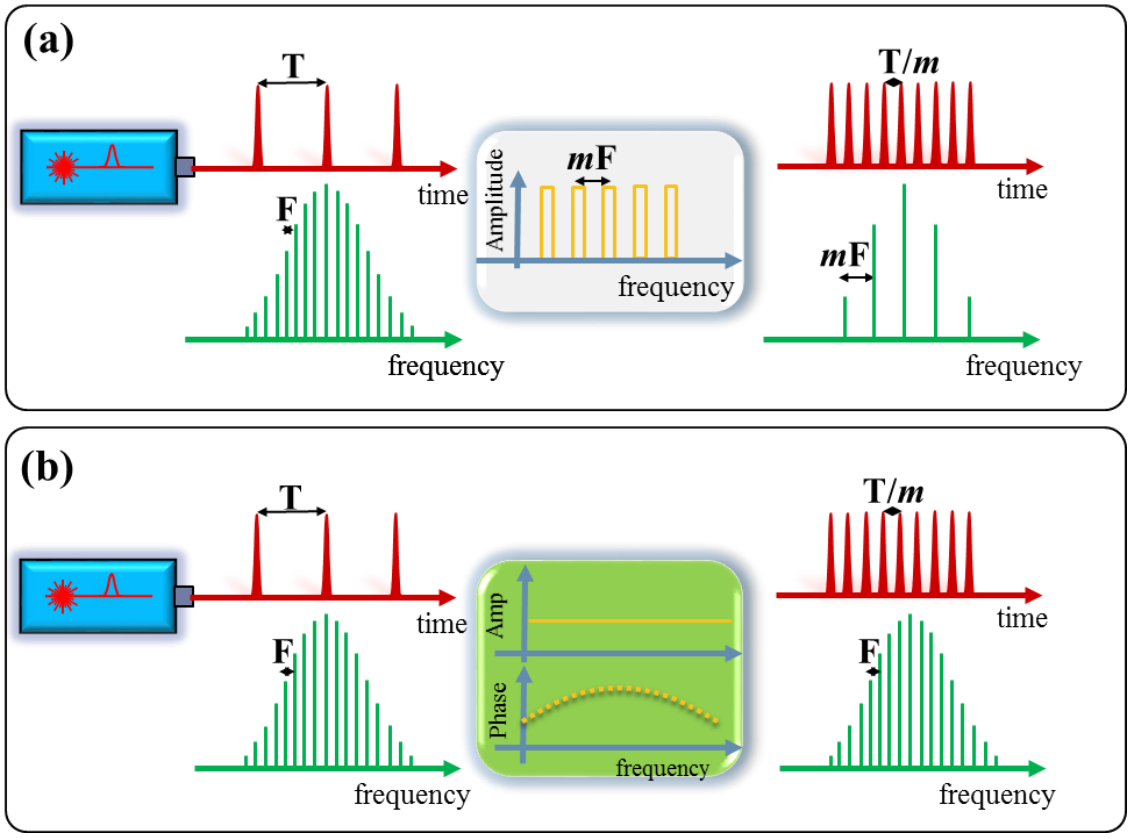

Figure 1.16 – Pulse repetition-rate multiplication techniques based on (a) linear spectral amplitude filtering and (b) spectral phase filtering.

However, despite its attractive set of advantages, Talbot-based PRRM requires the use of a proper, fixed amount dispersion for a given multiplication factor; once the dispersion is fixed, typically through a Section of dispersive fiber or a chirped fiber Bragg grating (FBG), it is not straightforward to tune or program the rate-multiplication factor without significant system configuration changes (i.e., changing the dispersive medium). Moreover, the method is limited to output repetition-rates that are only integer multiples of the initial pulse repetition-rate, i.e. *m* is an integer number. This same fundamental restriction applies to all PRRM methods reported to date.

1.4 Objective and Organization of the Thesis

Energy consumption, and the associated thermal issues, have been a driving consideration behind much of the progress made by the electronic industry over the past half century. In comparison, the optical signal processing research community has paid scant attention to the question of energy consumption. It is often argued that optical signal processing will replace digital signal processing because of its high-speed capabilities. However, simplistic arguments based on speed alone often miss the critically important point that optical devices are generally very energy hungry. Unless there are many-orders-of-magnitude improvement in the energy efficiency of optical processors, electronics is likely to remain the technology of choice for the vast majority of signal processing and switching applications in telecommunication networks.

A key objective of this dissertation is to highlight the importance of energy consumption as a measure of performance in optical signal processing and to try to provide a technological solution to the problem of energy consumption in relevant optical processors. In particular, in this dissertation, we explore the possibility of using energy-efficient, passive/active linear techniques for optical signal processing, avoiding the use of conventional energy-hungry optical active and/or nonlinear mechanisms; we choose a linear active temporal modulation scheme, i.e., electro-optic modulation, that provides the simplest and most energy-efficient (i.e., the lowest consuming energy) mechanism for temporal modulation of an optical signal. In particular, we introduce novel concepts and innovative approaches for implementation of important signal-processing operations using temporal phase modulation and/or spectral phase filtering processes that inherently preserve the entire input signal energy without requiring additional light sources. Through these concepts, the incoming signal's energy is effectively redistributed to build up the target output signal without energy loss and without using any additional external optical power.

This dissertation is mainly focused on optical signal processing of periodic and aperiodic (data) signals. Figure 1.17 shows a summary of the proposed functionalities in these two categories in my PhD research program.

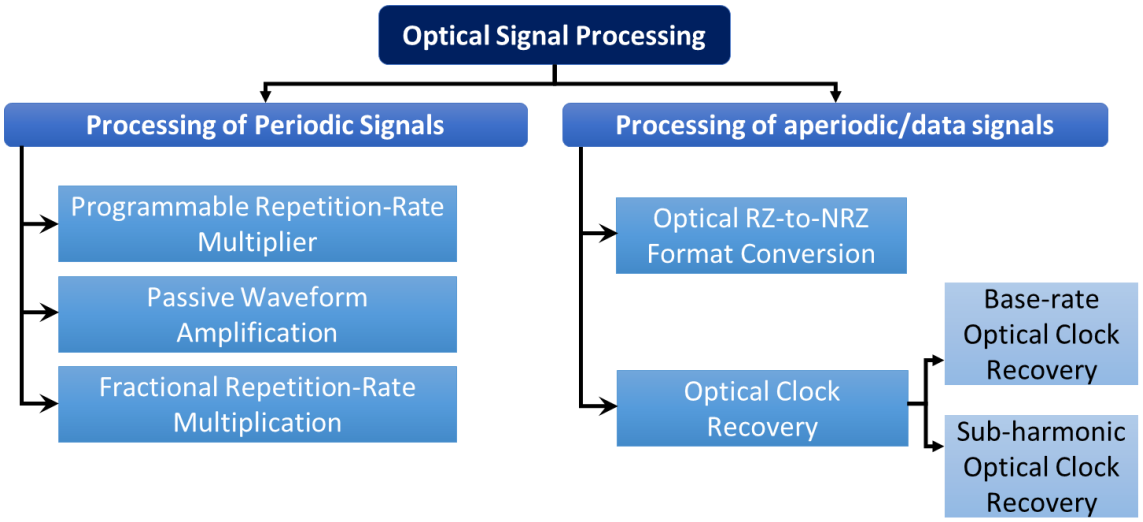

Figure 1.17 – Overall schematic of the pursued objectives during this PhD program.

Figure 1.18 shows an application example of the studied functionalities in the context of an optical router. The input data packet, consisting of the actual data (payload) and the destination information of the packet (header), is first clock recovered; the header is subsequently extracted using the recovered clock. The extracted header is processed in the optical processing unit to find the destination route and also to create a new header. Then, the new generated packet, including the payload and the new header, is directed to the appropriate destination by optical switch. The three functionalities studied in this dissertation are (i) versatile energy-efficient optical pulse source, used in the optical processing and header generation units, (ii) the optical clock recovery unit, and (iii) the format conversion unit.

Therefore, first, we demonstrate an energy-efficient scheme to obtain a reliable source of picosecond pulses with an unprecedented degree of repetition-rate control and programmability, involving a combination of phase-only temporal modulation and spectral filtering processes (e.g., group-velocity dispersion). Next, this Thesis proposes phase-only spectral filtering methods for performing two basic signal processing operations in the context of optical communications: optical base-rate and sub-harmonic clock recovery from data signals and RZ-to-NRZ optical format conversion.

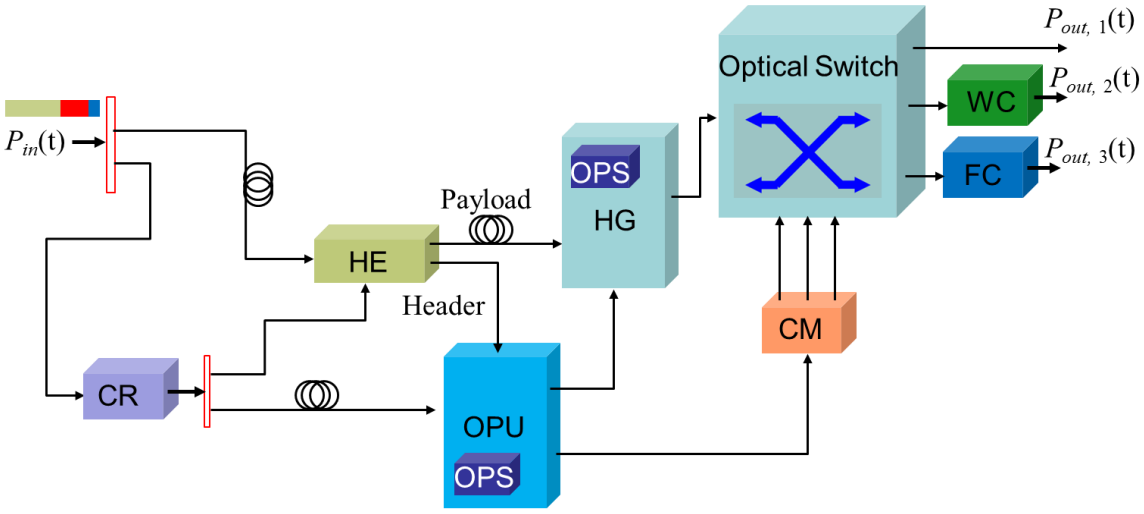

Figure 1.18 – Example of an optical router architecture. CR: Clock recovery, HE: Header extraction, OPS: Optical pulse source, OPU: Optical processing unit, HG: Header generation, CM: Control Module, FC: Format conversion, WC: Wavelength Conversion. Extracted from [128, 129, 130, 105].

Each chapter in this Thesis is centered on a different achievement of this PhD research. **Chapter 2** provides a comprehensive introduction to the temporal Talbot effect, where the analytic description of the method and its fundamental properties are discussed. The combination of temporal phase modulation and temporal self-imaging (Talbot) effect (i.e., spectral phase filtering) are employed for implementing new functionalities to process incoming periodic arbitrary waveform (e.g., pulse) trains. Application of a prescribed temporal phase-modulation profile to an input periodic pulse train produces new frequency components, and the subsequent dispersion-induced temporal self-imaging effect temporally re-distributes the new spectrum to produce the target output signal. Depending on the prescribed phase modulation and amount of used dispersion, different signal manipulations can be produced at the system output, according to the requirements of different target applications. In particular, using appropriate combinations of temporal and spectral linear filtering, we will show (i) a ***programmable*** repetition-rate multiplication technique, where the output repetition-rate can be electrically programmed to be any integer multiple of the input repetition-rate, and (ii) a ***fractional*** repetition-rate multiplication technique, where the repetition-rate of the output signal can be tailored to be any fractional multiple of the input signal, and (iii) an energy-preserving repetition-rate ***division*** mechanisms, producing undistorted passive

amplification of each resulting individual waveform, i.e. a passive waveform amplifier without using active gain.

Chapter 3 introduces novel energy-efficient signal processing concepts and technologies for optical data signals. For this purpose, we define, design, and develop two relevant set of processors: (i) A novel approach for all optical return-to-zero (RZ)-to-non-RZ (NRZ) telecommunication data format conversion, which has been experimentally implemented at a bit rate of 640 Gbit/s. In this approach, we show how a proper phase-only manipulation of the frequency content of a RZ data signal can be used to implement conversion of the RZ signal into the equivalent NRZ time-domain data. (ii) Novel approaches for base-rate and sub-harmonic clock recovery from on-off-keying (OOK) data signals. The former is implemented based on phase-only linear optical filtering of the incoming RZ signal whereas the latter exploits the so-called 'inverse' self-imaging effect.

Chapter 4 summarizes the work presented in this Thesis and proposes potential prospects for future work.

Chapter 2

Energy-preserving pulse repetition-rate control for high-speed optical systems

2.1 Introduction

The Talbot (self-imaging) effect, also referred to as lensless imaging, is a concept with a distinguished pedigree. The Talbot effect is a Fresnel (near-field) diffraction effect in which incident plane waves on a periodic structure produce self-images or Talbot revivals. This effect was originally discovered by Talbot more than 170 years ago [131]. Over the years, investigators have come to understand different aspects of this phenomenon, and a theory of the Talbot effect based upon classical diffraction theory has emerged that is capable of explaining various observations. Additionally, in the framework of the space-time duality, the temporal analog of the Talbot effect was first described in 1981 (about 35 years ago) [132] by propagating a periodic temporal signal (for instance, a stream of short optical pulses) through a dispersive medium under first-order dispersion conditions. Since then, the temporal Talbot effect has attracted considerable interest and has found various applications [133, 41, 134, 135, 136, 137].

In this Chapter, we use the temporal Talbot effect as the basis of our proposed concepts and methods for generation and repetition-rate control of picosecond pulse trains. As such, we first provide an overview of the fundamentals of the temporal Talbot self-imaging effect (Section 2.2). Next, this effect has been successfully employed for the design and realization of (i) a *programmable* repet-ition-rate multiplication technique, where the output repetition-rate can be

electrically programmed to be any integer multiple of the input repetition-rate (Section 2.3), (ii) a lossless *fractional* repetition-rate multiplication technique, where the repetition-rate of the output signal can be set to any fractional multiple of the input signal (Section 2.4) and (iii) a lossless repetition-rate *division* technique, where the energy of input repetitive pulses are coherently accumulated to fewer replica pulses to build up an output signal with a reduced repetition-rate and intensity-amplified pulses (Section 2.5).

2.2 The Talbot effect

"Self-imaging" means image formation without a lens or any other instrument in the space between the object and the image. While doing research on photography in 1836, William Henry Fox Talbot (1800-1877) first discovered the self-imaging phenomenon. Talbot was a British scientist, mathematician, politician, and photography pioneer who invented the salted paper and calotype processes, precursors to photographic processes of the later 19th and 20th centuries [138]. When he was examining diffraction gratings under white light illumination with a magnifying lens, he found that the image of the grating was repeated even when he moved the lens out of focus [131]. Talbot presented the results of his experiment at a meeting of the British Association in Bristol [138]:

> "*It was very curious to observe that though the grating was greatly out of the focus of the lens ... the appearance of the bands was perfectly distinct and well defined. The experiments are communicated in the hope that they may prove interesting to the cultivators of optical science*."

About half a century later, in 1881, Lord Rayleigh was the first scientist to explain this experiment analytically in a paper entitled: "*On copying diffraction-gratings, and on some phenomena connected therewith*" [139]. Chronologically, the next studies related to this phenomenon were by Winkelmann (1908) [140], Weisel (1910) [141], and Wolfke (1911-1913) [142] who examined grating image formation in microscopy. Once again, many years passed until the problem was further investigated, in the 1950s, by Cowley, Moodie [143] and later by Montgomery [144]. The terminology "self-imaging" was introduced by Montgomery and has been used together with the term "Talbot effect" in the literature since the 1970s.

In what follows, we first briefly review some of the main highlights of the physics of the classical (optical) self-imaging effect, starting from the fundamentals of light diffraction.

When a light field encounters an object or passes through a slit (or aperture), that is physically the approximate size of that light's wavelength (λ), its propagation deviates from that predicted by the theory of geometrical optics (that light travels in straight lines). This phenomenon is a result of the wave nature of light and is termed diffraction. An important historical example of diffraction is Thomas Young's double-slit experiment [145]. In this experiment, he used three screens placed at a set distance from each other. In the first screen, he cut a narrow slit and into the second screen, he cut two slits approximately 1mm apart. When Young shone light through the single slit, the light spread out or diffracted before passing through the two narrow slits, forming two sources of light which again diffracted. On the third screen placed behind the two slits, he observed a central bright band of light that appeared with alternate light and dark bands on either side. From this experiment, he learnt that as the light waves from the two slits spread out, they come into contact and interfere with each other and form an interference pattern.

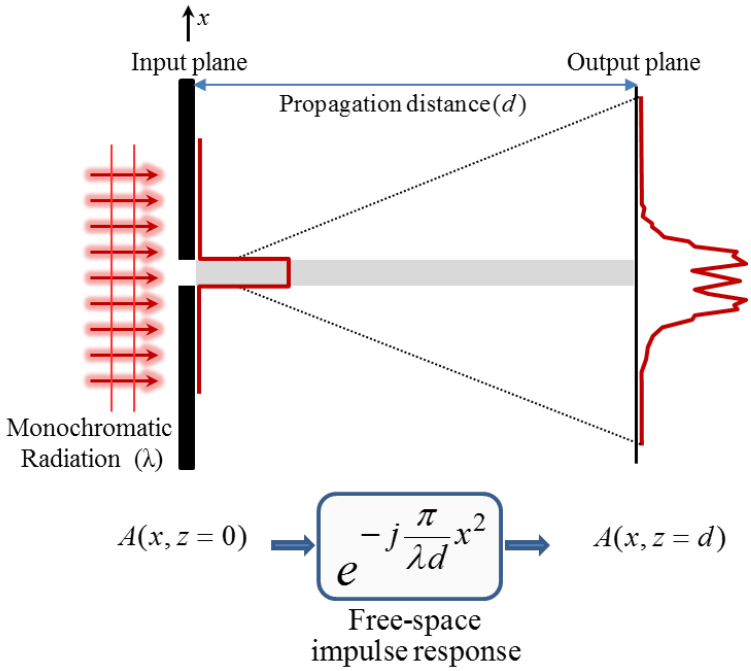

Figure 2.1 – Modelling of light Fresnel diffraction from a slit (aperture). Shaded area is the geometrical shadow of the slit. The dashed line is the width of the Fresnel diffracted light.

As detailed in classic treatments, the calculation of the light field immediately behind the diffracting object or slit is a subject of great interest. Figure 2.1 shows a slit (aperture) at the input plane illuminated by a plane-wavefront monochromatic light, and the resulting light diffraction at the output plane behind the slit, with an *x*-*z* coordinate system where *z* is the optical propagation axis and *x* is the transverse axis. For simplicity, only one transverse dimension is assumed, *x*-axis, but the same behavior would be observed in the *y*-axis. The dynamics of the complex amplitude of the light field behind the diffracting object $A(x,z=0)$ (at the input plane) is described by the wave equation approximation:

$$\frac{\partial A}{\partial z} = \frac{i}{2k}\frac{\partial^2 A}{\partial x^2} \tag{2.1}$$

where $k=2\pi/\lambda$ is the propagation constant with λ being the light wavelength. Under the so-called Fresnel approximation, this equation can be solved by the well-known Fresnel diffraction integral [146, 147]. Mathematically, this integral can be also modelled as the convolution of the complex amplitude function of the diffracting object $A(x,z=0)$ and the impulse response of light propagation in free space (sometimes called the impulse response of free space), displaying a rich set of properties associated with general linear systems [147]. This description of light propagation in free space, by an impulse response, implies that the diffraction imaging system is linear and shift invariant. The amplitude impulse response of light propagation in free space is an expanding quadratic-phase function [41]:

$$\tilde{h}_d(x) \propto exp\left(-j\frac{k}{2d}x^2\right) \tag{2.2}$$

where $z = d$ is the propagation distance (at the output plane) from the input plane. Figure 2.1 shows the diffraction pattern at the distance *d* from the illuminated slit: The intensity of the light field just behind the slit ($|A(x,z=0)|^2$) and at a distance *d* away from the input plane ($|A(x,z=d)|^2$) (i.e., the diffraction pattern) are displayed as a function of the transverse position (*x*-axis) in the input and output planes, respectively. As mentioned above, the resulting diffraction pattern can be predicted by convolving the input field amplitude $A(x,z=0)$ with the impulse response function of light propagation $\tilde{h}_d(x)$ (Eq. (2.2)).

In a linear systems, the expression for the impulse response naturally leads to the concept of the transfer function. The related transfer function of free-space propagation can be obtained by taking the Fourier transform of the impulse response in Eq. (2.2):

$$H_d(k_x) \propto exp\left(j\frac{z}{2k}\,k_x^2\right) \tag{2.3}$$

where k_x is the transverse wavenumber of the beam or spatial angular frequency. Therefore, the output light field can also be evaluated along the propagation direction by directly multiplying the *k*-space spectrum of the input field (at the input plane) and the transfer function $H_d(k_x)$. The transfer function in Eq.(2.3) implies that in *k*-space (spatial angular frequency domain), the diffraction imparts a quadratic phase shift on the light field. Indeed, this phase is a measure of the degree of beam divergence in the *x* direction.

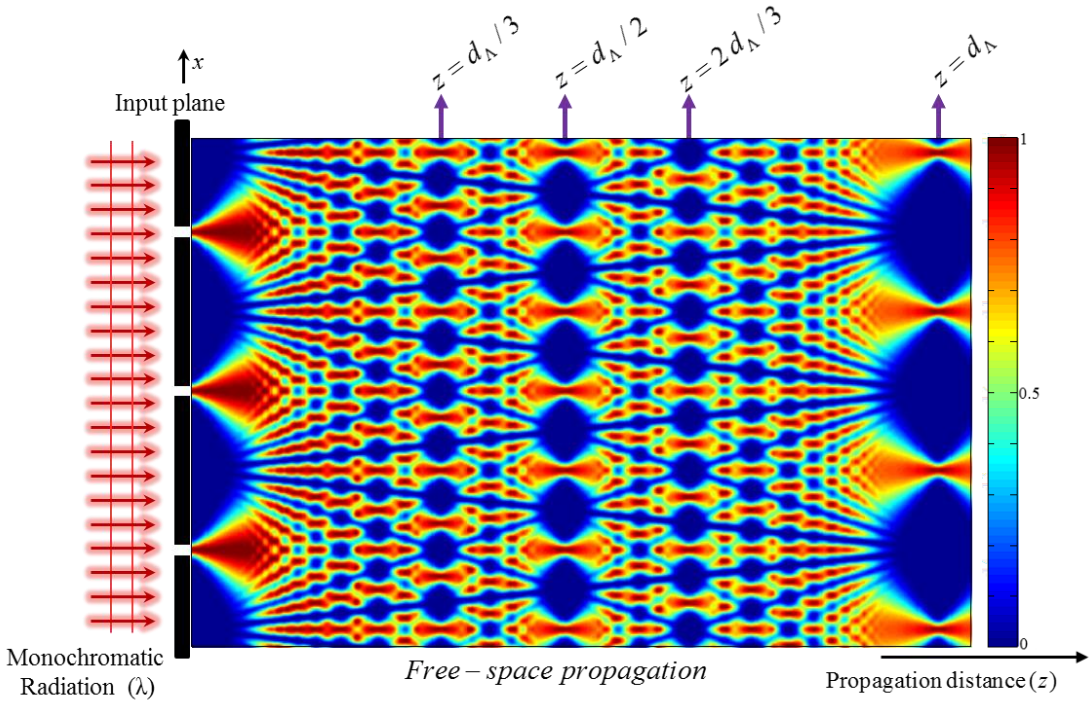

Figure 2.2 – The spatial Talbot effect for a monochromatic light, shown as a "Talbot carpet". The color-bar represents normalized signal intensity in each vertical cross-section along the propagation direction.

In the Fresnel diffraction regime, a counterintuitive situation occurs when considering not only a single slit, or a pair of them, but a periodic array of slits (or apertures), with the period of the

array Λ in the input plane, each contributing to the diffraction pattern. This is for instance the case for a spatial diffraction grating, illuminated by a monochromatic light beam. By using Fresnel diffraction theory, Eq.(2.2), one can still evaluate the transverse field amplitude along the direction of propagation *z*. Figure 2.2 shows the resulting diffraction pattern behind the input plane. Interestingly, we find that the original periodic pattern is reproduced exactly behind the input plane at distances $z = d$:

$$d = s\frac{\Lambda^2}{\lambda} \tag{2.4}$$

where $s = 2, 4, 6, \ldots$ (even integers), a formula first derived by Lord Rayleigh in 1881 [139]. This is the basic "Talbot" or "self-imaging" effect. At distances, satisfying Eq.(2.4), but for $s = 1, 3, 5, \ldots$ (odd integers), we find that the original pattern is also reproduced, but with a half-period (Λ/2) shift. Originally, the Talbot effect was only described for this basic situation according to which the field reproduces itself when *z* is a multiple of the so-called Talbot distance ($d_\Lambda = \Lambda^2/\lambda$). This is what is known as the *integer Talbot effect*.

In addition to the described reconstruction images, there also exists another set of distances where one finds other interesting diffraction patterns, Figure 2.2. At positions $z = d$, such that

$$d = \frac{s}{m}d_\Lambda = \frac{s}{m}\frac{\Lambda^2}{\lambda} \tag{2.5}$$

with $s = 1, 2, 3, \ldots$ and $m = 2, 3, 4, \ldots$, such that (s/*m*) is a noninteger and irreducible rational number, the original periodic pattern reappears, but with a periodicity of Λ/*m*. This sub-images were first identified by Winthrop and Worthington [148], and this effect now is known as the *fractional or sub-Talbot effect*. For example, at distances $z = d_\Lambda/3$ and $z = d_\Lambda/2$, the periodicity of the original pattern (in the input plane) is reduced by factors of $m = 2$ (to Λ/2) and $m = 3$ (to Λ/3), respectively. Visualization of the intriguing wave patterns behind a periodic array of slits (such as a diffraction grating) due to Talbot effect is referred to as the "Talbot carpet", resembling a Persian rug in intricate but repeating patterns, as shown in Figure 2.2. A picture of the Talbot carpet is displayed in the header of the Nature Physics website.

It is worth noting that the maximum value of m that gives rise to this effect depends only on the transverse width of the diffracting slits that constitute the original field pattern: the effect is observed only when the width of the input individual slit is narrower than Λ/m, and as a result, the different slits do not spatially overlap.

Since the advent of affordable coherent light sources in 1960s, the Talbot effect has received greater attention within the research community. In particular, the simplicity and beauty of the effect has triggered a surge of research related to coherent optical signal processing and has resulted in numerous interesting and original applications that provide competitive solutions to various scientific and technological problems [149]. In a comprehensive review, Patorski [150] compiled a detailed survey of the self-imaging phenomenon and its applications to imaging processing and synthesis, photolithography, optical testing, optical metrology, and spectrometry. This survey summarizes the progress made in this research area before 1990. There are also applications of the Talbot effect in other fields beyond traditional optics such as acoustics, Bose-Einstein condensates, electron microscopy, x rays, nonlinear optics, and quantum optics [151].

Additionally, by using the concept known as space–time duality, it is possible to transfer the spatial Talbot effect for applications in the temporal domain, representing a very powerful tool for temporal processing of periodic an aperiodic signals. The temporal counterpart of the spatial Talbot effect is referred to as the "temporal Talbot/self-imaging effect", which is the subject of the next sub-Section and the basis of the first half of this Thesis.

2.2.1 Temporal Talbot effect

There exists a well-known duality between the Fresnel (paraxial) diffraction of light beams in space and the temporal first-order dispersion of narrowband pulses in a dielectric dispersive medium. This was first pointed out by Akhmanov et al. (1968) in a general treatment of second- and third-order nonlinear optical interactions [152, 153]. This duality has been widely studied since then, and many researchers have used the similarity to propose and create temporal analogs of spatial systems [154, 69, 155].

Since we will deal extensively with the "dispersive medium" term throughout this dissertation, let us first define the characteristics of a dispersive medium. When an electromagnetic wave

interacts with a dielectric, the medium response, in general, depends on the optical frequency ω. This property, referred to as chromatic dispersion, manifests through the frequency dependence of the refractive index $n(\omega)$. This dispersion plays a critical role in the problem of propagation of short optical pulses because different spectral components associated with the pulse travel at different speeds given by $c/n(\omega)$, c being the speed of light in free space, causing pulse broadening, see Figure 2.3. Mathematically, the effects of dispersion are accounted for by expanding the propagation constant $\beta(\omega)= n(\omega)\ \omega/c$ in a Taylor series [42]. As will be detailed later in this Section, a dispersive medium can be modeled as an LTI system with a transfer function $H(\omega)=|H(\omega)|\ exp(j\ \Phi(\omega))$, with $\Phi(\omega) = \beta(\omega) \times z$ where z is the propagation distance in the dispersive medium. The Taylor expansion of $\beta(\omega)$ over a spectral bandwidth $\Delta\omega$ around the frequency ω_0 at which the pulse spectrum is centered may be written as

$$\begin{aligned}\Phi(\omega)=&\left.\frac{d\beta(\omega)}{d\omega}\right|_{\omega=\omega_0}(\omega-\omega_0)z+\frac{1}{2}\left.\frac{d^2\beta(\omega)}{d\omega^2}\right|_{\omega=\omega_0}(\omega-\omega_0)^2z+\frac{1}{6}\left.\frac{d^3\beta(\omega)}{d\omega^3}\right|_{\omega=\omega_0}(\omega-\\ &\omega_0)^3z\ldots=\beta_1(\omega-\omega_0)z+\frac{1}{2}\beta_2(\omega-\omega_0)^2z+\frac{1}{6}\beta_3(\omega-\omega_0)^3z+\ldots=\\ &\phi_1(\omega-\omega_0)+\frac{1}{2}\phi_2(\omega-\omega_0)+\frac{1}{6}\phi_3(\omega-\omega_0)+\ldots\end{aligned} \tag{2.6}$$

where

$$\phi_m=\beta_m z=\left.\frac{d^m\beta(\omega)}{d\omega^m}\right|_{\omega=\omega_0}z \tag{2.7}$$

In particular, the parameters β_1 and β_2 are related to the refractive index $n(\omega)$ and its derivatives through the relations

$$\beta_1=\frac{1}{v_g}=\frac{1}{c}\left(n+\omega\frac{dn}{d\omega}\right) \tag{2.8}$$

$$\beta_2=\frac{1}{c}\left(2\frac{dn}{d\omega}+\omega\frac{d^2n}{d\omega^2}\right) \tag{2.9}$$

The first-order term, β_1, contains the inverse group velocity, v_g, (i.e., the group delay per unit length) and describes an overall time delay without an effect on the pulse shape. The second-order

term parameter, β_2, represents dispersion of the group velocity and is responsible for pulse broadening. This phenomenon is known as group-velocity dispersion (GVD), and β_2 is the GVD parameter.

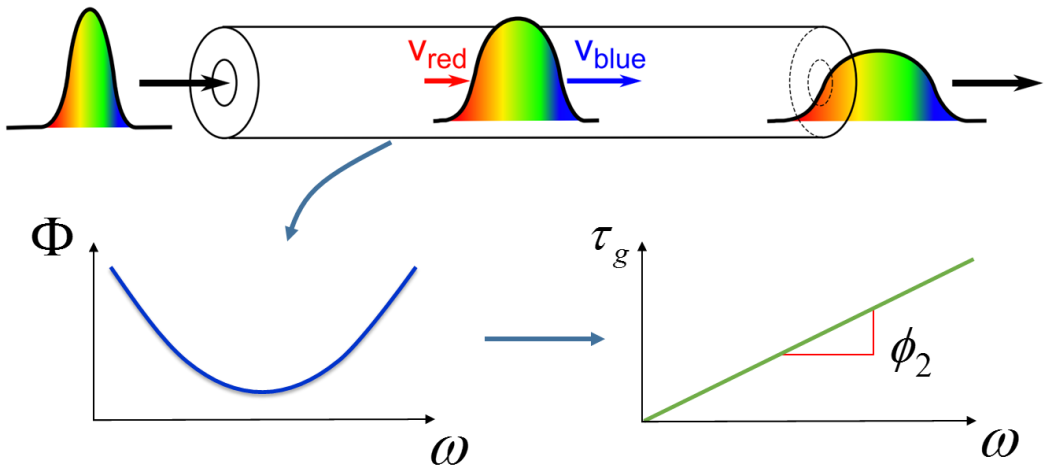

Figure 2.3 – Characterization of a first-order dispersion medium.

In addition to these two parameters, higher-order parameters also appears in Eq. (2.6). The coefficient β_3 appearing in Eq. (2.6) is called the third-order dispersion (TOD) parameter. Higher-order dispersive effects can distort ultrashort optical pulses both in the linear and nonlinear regimes. As the contribution of the higher-order dispersion terms in most typical dielectric media and structures (e.g., optical fibers) is quite small for picosecond pulses, these terms can be neglected in our following discussions. In the absence of higher-order dispersive effects, retaining only the two first terms of the Taylor expansion of the dispersive medium, $\Phi(\omega)$ is approximated by a quadratic function, as shown in Figure 2.3. This approximation is referred to as first-order dispersion approximation, leading to $H(\omega)$ having an all-pass amplitude with a quadratic phase response. Therefore, the group delay of the dispersive medium, defined as $\tau_g = d\Phi(\omega)/d\omega = \phi_1 + \phi_2(\omega-\omega_0)$, exhibits a linear variation as a function of frequency. A first-order dispersive medium is characterized by the slope of the group delay as function of ω, ϕ_2, referred to as the first-order dispersion coefficient. As mentioned above, the first-order dispersion coefficient is related to the GVD parameter β_2 through $\phi_2 = \beta_2 \times z$.

Now, going back to the space-time duality, let us consider the temporal analogue of a slit or aperture. A good representation is provided by a short light pulse in the time domain. The pulse

width and shape correspond to the width and shape of the individual slit. The temporal analogue of diffraction is group velocity dispersion, and the propagation of a pulse with amplitude $A(t, z=0)$ in a dispersive medium is described by

$$\frac{\partial A}{\partial z} = \frac{i\beta_2}{2}\frac{\partial^2 A}{\partial t^2} \tag{2.10}$$

where $t = \tau - z/v_g$ is the retarded time. As a matter of fact, equations (2.1) and (2.10) are mathematically equivalent. It is important to note that both equations represent an approximated form of the wave equation. The paraxial approximation is used in Eq. (2.1), which assumes that the field amplitude $A(x, z)$ varies slowly with z on the scale of a wavelength, whereas the derivation of Eq. (2.10) uses the slowly varying envelope approximation, which assumes that the amplitude $A(t, z)$ varies slowly with z on the scale of an optical cycle. The only difference between diffraction and dispersion is that the GVD parameter β_2 in Eq. (2.10) can be positive or negative, whereas the propagation constant k in Eq. (2.1) can be only positive. This implies that in the case of diffraction, the free-space propagation necessarily exhibits a positive wavelength-distance product ($\lambda \times z$), i.e., high spatial frequencies travel faster laterally than low spatial frequencies. In contrast, in case of group velocity dispersion, a normal dispersive medium ($\beta_2 > 0$), such as dispersion compensating fibers, exhibits a positive frequency chirp ($\beta_2 z > 0$) – low frequencies travel faster than high frequencies – and an anomalous dispersive medium ($\beta_2 < 0$), such as conventional single-mode optical fibers, exhibits a negative group delay ($\beta_2 z < 0$) – high frequencies travel faster than low frequencies. The possibility of having positive or negative dispersion adds an important extra degree of versatility to design and build optical information processors.

The duality between the temporal dynamics of optical waveforms and the spatial evolution of optical beams is based on the mathematical equivalence between Eqs. (2.1) and (2.10). In particular, the free-space propagation distance in the spatial-domain light propagation, which determines by how much a beam is diffracted, is analogous to the total group delay dispersion, ϕ_2, in a dispersive medium.

As mentioned above, in the Fourier domain, the transfer function of free-space diffraction imparts on the field a quadratic phase shift in k-space. Similarly, in the linear regime, the transfer function of first-order dispersion imparts a quadratic spectral phase in the frequency domain:

$$H(\omega) \propto exp(j\,\Phi(\omega)) = exp\left(j\frac{\beta_2\, z\, \omega^2}{2}\right) = exp\left(j\frac{\phi_2 \omega^2}{2}\right) \tag{2.11}$$

Since the linear term of $\Phi(\omega)$, β_1, represents a temporal delay and does not affect the pulse shape, it can be neglected for the discussions at hand, without loss of generality. Eq.(2.11) describes pulse distortion in dispersive media that provide nearly a constant amplitude response and a quadratic phase response (i.e., linear group delay) over the pulse's bandwidth. The related impulse response $\tilde{h}\,(t)$ of a dispersive medium can then be obtained by taking the inverse Fourier transform of this transfer function:

$$\tilde{h}\,(t) \propto exp\left(-j\frac{1}{2\beta_2 z}t^2\right) = exp\left(-j\frac{1}{2\phi_2}t^2\right) \tag{2.12}$$

The temporal impulse response in Eq. (2.12) has the same mathematical structure as the spatial impulse response in Eq. (2.2), which definitely shows that the distortion of a pulse in a dispersive medium, because of first-order chromatic dispersion, is mathematically identical to Fresnel diffraction.

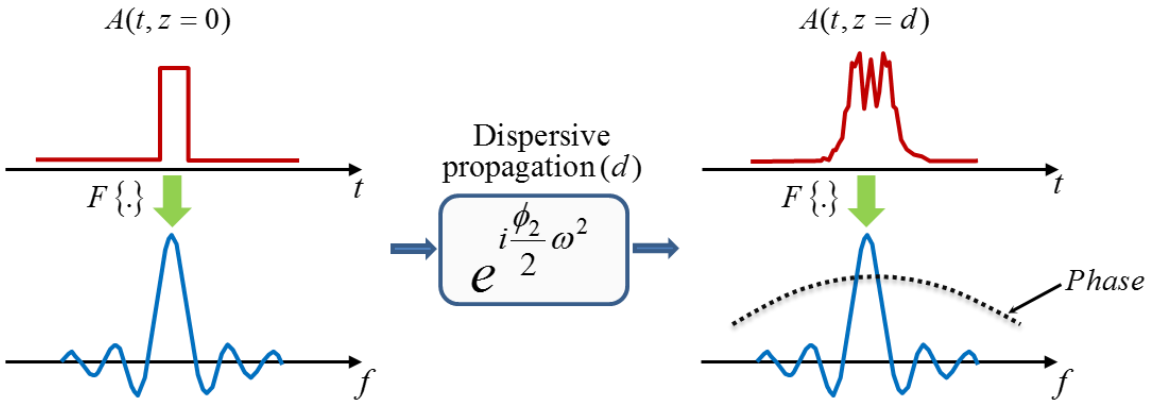

Figure 2.4 – Propagation of a temporal rectangular pulse through a first-order dispersive medium. *t*: time; *f*: frequency; F{.}: Fourier transform.

Figure 2.4 shows the analog of Fresnel diffraction (depicted in Figure 2.1) in the time domain when a temporal rectangular pulse is transmitted through a dispersive medium. In this case, the spectrum of the output waveform acquires a quadratic phase shift imposed by the dispersive medium. Examples of dispersive media widely used in the context of optical communications and

related applications include optical fibers, linear chirped fiber Bragg gratings (LC-FBGs)[17], prisms, and diffraction gratings [156, 41].

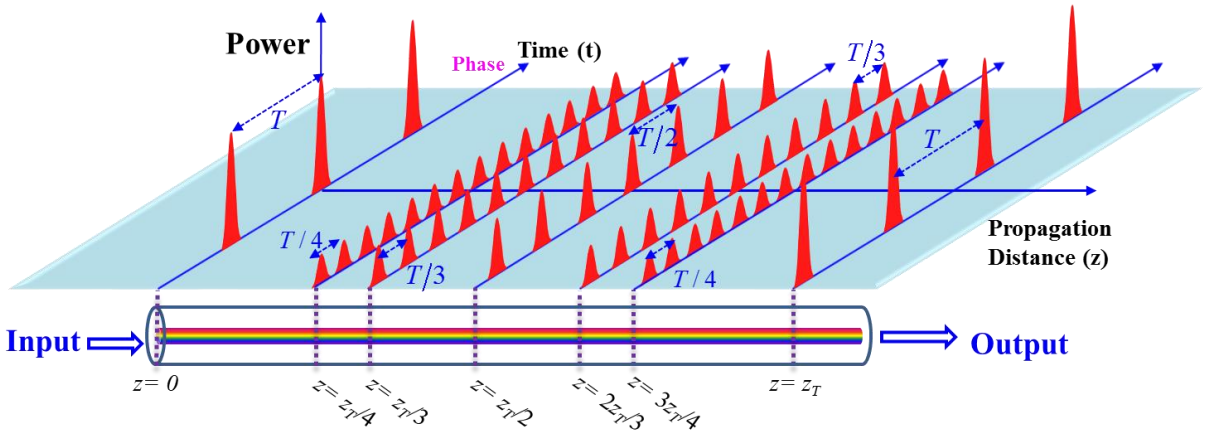

Figure 2.5 – Temporal Talbot effect. Evolution of a repetitive input pulse train through propagation along a first-order dispersive medium.

The other basic spatial propagation geometry that illustrates the space–time duality is the spatial Talbot effect. The temporal counterpart of the Talbot effect occurs when a periodic temporal signal (the temporal analogue of a periodic array of slits), for instance a stream of short optical pulses repeating with temporal period of T, e.g., as generated from a mode-locked laser, propagates through a dispersive medium, under first-order dispersion conditions. The temporal Talbot effect was first described by Jannson and Jannson [132], who proposed using the effect for the transference of information contained in periodic signals along an optical fiber. As can be observed in Figure 2.5, as the periodic temporal pulses propagate along the dispersive medium, such as an optical fiber, they broaden until their wings begin to overlap. At this point one usually considers further propagation of no use because the pulses do not retain their individuality, a detrimental effect for information transfer. However, when the propagation continues on, the broaden pulses in the stream start to interfere and by way of analogy, we expect that at a certain distance the original pulse train will be exactly replicated (*integer temporal self-imaging effect*).

[17] LC-FBG is a periodic perturbations of the refractive index along the core of an optical fiber. A LC-FBG, working in reflection, provides a propagation delay that is a linear function of frequency over its reflected spectral band, therefore, different frequencies of the input signal are reflected at different times [42].

At some other distances, the original pulse sequence reappears but with a repetition-rate that is an integer multiple of the original one (*fractional temporal self-imaging effect*).

The derivation of the mathematics of temporal Talbot effects has been covered in deep detail by Azaña et al (2001) [41]. We briefly review this derivation and conditions for the formation of temporal Talbot images in a dispersive medium.

Figure 2.5 represents the evolution of an input periodic signal through propagation along a first-order dispersive medium; here a piece of optical fiber is assumed, where the slope of group delay increases linearly with the propagation distance, i.e., $\phi_2 = \beta_2 \times z$. The complex envelope of the input periodic signal $A_{in}(t)$, shown in Figure 2.5 at $z = 0$ (where z represents the axial propagation coordinate) can be expressed as

$$A(t, z=0) = A_{in}(t) = \sum_{p=-\infty}^{\infty} a_0 (t - pT) \tag{2.13}$$

where $a_0(t)$ (signal in each period or individual pulse) is an arbitrary complex function in the interval $|t| \leq T/2$, and $a_0(t) = 0$, for $|t| > T/2$. Obviously, the corresponding average optical power is also a periodic function, i.e., $P_{in}(t) = | A_{in}(t) |^2 = \sum_{p=-\infty}^{\infty} P_0(t-pT)$, with $P_0(t) = | a_0(t) |^2$.

As mentioned above, the linear propagation through a dispersive medium under the first-order dispersion approximation can be characterized by the spectral transfer function in Eq.(2.11), or the related temporal impulse response in Eq.(2.12). In this way, the complex envelope $A_{out}(t)$ of the output pulse can be obtained by convolving the complex envelope of the input pulse $A_{in}(t)$ with the impulse response function Eq.(2.12). Alternatively, one can also operate in the frequency domain: the output complex envelope spectrum $\hat{A}_{out}(\omega)(=\mathcal{F}\{A_{out}(t)\})$ ($\mathcal{F}$ represents Fourier transform) can be obtained by directly multiplying the spectrum of the input complex envelope $\hat{A}_{in}(\omega)(=\mathcal{F}\{A_{in}(t)\})$ and the spectral transfer function $H(\omega)$ in Eq.(2.11):

$$\hat{A}_{out}(\omega) = \hat{A}_{in}(\omega) \times H(\omega) \tag{2.14}$$

The output signal complex envelope is simply found by taking the inverse Fourier transform of the output spectrum $A_{out}(t) = \mathcal{F}^{-1}\{ \hat{A}_{out}(\omega)\}$ ($\mathcal{F}^{-1}$ represents inverse Fourier transform). As mentioned above, in the chosen dispersive medium, an optical fiber, the dispersion value increases

linearly with the propagation distance z ($\phi_2 = \beta_2 \times z$) which in turn affects the spectral transfer function $H(\omega)$. Therefore, for different propagation distances, we expect to observe various forms of output signal. At some specific distances, the original signal is reconstructed (self-imaged) either with the same or a multiplied repetition-rate. For instance, as shown in Figure 2.5, the input pulse train is exactly self-imaged after dispersive propagation through an integer multiple of the Talbot distance (integer Talbot self-images) defined as:

$$z_T = s\frac{T^2}{2\pi\beta_2} \tag{2.15}$$

where s = 1, 2, 3, …. Similar to spatial Talbot effect, for even values of s, we find that the output signal is an exact replica of the input signal. For odd values of s, we find that the original periodic signal is also reproduced but with a half-period shift $T/2$, recall that the time variable 't' is relative to group delay, therefore, the $T/2$ delay is in addition to the group delay. In summary, if the repetition period of the input pulse train verifies condition (2.15), the signal is reproduced without undergoing distortion. In addition to the described reconstruction images, one finds other interesting patterns. At fractional distances of:

$$z = \frac{s}{m}z_T = \frac{s}{m}\frac{T^2}{2\pi\beta_2} \tag{2.16}$$

with s = 1, 2, 3, …, m = 2, 3, 4, . . ., such that s/m is a noninteger rational number, the output signal is a copy of the periodic input signal (where an individual pulse maintains its shape and temporal width), but with a repetition-rate m times that of the input signal. In this case, ideally the individual pulse power is correspondingly decreased by the factor of m, ignoring the insertion losses of the dispersive medium. Figure 2.5 shows examples of output pulse trains at the fractional Talbot distances $z = z_T/4$, $z_T/3$ and $z_T/2$ where the input repetition-rate has been multiplied by factors of m = 4, 3 and 2, respectively. Note that this rate multiplication process only multiplies the repetition-rate of the signal's intensity, while the spectrum magnitude remains unchanged, thus leaving a deterministic pulse-to-pulse residual temporal phase structure on the output pulse train. It is also worth mentioning that the maximum repetition-rate at the output is only limited to the input pulse width. The input pulse width must be short enough to prevent pulse overlapping in the multiplied output train; in particular, assuming that the Talbot condition is satisfied, then $m \leq D_{out\_\max}\, T/t_{in}$

where t_{in} is the input pulsewidth and D_{out_max} is the maximum duty cycle of output pulses before pulse-overlapping occurs [118]. This is a fundamental limitation that is imposed by the input low-rate source specifications (i.e., temporal pulsewidth) and that applies to all linear repetition-rate multiplication methods.

Mathematically, the absolute value of the output signal for a given set of parameters, *m* and *s*, may be written as [41]:

$$|A_{out}(t)| = \frac{1}{\sqrt{m}} \sum_{p=-\infty}^{\infty} |a_0\left(t - \frac{p}{m}T\right)|, \ (m \cdot s)\ even \tag{2.17}$$

$$|A_{out}(t)| = \frac{1}{\sqrt{m}} \sum_{p=-\infty}^{\infty} |a_0\left(t - \frac{p}{m}T - \frac{T}{2m}\right)|, \ (m \cdot s)\ odd$$

Another intuitive way to visualize the principle of the temporal Talbot effect is to use joint time-frequency (TF) representations of the involved signals, as shown in Figure 2.6. For each TF representation, the bottom plot represents the temporal variation of the pulse train and the plot at the left represents the corresponding spectrum, with the 2-D energy distribution shown in the larger, central plot. For the input signal, for example, this representation shows that each pulse in time domain is composed by all the discrete frequency components or equivalently, each frequency components is involved in the formation of each and all of the temporal pulses. Figure 2.6(a), as a first example, shows the case when the integer Talbot effect is considered (i.e., m = 1). The dispersive medium, with dispersion slope of $\phi_2 = \beta_2 \times z = T^2/2\pi$ (Eq.(2.16) with m =1), introduces a group delay ($\Delta\tau_g = \phi_2 \Delta\omega$) of T between two adjacent discrete frequency components with frequency spacing of F (= 1/T), i.e., $\Delta\omega = 2\pi/F$. Therefore, the frequency components of the pulses are redistributed into different temporal positions separated again by input pulse period of T. Spectral superimposition of the resultant dispersed pulse train produces an exact self-image of the original pulse train at the fiber output, as illustrated in Figure 2.6(a), right.

Figure 2.6(b) shows the case when we target a multiplication factor of two (m = 2). The dispersion coefficient is set to $\phi_2/2 = \beta_2 \times z/2 = T^2/4\pi$ (Eq.(2.16) with m =2). The propagation of the pulse train through the same amount of dispersion now induces a delay of $T/2$ between two adjacent discrete frequency components with frequency spacing of F (= 1/T) leading to the

predicted creation of new pulses along the time domain with a temporal period of $T/2$, as shown in Figure 2.6(b).

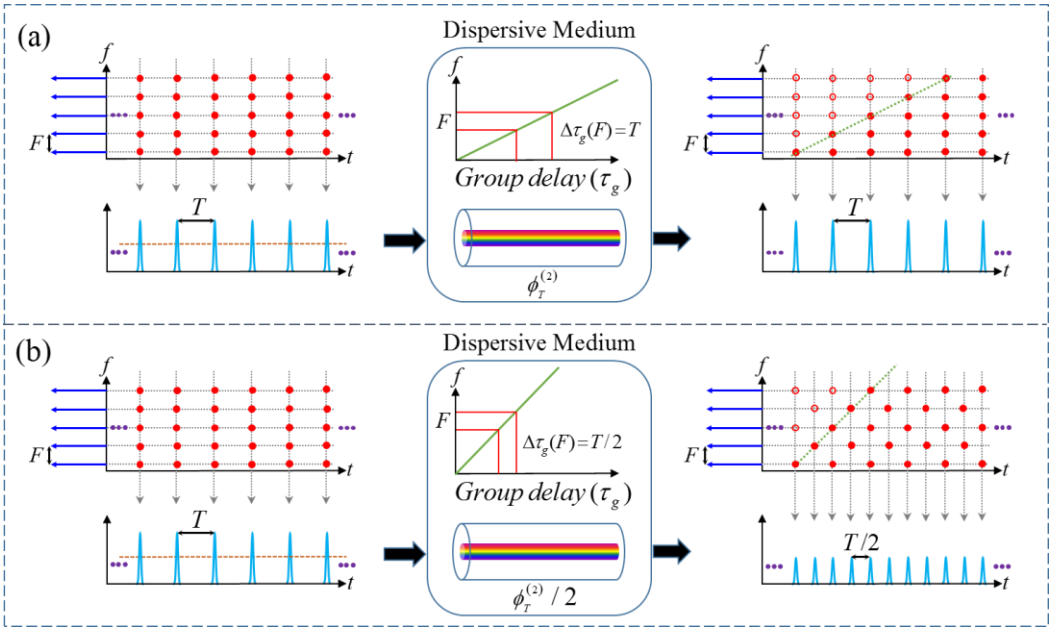

Figure 2.6 – Joint time-frequency (TF) illustration of the temporal Talbot effect. *t*: time; *f*: frequency.

As mentioned above, other than optical fibre, there exist a variety of dispersive media, such as LC-FBG, with which to impose the required spectral phase for observing the Talbot effect, i.e. so long as they provide linear first-order dispersion over the bandwidth of the pulse train [157], see Figure 2.7(a). An alternative method for applying the required spectral phase filter without dispersive delay is spectral line-by-line pulse shaping, enabling individual control of the phase on each discrete spectral component of the optical pulse train as illustrated in Figure 2.7(b) [158]. We define the frequency of spectral lines of the input signal as $\omega_n=\omega_0+n\omega_i$ where ω_0 is the central radial frequency of the signal, ω_i is the frequency spacing between the pulse train's spectral lines equal to the pulse repetition-rate, i.e., $\omega_i=2\pi f_0= 2\pi/T$, and n is an integer. The phase shifts to be applied to the different spectral lines of the input signal, $\omega_n=\omega_0+n\omega_i$, by a line-by-line pulse shaper, to obtain repetition-rate multiplication with a factor of m, is [158]:

$$\phi(\omega_n)=\frac{s}{m}\pi\, n^2 \tag{2.18}$$

Indeed, the multistep spectral phase in Eq.(2.18) is obtained from the phase term in Eq.(2.11), when only considering the relevant set of spectral phases at frequencies ω_n. The output pulse train after the pulse shaper is similar to the result shown in Figure 2.7(a). We notice again that, in both cases, only the intensity profile is multiplied, and the output train exhibits a pulse-to-pulse phase variation, not shown in the figures.

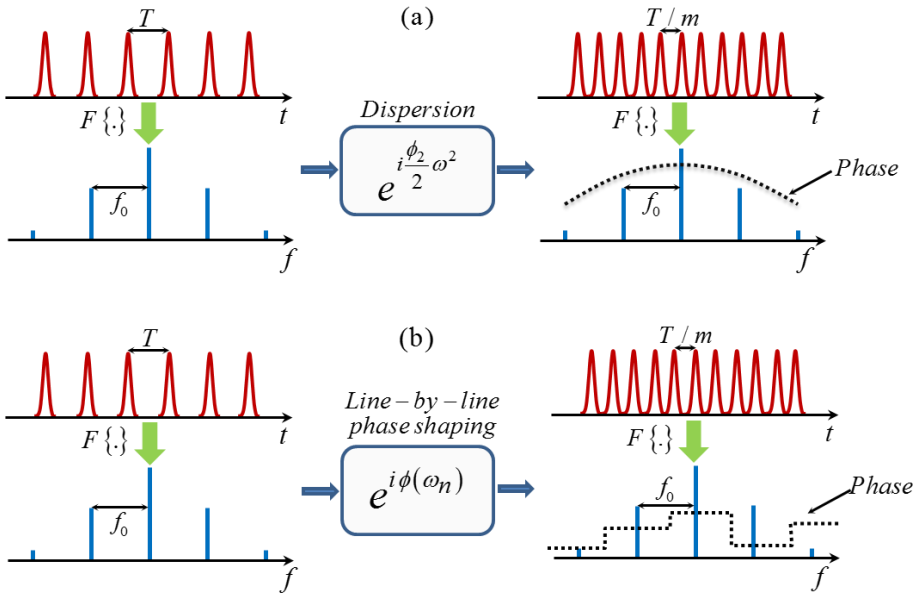

Figure 2.7 – Implementation of the temporal Talbot effect using (a) a quadratic phase-only filter and (b) line-by-line phase-only filtering. *t*: time; *f*: frequency, $\omega_n=\omega_0+n\omega_i$ and $\omega_i=2\pi f_0$.

2.2.2 The spectral Talbot effect

In addition to the duality between space and time, a duality between time and frequency has been also identified [66, 159]: the function of the dispersion operator in the frequency domain is equivalent to the function of a time-lens operator in the time domain. The latter refers to the time-domain counterpart of a spatial thin lens, and is essentially characterized by a quadratic phase temporal modulation of the form

$$p(t) \propto \exp\left(j\frac{\alpha}{2}t^2\right) \tag{2.19}$$

where α is the linear chirp coefficient of the time-lens process. An important consequence of this duality is the frequency-domain counterpart of the temporal self-imaging effect, the so-called spectral self-imaging (Talbot) effect [159]. Spectral self-imaging (Talbot) effect occurs when a periodic sequence of optical pulses (periodic comb in the frequency domain) is linearly chirped by a time-lens process. Under specific temporal linear chirping conditions, the input periodic frequency comb is essentially unaffected by the time lens (integer spectral self-imaging), whereas for other linear chirping conditions, the free spectral range (FSR) of the frequency comb is divided by an integer factor (fractional spectral self-imaging), without undergoing any further distortion in its spectral envelope, as shown in Figure 2.8(a).

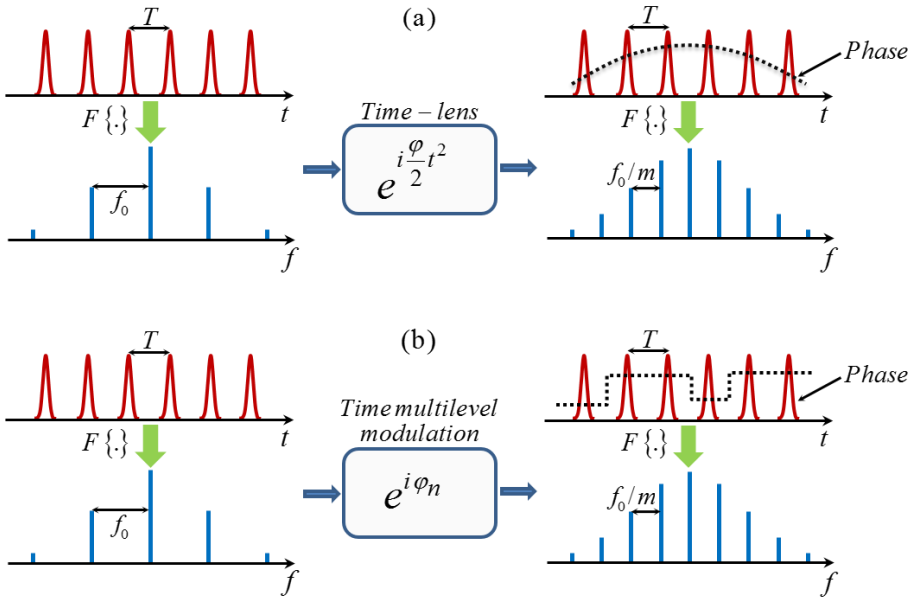

Figure 2.8 – Illustration of the spectral Talbot effect (a) using quadratic phase modulation in the time domain (time lens) and (b) by multilevel time phase modulation. *t*: time; *f*: frequency.

The spectral self-imaging condition on the linear chirp coefficient can be obtained from the frequency-domain analog of the well-established temporal self-imaging theory [41] such that the needed temporal phase modulation function is:

$$\varphi(t) = \frac{\alpha}{2}t^2 = \frac{s}{m}\frac{\pi}{T^2}t^2 \tag{2.20}$$

where the positive integer m is the FSR division factor induced by the spectral self-imaging effect under consideration (m = 1 for integer effects and m = 2, 3, … for fractional effects), and s is an arbitrary positive integer such that s and m are co-prime. We recall that when Eq.(2.20) is satisfied, the comb spectral envelope is unchanged after temporal phase modulation (time-lens) either (i) keeping the same FSR as the input (integer effects, m = 1) or (ii) with a reduced FSR by a factor m (fractional effects, m = 2, 3, 4, …).

Similarly, again by calculating the relevant temporal phase shifts in Eq.(2.20) according to the pulse positions in the input pulse train, it is straightforward to conclude that an appropriate time-domain periodic multistep phase modulation of the pulse train also leads to the spectral self-imaging effect. The phase shifts are directly derived from Eq.(2.20), yielding

$$\varphi_n = \frac{s}{m}\pi\, n^2 \tag{2.21}$$

where φ_n is the phase shift applied on the pulse n in the sequence. If these phase shifts are reduced to a 2π range, a periodic sequence of phase steps is obtained. A schematic diagram of the spectral self-imaging effect by the alternative time-domain multilevel phase modulation is sketched in Figure 2.8(b). We will use the multistep phase modulation method to induce spectral self-imaging in our proposals in this Chapter.

2.2.3 Applications of temporal Talbot effect

Since the discovery of the temporal Talbot effect, besides the intrinsic physical interest of the phenomenon itself, the effect has found main practical applications in various scientific areas. The primary motivation to use the temporal Talbot effect comes from the fact that, as mentioned above, the phenomenon can be exploited to multiply the repetition-rate of periodic pulse sequences through fractional Talbot effect. Generation of optical pulse trains with ultrahigh repetition-rate is of great interest for future ultrahigh-rate optical communications and optical computing systems, ultrafast data processing, and other scientific areas [133, 41, 134, 135, 136]. In addition to this popular application of the temporal Talbot effect, there have been other sets of applications. For instance, the inherent buffering ability of the temporal Talbot effect have been leveraged for the realization of an optical clock recovery technique from RZ optical communication data [100, 99].

Additionally, the temporal Talbot effect was used as the central component of an invisibility cloaking system proposed in [160], which exploits temporal interference to generate intensity gaps about the time domain, and was also employed in pulsed fiber lasers for suppressing dispersion effects [161]. This phenomenon has been also investigated theoretically to be an accurate technique for measuring the first-order dispersion coefficient of dispersive media [135]. In quantum mechanics realm, the temporal Talbot effect also has a potential application in the temporal domain for multiplying the repetition-rate of two-photon pulse trains [162].

In this Section, we focus our attention on reviewing two of the Talbot effect's most prominent applications in the time domain: energy-preserving pulse repetition-rate control and clock recovery from data signals.

As mentioned in the introduction Chapter, extensive research has been devoted to develop techniques for generating optical pulse sequences at repetition-rates beyond those achievable by conventional mode-locking techniques or by direct modulation of semiconductor lasers. The fractional Talbot effect can be applied for increasing the repetition-rate of a periodic optical pulse sequence, without affecting the individual pulse features (shape and duration) and essentially without loss of energy, simply by propagating the original sequence through a suitable first-order dispersive medium. Figure 2.9 shows the diagram of a repetition-rate multiplier based on the temporal Talbot effect implemented by using either an optical fiber or a LC-FBG as the dispersive medium.

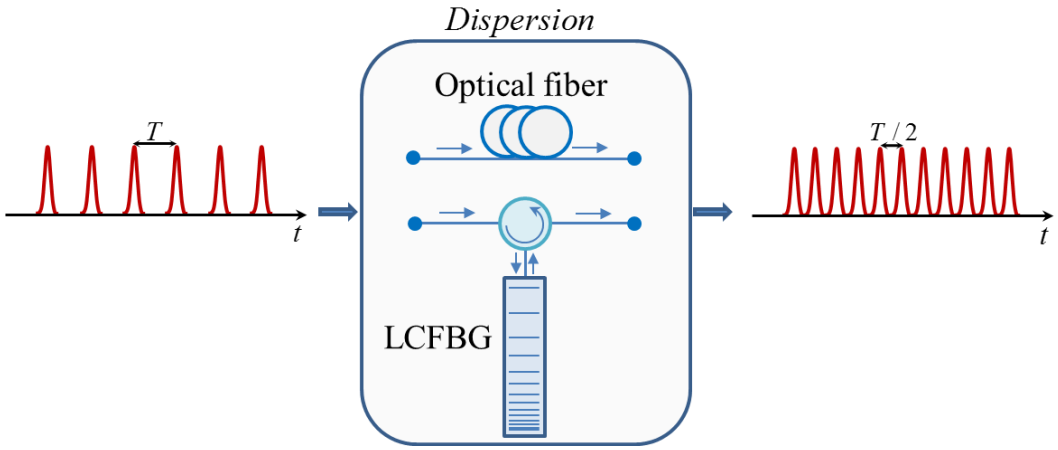

Figure 2.9 – A repetition-rate multiplier based on temporal Talbot effect; rate multiplication by a factor of *m*=2 is shown here. *t*: time.

For a given input pulse sequence with a temporal period of T (output of a fiber mode-locked laser, for example), the dispersive medium is designed to satisfy Eq.(2.16) for a target rate multiplication factor, m.

Figure 2.9 shows the dispersed output intensity which is constituted by pulses with identical intensity shape but the repetition-rate increased by a factor of m (we schematically show an example of a rate multiplier based on the temporal Talbot effect with $m = 2$ in this figure). Using this method, repetition-rates beyond the THz regime can be obtained from typical mode-locked sources operating at a few GHz [163]. For example, Figure 2.10 shows experimental results of a repetition-rate multiplier based on the temporal Talbot effect, reported in [120], fed by a 10-GHz input pulse train. The dispersive medium is set to a rate multiplication factor of $m = 10$. The autocorrelation traces of the 10-GHz input and 100-GHz output signals are displayed in Figure 2.10.

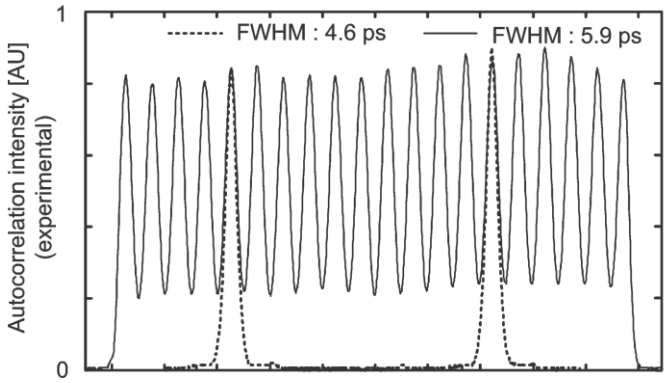

Figure 2.10 – Experimental results of rate multiplication based on temporal Talbot effect. Autocorrelation of the input 10-GHz train (dotted line) and of the output 100-GHz train (solid line) [164].

Note that this multiplication technique only multiplies the repetition-rate of the signal's amplitude envelope, while the spectrum magnitude remains unchanged. The resulting multiplied self-images exhibit pulse-to-pulse phase variations, hence the process is being often referred to as pseudo-multiplication. Nonetheless, such a technique is sufficient for applications in which the signal phase is irrelevant; otherwise various approaches, such as cross phase modulation in nonlinear fibers [165, 166], can be used to achieve true rate multiplication from the Talbot-multiplied output pulse train.

Regarding our discussion in Chapter 1, a repetition-rate multiplication system based on temporal Talbot effect has a very simple structure including only a dispersive medium, a purely fiber-optics configuration, higher energy efficiency and it is robust against possible misalignments. Despite these advantages, however, a Talbot-based rate multiplier requires the use of a proper, fixed amount dispersion for a given multiplication factor, *m*, as such it is not straightforward to tune or programme the rate-multiplication factor. As can be inferred from Eq.(2.16), for a given input signal with a repetition period of *T*, the amount of dispersion to achieve a desired fractional self-image is inversely proportional to the multiplication factor, *m*. Hence, in order to modify the multiplication factor in this technique, one needs to change the dispersive medium accordingly. This has been the primary obstacle to realize a tunable multiplication technique based on dispersion-induced Talbot effect, owing to the fact that available dispersive media (e.g., optical fibers or LC-FBGs) do not possess the flexibility to modify their group delay dispersion without mechanical manipulation. There have been some efforts to alleviate this problem by designing tunable dispersive media so as to modify the dispersion for various Talbot conditions, corresponding to different multiplication factors [167, 168]. For instance in [167], as shown in Figure 2.11(a), identical LC-FBGs are interconnected via multiport switches and the dispersion is tuned by those switches, or in [168], as shown in Figure 2.11(b), a mechanically tunable LC-FBG has been used where the dispersion is tuned by adjusting the bending angle. Nevertheless, in addition to their inherent complexity, all these schemes exhibit very limited reconfigurability (i.e., tuning range of the rate-multiplication factor). Later in this Chapter, we demonstrate an electrically-tunable, fiber-optics pulse repetition-rate multiplication approach based on dispersion-induced temporal Talbot effect, in which the output pulse repetition-rate can be electrically reconfigurable to be any integer multiple of the input repetition-rate.

For the second example of temporal Talbot effect applications, we gear our focus towards a system-level application within the context of high speed communication systems. More specifically, we review briefly an all-optical clock recovery scheme for RZ transmission systems utilizing the temporal Talbot effect as the core of the described recovery process. Since the temporal Talbot effect is based on the interference of dispersed pulses, there is no direct one-to-one correspondence between the input and output pulses. As a result, the effect has an interesting inherent ability to generate a regular pulsed output, even for an aperiodic train of pulses.

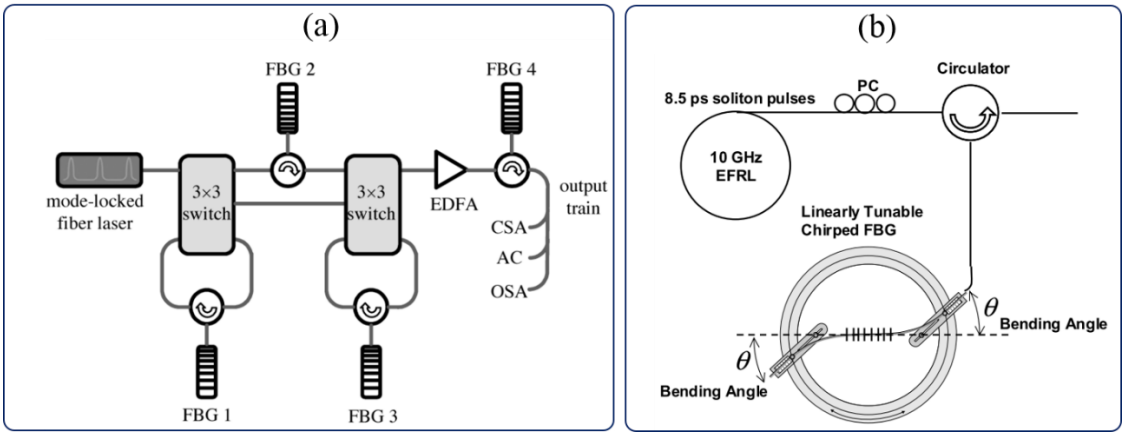

Figure 2.11 – (a) Cascading LC-FBGs interconnected via multiport switches [167], (b) Mechanically tunable LC-FBG [168].

This inherent property of the temporal Talbot effect has been applied toward a simple, passive, and polarization-insensitive all-optical base-rate clock recovery scheme for RZ transmission systems by Pudo et al [100, 99]. The term base-rate refers to the fact that, in the clock recovery process, the repetition-rate of the output signal is equal to the input data signal's bit rate. For this purpose, the integer temporal Talbot effect (when $m = 1$) is used for designing the clock recovery setup.

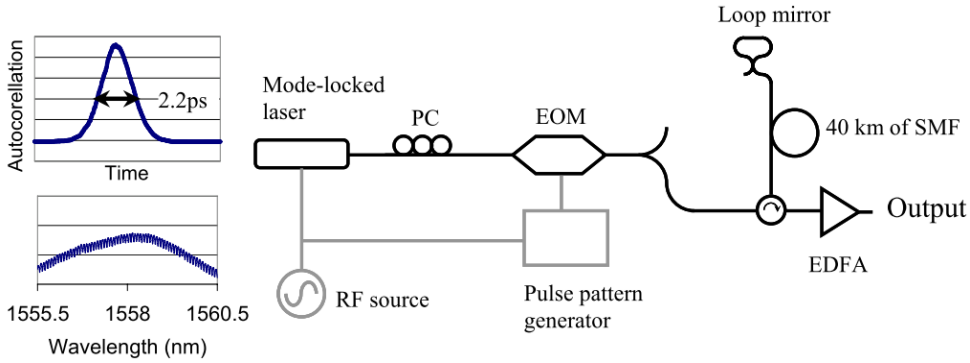

Figure 2.12 – Experimental setup used for proof-of-principle demonstration of all-optical clock recovery using the temporal Talbot effect. The insets depict the autocorrelation and optical spectrum of the input pulses [100, 99].

Figure 2.12 depicts the experimental setup of the clock recovery technique [100, 99]. The output from a mode-locked fiber laser at 9.25 GHz is modulated by an electro-optic Mach–Zehnder

modulator (EOM) driven by a pulse pattern generator. The generated data signal was then propagated through an 80 km of optical fiber, acting as a Talbot self-imaging system.

Figure 2.13 shows the experimental demonstration of the all-optical clock recovery. In particular, it shows how an input sequence consisting of ones and zeros (observed by an eye diagram with a zero base line) is transformed after propagation into a sequence of only ones (an eye diagram without zero base line).

In Chapter 3, we extend this clock recovery technique and use the buffering ability of the temporal Talbot effect to produce periodic sub-harmonic (rate-divided) pulse trains from aperiodic RZ data signals, i.e. sub-harmonic clock recovery.

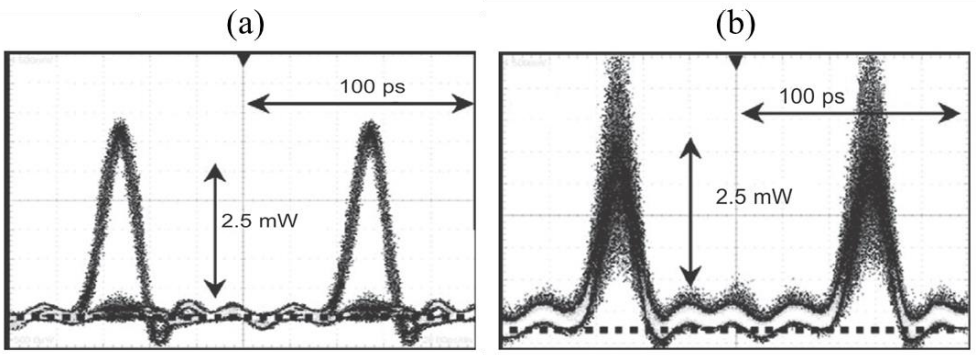

Figure 2.13 – Experimental demonstration of the temporal Talbot effect for restoring an imperfect sequence. (a) Eye diagram of the input signal. (b) Output after travelling through the dispersive medium satisfying the integer Talbot condition [100, 99].

2.2.4 Influence on random amplitude noise and timing jitter

Amplitude fluctuations (pulse-to-pulse fluctuations) and timing jitter are two major issues limiting the performance of any application relying on the precise regularity and periodicity of optical pulse trains. All-optical sampling, frequency metrology, and optical clock schemes [169, 170] are especially sensitive to any variations in the pulse amplitude and timing. Therefore, the amplitude fluctuations and timing jitter characteristics should be considered as critical parameters in the generation of stable pulse sources. There have been many theoretical and experimental works to investigate and reduce the timing jitter and amplitude noise in optical pulse sources [171, 172, 173, 174, 175, 176, 170, 177]. These methods include using an intracavity etalon [174], using

optical injection into the laser cavity [176], exploiting the dispersion effect inside the cavity [175], using phase modulation followed by dispersion outside the laser cavity [170], etc.

It has been shown that the temporal Talbot effect also has an intrinsic property of mitigating the standard deviation of both amplitude fluctuations and timing jitter present on an optical pulse train [178, 179, 180], either when used for multiplying the initial repetition-rate (fractional Talbot effect) or when the repetition-rate is kept unchanged (integer Talbot effect) - another interesting property of the Talbot effect. Fernández-Pousa et al. [179] first theoretically demonstrated that a fluctuating timing jitter within a single input pulse period, where for example, the pulse's edges suffer from larger variations than their peak, is smoothened at the output. In Pudo et al. [178], it was also predicted that the Talbot effect has mitigating properties on both amplitude noise and timing jitter with a Gaussian distribution, and developed simple expressions to predict the standard deviations of the amplitude fluctuations and timing jitter of an input pulse train subject to the temporal Talbot effect. Finally, Malacarne et al. analyzed the noise performance of a set of commonly equivalent spectrally periodic phase-only filters for implementing pulse repetition-rate multiplication. To best of my knowledge, the only experimental demonstration of timing jitter reduction through integer temporal Talbot effect was reported in [180].

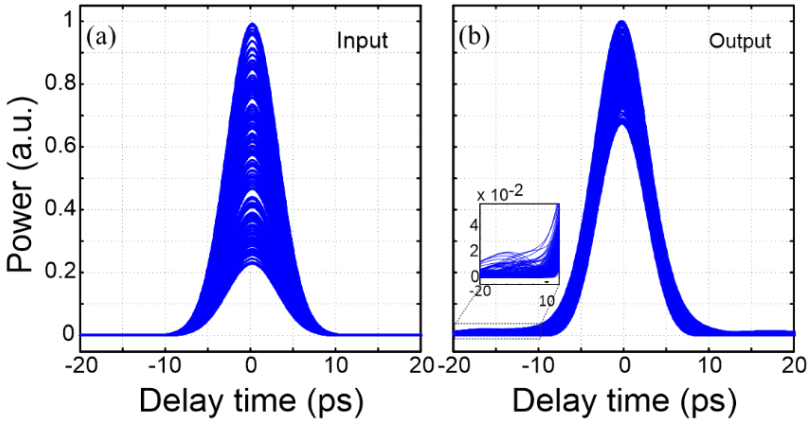

Figure 2.14 – Pulse-to-pulse amplitude fluctuation mitigation of an input signal after Talbot propagation (*m*=1). Input pulse sequence consists of 7ps FWHM Gaussian pulses with a temporal period of 100ps, i.e., the repetition-rate of 10GHz. The amplitude modulation of the input and output signals are 6.5dB and 1.7dB, respectively.

In the temporal Talbot effect, each output pulse results from cumulative interference of dispersed input pulses. Thus, after Talbot propagation, the amplitude fluctuations and timing jitter are averaged out, thereby reducing the amplitude and timing variations in the original pulse train.

Figure 2.14 and Figure 2.15 show simulation results of the mitigation effects of the Talbot effect on timing jitter and amplitude fluctuations present in the original signal. In both simulations, the input signal is a train of 7ps full width at half maximum (FWHM) Gaussian pulses with a repetition-rate of 10GHz (a temporal period of 100ps). Figure 2.14(a) shows superposition of input pulses smeared to amplitude fluctuation noise, modeled in the time domain with a random Gaussian distribution, with amplitude modulation (highest to lowest pulse ratio) of 6.5dB. The amplitude modulation is reduced to 1.7dB at the output self-imaged pulses with $m = 1$, as demonstrated in Figure 2.14(b). A deterioration on the pedestal of each output pulse train is also evident. To examine the timing jitter performance of the Talbot effect, a severe timing jitter is imposed to the input signal with a peak to peak amplitude of 7ps, See Figure 2.15(a). Figure 2.15(b) shows how the timing jitter in the temporal domain is smoothed to ~3 ps by a self-imaging effect. However, in this case, additional pulse-to-pulse amplitude fluctuations are observed in the output pulses.

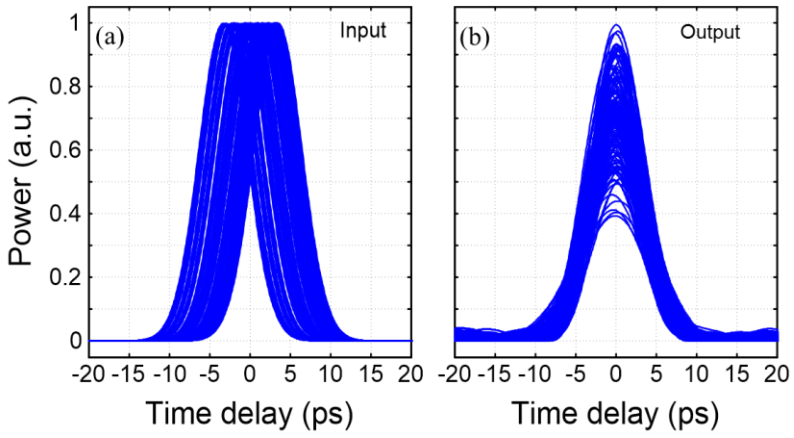

Figure 2.15 – Simulation results for timing jitter mitigation of an input signal after dispersive propagation under integer Talbot condition ($m = 1$). Input pulse sequence consists of 7ps FWHM Gaussian pulses with a temporal period of 100ps. The emulated timing jitter of the input signal is 7ps and the timing jitter at the output is 3ps.

2.2.5 *Temporal phase variations in the temporal Talbot effect*

Most of the practical applications of the Talbot effect presented to date have made use of the temporal distribution of the input signal's intensity, and the phase properties have triggered relatively limited interest. However, in the rest of this Chapter, we show that the phase properties yield a powerful tool to provide an unprecedented degree of flexibility to control and manipulate the output pulse repetition-rate.

As shown in Figure 2.16, in an integer self-image, the uniform temporal phase profile of the input is also restored. However, the multiplied self-images, such as those observed at distances $z_T/2$and $z_T/3$, are affected by a deterministic pulse-to-pulse residual temporal phase structure (dashed black lines in Figure 2.16). The residual phase for a particular fractional image can be analytically calculated for a given *s* and *m* [181].

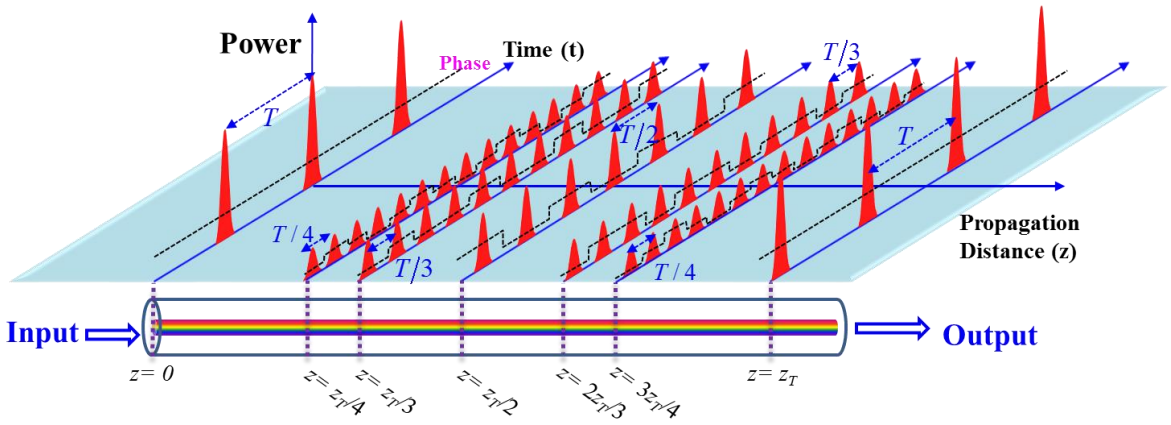

Figure 2.16 – Temporal Talbot carpet. The multiplied self-images are affected by a deterministic pulse-to-pulse residual temporal phase profile (dashed black).

In particular, the phase function of the *n*-th pulse of a particular fractional image, for a given *s* and *m*, is defined by the following [181]:

when *s* is even and *m* is odd or vice versa,

$$\varphi_n = -\frac{s}{m}\left(\left[\frac{1}{s}\right]_m\right)^2 \pi n^2 \qquad (2.22)$$

when both *s* and *m* are odd

$$\varphi_n = -2\frac{s}{m}\left[\frac{1}{2}\right]_m \left(\left[\frac{l}{2s}\right]_m\right)^2 \pi(2n+m)^2 \qquad (2.23)$$

where $\left[\frac{1}{a}\right]_b$ is the inverse of a modulo b. If these phase shifts are reduced to a 2π range, a periodic sequence of phase steps with a fundamental period equal to m, namely $\varphi_n = \varphi_{n+m}$, is obtained; see examples of phase profiles shown in Figure 2.16. It is worth mentioning that the phase functions defined in (2.22) and (2.23) show a quadratic dependence with the pulse position, identified by the factor n. This behavior is actually equivalent to the effect of a continuous temporal quadratic phase modulation, a time lens, at the discrete time pulse positions (i.e., at $t = nT$). This quadratic variation of the phases in time recently has been proved that corresponds to the phases that are needed to be induced for spectral self-imaging [182].

DOI : 10.1109/JLT.2015.2500538

2.4 Lossless fractional repetition-rate multiplication of optical pulse trains[19]

2.4.1 Abstract

We propose and experimentally demonstrate repetition-rate multiplication of picosecond optical pulse trains by a fractional factor based on temporal self-imaging, involving temporal phase modulation and first-order dispersion. Multiplication factors of 1.25, 1.33, 1.5, 1.6, 1.75, 2.25, 2.33 and 2.5 are achieved with high fidelity from a mode-locked laser with an input repetition-rate between 10 and 20 GHz.

2.4.2 Introduction

The generation of high repetition-rate optical pulse trains is of great interest for high bit-rate optical communications, optical computing systems, and both optical and microwave waveform generation [190, 191]. One attractive method for generating high repetition-rate optical pulse trains is to multiply the repetition-rate of a lower repetition-rate pulse train in the optical domain as opposed to electronically, overcoming bandwidth limitations of high speed electronics [121, 123, 192, 124, 120, 41]. Among previously demonstrated pulse repetition-rate multiplication (PRRM) techniques, the approach based on the temporal self-imaging (TSI) or Talbot effect [120, 41] has attracted a great deal of attention over the years. This approach provides the desired multiplied repetition-rate copy of an incoming optical pulse train without distorting the individual pulse features (shape and time width) simply by applying a proper dispersion-induced spectral phase profile on the original pulse train. Additionally, this method provides increased energy efficiency since fundamentally no energy is lost in the phase-filtering process. However, despite the advantages of TSI-based PRRM, the method is limited to output repetition-rates that are integer multiples of the initial pulse repetition-rate. This same restriction applies to all PRRM methods reported to date [121, 123, 192, 124, 120, 41].

---

[19] R. Maram, J. Van Howe, M. Li, and J. Azaña, "Lossless fractional pulse repetition-rate multiplication of optical pulse trains," Optics Letters, vol. 40, no. 3, pp. 375-378, (2015).

In this Letter, we propose and experimentally demonstrate, for the first time to our knowledge, "fractional" pulse repetition-rate multiplication (F-PRRM) based on TSI. Using our newly proposed method, the output pulse train repetition-rate can ideally be designed to be any fractional multiple of the input repetition-rate. The proposed concept shares the above-mentioned advantages of TSI-based PRRM yet it provides an additional, unprecedented degree of flexibility to set the output pulse repetition-rate.

2.4.3 The operation principle

The principle of our proposed fractional pulse repetition-rate multiplication concept is illustrated in Figure 2.23. Figure 2.23(a) represents the well-known standard temporal self-imaging (Talbot) effect in which a flat-phase repetitive input waveform (signal at $z = 0$) is self-imaged after dispersive propagation through an integer number of Talbot distances, z_T. In this representation, first-order dispersive propagation, involving a linear group delay profile, is assumed. Moreover, in addition to the mentioned 'integer' self-images, rate-multiplied self-images of the original input waveform train are obtained at fractional values of the fundamental Talbot distance, z_T, as defined by the "Talbot Carpet" [41]; see examples in Figure 2.23(a) at the fractional Talbot distances z_T /2, $2z_T$ /3 and $3z_T$ /4. Dispersive propagation speeds up and slows down the different frequency-components 'colors', originally in-phase that make up the waveform train, redistributing the original signal energy into the mentioned different temporal intensity patterns. An integer self-image exhibits the same repetition-rate as the input, whereas in the multiplied self-images, the repetition-rate is increased by an integer factor. In particular, the repetition-rate multiplication factors for the multiplied self-images shown in Figure 2.23(a) at z_T /2, $2z_T$ /3 and $3z_T$ /4 are integer numbers of 2, 3 and 4, respectively. We also recall that the term self-image refers to the fact that the temporal shape of each individual waveform in the Talbot patterns is an exact, undistorted copy of the input (under ideal conditions that the input is completely periodic and that the output is generated by purely linear group delay). Additionally, in an integer self-image, the uniform temporal phase profile of the input is also restored. However, in the multiplied self-images, such as those observed at distances z_T /2, $2z_T$ /3 and $3z_T$ /4, there exists a waveform-to-waveform residual temporal phase structure (dashed black lines in the figure). This residual temporal phase represents

instances where the waveform field-amplitude has been advanced or delayed in relation to the envelope center.

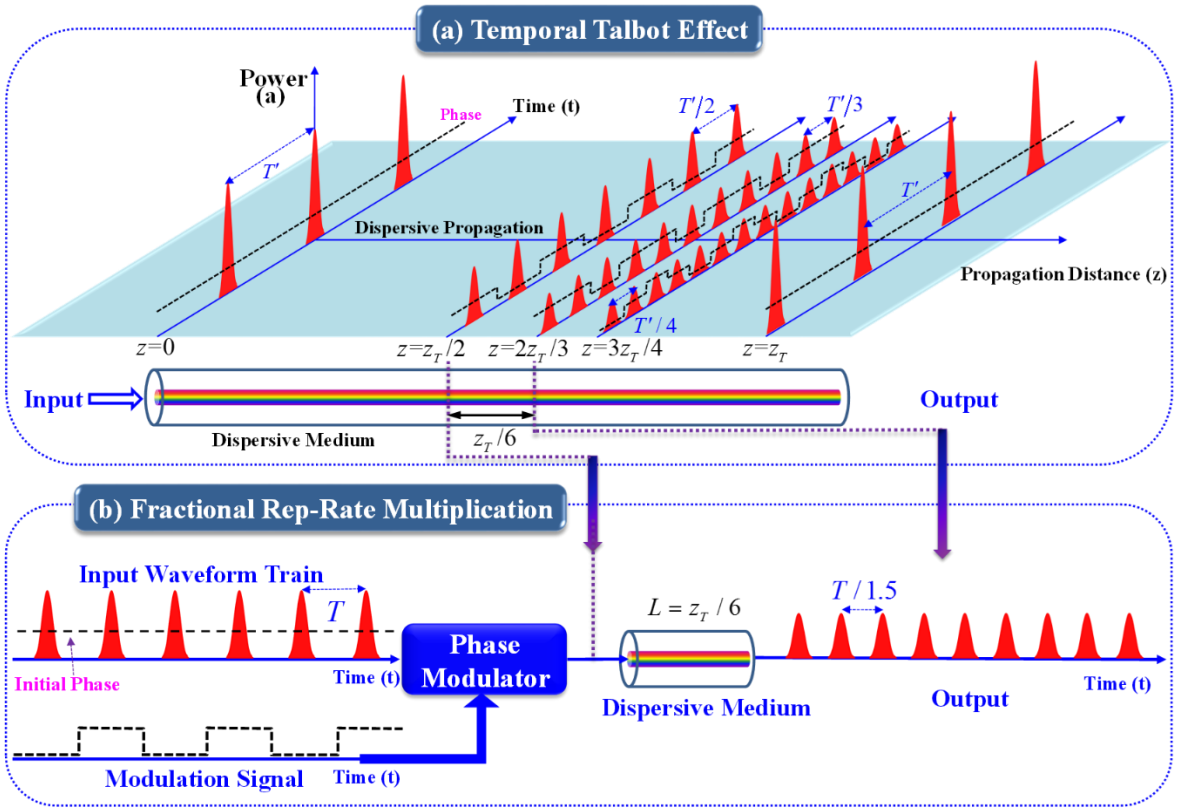

Figure 2.23 – Fractional pulse repetition-rate multiplication (F-PRRM) concept. (a) Standard temporal self-imaging (Talbot) effect, (b) A F-PRRM example with multiplication factor of 1.5 (*s* = 3; *m* = 2).

By using a multiplied image at a fractional distance as the input, instead of the conventional phase-free input at $z = 0$, further dispersive propagation to a next fractional distance produces output with a multiplied repetition-rate that is not necessarily limited to an integer rate-multiplication factor. As shown in Figure 2.23(a), repetition-rate of a pulse train starting at the fractional distance $z_T/2$ will be multiplied by a fractional factor of $k = 3/2 = 1.5$ at the fractional distance $2z_T/3$. Likewise, a pulse train starting at the fractional distance $2z_T/3$ will be repetition-rate multiplied by fractional factor of $k = 4/3 = 1.33$ at the fractional distance $3z_T/4$. This requires the application of a prescribed temporal phase modulation profile to the repetitive input signal to make it appear as if it has already propagated from $z = 0$ through an amount of dispersive delay equivalent to the target multiple self-image. For example, Figure 2.23(b), shows how if we

condition a typical flat-phase repetitive input pulses to look like the waveform train at $z_T/2$ by proper temporal phase modulation (dashed black line), subsequent propagation through $z_T/6$ more of dispersive delay will give the output shown at $2z_T/3$, one and a half the input repetition-rate ($k = 1.5$). Notice that the described processes involve only a suitable manipulation of the input signal temporal and spectral phase profiles, not magnitude, ensuring that the original signal energy is ideally preserved. According to the Talbot carpet, any desired fractional repetition-rate multiplication factor can be obtained, as long as the output period is sufficiently long so that individual pulse waveforms do not overlap along the time domain.

Notice that one can use the F-PRRM technique to also obtain integer factors, providing added versatility in the PRRM process design. As an example, the repetition-rate of a pulse train starting at the fractional distance $z_T/2$ will be multiplied by an integer factor of 2 at the fractional distance $3z_T/4$. Moreover, the target PRRM factor can be smaller than 1, actually implementing a repetition-rate division process [188].

2.4.4 System design

The required temporal phase modulation profile can be deduced from the self-imaging theory [41]. Assume that we target increasing the original repetition-rate ($F = 1/T$) by a desired fractional factor $k = (s/m)$ with $s = 1, 2, 3, \ldots$ and $m = 2, 3, 4, \ldots$, where s and m are co-prime integers. Accordingly, the temporal period of the output pulse train will be $T_{Out} = T / k = (m/s)T$, ($F_{Out} = 1/T_{Out}$ being the output repetition-rate). In this case, a temporal phase of

$$\varphi_n = \frac{m\text{-}1}{m}\pi n^2 \qquad (2.36)$$

must be applied on the n-th incoming temporal pulse ($n = 0,1,2,\ldots, m\text{-}1$). The temporal phase φ_n can be assumed to be applied on time slots equal to the pulse repetition-rate. In practice, however, it is sufficient to apply the same phase over the pulse duration. If these phase shifts are reduced to a 2π range, a periodic sequence of phase steps with a fundamental period equal to m, namely ϕ_{n+m}, is obtained. These phase shifts have been shown to induce a spectral self-imaging effect on the modulated pulse train [188, 75]. In particular, the temporal phase modulation process reduces the comb frequency spacing of the input signal by m times [75]. As mentioned above, prescription of

the phase profile to the input signal makes it appear as though it has already propagated through an amount of dispersive delay equivalent to the *m* multiple image.

The phase-conditioned pulse train is then propagated through a first-order dispersive medium, providing a linear group delay (quadratic spectral phase) across the entire input pulse frequency bandwidth. According to TSI theory [41], in order to produce a pulse repetition-rate by a factional factor *k*, the dispersive medium should introduce a total dispersion value of

$$\phi_0^{(2)} = \frac{q}{k}\frac{T^2}{2\pi\beta_2} \tag{2.37}$$

where *q* is a positive integer and co-prime with *s* and *m*, and $\phi_0^{(2)}$ is the group-delay slope as a function of radial frequency around the central frequency of the input pulse train. Notice that *q* = 1 ensures the minimum dispersion value required to obtain the target fractional rate multiplication. The multiplication factor is given by $k = s / m$ which is the fractional when $s > m$ and s / m is a non-integer. Maximum repetition-rate multiplication is limited by the desired output duty cycle, which must be short enough to prevent pulses overlapping in the multiplied train. Care also must be taken to precisely meet the Talbot condition, Eq.(2.37), in order to prevent mismatch between input and output pulse shape.

2.4.5 Experimental demonstration

In our experimental demonstrations, a MLFL generating uniform-phase 6-ps Gaussian-like optical pulses at 1550nm is used as the input optical pulse train source. The input pulse train with repetition-rate between 10 and 20 GHz is first appropriately phase-modulated in the time-domain by a commercial fiber-integrated electro-optic phase modulator, driven by an arbitrary waveform generator (AWG). After temporal modulation, pulses are propagated through a dispersion-compensating fiber (DCF) module, providing a fixed first-order dispersion coefficient of $\phi_0^{(2)}$~890 ps^2/rad.

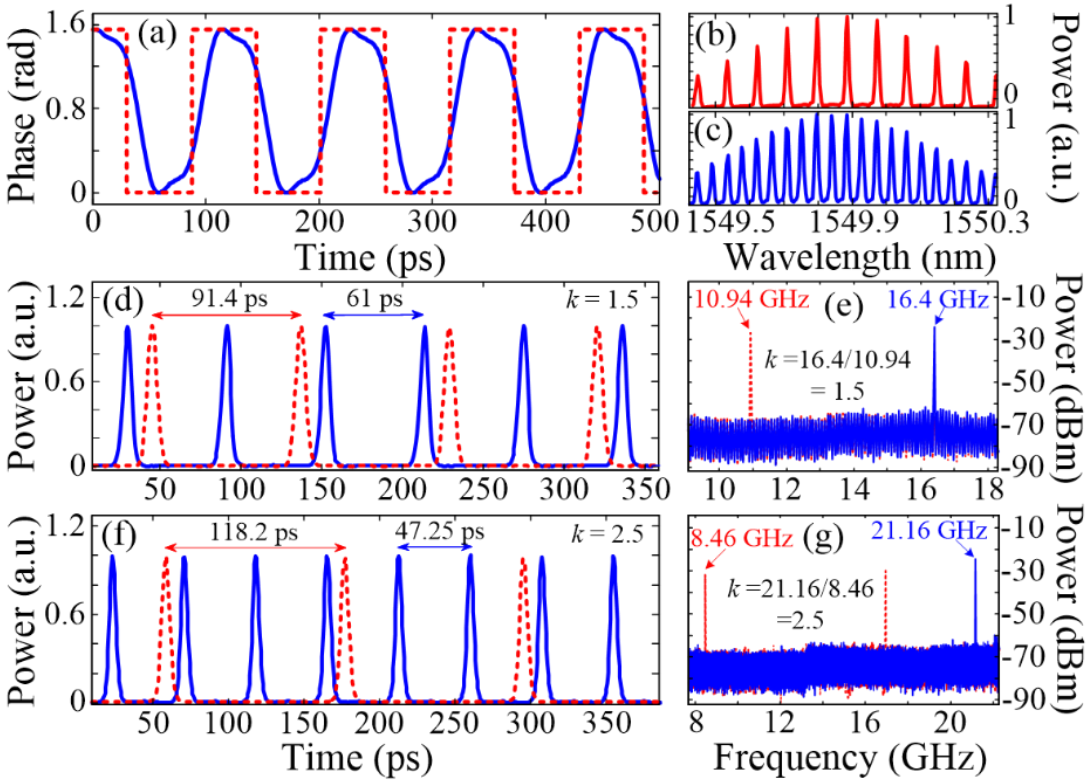

Figure 2.24 – Results for fractional rate multiplication by k = 3/2 = 1.5 and 5/2 = 2.5 with m = 2. (a) Prescribed temporal phase modulation profiles, ideal (dashed red) and experimental (solid blue) for the case of m = 2. (b) and (c) Measured optical spectra input signal before and after temporal phase modulation (d) and (f) Measured temporal waveforms of the 10.94-GHz and 8.46-GHz input pulse trains (dashed red) together with their self-imaged rate-multiplied copies (solid blue). (e) and (g) RF spectra of the temporal pulse trains (intensity waveforms) shown in (d) and (f), respectively.

We first start with experimental demonstration of fractional rate multiplication by factors of k = 1.5, 2.5, … where the denominator of the fractional factor k (= s/m) is m = 2. To this end, the required phase profile can be derived using Eq.(2.36) with m = 2. Figure 2.24(a) shows the obtained two-level periodic phase modulation profile {0, π/2, 0, π/2, …}. The dashed red curve shows the ideal temporal phase profile, and the solid blue curve shows the actual phase drive delivered by the AWG. This phase profile is then prescribed electro-optically to the input optical pulses generated by the MLFL. We select the repetition-rate of the input pulse train to be F = 10.94GHz ($=1/T=1/(k2\pi\phi_0^{(2)}q)^{1/2}$, from Eq.(2.37) above) for the case when we target a fractional multiplication factor of k = 1.5 (with q = 1). Figure 2.24(b) and (c) show the optical spectra of the

input data signal before and after temporal phase modulation, respectively, showing the predicted spectral self-imaging effect, leading to the anticipated decrease in the comb frequency spacing of the input signal by a factor of $m = 2$. The optical spectra were recorded with a standard optical spectrum analyzer with 0.01 nm resolution bandwidth.

Figure 2.24(d) illustrates the temporal intensity waveforms of the 10.94-GHz input pulse train (dashed red) and the resultant 16.4-GHz multiplied pulse train (solid blue) at the output of the dispersive medium, measured by a 500-GHz bandwidth optical sampling scope (Exfo PSO-101). Figure 2.24(e) shows the corresponding measured RF spectra of the input and output pulse trains. Together, Figure 2.24(d) and (e) clearly approve that the target fractional PRRM factor of 1.5 was obtained. Notice that within our ability to record the waveforms, the output pulses are undistorted copy of the input ones. This implies a linear group delay over signal's bandwidth and insignificance of the higher order dispersion. However, for very long dispersive lengths or high bandwidth pulses, distortion from higher order dispersion will not be negligible.

We further observe that by changing the repetition-rate of the input to satisfy Eq.(2.37) with $k = 2.5$ and $q = 1$, such that $F = 8.46$GHz, the repetition-rate of the output pulse train is again a self-imaged version of the input pulse train, but this time with a repetition-rate multiplied by factor 2.5. Figure 2.24(f) shows the sampling scope time traces and Figure 2.24(g) shows the corresponding RF spectra. As expected for a self-imaging effect, in all cases, the output temporal pulses are nearly undistorted copies of the input pulses.

For the second set of experiments, Figure 2.25 presents the experimental results for F-PRRM with multiplication factors of $k = 1.33$, 1.66 and 2.33 (where the denominator of k is $m = 3$ and numerators are $s = 4$, 5 and 7, respectively). First, the repetition-rate of the input signal is set to satisfy Eq.(2.37) with $k = 1.33$ and $q = 1$, i.e. $F = 11.64$GHz. As shown in Figure 2.25(b) and (c), the comb frequency spacing of the 11.64GHz input signal is reduced by a factor of 3 following application of the periodic temporal phase modulation $\{0, 2\pi/3, 2\pi/3, 0, 2\pi/3, 2\pi/3, \ldots\}$ as derived from Eq.(2.36) with $m = 3$, Figure 2.25(a).

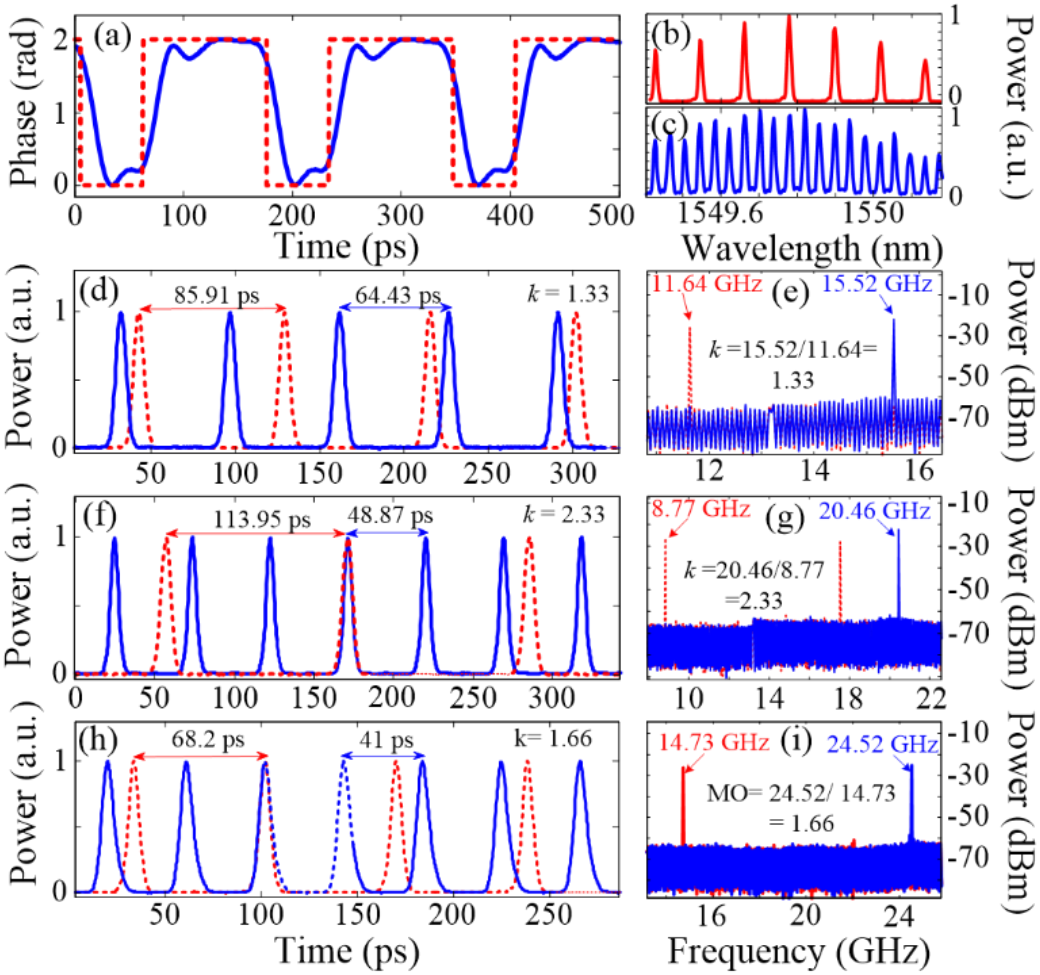

Figure 2.25 – Experimental results for fractional rate multiplication by k = 1.33, 2.33 and 1.66 with m = 3, with the same captions as for the Fig. 2.

The slight reduction in the fidelity of the Gaussian spectral envelope is due to the time-resolution limitations of the AWG, which fails to reproduce the ideal temporal phase drive. Because a constant phase is only required over the pulse width, it may be possible to synthesize smoother phase profiles to relax the bandwidth requirement of the AWG. Figure 2.25(d) shows that the output signal (solid blue) reproduces the input signal (dashed red) but with 1.33 times the repetition-rate, confirmed further by the corresponding RF spectra in Figure 2.25(e). Next, we consider input pulse trains with repetition-rates of F = 8.77GHz and 14.73GHz (calculated to satisfy Eq.(2.37) with k = 2.33 (q = 1) and 1.66 (q = 2), respectively). At the output of the setup we obtain the predicted 20.46-GHz and 24.52-GHz optical pulse trains, achieving the target repetition-rate multiplication by 2.33 and 1.66, respectively, as illustrated in Figure 2.25(f),(h) and

the corresponding RF spectra in Figure 2.25(g),(i). Again, the individual output pulses are nearly undistorted replicas of the input pulses.

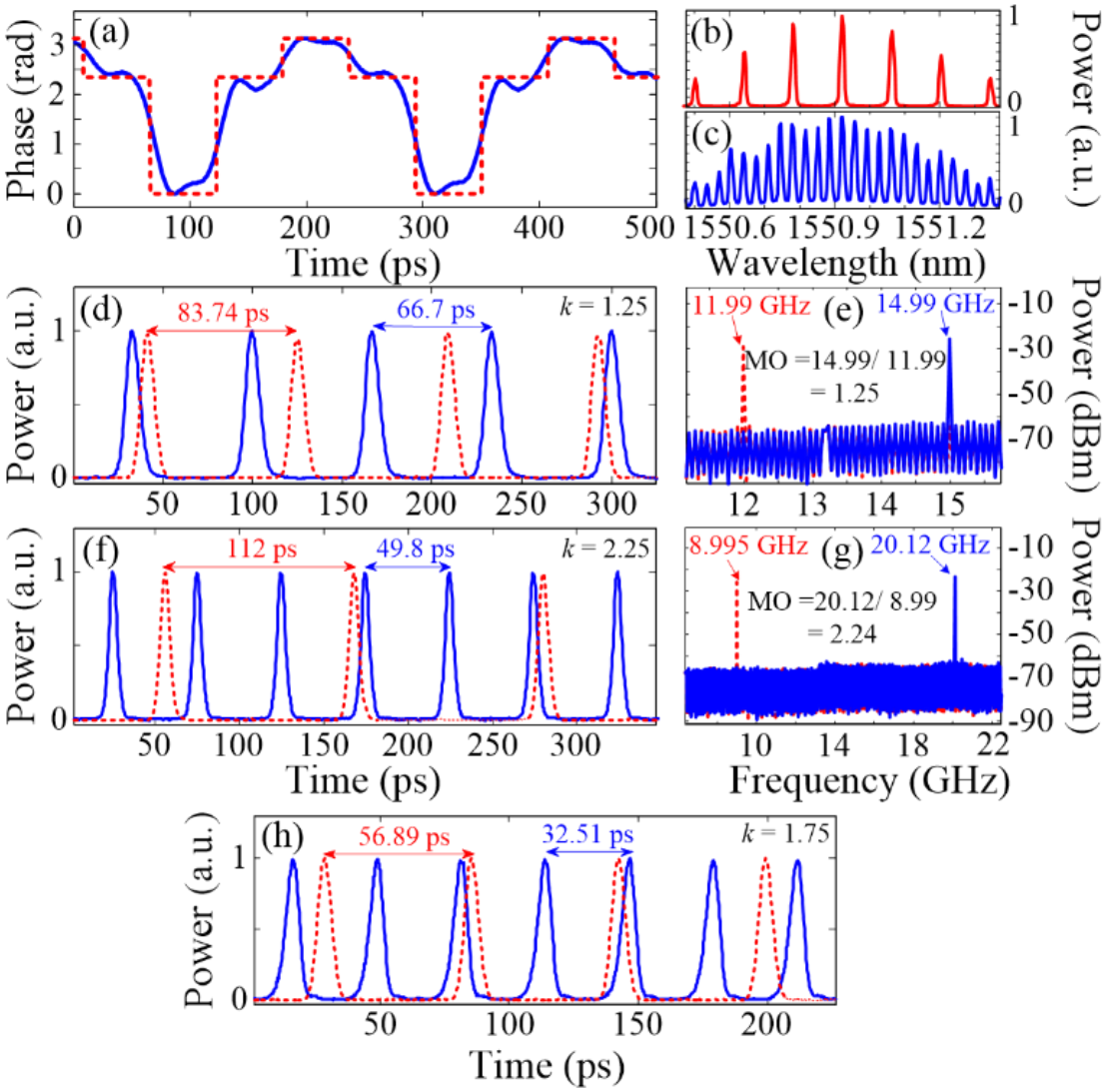

Figure 2.26 – Results for fractional rate multiplication by k = 1.25 (, 2.25) and 1.75 (with m = 4, with the same captions as for Fig. 2. RF spectra on the last experiment shown in (h) Corresponding RF spectrum not shown due to insufficient frequency bandwidth of our measurement instrument (limited to ~26GHz) to capture the output train at a rate at 30.8 GHz.

In the last set of experimental demonstrations, we target fractional multiplication factors of k = 1.25, 1.75 and 2.25 where the denominator of the fractional factor k is m = 4. Figure 2.26(a) shows the prescribed electro-optic phase modulation profile to the input optical pulses generated by the MLFL with repetition-rate of F = 11.99GHz, to satisfy Eq.(2.37) for k = 1.25 (with q = 1).

The periodic temporal phase profile is {0, 3π/4, π, 3 π/4, 0, 3 π/4, π, …} when m = 4 in Eq.(2.36), Figure 2.26(a). Likewise our previous demonstrations, the comb frequency spacing of the input signal is reduced after phase modulation, in this case, by a factor of m = 4, as depicted in Figure 2.26(b) and (c). Figure 2.26(d) and (e) show experimental temporal scope traces and RF spectra for both the input (F = 11.99GHz) and 1.25 times repetition-rate output (F_{Out} = 14.99GHz). Finally, by adjusting the repetition-rate of the input pulse train to 8.99GHz (with q = 1) and 17.6GHz (with q = 3), we would have the 2.25 and 1.75 multiplied pulse trains with 20.12 and 30.8GHz repetition-rates, respectively, as shown in Figure 2.26(f)-(h).

2.4.6 Conclusion

In summary, we have proposed and experimentally demonstrated a simple and practical lossless method for undistorted optical PRRM by any desired fractional factor. The demonstrated technique offers an unprecedented degree of flexibility compared with previously reported PRRM approaches, which are generally limited to integer repetition-rate multiplication factors. The method exploits temporal self-imaging effects and it involves temporal phase modulation combined with dispersive (phase-only spectral) filtering, fundamentally preserving the input pulse train energy.

2.5 Noiseless Intensity Amplification of Repetitive Signals by Coherent Addition using the Temporal Talbot Effect[20]

2.5.1 Abstract

Amplification of signal intensity is essential for initiating physical processes, diagnostics, sensing, communications, and measurement. During traditional amplification, the signal is amplified by multiplying the signal carriers through an active gain process, requiring the use of an external power source. Additionally, the signal is degraded by noise and distortions that typically accompany active gain processes. We show noiseless intensity amplification of repetitive optical pulse waveforms with gain from 2 to ~20 without using active gain. The proposed method uses a dispersion-induced temporal self-imaging (Talbot) effect to re-distribute and coherently accumulate energy of the original repetitive waveforms into fewer replica waveforms. In addition, we show how our passive amplifier performs a real-time average of the wave-train to reduce its original noise fluctuation, as well as enhances the extinction ratio of pulses to stand above the noise floor. Our technique is applicable to repetitive waveforms in any spectral region or wave system.

2.5.2 Introduction

Waveform amplification refers to a process by which the amplitude of the waveform is increased without affecting its other signal features, particularly temporal shape. Intensity amplification of waveforms is necessary for increasing the peak power of signals for initiating physical processes, extracting information from the natural world, and communications. Almost every information-bearing electronic signal used for diagnostics, sensing, or fundamental measurement requires amplification between the source and the detector. Optical pulses amplified to high-intensities are necessary for nonlinear microscopy [193], materials processing [194], and relativistic optical processes [195] such as coherent x-ray generation, laser fusion, and particle

[20] R. Maram, J. Van Howe, M. Li and J. Azaña, "Noiseless intensity amplification of repetitive signals by coherent addition using the temporal Talbot effect" Nature Communications, vol. 5, 4827, (doi: 10.1038/ncomms6163), (2014).

acceleration. Additionally, optical amplification of signal intensity is critical for communications and becoming increasingly important for current work in optical computing and optical information processing [196, 197, 198]. During active amplification, the signal is amplified directly by multiplying the signal carriers through an active gain process using an external power source [199, 200, 201, 202, 203, 204, 205, 206]. Whereas active gain mechanisms are widely available for electrical and optical signals, suitable active gain processes for direct waveform amplification are limited over large regions of the electromagnetic spectrum and for other wave systems, such as mechanical, acoustic, and quantum probability waves.

Furthermore, for applications involving high-peak power pulse generation [193, 194, 195], traditional active amplification is extremely inefficient. In order to generate high-peak power optical pulses, many pulses in a wave-train are intentionally thrown away, "pulse-picking," either prior to amplification [207] or during the amplification process (regenerative amplification) [208], in order to concentrate energy from the external source in fewer remaining output pulses. In such processes, typically more than 99% of the signal energy is thrown away prior to boosting. While absolute power consumption in high-peak power amplification is dominated by the pumps on the high-power boosting amplifier after pulse-picking, carelessly throwing away 99% of the signal prior to active-amplification significantly reduces the signal-to-noise and is enough of a power hit to be a problem for high-peak power applications [209].

Finally, in applications where active amplification is employed, the active-gain process typically contributes amplitude and phase noise, such as amplified spontaneous emission (ASE) noise or timing jitter, and other signal distortions induced by limited gain frequency bandwidth. Because an active-gain process inherently amplifies input noise and also injects its own noise onto a signal, the output signal-to-noise ratio (SNR) degrades. This degradation is encapsulated by a common figure-of-merit of any active amplifier- the noise figure [210]. The noise figure of an active amplifier is the ratio of the SNR of the input signal to the SNR of the output signal. Though phase-sensitive amplifiers have been shown capable of realizing low-noise amplification (with noise figures as low as 1 dB [206]), the amplification of weak signals by conventional amplifiers typically renders the signal totally undetectable due to the amplification and injection of noise.

Coherent addition of repetitive optical pulses in a wave-train has been used in the past with the aim of overcoming the drawbacks described above. However, controlled coherent addition of

many identical waveforms is an extremely challenging process. Previous methods are based on precisely timing and storing pulses in a high-finesse cavity [209, 211]. As such, these methods require ultra-precise active phase control of the input signal envelope and carrier, i.e., carrier-envelope phase stabilization, in order to stabilize the input waveforms to cavity such that each pulse will add constructively. Otherwise, small phase misalignment in each pulse tends towards destructive interference. Though impressive results have been reported, these conditions are much too restrictive to be applied beyond a controlled lab environment.

Using optical pulses, we demonstrate a noiseless waveform amplification method for repetitive signals with experimental intensity gain from 2 to ~20, without using an active gain process, through coherent addition. Our new concept of passive amplification exploits the intrinsic coherence revival times of periodic waveform trains provided by passive dispersive broadening, known as temporal "self-imaging" or the temporal Talbot effect [41] (illustrated in Fig. 1, top). In particular, passive amplification is achieved by effectively re-distributing and coherently adding the overall input energy of a repetitive waveform signal into fewer waveforms, resulting in each output individual waveform to be an amplified copy of the input. Essentially, we implement a "lossless" pulse picking process by using a suitable combination of phase-only temporal and spectral modulation operations, in order to preserve the overall input signal energy. This can be interpreted as coherently adding a desired number of identical copies on top of one another to produce the desired amplified output. However, in sharp contrast to previous pulse coherent-addition methods, our technique implements a similar process without using a cavity and therefore without the associated stringent timing and stabilization conditions. The only condition on the input waveform is that it is repetitive and maintains coherence over the output repetition-rate. Because our passive amplification technique for repetitive signals is based upon the fundamental process of linear superposition of waves, it can be applied to any wave system, introducing a method for multiplying signal intensity in systems where active gain processes for waveform amplification are limited or do not exist.

Last but not least, we report numerical and experimental results to demonstrate that during passive intensity amplification, the SNR does not degrade. In fact, the proposed Talbot-based amplification technique improves random (white) intensity noise, ASE-like fluctuations, present on the input temporal signal, similarly to a real-time averaging process, as well as enhances the

extinction ratio compared to the input waveform train in the time-domain. In particular, consistent with simulation, we show experimentally that Talbot-based passive amplification increases the extinction ratio by approximately the passive gain factor, *m*, as well as performs a real-time average of the waveform train by about *m* averages. These noise-mitigating effects allow us to show in a side-by-side comparison in one of our experiments how Talbot-amplification can extract a weak noisy signal nearly buried beneath a noisy background whereas a typical active amplifier buries the signal further beneath the noise. We also anticipate that Talbot amplification improves pulse-to-pulse fluctuation [212] and timing-jitter present on the input signal as the passive gain factor increases. This is consistent with previous experiments which show improvement in timing-jitter and pulse-to-pulse fluctuation for simple self-imaging (passive gain factor of $m = 1$) [178, 179]. Noise mitigation using Talbot passive amplification therefore shows promise for further signal regeneration than the results presented in this report.

2.5.3 Concept and operation principle

Figure 2.27 illustrates the concept of our passive amplification technique. We effectively exploit an "inverse temporal Talbot effect" in which the final amplified temporal image is recovered from a previous multiplied self-image. As shown in Figure 2.27, top, in the standard temporal Talbot effect, a flat-phase repetitive input waveform (signal at $z = 0$) is self-imaged, after dispersive propagation through a distance z_T (integer Talbot distances). There also exists an infinite amount of fractional distances, given by the "Talbot Carpet" (a map of all possible coherence revivals resembling a Persian rug in intricate but repeating patterns) [41] that give multiplied self-images; see examples at the fractional Talbot distances $z_T/2$ and $2z_T/3$, Figure 2.27, top. Dispersive propagation speeds up and slows down the different frequency-components 'colors', originally in-phase that make up the waveform train, redistributing the original signal energy into the mentioned different temporal intensity patterns. An integer self-image exhibits the same repetition-rate and individual waveform intensity as the input, whereas in the multiplied self-images, the repetition-rate is increased, and the individual waveform intensity is correspondingly decreased by an integer factor. The repetition-rate-multiplication (intensity-division) factors for the multiplied self-images shown in Figure 2.27 at $z_T/2$ and $2z_T/3$ are 2 and 3, respectively. In an integer self-image, the uniform temporal phase profile of the input is restored. However, in the

multiplied self-images, such as those observed at distances z_T /2 and $2z_T$ /3, there exists a waveform-to-waveform residual temporal phase structure (dashed black). This residual temporal phase represents instances where the waveform field-amplitude has been advanced or delayed in relation to the envelope center.

By using a multiplied image at a fractional distance as the input instead of the conventional phase-free input at $z = 0$, further dispersive propagation to the distance z_T produces an output with an amplified intensity. As shown by Figure 2.27 top, a waveform starting at the fractional distance z_T /2 will be amplified in intensity by a factor of $m = 2$ at the output z_T. Likewise, a waveform starting at the fractional distance $2z_T$ /3 will be amplified by a factor of $m = 3$. This requires the application of a prescribed temporal phase modulation profile to an input signal to make it appear as though it has already propagated from $z = 0$ through an amount of dispersive delay equivalent to the target multiple image. For example, Figure 2.27, bottom, shows how if we condition a typical flat-phase input to look like the waveform train at $2z_T$ /3 by proper temporal phase modulation (dashed black line), subsequent propagation through z_T /3 more of dispersive delay will give the output shown at z_T, one-third the repetition-rate and three times the intensity. Notice that the described processes involve only a suitable manipulation of the input signal temporal and spectral phase profiles, not magnitude, ensuring that the signal energy is ideally preserved. The full Talbot carpet provides an infinite amount of fractional self-image locations and corresponding phase profiles, so that any desired repetition-rate division and corresponding amplification factor can be obtained, limited only practically by the control of temporal phase modulation and spectral phase filtering from dispersive propagation.

To passively amplify any arbitrary repetitive input signal by m times ($m = 2,3,4,...$), a temporal phase of

$$\varphi_n = \frac{m\text{-}1}{m}\pi n^2 \tag{2.38}$$

(where $s = m - 1$) is applied on the n-th temporal pulse ($n = 0,1,2,...$) of the input periodic signal. This is followed by propagation through a first-order dispersive medium, ideally providing a linear group-delay variation as a function of frequency over the signal spectral bandwidth. The dispersive medium should introduce a total dispersion value:

$$2\pi|\beta_2| = mT^2 \tag{2.39}$$

where T is the repetition period of the input pulse train, z_A is the length of the dispersive medium, and β_2 is the dispersion coefficient, defined as the slope of the group delay as a function of the radial frequency ω, per unit length. Mathematically, $\beta_2=\left[\partial^2\beta(\omega)/\partial\omega^2\right]_{\omega=\omega_0}$, where $\beta(\omega)$ is the propagation constant through the medium, i.e. $\tau_g(\omega)=z_A[\partial\beta(\omega)/\partial\omega]_{\omega=\omega_0}$ is the medium's group delay, and ω_0 is the central (carrier) frequency of the considered signal (periodic waveform train).

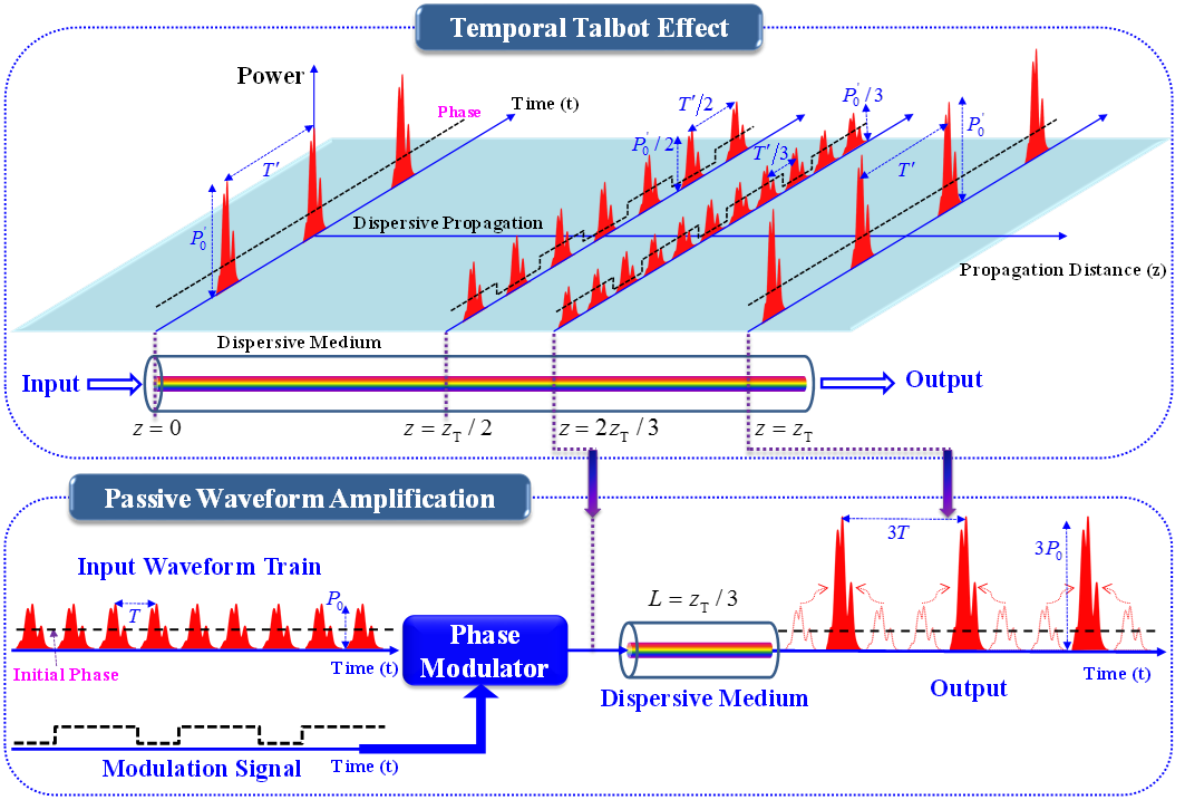

Figure 2.27 – Passive waveform amplification concept. A portion of the temporal Talbot carpet, top, provides the map of the temporal phase modulation and spectral phase-only filtering from dispersion required for passive amplification.

The temporal phase φ_n can be assumed to be applied on time slots equal to the pulse repetition-rate. In practice, however, it is sufficient to apply the same phase over the pulse duration. Notice that the phase profile φ_n is periodic with a fundamental period equal to the gain-factor m, namely $\varphi_n = \varphi_{n+m}$. If these phase shifts are reduced to a 2π range, a periodic sequence of discrete phase

steps in the range $[0, 2\pi]$ is obtained. The example illustrated in Figure 2.27 of the main text for $m = 3$ gives a repeating temporal phase profile of $\{0, 2\pi/3, 2\pi/3, 0, 2\pi/3, 2\pi/3, \ldots\}$, where the third phase level corresponding to $n = 2$ has been obtained by taking modulo 2π.

The temporal phase shifts φ_n are defined from the Talbot carpet [41]. These phase shifts induce a spectral self-imaging (Talbot) effect on the modulated pulse train [75]. In particular, the temporal phase modulation process produces new frequency components, reducing the frequency spacing of the input signal discrete comb-like spectrum by an integer factor of m. This is consistent with the repetition-rate division (temporal period increase) by a factor m that is subsequently achieved on the temporal pulse train following dispersive propagation.

2.5.4 Experimental demonstration

We experimentally demonstrate passive amplification using optical pulses generated from a standard commercial pulsed fibre laser, which does not incorporate any carrier-envelope phase stabilization mechanism. The pulses from the laser are input directly into a dispersive optical fibre and delivered at the fibre output through conventional integer temporal self-imaging [41]. Next, by adding a suitable temporal phase through electro-optic modulation to waveforms prior to dispersion, the waveform intensity will be locally amplified according to the amount of repetition-rate reduction. Because the absence of temporal phase modulation produces an integer Talbot self-image of the original pulse train at the fibre output, we are able to compare the cases of passively amplified and unamplified waveforms that have propagated through the same optical system. Any loss from the system will show up in both the passively amplified and unamplified data, allowing us to isolate the effectiveness of passive amplification alone.

Figure 2.28 shows the prescribed electro-optic phase modulation profiles to the ~7-ps Gaussian input optical pulses generated by the fiber laser for the cases when we target gain factors of $m =$ 2, 5, 15, and 27, respectively. The temporal phase functions are generated from an electronic arbitrary waveform generator (AWG). The solid red lines show the ideal temporal phase profiles, and the dashed blue lines show the actual phase drive delivered by the AWG. Figure 2.29 presents the optical spectra recorded with a high-resolution (20-MHz) optical spectrum analyzer after

temporal phase modulation showing the predicted spectral Talbot effect, leading to the anticipated decrease in the frequency comb spacing by factors of 2, 5, 15, and 27, respectively.

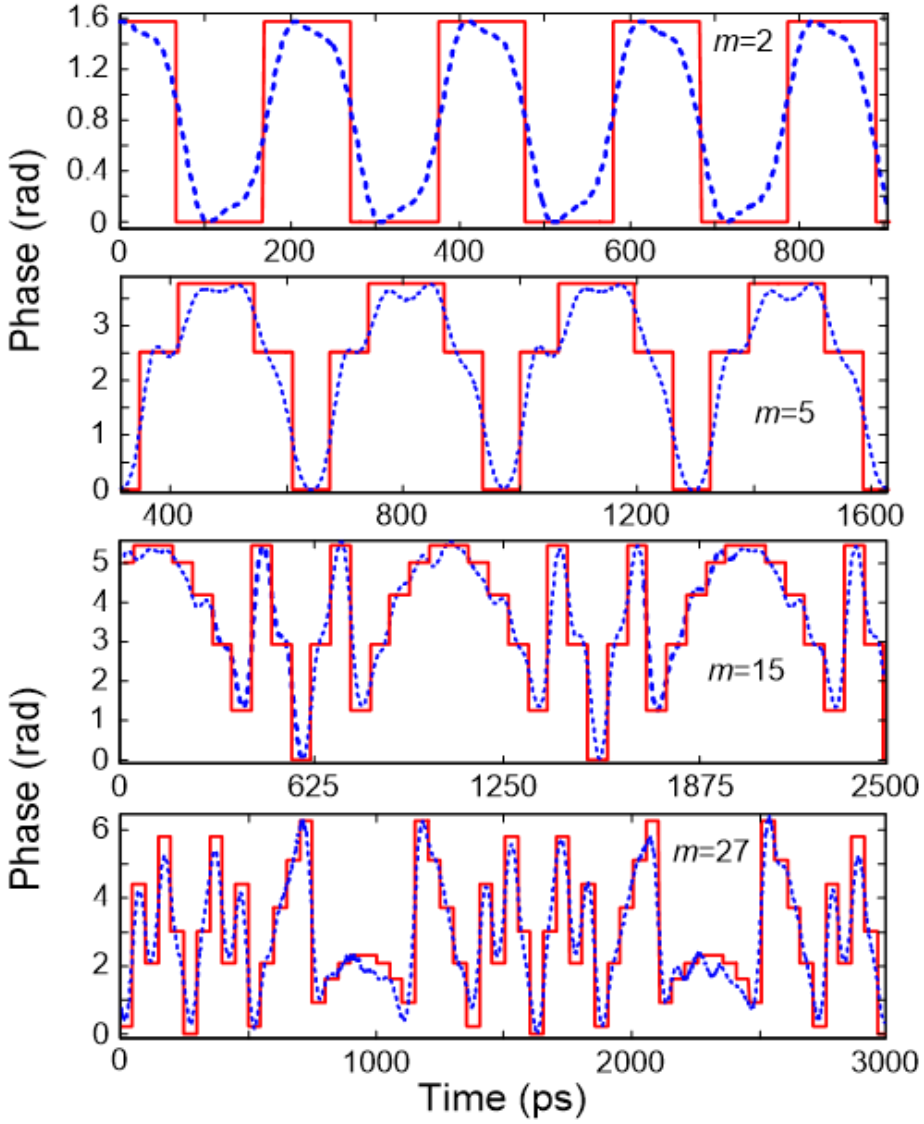

Figure 2.28 – Experimental prescribed phase modulation profiles. Temporal phase modulation patterns required for amplification factors *m* = 2, 5, 15, and 27, as determined by the Talbot carpet.

Figure 2.30(a) shows the experimental results of the demonstrated passive amplification, with gain factors of $m =$ 2, 5, 15, and 27, at the output of the dispersive fiber link (total dispersion ~2,650ps nm^{-1} in the case of m = 2 and m = 5, and ~ 8,000ps nm^{-1} for m = 15 and m = 27). In the case of m = 15 and m = 27, fiber losses from dispersion are significant, ~42 dB from a total of six

dispersion compensating fiber modules, so that we include active amplifiers, Erbium-doped fiber amplifiers (EDFAs), in our system in order to detect the signal at the end of the span to show proof-of-concept for these higher amplification factors. This practical limitation can be overcome by using lower loss dispersive devices, such as chirped fiber gratings for losses as low as 3 dB for the entire dispersive spectral phase employed [213]. Another low loss alternative method is spectral line-by-line shaping [158], for which the desired spectral phase shifts can be restricted to the range $[0, 2\pi]$.

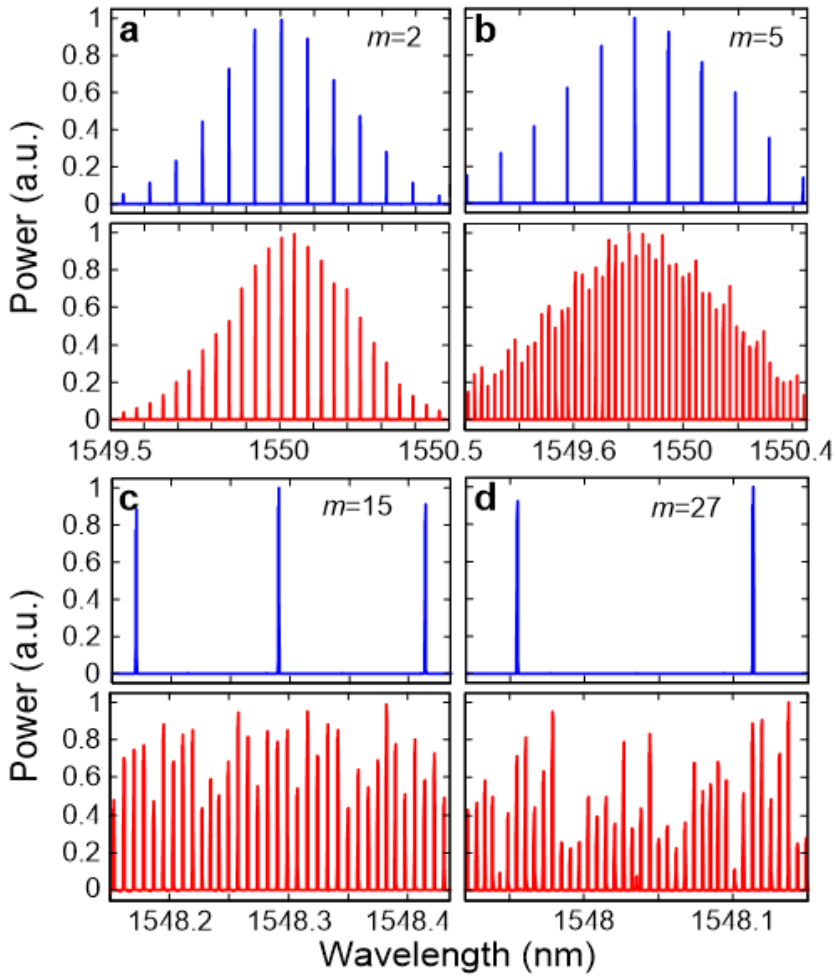

Figure 2.29 – Measured optical spectra of the optical pulse trains. Optical spectra of the optical pulse trains after phase modulation with the phase modulator turned off (blue, top plot) and with the phase modulator turned on (red, bottom plot), demonstrating the expected decrease in the frequency comb spacing by factors of (a) *m* = 2, (b) *m* = 5, (c) *m* = 15, and (d) *m* = 27, respectively.

The original repetition-rates of the input pulse trains in the four reported experiments are 9.7 GHz, 15.43GHz, 15.43 GHz, and 19.75 GHz, respectively. The reduced rates after passive amplification are 4.85 GHz, 3.08 GHz, 1.03 GHz, and 0.73 GHz, as measured by the radio frequency (RF) spectra of the detected output optical pulse trains, Figure 2.31, in excellent agreement with the desired amplification factors. Figure 2.30(a) shows the optical sampling oscilloscope (OSO) trace (500-GHz measurement bandwidth) of the pulse train after dispersion in the case with a phase-conditioned input (solid red) and without (dashed blue). For $m = 2$, the pulse train intensity, as measured by the OSO, doubles as predicted. For $m = 5$, 15 and 27 the ideal amplification factors are nearly obtained, 98% of the desired $m = 5$, 96% of the desired $m = 15$, and 75% of the desired $m = 27$.

In all cases, the amplified temporal waveforms are nearly undistorted replicas of the unamplified Gaussian pulses. The reduction in the fidelity of the Gaussian spectral envelope (Figure 2.29) for amplification factors $m = 15$ and $m = 27$, and the associated slight decrease of the expected gain, is mainly due to the time-resolution limitations of the AWG, which fails to reproduce the ideal temporal phase drive for more complicated phase patterns, Figure 2.28.

Figure 2.30(b) further proves how Talbot passive amplification is achieved without affecting the temporal shape of the input waveform. Here, the laser pulses are re-shaped prior to amplification to exhibit a sinc-like pulse waveform in the time-domain. Using the same scheme that was applied to Gaussian pulses for amplification by 15 times, we similarly demonstrate passive amplification of the sinc-like pulses by a factor of ~12.6. The Talbot passive amplification approach can be applied on any arbitrary waveform with no fundamental limitation on the signal frequency bandwidth. It is only practically limited by the spectral bandwidth of the linear region of the particular dispersive medium. In the case of dispersive delay provided by optical fiber as employed in this work, linear dispersion around 1550 nm greatly exceeds the pulse bandwidth. For other wavelength regions or wave systems care may need to be taken to ensure a linear chirp provided by dispersive delay.

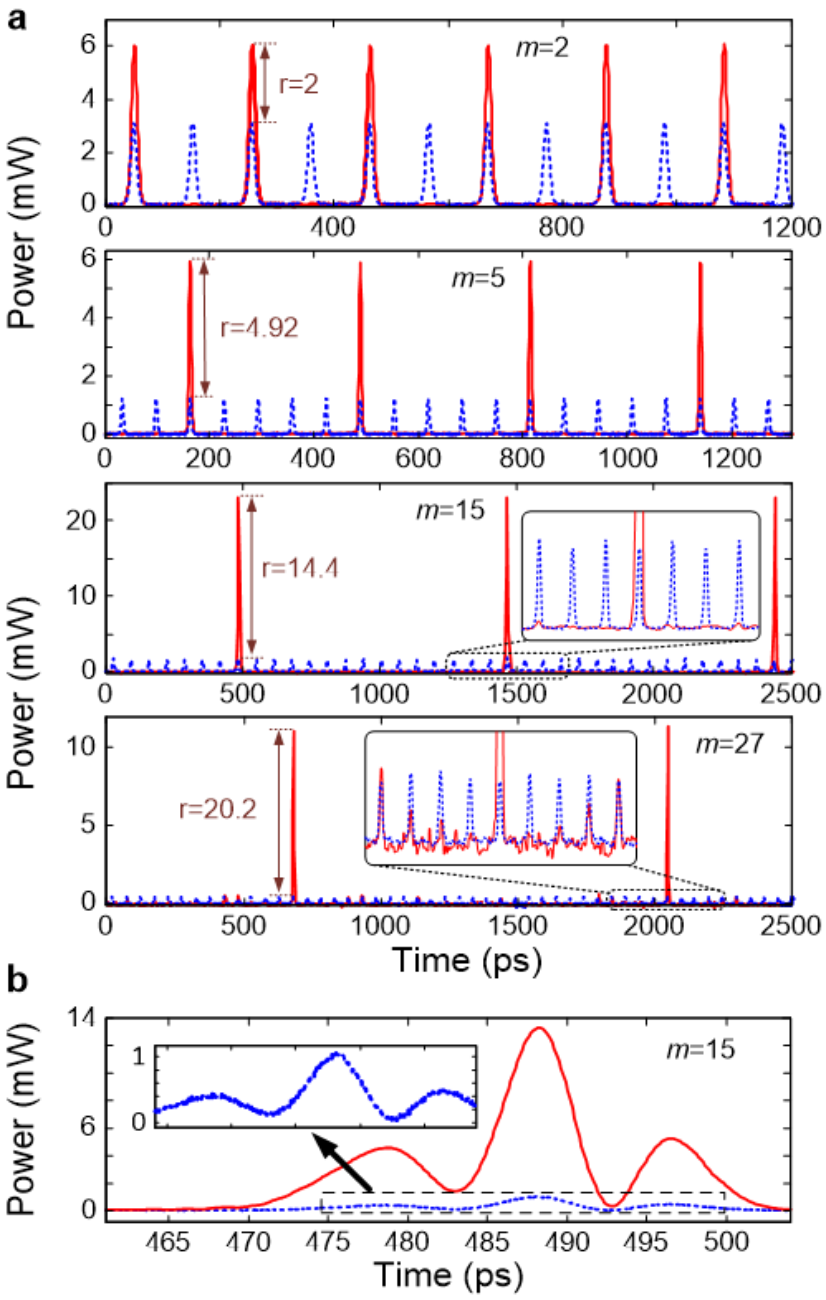

Figure 2.30 – Experimental demonstration of passive waveform amplification. (a) Optical sampling oscilloscope time trace of pulse trains at the dispersive fiber output before passive amplification (dashed blue, with the phase modulator turned off) and after passive amplification (solid red, with the phase modulator turned on) for the desired amplification factors of *m* = 2, 5, 15, and 27. (b) Passive amplification of an arbitrary waveform demonstrating the insensitivity of the Talbot method to temporal signal shape.

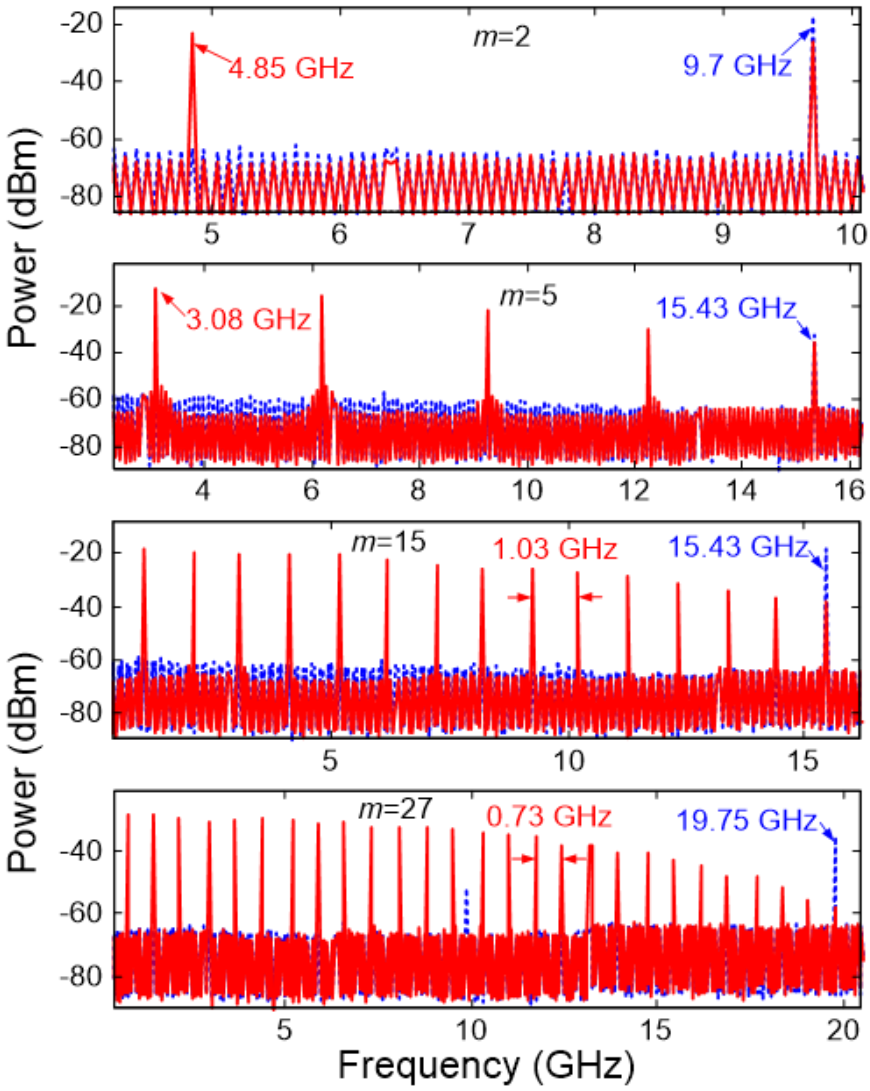

Figure 2.31 – Experimental verification of repetition-rate division for passive amplification. Traces show the RF spectra of the optical pulse trains after photo-detection at the dispersive fiber output without passive amplification (dashed blue, with the phase modulator turned off) and with passive amplification (solid red, with the phase modulator turned on) for the desired amplification factors of 2, 5, 15 and 27.

2.5.5 Analysis of noise performance

The plots in Figure 2.32 demonstrate the phenomenon of passive amplification without the injection of intensity noise. In these experiments, no active amplification was used in the dispersive span. The identical match of the spectra, in the presence and absence of passive amplification,

particularly at the noise-floor, indicates our technique does not contribute any measurable intensity noise, consistent with what one would expect from a passive system. Using the spectral linear interpolation method, the data show that the optical signal to noise ratio (OSNR) remains the same in the presence of amplification. To be more concrete, Figure 2.32(a) shows the OSNR, in a 1 nm resolution bandwidth of the optical spectrum analyzer, to be 50 dB without passive amplification, PM-OFF (dashed blue), and 50 dB with passive amplification, PM-ON (red), indicating a noise figure of 0 dB. Within our ability to measure OSNR, we show there is no injected intensity noise from passive amplification.

On the other hand, when an active amplifier (EDFA) is used at the end of the same network instead of passive amplification, the OSNR degrades from 50 dB to 36 dB, PM-OFF + EDFA (dot-dashed green), due to the injected ASE noise from the active amplifier. Notice that all the spectra traces are normalized to their respective amplitude peaks. The injected noise from active amplification can also be inferred from the time traces shown in Figure 2.32(b). Although both active and passive amplification amplify the peak of the signal by approximately 7 dB (corresponding to passive gain of $m = 5$ and the equivalent active gain of 5), the active amplification also raises the average noise floor by 7 dB (dot-dashed green) whereas passive amplification leaves the floor at its original level (red). Figure 6c shows optical oscilloscope traces with zero averaging, clearly confirming an increased fluctuation when active amplification is employed (top trace) as compared to passive amplification (bottom trace).

Figure 2.33 shows enhancement of extinction ratio (ER) as the passive amplification factor m increases for a noisy input with OSNR=10. In this experiment, ASE noise was injected onto the pulse train in a controlled fashion using an EDFA, paired with a variable attenuator, at the input of the phase modulator and placing two more EDFAs in the dispersive span. We define ER enhancement as the ratio of the ER of the Talbot-amplified signal with respect to the ER of the input train, where ER is given by the ratio of the average peak intensity of the waveform to the average intensity of the noise floor.

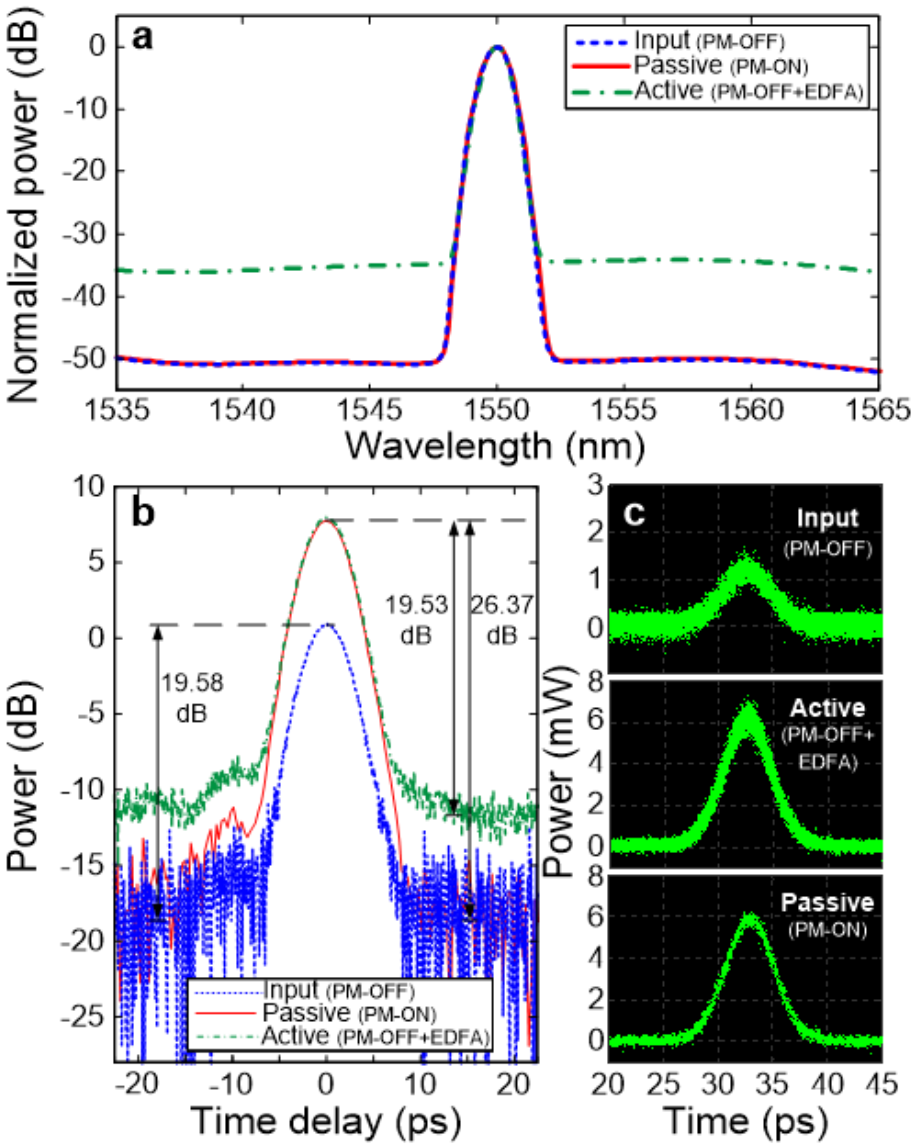

Figure 2.32 – Experimental verification of noiseless amplification. (a) Optical spectra of the pulse trains measured at the dispersive fiber output before passive amplification (phase modulator turned off, PM-OFF), (dashed blue), after passive amplification (phase modulator turned on, PM-ON) with *m*=5 (red), and with active amplification (EDFA) with gain of 5 (dot-dashed green). Notice that all the spectra are normalized to their respective amplitude peaks. (b)-(c) Corresponding optical sampling scope time traces in averaging mode and sampling mode (no averaging), respectively.

Figure 2.33(a) shows simulated data (blue squares) of how the ER scales linearly with m, and experimental data points for $m =$ 2, 5 and 15 overlaid (red triangles). The dashed blue line shows the expected linear trend for ER enhancement. Passive amplification increases the waveform peak

intensity by m times, while leaving the noise floor at its average value. After phase modulation, energy is distributed into m-times more frequency tones. After temporal redistribution by dispersive delay, the individual frequency components of the waveform will add coherently to give an average peak-power that is m-times the original signal. The noise floor, however, will remain the same. This is shown clearly in the optical sampling scope trace in Figure 2.32(b), as well as Figure 2.33(b) and (c), which show the optical sampling oscilloscope time traces with passive amplification (red) and without (dashed blue) for $m = 5$ and $m = 15$, respectively. Note that traces in Figure 2.33(b) and (c) have been normalized to the same peak power rather than the noise floor to better show ER enhancement. So long as the new frequency components generated during phase modulation are the correct ones (dictated by a correct phase drive), the noise floor will have the same average level from the destructive interference as before. Intensity noise present at the top of the waveform signal will also keep the same average value through the passive amplification process, in such a way that the ER enhancement actually increases linearly by a factor lower than m (approaching m for a higher input OSNR).

Talbot amplification is not simply a time-domain equivalent of band-pass filtering (BPF) but does actually redistribute signal energy from in-band noise. In order to show this important feature of our technique, we additionally show data of Talbot amplification used in conjunction with band-pass filtering and compare it to Talbot amplification without band-pass filtering, and to band-pass filtering alone. Figure 2.33(a) shows the experimentally expected enhancement to ER when band-pass filtering is employed without Talbot-amplification (solid violet). Here the filter used had a nearly flat-top spectral response with a 40 dB bandwidth of 2.8nm. For this case of OSNR=10, Figure 2.33(a) shows that BPF is better at enhancing the ER than passive amplification alone for $m = 5$, and that it is equivalent for $m = 15$. This can be also seen in the difference between the solid red and dot-dashed green curves in Figure 2.33(b) and (c). However, when a BPF is used in conjunction with Talbot amplification, the ER improves drastically since the BPF gets rid of the out-of-band noise, and the passive amplification additionally enhances the resulting ER as discussed above.

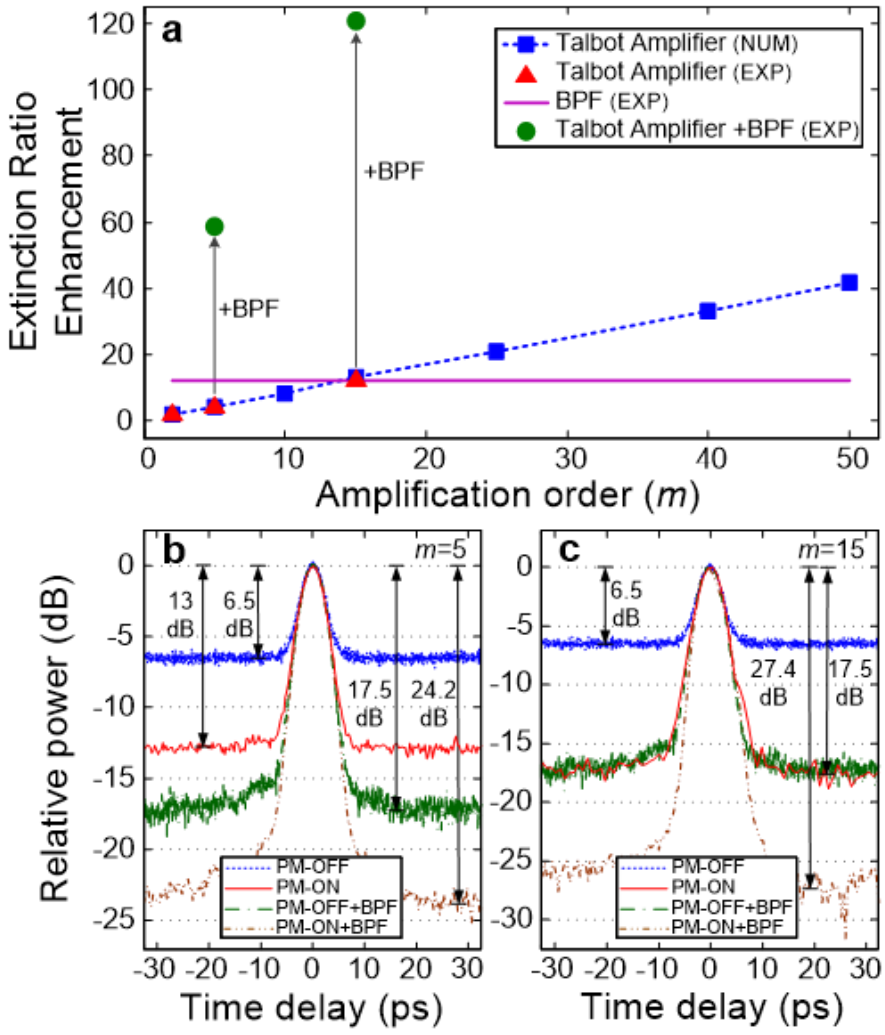

Figure 2.33 – Extinction ratio enhancement. (a) The experimental data points (red triangles) for *m* = 2, 5 and 15 are overlaid with the simulation trend (blue squares). The solid violet line shows the experimentally measured ERE when a band-pass filter is employed without Talbot-amplification. Solid green circles show experimental data points of ERE when a band-pass filter is used in conjunction with Talbot amplification. (b) Optical sampling oscilloscope time traces with passive amplification (red, PM-ON), without passive amplification (dashed blue, PM-OFF), with a BPF alone (dot-dashed green), and with both the use of a BPF and passive amplification (double-dot-dashed brown), for *m* = 5. (c) Similar optical sampling oscilloscope traces as in (b) but with *m* = 15 .

In the case of m = 15, the ER enhancement increases to 20.9 dB rather than ~11 dB from passive amplification alone. Likewise the ER enhancement for m = 5 shifts to 17.7 dB rather than ~6.5 dB from passive amplification alone. We note that the ER enhancement from the BPF

depends on the OSNR while the ER enhancement for Talbot amplification depends both on level of noise and amplification factor *m*. Talbot amplification becomes particularly effective for enhancing ER at low OSNRs whereas BPFs are less effective.

Figure 2.34 shows how Talbot amplification behaves as a conventional averaging process, e.g., scope averaging, on ASE-like intensity noise fluctuations. Figure 2.34(a) shows experimental data for the coefficient of variance (CV), the ratio of the standard deviation to the mean for the top level, of a noisy pulse (OSNR=10) vs. the inverse of the square root of amplification factor $m = \mathrm{N}$ (red squares). Also shown is the CV vs. the inverse of the square root of number of scope averages N (blue circles), demonstrating the equivalence of Talbot amplification to averaging. The theoretical trendline for scope averaging, which scales as $\sqrt{\mathrm{N}}$, is overlaid (dashed green). Experimental sampling oscilloscope traces in Figure 2.34(b) and c show how the point-to-point fluctuation is nearly the same for scope averaging and Talbot amplification. Figure 2.34(b) (blue) shows results for a pulse without passive amplification and a regular scope average of $\mathrm{N} = 15$, and Figure 2.34(c) shows results for a Talbot-amplified pulse by $m = 15$ with no scope averaging. OSNR=10 for the experimental traces. Here the realignment of newly created frequencies with old ones, with just as much negative and positive fluctuation, creates an averaging effect. Because there are m-times as many frequency tones adding together, the reduction in fluctuation (CV of intensity noise) at the waveform top nearly follows the conventional counting rule and goes like the square root of m.

Passive amplification is therefore equivalent to a real-time optical average. Said another way, Figure 2.34(c) is the equivalent of Figure 2.34(b) without the need for detection and post-processing. Such a real-time average could be particularly important where a clean pulse is needed directly in the optical domain. Notice also that whereas Talbot amplification is equivalent to scope averaging concerning its effect on white noise fluctuations, Talbot amplification additionally enhances the waveform train ER as the gain factor is increased. This is in sharp contrast to conventional scope averaging, where the noise floor and peak always average to their same respective levels, keeping ER constant.

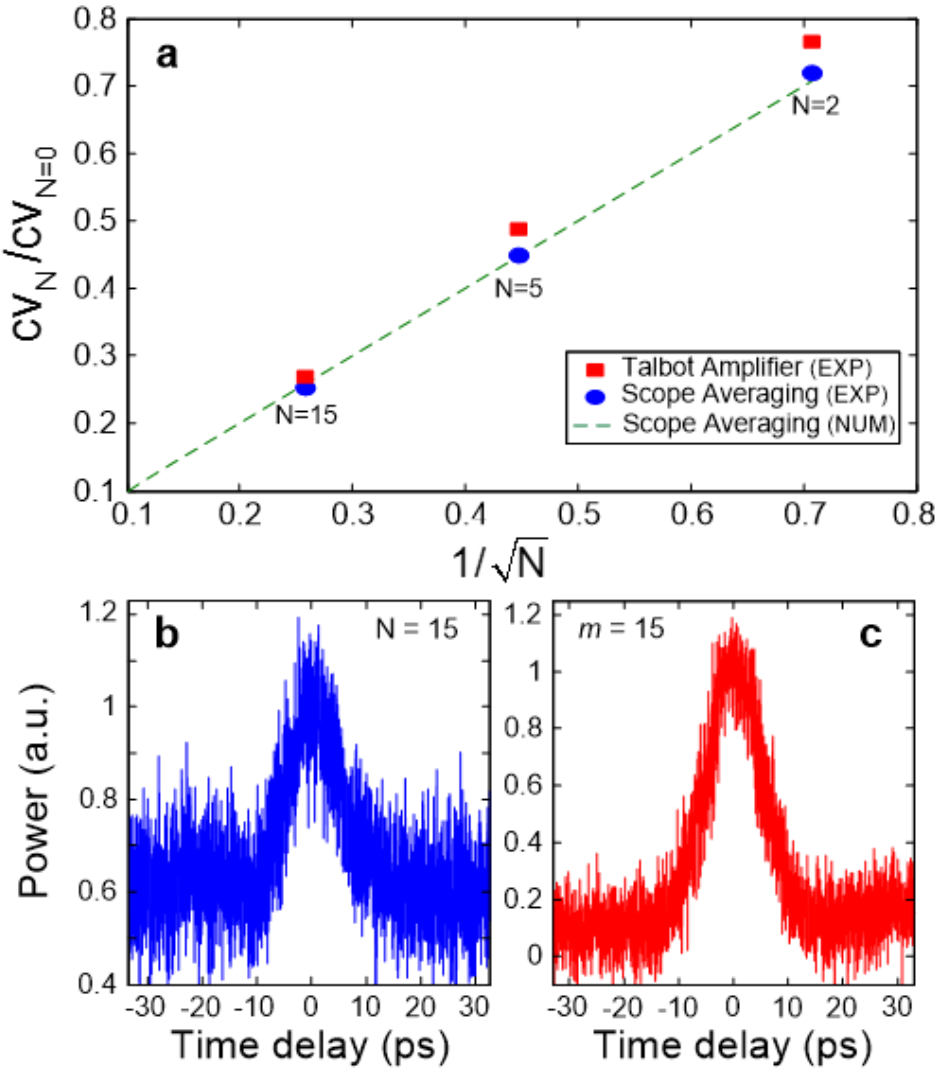

Figure 2.34 – Averaging effect of Talbot amplification for ASE-like noisy fluctuations. (a) Red squares show experimental data for the coefficient of variance (CV) of a passively amplified noisy pulse (OSNR=10) for a given passive amplification factor vs. the inverse of the square root of the amplification factor with no scope averaging. (b) Experimental sampling oscilloscope trace for a pulse without passive amplification using scope averages, (c) Experimental sampling oscilloscope trace of the same pulse train as in (b) but using passive Talbot amplification with and no scope averaging.

Finally, Figure 2.35 shows a side-by-side comparison of the oscilloscope time-trace of a Talbot amplified pulse train versus an actively amplified pulse train using an EDFA. Both amplification techniques amplified a very noisy input pulse train with an input OSNR=5, and both had a gain of 15.

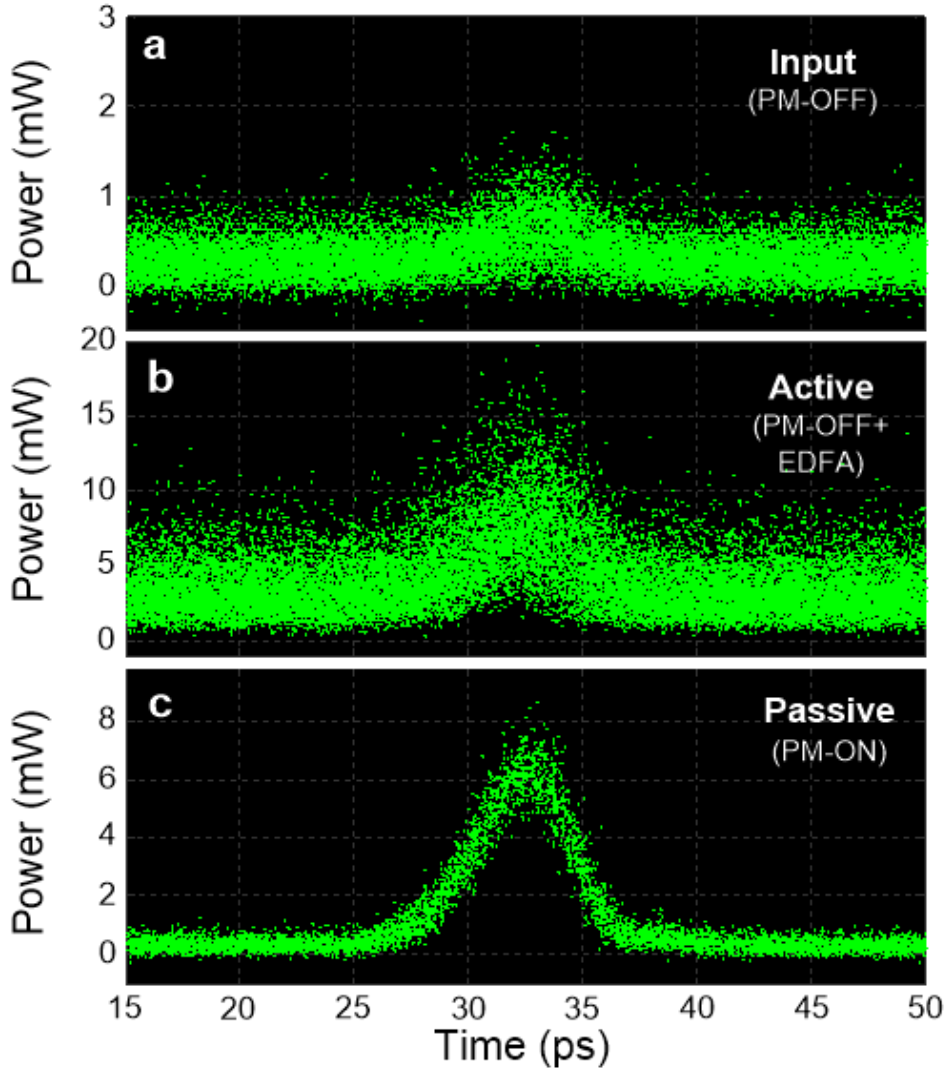

Figure 2.35 – Comparison of passive and active amplification. Oscilloscope time-traces of (a) a noisy pulse train (OSNR = 5) measured at the dispersive span output before passive amplification (PM-OFF), (b) Oscilloscope time-trace of the noisy signal shown in trace (a) after active amplification using an EDFA with a gain of 15, and (c) Oscilloscope time-trace of the noisy signal shown in trace (a) after passive Talbot amplification (PM-ON) with passive gain of 15.

The noisy input is shown in the top trace, and after active amplification, bottom trace, the pulse is significantly degraded. Noise is injected onto the already-noisy train, and both the noise floor and pulse peak are amplified about the same amount, negatively affecting the pulse quality. However, in the case of passive amplification, no noise is injected, the ER is enhanced by a factor approaching m - the peak is amplified while the noise floor is not, and the point-to-point

fluctuations from ASE noise are reduced by a real-time optical average in which 15 averages have been taken. Both scope traces show zero averaging in the scope representation, but the Talbot amplified pulse has notably better extinction and less noise fluctuation. This signal recovery resembles the strategies used in optical spread-spectrum methods to hide an optical pulse in noise and recover it from the noisy background through the use of a pseudo-random spectral phase mask (transmitter) and its conjugate (receptor) [214]. However, for Talbot passive amplification the analogous "phase masks" are in time and frequency, respectively, instead of frequency alone, effectively implementing a coherent addition of multiple consecutive waveform copies.

2.5.6 Discussion

Even though phase-only temporal and spectral manipulation processes ideally preserve the input signal energy, practical devices introduce losses, and these should be minimized in the design of amplification systems aimed at achieving input-to-output gain. Typically, highly-dispersive elements require large spectral phase shifts and these are typically achieved through long transmission paths, such as for the optical fiber solution shown here, which readily leads to loss. However, devices and materials can be engineered to simultaneously provide high levels of dispersion with high transmission. So long as the dispersive device provides linear dispersion over the bandwidth of the pulse train, there exist a variety of different options other than optical fiber with which to impose spectral phase. For example, in the optical region, chirped fibre Bragg gratings are available offering dispersion levels greatly exceeding 10,000ps nm^{-1} with less than 3dB loss [213]. Additionally, alternative methods exist for applying the spectral phase that is required for self-imaging without dispersive delay, such as spectral line-by-line shaping [158], for which spectral phase shifts can be restricted to the range $[0, 2\pi]$, though the limited spectral resolution of current line-by-line shapers restricts the amount of gain factor that could be practically achieved.

Though our technique cannot readily be used with aperiodic data, such as a random bit sequence, a single shot, or a sequence of data that is pulse-position coded, it can be made to work if such aperiodic data is made to repeat over some repetition period, even at a much slower rate. For example, the correct phase drive and subsequent dispersion could be engineered to amplify a repeating aperiodic sequence of 100 bits such that every set of 100 bits would coherently add.

Alternatively, one could purposely modulate data at a faster rate in order to use Talbot-amplification to coherently add and amplify it at a slower desired output rate. Though our technique cannot generally be applied to data sequences, there are important exceptions where it can be engineered to work.

Because dispersion in many wave systems can be controlled along wave propagation (as in the case of optical fibre links shown here), our method can also be used to tailor amplification to occur only at specific locations far away from any power source, offering the unique possibility of remote or localized waveform amplification. Perhaps of greater significance is how passive amplification using our method can be readily applied to other spectral regions or wave systems. Passive amplification by self-imaging is applicable to any wave system in which the temporal and dispersive spectral phase can be controlled. Such control is not only available throughout the entire electromagnetic spectrum [215], but also for many other wave systems, such as acoustic [216] and matter waves [217, 218], for which active gain mechanisms are extremely challenging to implement or simply not available. For example, direct passive amplification of acoustic and vibrational waveforms without the need for transducers could be useful in micro-electro-mechanical systems (MEMS) design [219], sonar, and ultrasonic sensing and imaging. Additionally, passive probability amplification of matter-waves could provide another tool for atom optics to control and manipulate quantum states of matter [217, 218] as well as single photon pulses [220].

2.5.7 Conclusion

In summary, we have proposed and experimentally demonstrated a new concept for waveform intensity amplification without using active gain by recycling energy already stored in the input signal. Our method uses dispersive self-imaging phenomena, temporal Talbot effects, which exploit the intrinsic repetitive nature of waveform signals to precisely redistribute the input signal energy into fewer waveforms in order to achieve noiseless amplification of each individual waveform. This technique allows us to overcome critical limitations of present active-gain based amplification methods. In particular, our demonstrated passive waveform amplification technique represents an amplification method that can be potentially applied to repetitive signals in all wave systems, eliminates the wasted power inherent in applications requiring peak-power amplification,

does not amplify or inject noise in the output signal, and even enhances the extinction ratio and reduces noise fluctuation of the input waveform train.

2.5.8 Methods

A. Optical waveform generation and phase modulation

We used a commercial actively mode-locked fibre laser (Pritel - Ultrafast Optical Clock) to generate a repetitive input optical pulse train with tunable repetition-rate. Temporal pulses directly generated from the laser are Gaussian in shape, approximately 7.0 ps intensity full width at half maximum (FWHM). Generation of optical pulses with a sinc-like temporal shape was achieved by filtering the input pulse train with a square-spectrum filtering function using an optical wave-shaper (Finisar 4000S). The appropriate multilevel temporal phase modulation required for a desired amplification factor was applied to the optical pulses with a commercial fibre-integrated electro-optic phase modulator (EOspace, 25 GHz bandwidth) driven by an electronic arbitrary waveform generator (Tektronix AWG7122C, 7.5 GHz analog bandwidth).

B. Dispersive medium

The subsequent first-order dispersion was provided by six dispersion-compensating fibre modules (Corning PureForm DCM-D-080-04), with a total of ~8,000ps nm^{-1} for $m = 15$ and $m = 27$ and ~2,650ps nm^{-1} for $m = 2$ and $m = 5$. Each module had a loss of 7 dB. Because the amount of dispersion required for coherent addition grows linearly with the desired amplification factor and quadratically with the temporal period of the repeating input waveform, changing the repetition-rate of the input pulse train allowed us the experimental convenience of demonstrating different amplification factors at the output of the similar length of dispersive optical fibre link.

C. Noise emulation

For noise mitigation experiments, ASE noise was purposely injected onto the pulse train using an EDFA at the input of the phase modulator and placing two additional EDFAs in the dispersive span. Using a variable attenuator prior to the input EDFA, we controlled the input power, versus the fixed amount of injected ASE noise from the EDFAs in the system, thereby implementing a desired value of OSNR. For simulation, noise was modeled in the frequency-domain as random Gaussian fluctuation in both phase and amplitude, with mean spectral amplitude- and phase-noise

components as zero and a standard deviation per frequency point normalized to sum to the desired average noise power, and corresponding desired OSNR.

D. Optical characterization

All optical time-traces were recorded with a 500-GHz bandwidth optical sampling oscilloscope (Exfo PSO-100), the optical spectra were recorded with high-resolution (20-MHz) optical spectrum analyzer (Apex, AP2440A), the RF phase drive was recorded with a 40-GHz bandwidth electrical sampling oscilloscope (Tektronix CSA8200), and RF spectra were recorded by detecting the optical pulse train with a 45-GHz photo-detector (New Focus Model 1014) which was then input into a 26-GHz RF spectrum analyzer (HP 8563E).

Chapter 3

Energy-Efficient Optical Signal Processors

3.1 Introduction

In this Chapter, we develop novel energy-efficient signal processing concepts and technologies for optical data signals used for telecom applications. For this purpose, we define, design, and develop two relevant set of processing approaches: (i) novel approaches for base-rate and sub-harmonic clock recovery of on-off-keying (OOK) data signals. The former is implemented based on phase-only linear optical filtering of the incoming RZ signal (Section 3.2), whereas the latter exploits the so-called 'inverse' self-imaging effect (Section 3.3). (ii) a novel approach for all optical return-to-zero (RZ)-to-non-RZ (NRZ) telecommunication data format conversion, which has been experimentally implemented at a bit rate of 640 Gbit/s. In this approach, we show how a proper phase-only manipulation of the frequency content of a RZ data signal can be used to implement conversion of the RZ signal into the equivalent NRZ time-domain data (Section 3.4).

3.2 Ultrafast All-Optical Clock Recovery Based on Phase-Only Linear Optical Filtering[21]

3.2.1 Abstract

We report on a novel, efficient technique for all-optical clock recovery from RZ-OOK data signals based on spectral phase-only (all-pass) optical filtering. This technique significantly enhances both the recovered optical clock quality and energy efficiency in comparison with conventional amplitude optical filtering approaches using a Fabry–Perot filter. The proposed concept is validated through recovery of the optical clock from a 640 Gbit/s RZ-OOK data signal using a commercial linear optical waveshaper.

3.2.2 Introduction

In all-optical clock recovery, the receiver retrieves timing information from an incoming optical data stream and produces an optical clock signal at a base rate or sub-harmonic rate without an intermediate electrical stage. The recovered clock signal is then used for many key functionalities that require synchronous operations, such as re-shaping and re-timing, OTDM demultiplexing, modulation format conversion and signal processing [46].

So far, a number of all-optical clock recovery techniques have been reported, which, in general, may be classified in two main categories [46, 221]: active pulsating and passive filtering techniques. Active pulsating techniques employ an opto-electronic oscillator or a self-pulsating laser to produce a high-quality clock signal, however, usually at the price of higher device complexity. On the other hand, passive filtering techniques typically benefit from simple construction. Their challenge is on the quality of the recovered clock signal though. Optical clock recovery based on a Fabry–Perot filter (FPF) is among the most studied passive techniques in order to recover the clock signal from a return-to-zero on-off-keying (RZ OOK) incoming optical data signal. A FPF is, in fact, an amplitude filter whose spectral transmission peaks are periodic over

[21] R. Maram, D. Kong, M. Galili, L. K. Oxenløwe and J. Azaña, "All-optical clock recovery based on spectral phase-only optical filtering" Optics Letters, vol. 39, no. 9, pp. 2815-2818, (2014).

the optical frequency bandwidth of interest and where the transmission spectral bands are typically narrow. This filter, with a free spectral range (FSR) tuned to the bit rate of the incoming optical data signal, preserves the discrete clock spectral components from the incoming optical data signal and removes the rest of the signal's continuous spectral content, which typically contains around 50% of the overall energy of the incoming data signal. Since a FPF is a fully passive device, the operation speed of techniques based on FPF is ideally unlimited. However, to achieve a high-quality clock signal, a high finesse FPF is required to average out the incoming data pattern. The needed high finesse imposes a very stringent tolerance for mismatching between the filter specifications (resonant frequency and FSR) and the incoming data signal specifications (central wavelength and bit rate, respectively). On the other hand, a lower FPF finesse leads to amplitude modulation (AM) in the clock signal. To minimize this AM, the FPF should be followed by a nonlinear subsystem [46], e.g., a semiconductor optical amplifier (SOA), an ultrafast nonlinear interferometer or a Mach–Zehnder interferometer, acting as an optical power equalizer. Not only does this increase the clock-recovery circuit complexity but additionally, these subsystems may limit the system operating data rate, e.g. to tens of Gbit/s when using SOAs.

In this paper, we demonstrate a novel, simple passive all-optical clock recovery technique based on spectral phase-only (all-pass) optical filtering for RZ-OOK data signals. This technique overcomes the above-mentioned crucial drawbacks of the FPF method. In particular, the proposed technique offers a significantly improved performance, e.g. leading to significantly smaller AM in the recovered clock signal for similar filter specifications (particularly finesse), in comparison to an amplitude filter, such as a FPF. It also provides higher energy efficiency, at least a two-fold improvement, since fundamentally no signal energy is lost in the phase-only optical filtering process. The novel scheme is demonstrated using numerical simulations and through a successful proof-of-concept all-optical clock recovery experiment on a 640 Gbit/s data signal using a commercial linear optical waveshaper.

3.2.3 The operation principle

All-optical clock recovery of an RZ-OOK data signal can be achieved by extracting the discrete clock spectral components of the incoming signal, which implies suppressing the continuous frequency content of the signal optical spectrum. A periodic optical amplitude filter whose FSR is

matched to the signal bit rate (f_0) and a sufficiently narrow spectral line-width (F_b), i.e., high finesse (= FSR/F_b), can effectively implement this operation, as shown in Figure 3.1, left.

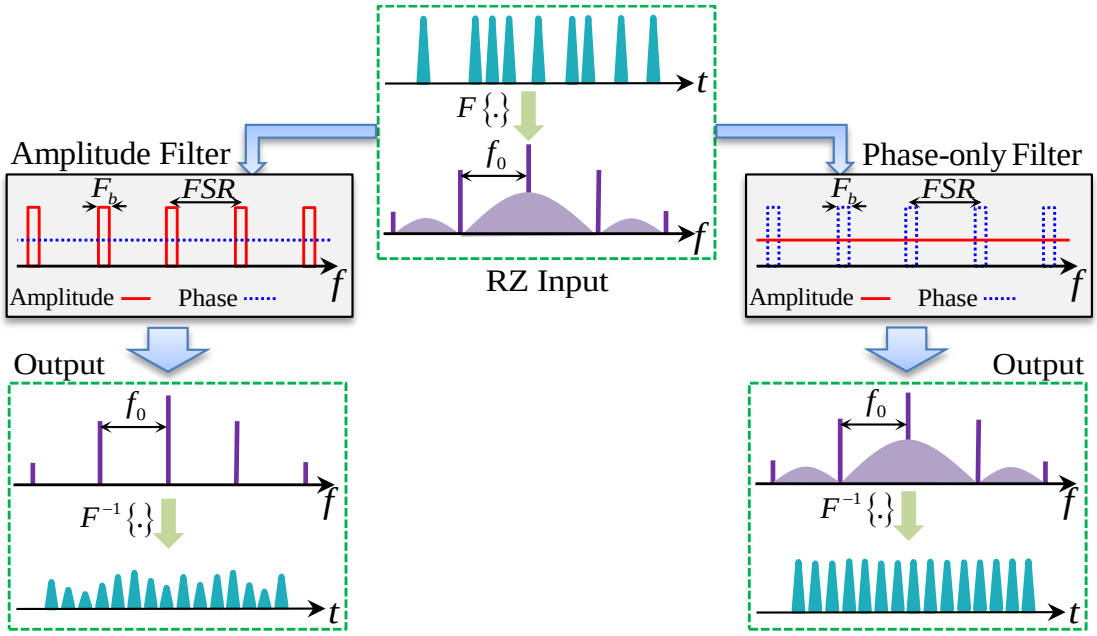

Figure 3.1 – Principle of the optical clock recovery methods based on amplitude (left) and phase-only (right) filtering. F stands for Fourier transform.

In this clock recovery process, approximately 50% of the energy of the input optical signal is lost in order to extract the desired optical clock signal. Additionally, the extracted signal also suffers from an increased amplitude modulation (AM: highest to lowest pulse ratio) as the finesse of the filter is decreased, i.e. as the spectral line-width F_b is increased. However, we show here that a spectrally periodic phase-only filter can be properly designed to achieve the same clock recovery result with significantly reduced AM, for the same value of filter finesse (defined now as the spectral *phase* line-width), and without removing any spectral component of the input signal and hence, without fundamentally losing any energy in the filtering process. Figure 3.1, right, shows schematically the spectral phase profile of the proposed all-pass filter: the discrete clock spectral components in the input optical signal must be phase shifted by $\pi/2$ with respect to the rest of the signal spectrum. Thus, the FSR of the spectral phase profile must be also fixed to match the data signal bit rate. Indeed, the operation principle of the phase filtering technique is inspired from the amplitude filtering approach, in which the extraction of either the discrete clock spectral

components or continuous spectral content leads to the creation of periodic optical pulse trains along the time domain. However, in the former, all pulses are in-phase whereas in the latter, pulses are phase-shifted by π in the temporal locations corresponding to the "zeros" of the input signal. In the reverse direction, summation of these pulse trains will retrieve the input signal. However, in the phase filtering approach, the temporal periodic pulses corresponding to the discrete clock components and continuous spectral content are all phase-shifted by $\pi/2$ with respect to each other. Thus, the two components beat in intensity leading to the observed generation of the periodic optical clock pulse train. The defined phase filtering can be practically implemented using a variety of technologies such as line-by-line optical pulse shapers, Fiber Bragg Gratings (FBG), thin film filters, photonic ring resonators, and photonic crystals, among others [222]. Polarization-independent clock recovery can be achieved as long as a polarization-insensitive optical filtering technology is used. In the experiment reported here, we use a line-by-line optical pulse shaper, which allows for high-resolution, independent manipulation of the phase of the individual spectral lines. Line-by-line pulse shapers with frequency resolutions (F_b) as low as ~890 MHz have been reported [223].

3.2.4 Performance analysis and simulation results

The described operation principle has been first validated and compared with the use of a FPF with similar filtering specifications (shape, FSR and finesse, ignoring insertion loss) through numerical simulations based on the standard frequency-domain method for linear processes. Figure 3.2 shows the transmission spectrum and spectral phase of the used (a) FPF and (b) phase filter, respectively. The finesse of the two filters is assumed to be 103. As for the input data signal, we assume RZ-OOK data with a pseudorandom bit sequence (PRBS) of 2^7-1 bits, 400-fs FWHM Gaussian pulses, with peak power of 100 mW, and a bit rate of 640 Gbit/s.

Figure 3.3 presents the simulation results of all-optical clock recovery from the 640 Gbit/s input signal. Each row shows temporal waveform and optical spectrum of the input signal ((a) and (b)), the recovered optical clock after the FPF ((c) and (d)), and the recovered clock after the phase filter ((e) and (f)), respectively.

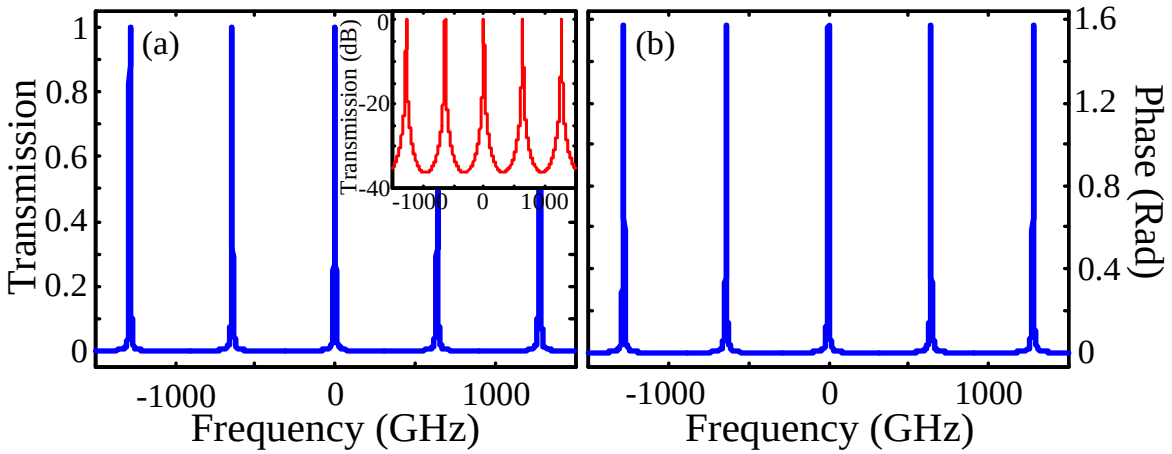

Figure 3.2 – (a) Transmission spectrum of the FPF and (b) spectral phase profile of the phase filter, used for numerical simulations.

The corresponding persistent-mode temporal waveforms of the extracted optical clocks are illustrated in Figure 3.4(a) and (b), respectively.

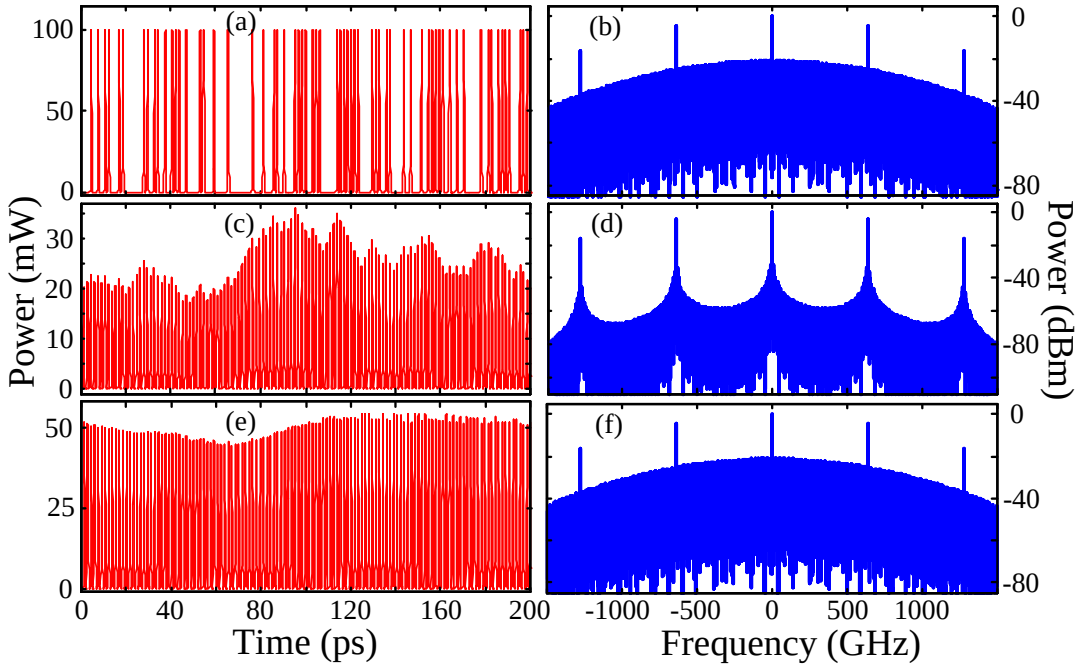

Figure 3.3 – Simulation results of all-optical clock recovery from a 640 Gbit/s input signal. Temporal waveforms and optical spectra of (a)-(b) the input signal, (c)-(d) the recovered optical clock using amplitude filter, and (e)-(f) the recovered clock using phase filter.

The waveform of the recovered clock through phase filtering shows a clear reduction in AM, down to 0.86 dB, in comparison with the FPF-recovered clock, with AM of 3.2 dB. Due to the strong suppression of spectral content by the FPF, the discrete clock components appear strongly emphasized in the optical spectrum of the corresponding extracted optical clock, whereas the optical spectrum of the extracted optical clock by the phase filter remains unchanged with respect to that of the input signal. This yields a nearly two-fold energy improvement for the phase-only filtering approach as compared with the FPF approach, as can be also directly inferred by comparison of the power levels of the temporal waveforms in Figure 3.3(c) and (e). Figure 3.4(c) shows the AM variation as a function of the finesse of the FPF and phase filter.

As expected, AM decreases with filter finesse. The AM in the extracted clock is significantly lower for the phase filter than for the FPF. This means that to achieve the same degree of AM, the FPF should have a significantly higher finesse than the phase filter. As an example, to acquire a recovered clock with an AM of 0.1 dB, the phase filter requires a finesse of 447 while this should be increased to 3489 for the FPF. Note that for a given filter finesse, AM increases as the number of consecutive zeros in the input signal's pattern increases. For instance, for a filter finesse of 103, the AM of the recovered clock approaches 8 dB when there are 38 consecutive zeros if using a FPF, and 67 consecutive zeros when using a phase filter.

To analyze the performance of the FPF and phase filter in regards to timing jitter, a 1-GHz sinusoidal jitter is numerically simulated on the input signal. Figure 3.4(d) shows the root mean square (rms) timing jitter of the recovered optical clock (output), which is calculated by integrating the single-sideband-to-carrier ratio (SSCR) phase-noise from an offset frequency of 1 kHz to 5 GHz, as a function of the applied input timing jitter. The two filters exhibit a roughly similar performance in terms of timing jitter for moderate to high finesses, e.g. the output rms jitter is approximately equal to the input one for both filters when the filter finesse is 103. Both filters have the capability of reducing the input timing jitter for a sufficiently high finesse, though the FPF typically exhibits a better performance than that of the phase filtering approach, e.g. the output timing jitter is reduced by 37% in the FPF case vs. 25% for the phase filtering case when the finesse is increased to 500. This is so because at higher values of finesse, the FPF attenuates more strongly the noise frequency peaks, created by the imposed jitter, with respect to the clock spectral components.

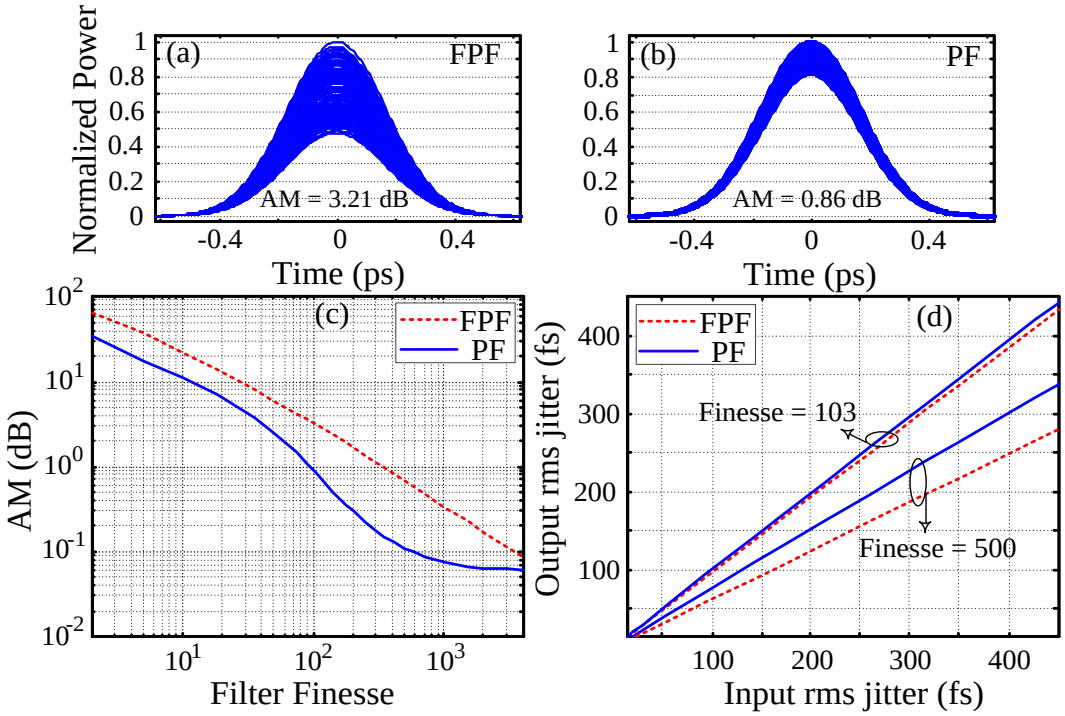

Figure 3.4 – Results from numerical simulations: (a), (b) Persistent-mode waveforms of the recovered clock signals in Figs 2(a) and 2(c), respectively; (c) Amplitude modulation versus filter finesse; (d) Output versus input rms jitter. FPF: Fabry-Perot filter, PF: phase filter.

3.2.5 Experimental demonstration

We furthermore report on a proof-of-concept experiment to validate the proposed concept by performing clock recovery from a 640 Gbit/s RZ OOK data signal. The used experimental setup is sketched in Figure 3.5. The setup consists of three main blocks: 1- the transmitter, to generate a 640 Gbit/s phase-coherent RZ OOK signal, 2- the spectral phase-only (all-pass) optical filter, to recover the clock signal, and 3- the receiver, to measure the temporal waveform and spectrum of the recovered optical clock signal.

In the transmitter, optical pulses are generated by an erbium-glass oscillating pulse generating laser (ERGO-PGL) at 1542 nm with pulsewidth of 1.5 ps and 10-GHz repetition-rate. Subsequently, the pulses are compressed down to 720 fs by self-phase modulation in 400 m of dispersion-flattened highly nonlinear fiber (DF-HNLF) and filtered with an optical band-pass filter (OBPF) at 1537 nm with a 3-dB bandwidth of 16 nm.

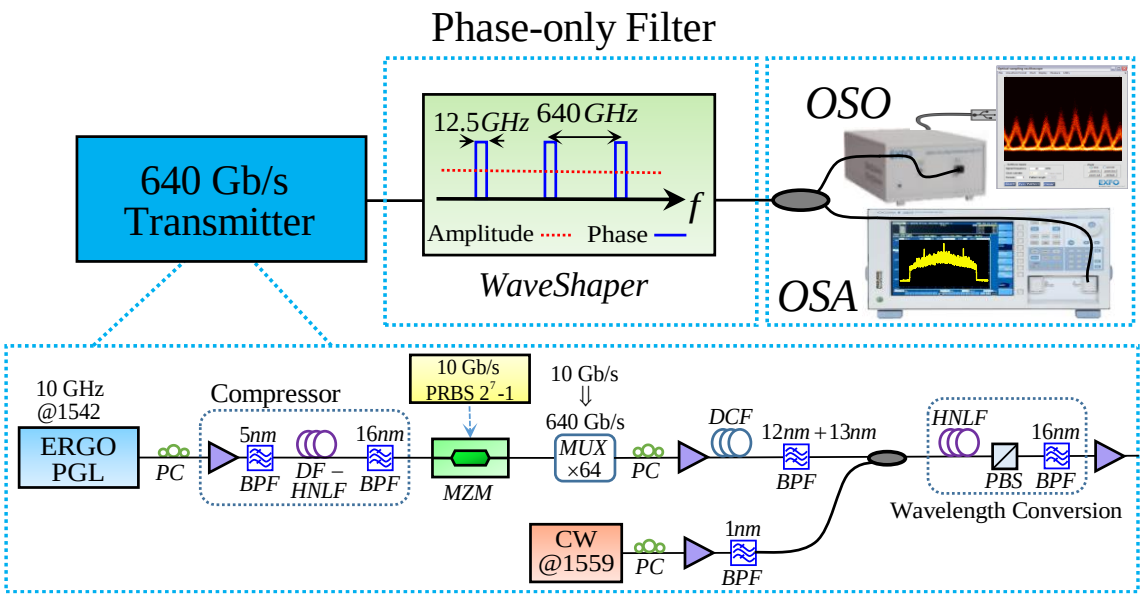

Figure 3.5 – Experimental setup of the all-optical clock recovery technique using a phase-only filter.

The pulses are then intensity modulated at the 10 Gbit/s base rate with a 2^7 -1 PRBS sequence. The modulated pulses are time-multiplexed in a passive fiber-based split-and-delay multiplexer (MUX) to constitute the 640 Gbit/s RZ OTDM signal. In the OTDM signal, the phases of the different tributary channels are uncorrelated, making the OTDM signal pulse-to-pulse incoherent. To successfully recover the clock signal, a phase-coherent RZ OTDM signal is however required, which can be obtained by wavelength converting the original incoherent OTDM signal. Therefore, the 640 Gbit/s RZ OTDM signal is subsequently wavelength converted using a polarization-rotating Kerr switch [104] to obtain the phase-coherent OTDM signal. The converted RZ signal is then amplified before being input to the phase-only filter. Notice also that in an actual optical transmission system, the optical signal should be dispersion-compensated prior to the clock recovery block in the receiver. An imperfect dispersion compensation may lead to a crosstalk between optical pulses in the clock signal in both the amplitude and phase filtering methods. The generated data signal is then delivered to the clock recovery block comprising the phase-only linear optical filter.

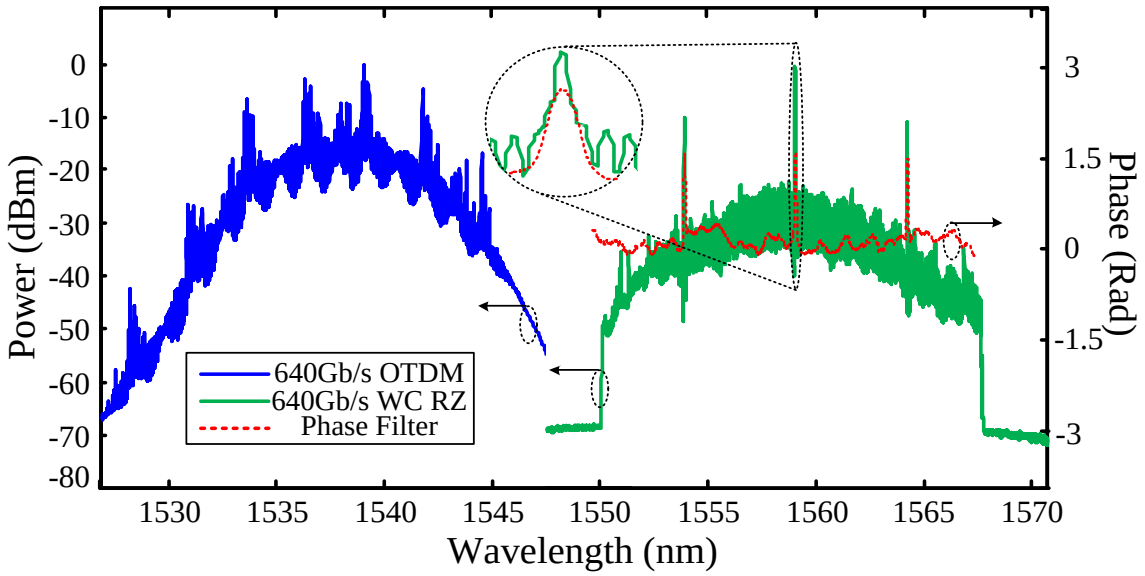

Figure 3.6 – (a) Spectra of the original OTDM (blue) and wavelength converted RZ (green) signals, as well as spectral phase profile of the used phase filter (red).

A line-by-line pulse shaper (Finisar WaveShaper 4000S) has been programmed to produce the needed filtering specifications, i.e., constant spectral amplitude and a spectral phase profile with periodic π/2 phase shifts over the desired bandwidth, with a spectral period of FSR = 640 GHz and a finesse of around 51. The employed filter finesse is determined by the minimum bandwidth (frequency resolution) of the utilized line-by-line pulse shaper, F_b = 12.5 GHz. The spectra of the original 640 Gbit/s OTDM and the generated 640 Gbit/s phase-coherent RZ signal, captured by a standard optical spectrum analyzer (OSA) with resolution bandwidth of 0.02 nm, together with the spectral phase profile of the filter are depicted in Figure 3.6. The spectral phase response of the phase filter was measured with an Optical Vector Analyzer (Luna Technologies).

Owing to the lack of pulse-to-pulse phase correlation between the tributary channels of the original 640 Gbit/s OTDM signal, one can notice that the OTDM spectrum (blue) does not contain strong clock components at frequencies corresponding to multiples of the bit rate. However, the 640 Gbit/s wavelength-converted RZ spectrum (green) displays clear and strong clock components and is thus suitable for the proposed clock recovery scheme. For this purpose, the spectral clock components of the 640 Gbit/s wavelength-converted RZ spectrum are phase-shifted by $\pi/2$ with respect to the rest of the signal spectrum by the phase filter, as shown in Figure 3.6. The OSNR of the input and clock signals are 41.5dB.

Figure 3.7 illustrates the temporal intensity traces of (a) the 640 Gbit/s input data signal and (b) the recovered clock signal at the output of the phase filter, measured by a 500-GHz bandwidth optical sampling scope (Exfo PSO-101). As can be clearly seen, the proposed concept has implemented the target optical clock recovery operation on the input data signal. Figure 3.8 shows the corresponding eye-diagram of the 640 Gbit/s input data signal and the waveform of the recovered clock signal, respectively.

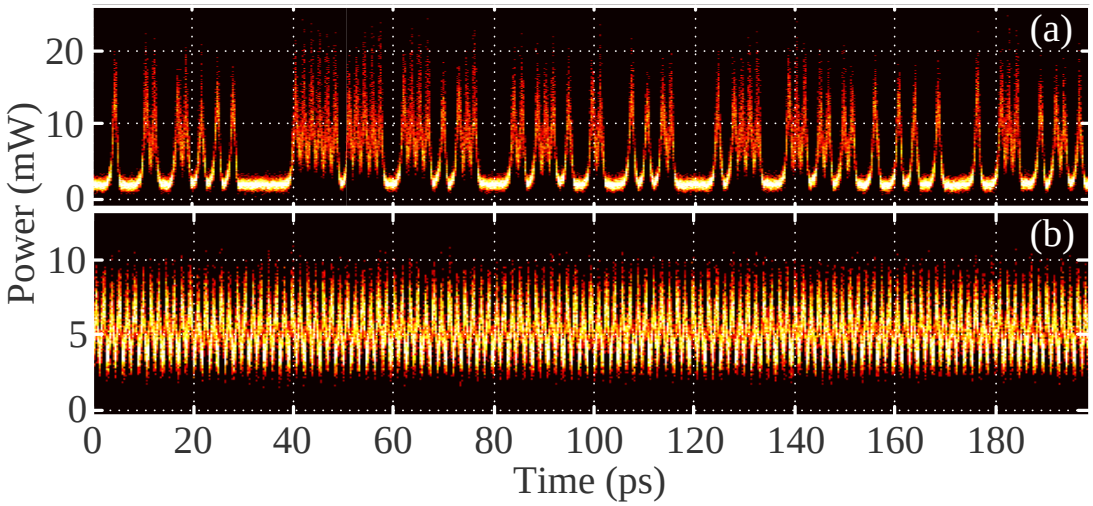

Figure 3.7 – Temporal traces of the 640 Gbit/s coherent input data signal and the extracted clock signal.

A clear waveform with low amplitude modulation is obtained for the 640 Gbit/s clock signal. The estimated AM for this clock signal is around 2.5dB, in good agreement with the Figure 3.4(c) for a phase filter with finesse of ~51. In comparison, according to this curve, a FPF with finesse of 140, beyond the frequency-resolution capabilities of the used pulse shaper, would be required to obtain the same amount of AM.

Even though no measures were taken to reduce timing jitter, the estimated rms timing jitter of the recovered clock signal is around 350 fs. Notice that using flat-top switching windows, a timing jitter up to 30% of the timeslot can be tolerated, which for 640 Gbit/s corresponds to around 500 fs [224]. If needed, we expect the timing jitter to become lower for higher finesse.

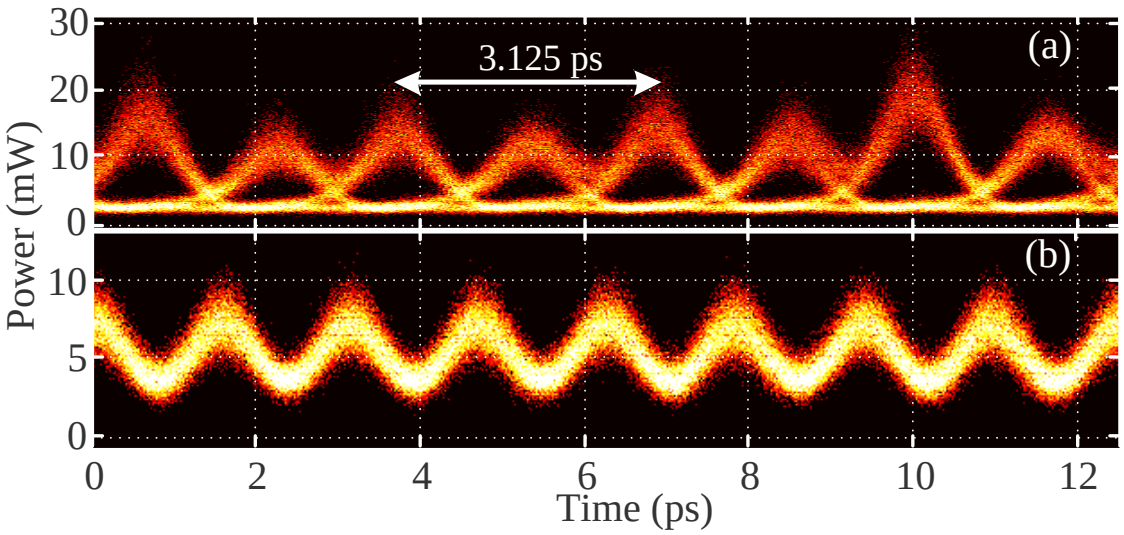

Figure 3.8 – Corresponding (a) eye diagram of the input data and (b) persistent-mode waveform of recovered clock signals in Figure 3.7

3.2.6 Conclusion

In summary, we have proposed and experimentally demonstrated a novel energy-efficient all-optical clock recovery concept based on all-pass (phase-only) optical filtering. Besides its intrinsic implementation simplicity, this technique enhances both the quality of the recovered optical clock and the energetic efficiency of the recovery process in comparison with conventional filtering approaches using a FPF. Proof-of-concept experiments at 640 Gbit/s have validated the proposed concept and predicted advantages.

3.3 Sub-harmonic periodic pulse train recovery from aperiodic optical pulse sequences through dispersion-induced temporal self-imaging[22]

3.3.1 Abstract

Temporal self-imaging effects (TSIs) are observed when a periodic pulse train propagates through a first-order dispersive medium. Under specific dispersion conditions, either an exact, rate multiplied or rate divided image of the input signal is reproduced at the output. TSI possesses an interesting self-restoration capability even when acting over an aperiodic train of pulses. In this work, we investigate and demonstrate, for the first time to our knowledge, the capability of TSI to produce periodic sub-harmonic (rate-divided) pulse trains from aperiodic sequences. We use this inherent property of the TSI to implement a novel, simple and reconfigurable sub-harmonic optical clock recovery technique from RZ-OOK data signals. The proposed technique features a very simple realization, involving only temporal phase modulation and first-order dispersion and it allows one to set the repetition-rate of the reconstructed clock signal in integer fractions (sub-harmonics) of the input bit rate. Proof-of-concept experiments are reported to validate the proposed technique and guidelines for optimization of the clock-recovery process are also outlined.

3.3.2 Introduction

The temporal self-imaging effect (TSI), also referred to as temporal Talbot effect, is the time-domain counterpart of the well-known spatial self-imaging phenomenon [41, 135]. This space-time duality is related to the mathematical isomorphism existing between the equations describing the paraxial diffraction of beams in space and the first-order temporal dispersion of optical pulses. The TSI occurs when a periodic train of optical pulses propagates through a dispersive medium in a first-order approximation; such a dispersive medium is characterized by a linear all-pass amplitude response and a quadratic phase variation in frequency. An appropriate amount of

[22] R. Maram, L. Romero Cortés and J. Azaña, "Sub-harmonic periodic pulse train recovery from aperiodic pulse trains through dispersion-induced temporal self-imaging," Optics Express, vol. 23, no. 3, pp. 3602-3613, (2015).

dispersion, given by the so-called self-imaging condition [41, 135], leads to either an exact reproduction of the original pulse train (integer TSI) or to repetition-rate multiplication by an integer factor (fractional TSI).

Besides the intrinsic physical interest of the TSI phenomenon, it has also been put into practical use in several areas. In particular, TSI has been extensively studied as a lossless mean to multiply the repetition-rate of a periodic pulse train, through fractional TSI [41, 135, 158, 185, 225, 226, 227]. This phenomenon also has been investigated theoretically to be an accurate technique for measuring the first-order dispersion coefficient of dispersive media [135]. Moreover, Pudo et al. [100, 99] have shown the inherent buffering ability of TSI to generate a periodic output, even from an aperiodic input pulse train. They have used this property to perform base-rate clock recovery (BRCR) of a return-to-zero on–off keying (RZ-OOK) optical data signal by utilizing single-mode fibers (SMFs) or linearly chirped fiber Bragg gratings (LCFBGs) as dispersive media.

Very recently a new feature of TSI, referred here to as inverse temporal self-imaging (I-TSI), has been reported to demonstrate passive amplification of repetitive optical signals [188]. I-TSI involves repetition-rate division of an incoming repetitive pulse train by an integer factor (m = 2, 3, …) through an ideally lossless redistribution of the input signal energy, effectively implementing a process equivalent to coherent addition of each m individual consecutive pulses. Similar to the TSI, the I-TSI is based on the distributed interference of dispersed pulses, i.e., there is no direct one-to-one correspondence between the input and output pulses. As a consequence, we anticipate that this effect should also possess the inherent property to generate a periodic output (with sub-harmonic repetition-rate), yet from an aperiodic input pulse train. This feature, therefore, could be appropriately used to recover the m-sub-harmonic clock signal of a RZ-OOK data signal. In optical communications, optical sub-harmonic clock recovery (SHCR) is a fundamental functionality for de-multiplexing optical time-division multiplexed (OTDM) systems and subsequent processing operations [228, 229, 94, 230].

In this paper, we propose and experimentally demonstrate the realization of a reconfigurable SHCR technique based on I-TSI. The proposed concept can be implemented using a very simple setup, involving a suitable combination of temporal phase modulation and dispersive spectral phase filtering of the original aperiodic (data) pulse train. This setup can be designed to reconstruct a periodic optical pulse train (clock) in which the pulses are spaced by m times the bit period of

the input data signal, i.e., the output is a sub-harmonic clock signal with a bit rate division factor of m. As detailed below, quality of the recovered clock signal is strongly related to the duty-cycle of the input pulses and the amount of dispersion used to implement the required spectral phase filter.

The proposed technique offers similar advantages to those of the TSI-based BRCR method [100, 99], namely simplicity, the potential for timing-jitter mitigation and high energy efficiency. The latest is associated with the fact that fundamentally, no energy is lost in the recovery process, since this involves only manipulations of the signal's phase information, in the time and frequency domains. Moreover, the SHRC scheme can be easily reconfigured to achieve clock recovery at the input signal's bit rate (BRCR, m = 1) by simply bypassing the temporal phase modulation process.

3.3.3 Concept and operation principle

Figure 3.9 illustrates the principle of our proposed concept. Figure 4.9(a) represents the well-known standard temporal self-imaging (Talbot) effect in which a flat-phase repetitive input train of pulses (signal at $z = 0$, where z represents the axial propagation coordinate) is self-imaged, after dispersive propagation through an integer multiple of the Talbot length, z_T (integer Talbot images). In this representation, first-order dispersive propagation, involving a linear group delay profile, is assumed. Additionally, rate-multiplied self-images of the original input waveform train are obtained at fractional values of the fundamental Talbot distance, z_T, as defined by the "Talbot Carpet" [41]; see examples in Figure 4.9(a) at the fractional Talbot distances $z_T/2$, $2z_T/3$ and $3z_T/4$. Dispersive propagation speeds up and slows down the different frequency-components, originally in-phase, of the pulse train, thus redistributing the energy of the signal into the mentioned different temporal intensity patterns. An integer self-image exhibits the same repetition-rate as the input signal, whereas in the multiplied self-images, the repetition-rate is increased. The repetition-rate-multiplication factors for the multiplied self-images shown in Figure 4.9(a) at $z_T/2$, $2z_T/3$ and $3z_T/4$ are 2, 3 and 4, respectively.

In an integer self-image, the uniform temporal phase profile of the input is restored. However, the multiplied self-images, such as those observed at distances $z_T/2$, $2z_T/3$ and $3z_T/4$ are affected by a deterministic pulse-to-pulse residual temporal phase profile (dashed black). This residual temporal phase represents instances where the pulse field-amplitude has been advanced or delayed

in relation to the envelope center [41, 188]. The residual phase for a particular fractional image can be mathematically calculated and pre-introduced to the input signal by means of a phase-modulation mechanism. This emulates the effect of a previous propagation through dispersion of the input signal. Further dispersive propagation of such signals to the distance z_T produces an output with a reduced repetition-rate. The repetition-rate of a pulse train starting at the fractional distance $z_T/2$ will be reduced by a factor of $m = 2$ at the output as depicted in Figure 4.9(b). Likewise, the repetition-rate of a pulse train starting at the fractional distance $2z_T/3$ will be reduced by a factor of $m = 3$.

Similarly, we anticipate that an aperiodic input pulse train (e.g. a RZ-OOK data signal) undergoing similar processing steps will also produce a periodic pulse train output, with a repetition-rate that is reduced by an integer factor of m with respect to the input bit rate, as shown in Figure 4.9(c). In this paper, we demonstrate and study this interesting property of the temporal Talbot effect, for the first time to our knowledge. We also show how this property can be applied towards a simple, passive optical sub-harmonic clock recovery scheme for OOK-RZ transmission systems. Notice that the required processes involve only a suitable manipulation of the input signal temporal and spectral phase profiles, ensuring that the signal energy is ideally preserved.

The complete Talbot carpet provides an infinite amount of fractional self-image conditions and corresponding phase profiles, so that any desired repetition-rate division factor can be obtained, only limited in practice by the degree of control that one can achieve on the temporal phase modulation mechanism and dispersion-induced spectral phase filtering.

The required temporal phase modulation profile can be deduced from the self-imaging theory [41, 188] so that in order to recover the sub-harmonic clock signal of a RZ-OOK input signal with clock division factor of m (= 2, 3, 4, …), a quadratic temporal phase variation must be applied, i.e.

$$\varphi_n = \frac{m\text{-}1}{m}\pi n^2 \tag{3.1}$$

where φ_n is the amount of temporal phase-shift to be applied on the n-th bit ($n = 0,1,2,\ldots, m\text{-}1$) of the input data signal. If these phase shifts are reduced to a 2π range, a periodic sequence of phase steps with a fundamental period equal to the clock division factor m, (i.e. $\varphi_n = \varphi_{n+m}$) is obtained. These phase shifts induce a spectral self-imaging effect on the modulated data signal [75, 189]. In

particular, the temporal phase modulation process reduces the spectral comb spacing of the clock component (i.e. the spectral separation between two adjacent lines) of the input data signal by an integer factor of *m*.

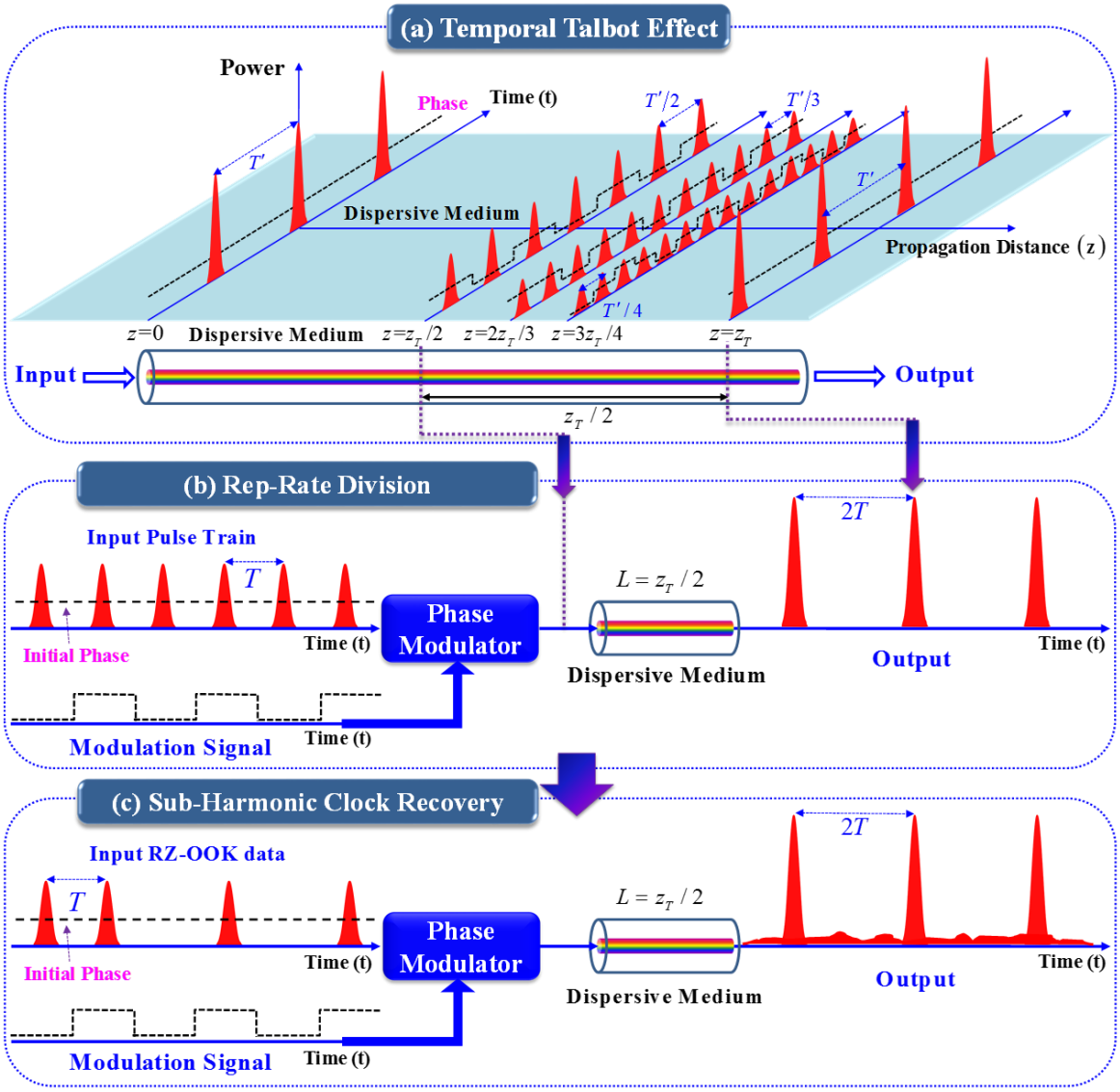

Figure 3.9 – (a) Standard temporal Talbot effect. Evolution of a repetitive input pulse train through propagation along a first-order dispersive medium. (b) Repetition-rate division by temporal self-imaging assisted [188]. (b) Illustration of the principle of operation of the proposed SHCR concept.

As per the TSI theory [41, 188], the subsequent dispersive medium should introduce a total dispersion value given by equation (3.2):

$$\phi_T^{(2)} = (s \times m + 1)\frac{mT^2}{2\pi} \tag{3.2}$$

where $s = 0,1,2,\ldots$, T is the bit period of the input data signal (inverse of the input bit rate), and $\phi_T^{(2)}$ is the slope of the medium's group delay vs. radial frequency. Notice that $s = 0$ ensures the minimum dispersion value required to obtain the target sub-harmonic clock signal. It should be mentioned that in the absence of temporal phase-modulation, the dispersion $\phi_T^{(2)}$ will produce an integer Talbot self-image of the original pulse train at the output of the dispersive medium. This fact allows one to re-program the scheme to achieve also clock recovery at the basic input bit rate (BRCR) by simply bypassing the temporal phase-modulation mechanism.

In order to present a more intuitive insight into the operation principle of the proposed sub-harmonic clock recovery technique, we use joint time-frequency (TF) representations of the involved signals, first for a periodic input pulse train as shown in Figure 3.10, and then for an aperiodic input pulse train (e.g. a RZ-OOK data signal), as shown in Figure 3.11. For each TF representation, the bottom plot represents the temporal variation of the pulse train and the plot at the left represents the corresponding spectrum, with the 2D energy distribution shown in the larger central plot.

Figure 3.10 shows the case when the input signal is a periodic pulse train and we target a repetition-rate division factor of two ($m = 2$), for example. In the absence of temporal phase-modulation, each repeating pulse of the input pulse train along the temporal domain is composed by all the discrete frequency components of the original pulse train, as shown in Figure 3.10(a), left. The dispersive medium, with dispersion coefficient of $\phi_T^{(2)} = 2T^2/2\pi$ [from Eq.(3.2), with $s = 0$] $\phi_T^{(2)} = T^2/2\pi$, introduces a group delay difference of $2T$ between two adjacent discrete frequency components with frequency spacing of $F = 1/T$. Spectral superimposition of the resultant dispersed pulse train produces an exact (integer) Talbot self-image of the original pulse train at the fiber output, as illustrated in Figure 3.10(a), right. Application of the prescribed temporal phase-modulation profile for the case $m = 2$, $\varphi_n = \{0, \pi/2, 0, \pi/2,\ldots\}$, derived from Eq.(3.1), to the input periodic pulse train, produces new frequency components, reducing the comb frequency spacing of the input signal by a factor of 2 (i.e. to $F/2$), as illustrated in Figure 3.10(b), left.

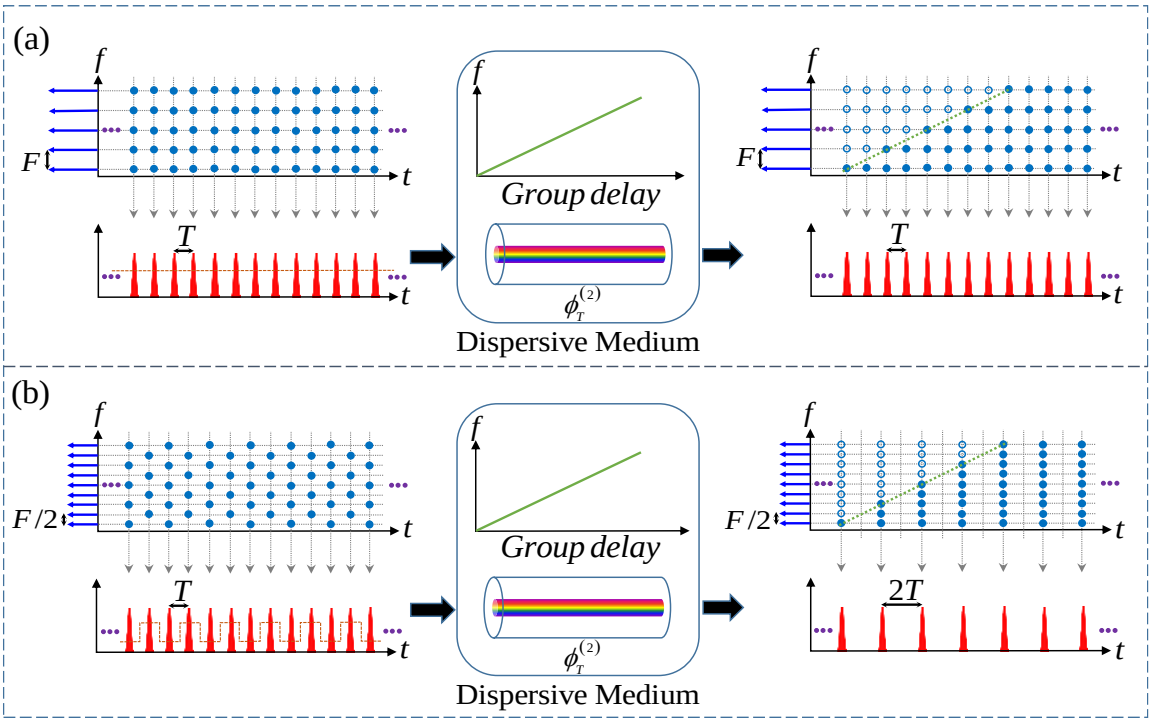

Figure 3.10 – Joint time-frequency analysis of (a) a flat-phase and (b) phase-conditioned periodic input pulse train propagating through a given dispersive medium. *t*: time, *f*: frequency.

Moreover, the induced pulse-to-pulse phase variation translates into instantaneous frequency fluctuations among the different optical pulses in such a way that alternating optical pulses exhibit a different frequency-shifted spectral content. Subsequent propagation of the phase-conditioned pulse train through the same amount of dispersion $\phi_T^{(2)}$ now induces a dispersive delay of T between two adjacent discrete frequency components (with frequency spacing of $F/2$). After the temporal redistribution induced by the frequency-dependent group delay, the individual frequency components of the pulse train will add coherently to build a new pulse train with twice the temporal period of the original signal. In other words, this delay, indeed, coherently shifts energy such that the output repetition-rate is reduced by a factor of two as shown in Figure 3.10(b), right.

Next, we assume an aperiodic pulse train such as a RZ-OOK data signal as the input signal, which comprises some missing pulses along time domain in comparison with a purely periodic optical pulse train. Figure 3.11(a), left shows the evaluation of such data signal along the temporal and spectral domains before dispersion in the absence of the prescribed temporal phase modulation. Notice that the spectrum of an arbitrary RZ-OOK data, indeed, consists of strong line

spectral components (clock components, spaced in frequency by the input bit rate) and a 'weaker' noise-like background that is distributed continuously along the signal spectrum between the frequency clock lines. Therefore, each individual pulse of the temporal signal actually consists of a continuous band of frequency components. However, herein, for illustrative purposes, to facilitate the interpretation of the resulting plots and without loss of generality, we just consider the signals' clock components, which play the main role in the clock recovery process. The influence of the weak noise-like spectral background will be briefly discussed later in this Section.

As compared to Figure 3.10, the same dispersive medium ($\phi_T^{(2)}=2T^2/2\pi$) introduces a group delay of $2T$ between two adjacent discrete clock frequency components with frequency spacing of $F = 1/T$. The spectral superimposition of the dispersed pulses on the temporal axis recovers the missing pulses of the input RZ signal and thereby produces a periodic pulse train with a repetition period equal to the input bit period (i.e. a base-rate clock signal with repetition-rate of $1/T$). Non-uniform distribution of the instantaneous frequencies among the different optical pulses, however, causes pulse-to-pulse amplitude variations in the recovered clock signal; such amplitude variations are more pronounced in the case of an input data signal with a longer series of zero bits. Nevertheless, higher-quality clock pulses with small pulse-to-pulse amplitude variations can be recovered when the input pulses are sufficiently short in comparison with the bit period, T, (i.e. low duty cycle). In this case a larger number of spectral clock components will contribute to the pulse reconstruction process so that the dispersed pulses can interfere with temporally apart pulses as well as adjacent ones.

Figure 3.11(b) shows how if we condition the input data signal by a proper temporal phase modulation derived from Eq.(3.1) ($\{0, \pi/2, 0, \pi/2,\ldots\}$) when we target to perform sub-harmonic clock recovery with clock division factors of $m = 2$. This leads to the anticipated spectral self-imaging and reduces the comb frequency spacing of the input signal by a factor of $m = 2$. Subsequent propagation through the dispersion $\phi_T^{(2)}$ induces a dispersive delay of T between two adjacent discrete clock frequency components with frequency spacing of $F/2$. This frequency-dependent delay will rearrange the instantaneous frequencies along the time domain and their coherent superimposition will produce a periodic pulse train with a repetition period twice that of the input signal (i.e. with the target sub-harmonic repetition-rate).

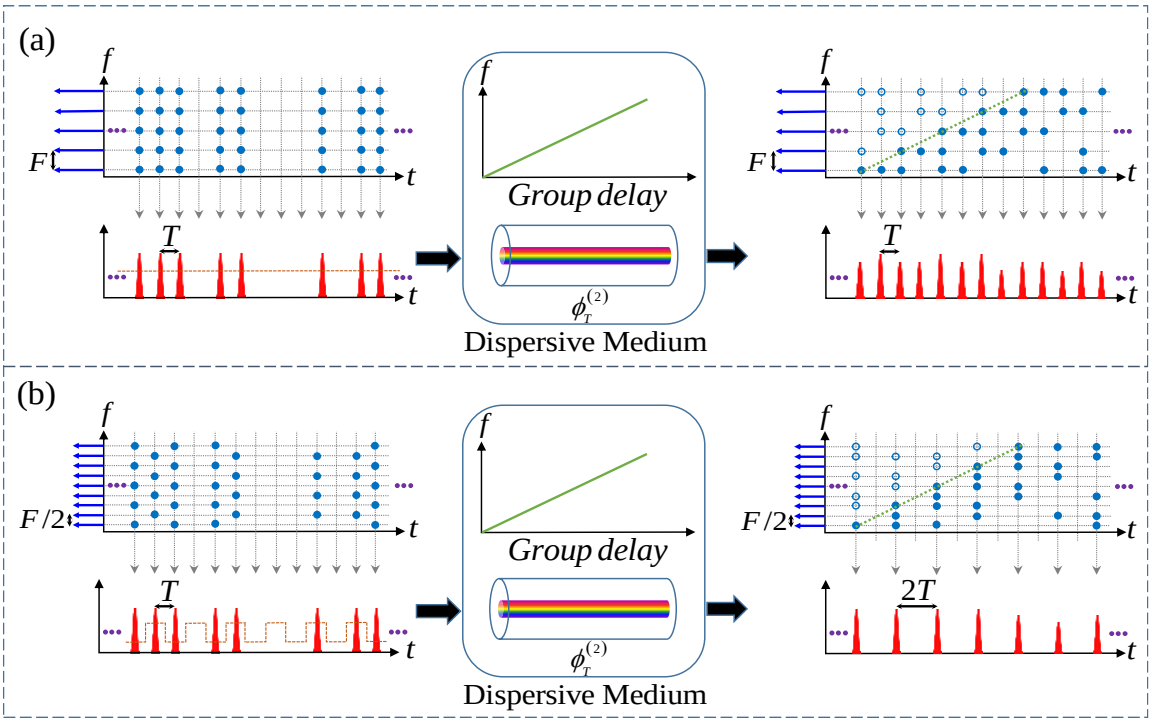

Figure 3.11 – Joint time-frequency analysis of (a) base-rate clock recovery and (b) sub-harmonic clock recovery from a RZ-OOK data signal using dispersion-induced TSI. *t*: time, *f*: frequency.

Similar to the preceding case, the recovered sub-harmonic clock pulses, however, suffer from pulse-to-pulse amplitude variations, which are particularly significant for input signals with a longer series of consecutive zero bits. Amplitude variations in the recovered clock envelope are less pronounced for lower duty-cycle input pulses. Still, if needed, these fluctuations could be further minimized by use of a higher amount of dispersion [i.e., higher value of the parameter *s* in Eq.(3.2)], or by incorporating an additional power equalizer, e.g. a semiconductor-optical-amplifier (SOA)-based fiber ring laser (SOA-FRL) [231]. A detailed numerical analysis and further discussions on the issue of amplitude fluctuations in the recovered clock signals are provided in the following Section 3.3.4.

Finally, we should mention that the continuous, noise-like spectral background component of the input signal adversely affects the clock recovery process and degrades the clock signal quality. After temporal dispersion, such a component will be spread randomly all over the time domain, inducing a certain pedestal on the output generated pulses, as illustrated in Figure 3.9(c).

3.3.4 Experimental demonstration and discussion

We next report on a proof-of-concept experiment to validate the proposed concept by performing SHCR with clock division factors of m = 2, m = 3 and m =4, as well as BRCR from a 9.7Gbit/s data signal. Notice that, any desired repetition-rate division factor can be essentially obtained in practice by appropriate control of the temporal phase modulation and dispersion-induced spectral phase filtering. Nevertheless, to obtain higher SHCR orders, higher dispersion values are required to realize the desired spectral phase filter. In this experiment, the highest repetition-rate division factor (m = 4) was practically limited by the available dispersive medium in our laboratories.

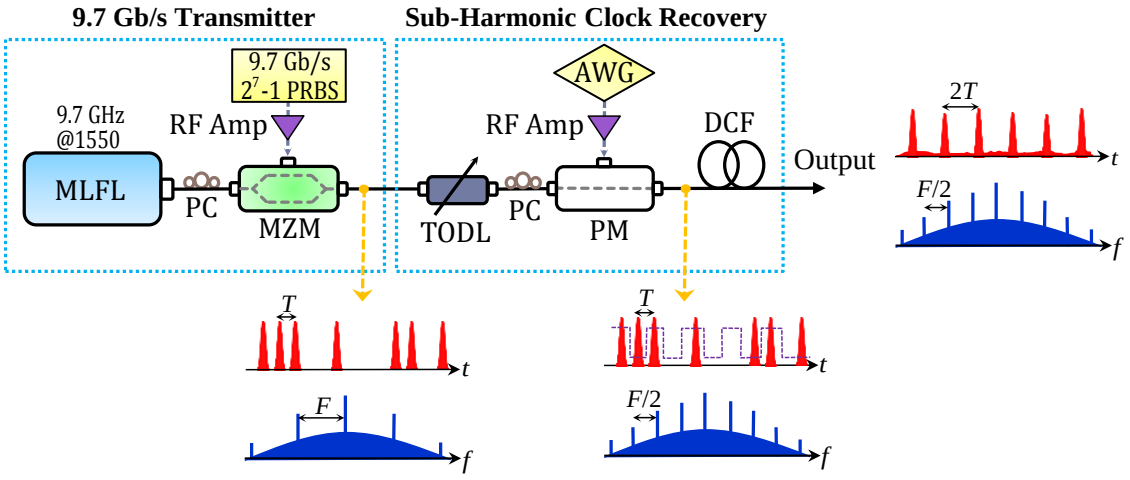

Figure 3.12 – Experimental setup of the sub-harmonic clock recovery technique through dispersion-induced temporal self-imaging. MLFL: Mode-Locked Fiber Laser, MZM: Mach-Zehnder Modulator, PC: Polarization Controller, AWG: Arbitrary Waveform Generator, DCF: Dispersion-Compensating Fiber, PM: Phase Modulator, TODL: Tunable Optical Delay Line, RF Amp: Radio-Frequency Amplifier, *t*: time, *f*: frequency.

The experimental setup used in our demonstration is sketched in Figure 3.12. The RZ-OOK data signal is produced by intensity modulation of ~4 ps (intensity FWHM) optical pulses generated by a mode-locked laser with a 9.7GHz repetition-rate at a central wavelength of 1550nm. The modulator driver is a 2^7-1 pseudo-random bit sequence (PRBS), thus generating a RZ-OOK modulated signal. The generated data signal is then delivered to the clock recovery circuit,

consisting of a commercial fiber-integrated electro-optic phase modulator driven by an arbitrary waveform generator (AWG), followed by dispersion-compensating fibers (DCFs).

Figure 3.13 shows the prescribed electro-optic phase modulation profiles in our reported experiments for the targeted SHCR factors of 2, 3 and 4, respectively. The periodic temporal phase profiles derived from Eq.(3.1) are $\{0, \pi/2, 0, \pi/2, \ldots\}$ for $m = 2$, $\{0, 2\pi/3, 2\pi/3, 0, \ldots\}$ for $m = 3$, and $\{0, 3\pi/4, \pi, 3\pi/4, 0, \ldots\}$ for $m = 4$. The dashed red lines show the ideal temporal phase profiles, and the solid blue lines show the actual phase drives delivered by the AWG. Figure 3.14 presents the optical spectra of the input data signal before (solid blue) and after (dashed red) temporal phase modulation, recorded with a standard optical spectrum analyzer. These measurements show the predicted spectral self-imaging effect, leading to the expected decrease in the spectral comb spacing by factors of 2, 3 and 4, respectively.

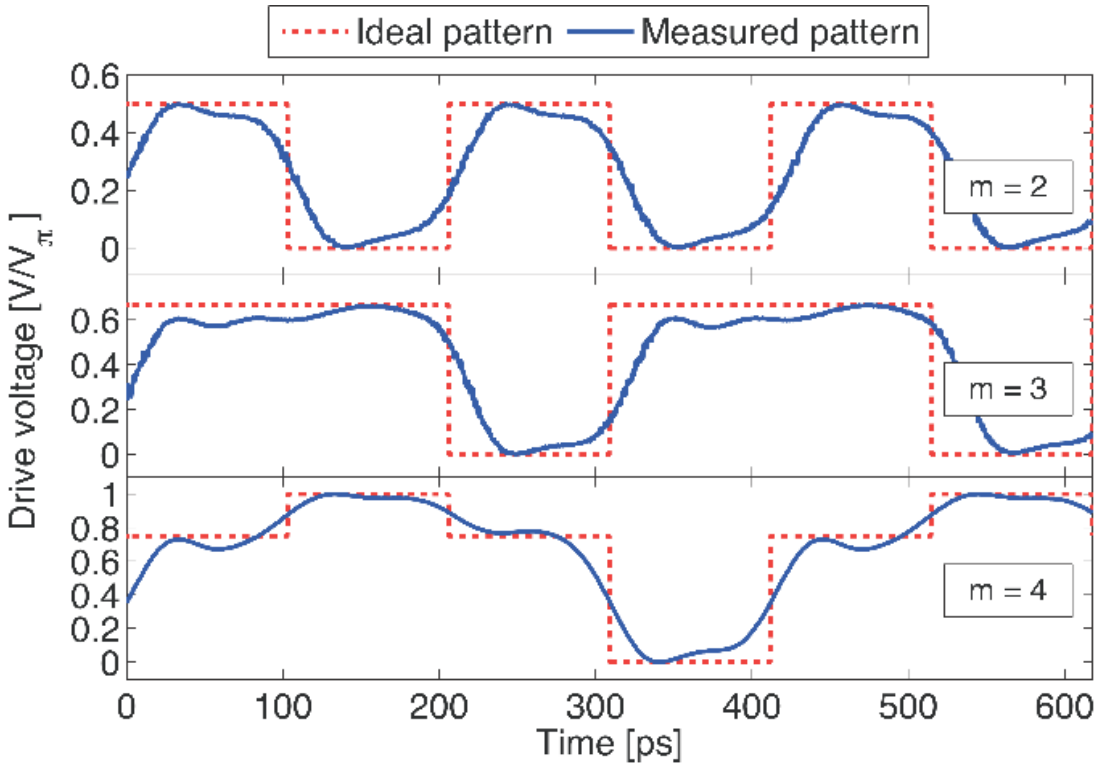

Figure 3.13 – Prescribed temporal phase modulation profiles. Ideal temporal phase profiles (dashed red) and measured phase drives, as delivered by the AWG (solid blue).

The required amount of first-order dispersion can be calculated using Eq.(3.2). In this set of experiments, we have considered the minimum required dispersion and set $s = 0$ in Eq.(3.2). The

corresponding dispersion values would be 3376 ps^2/rad (≈2647 ps/nm), 5065 ps^2/rad (≈3972 ps/nm) and 6752 ps^2/rad (≈5294 ps/nm) for SHCR orders of m = 2, 3 and 4, respectively. In practice, the required dispersion was provided by m dispersion-compensating fiber modules (Corning PureForm DCM-D-080-04, each having a nominal group-velocity dispersion of ≈1324 ps/nm) for the respective SHCR order. In this case (i.e. when s = 0), the dispersion values increases with the SHCR factor m. As mentioned above, when the temporal phase modulation is off, the defined dispersion directly implements BRCR from the input RZ-OOK signal.

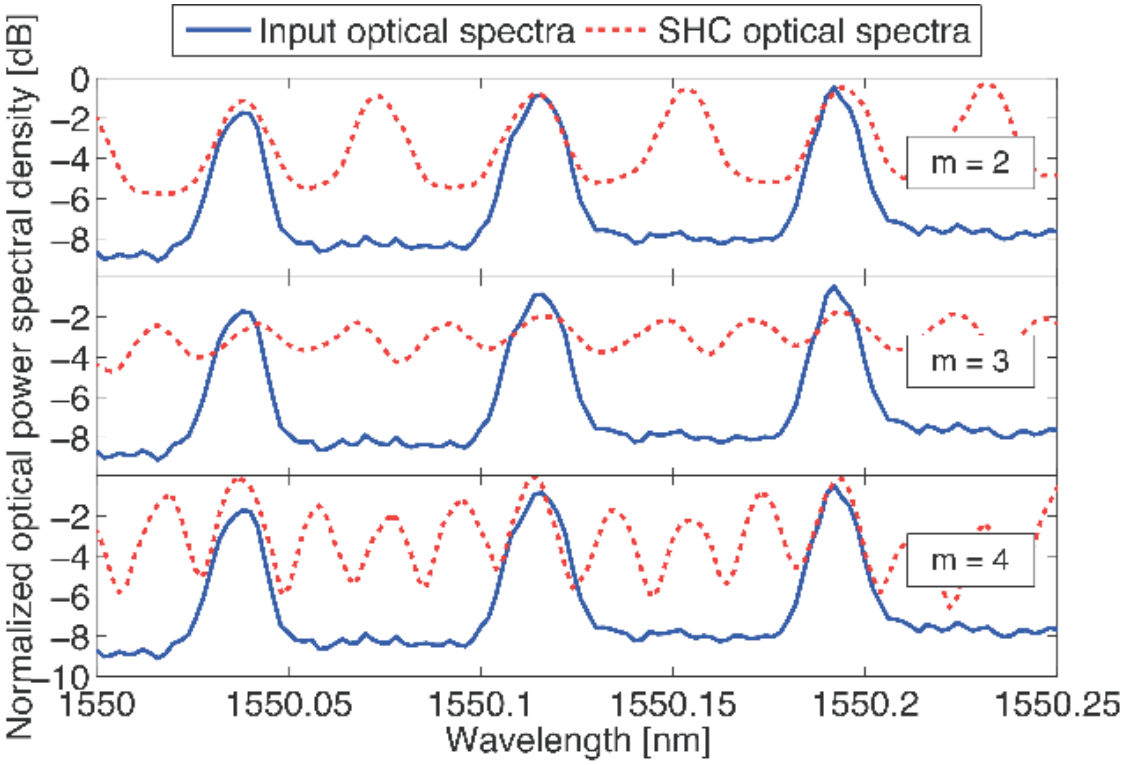

Figure 3.14 – Measured optical spectra of the input data signal before (solid blue) and after (dashed red) temporal phase modulation.

Figure 3.15 shows the temporal waveform, eye diagram and RF spectrum of the input data signal used in the experiments. The RF spectrum shows a clear bit rate frequency component at 9.7GHz and the PRBS data components around the bit rate frequency.

The experimental results of the demonstrated SHCR with clock division factors of 2, 3 and 4 are presented in Figure 3.16. Figure 3.16(a)– (c) display the measured temporal waveforms and eye diagrams of the 4.85GHz (m = 2), 3.23GHz (m = 3), and 2.43GHz (m = 4) sub-harmonic clock

signals, respectively, measured with a 40-GHz photodetector attached to an electrical sampling oscilloscope. The eye diagrams are depicted together with their amplitude histograms at the center of a pulse timeslot. The results clearly indicate the presence of a periodic pulse train at the output, highlighted by the absence of a baseline in the eye diagrams. Amplitude variations in the output pulses are evident, though, through the smearing in "one" level of the output eye diagram; nevertheless, the pulse's peaks are always well above the "zero" level.

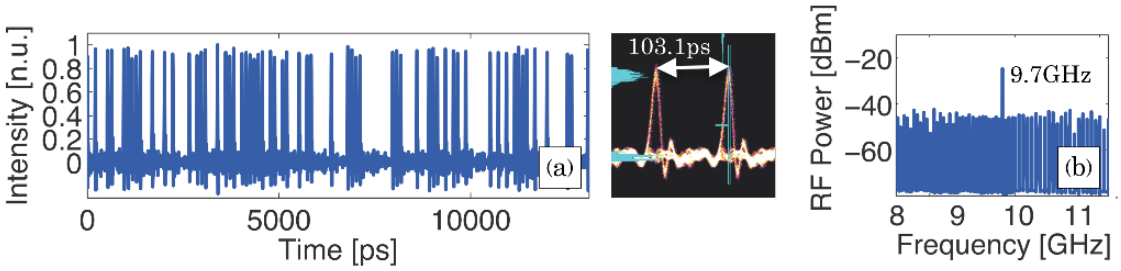

Figure 3.15 – Temporal waveform, eye diagram and (b) RF spectrum of the measured input 2^7 –1 PRBS signal (9.7Gbit/s) used for the experiments.

Figure 3.16(d)– (f) show the measured RF spectra corresponding to the temporal waveforms shown in Figure 3.16(a)– (c), respectively. Clearly visible peaks appear at 4.85GHz [Figure 3.16(d)], 3.23GHz [Figure 3.16(e)] and 2.42GHz [Figure 3.16(f)], confirming the target SHCR processes for m = 2, 3 and 4, respectively. Comparison of the measured RF spectra in Figure 3.16 and Figure 3.15 reveals that the frequency components of pseudo-randomly intensity-modulated signals [visible in Figure 3.15(b)] have been greatly suppressed through the clock recovery process. This proves that TSI operates as a periodic RF bandpass filter with central frequencies located at $(mT)^{-1}$ GHz and its harmonics. The pass bandwidth of each harmonic is inversely proportional to m (assuming s = 0 for all cases). As can be seen, the pass bandwidth becomes narrower with increasing m, and the RF spectral intensity of data components (restricted to the vicinity of clock frequency) is increasingly suppressed. Notice that a narrower pass bandwidth and a higher suppression rate of the data components in the RF spectra are indications of a higher-quality output clock signal, e.g., with lower pulse-to-pulse amplitude variations, also associated with an improved eye opening for the output pulse train. Therefore, provided that the minimum required dispersion is employed in each case [s = 0 in Eq.(3.2)], a higher quality optical clock is recovered as the SHCR order is increased; this can be attributed to the fact that a higher

order *m* requires a higher dispersion in the recovery system and increased dispersion induces a broader spreading of each input individual pulse, facilitating the desired inter-pulse interactions at the system output.

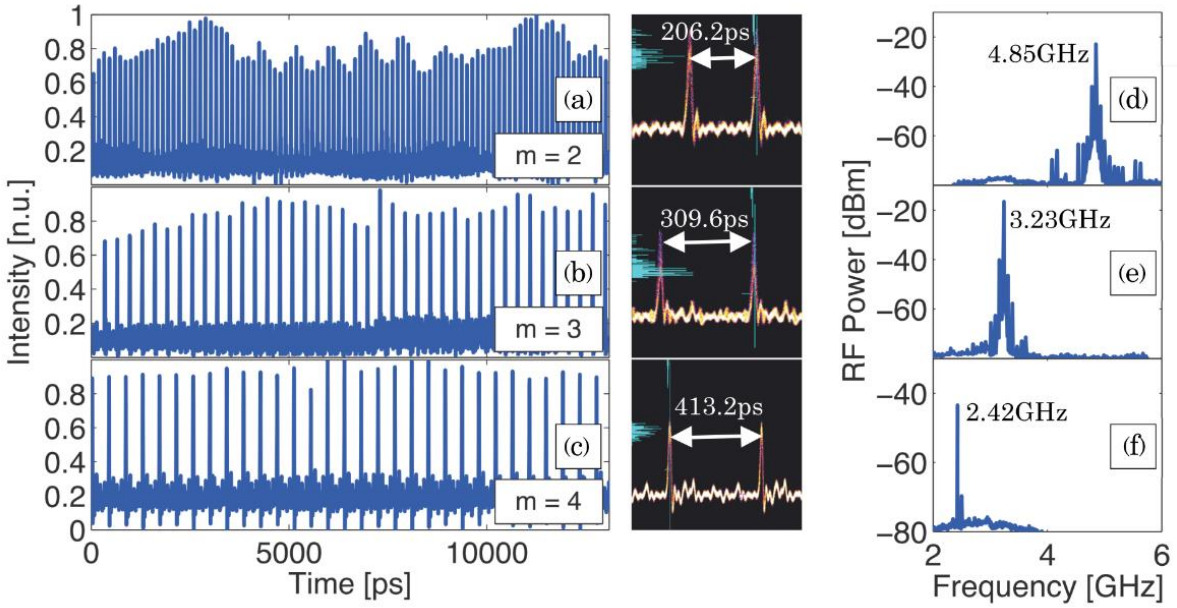

Figure 3.16 – Temporal waveforms and eye diagrams of the recovered 4.85GHz sub-harmonic clock signal when *m* = 2, 3.23GHz sub-harmonic clock signal when *m* = 3 and 2.42GHz sub-harmonic clock signal when *m* = 4 at the output of the circuit.

In line with our discussions in Section 3.3.3, the ability of the temporal self-imaging effect to produce uniform amplitude optical pulses from the input RZ-OOK data signal is strongly dependent on: 1- the number of spectral clock components in the input signal, namely the input pulse duty-cycle, 2- the amount of required dispersion, depending on both *s* and *m*, and 3- the PRBS pattern length. In order to quantitatively evaluate the magnitude of pulse-to-pulse amplitude variations in the clock signal in regard to these parameters, we define the "relative amplitude variation factor (RAVF)" as the ratio of the difference between the highest pulse's peak power (P_{max}) and the lowest pulse's peak power (P_{min}) to the highest pulse's peak power:

$$RAVF = \frac{P_{max}\text{-}P_{min}}{P_{max}} \tag{3.3}$$

Figure 3.17(a) plots the output pulses' amplitude variation (i.e. RAVF) as a function of the input pulse duty-cycle for different values of *m* and *s*. In this simulation, we used a RZ-OOK data with a 2^7-1 PRBS. One may notice that for a given *m* and *s*, the amplitude variations of recovered clock pulses are alleviated as the input pulse duty-cycle decreases. As mentioned earlier, lower input pulse duty-cycle incorporate a larger number of spectral clock components in the pulse reconstruction process. Therefore, pulses are temporally spread out more significantly by the same amount of dispersion and this facilitates their interference with temporally apart pulses as well as adjacent ones, so that in average the input pulses' energy is more uniformly redistributed over all the newly generated pulses.

In addition, for a given input pulse duty-cycle and SHCR order, the amplitude modulation of the recovered clock signal can be noticeably reduced when a higher value of dispersion is employed [i.e. higher *s* in Eq.(3.2)]. This can be attributed to the fact that a higher dispersion induces a broader temporal spreading of each input individual pulse, leading to more pronounced inter-pulse interactions. For example, assume the input pulse duty-cycle of 33% and SHCR order of *m* = 6, RAVF of the clock signal is reduced from 0.87 to 0.5 when *s* increases from 0 to 2.

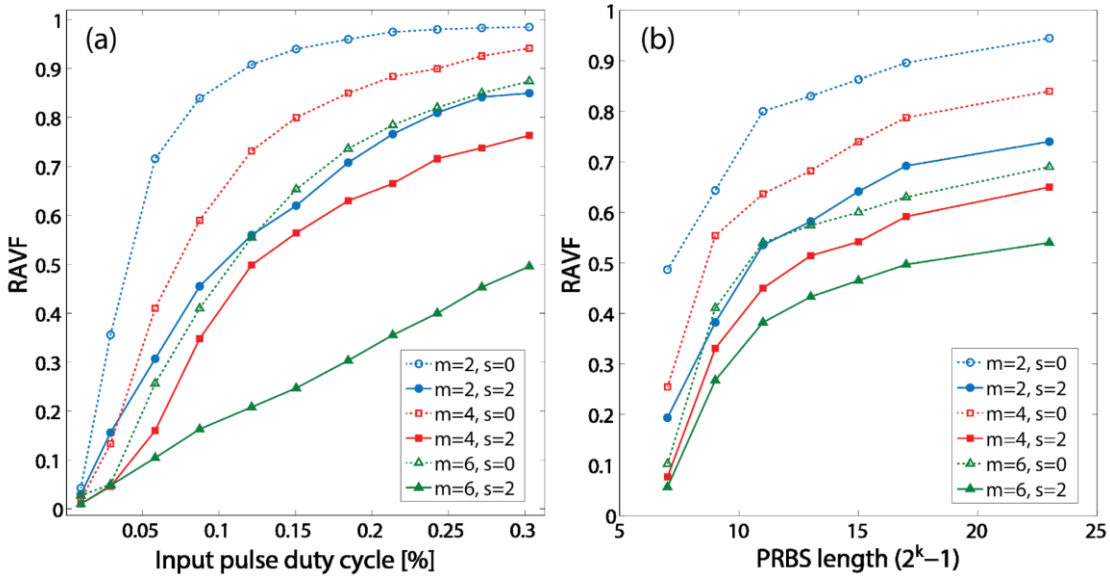

Figure 3.17 – Sub-harmonic clock signal's amplitude-variations as a function of (a) input pulse width and (b) the number of consecutive zeros in the input signal's pattern.

Figure 3.17(b) shows that the amplitude variations at the output pulse train increases as the PRBS pattern length (2^k-1) of the input data increases. For example, for *m* = 2 and *s* = 0, RAVF

reaches almost 1 for PRBS patterns with lengths more than 2^{23}-1. Note that a PRBS with a length of 2^k-1 may have a sequence of up to "k" (or "k-1") consecutive zeros in its pattern. In this case, the temporally apart pulses in the two sides of the long sequence of zeros (i.e. long zero gap), indeed, do not get to interfere with each other and, therefore, the clock pulses along this sequence is not recovered. However, for SHCR order of m = 2 with s = 2, for example, the required dispersion is five times that for m = 2 and s = 0 and then, pulses are temporally dispersed more strongly, so that they get to pass the long zero gap and interfere with the other side pulses, creating the desired new pulses in the long zero gap zone. The pulse time-width in the input data pulse train is fixed to 4 ps in this simulation.

Finally, Figure 3.18 shows the outcome of the same clock recovery circuit, in the absence of temporal phase modulation. In this case, a 9.7GHz base-rate clock signal can be obtained at the output of the circuit, no matter which SHCR order (m) is used, as confirmed by the corresponding RF spectra in Figure 3.18(d)–(f). Similarly to the SHCR case, the optical clock quality increases as the factor m is increased. It is important to mention that the bit rate in our proof-of-concept experiment was limited by available equipment.

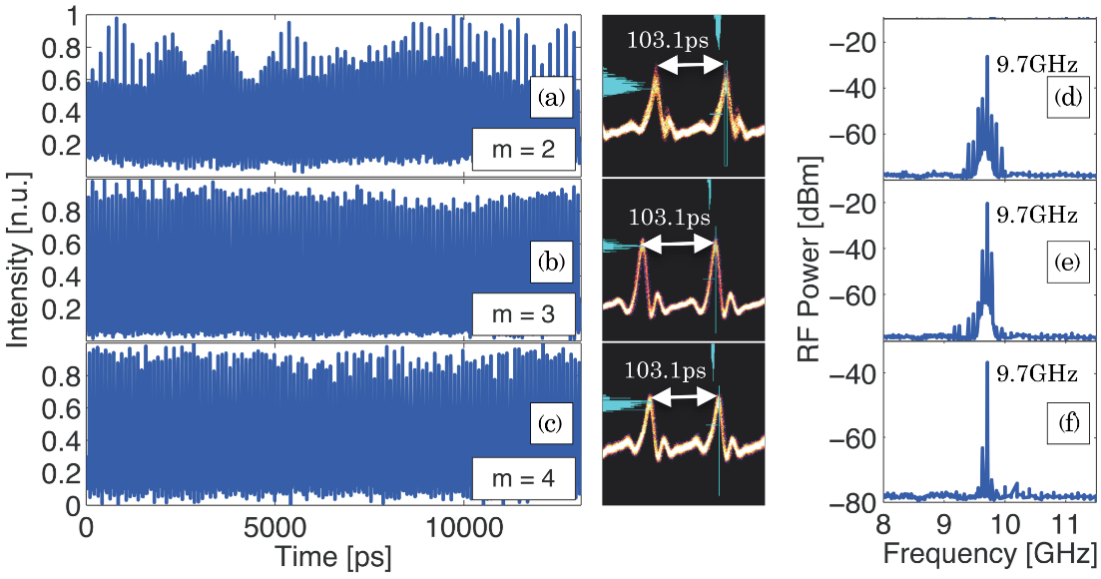

Figure 3.18 – Temporal waveforms and eye diagrams of the recovered 9.7GHz base-rate clock signal in the absence of temporal phase modulation.

It is well known that TSI is more easily observable as the pulse bit rate is increased since a lower dispersion amount is then required. Moreover, alternatively, the quadratic time phase modulation can be applied using non-linear optical processes, e.g. cross-phase-modulation with a parabolic pump pulse train, overcoming the intrinsic speed limitations of electro-optic phase modulation [232].

3.3.5 Conclusions

In summary, the effect of inverse temporal self-imaging (I-TSI) on aperiodic pulse trains have been investigated and studied. Results on this study suggest a novel scheme for reconfigurable sub-harmonic optical clock recovery based on I-TSI, involving phase-only temporal modulation and dispersive spectral filtering of the input data pulse train. The scheme can be easily reconfigured to achieve base-rate clock recovery by simply bypassing the temporal phase-modulation step. The proposed scheme has been validated through experimental demonstrations, and in particular, we have reported successful extraction of 4.85-GHz and 3.23-GHz sub-harmonic clock signals as well as the 9.7-GHz base-rate clock signal from a 9.7-Gbit/s RZ-OOK data signal under a 2^7-1 PRBS pattern. The quality of the recovered optical clock signal is improved for a higher sub-harmonic rate factor, a higher dispersion amount for temporal self-imaging [higher ‘s’ in Eq. (2)], or lower duty-cycle input pulses.

3.4 640 Gbit/s return-to-zero to non-return-to-zero format conversion based on optical linear spectral phase filtering[23]

3.4.1 Abstract

We propose a novel approach for all-optical return-to-zero (RZ)-to-non-RZ (NRZ) telecommunication data format conversion based on linear spectral phase manipulation of an RZ data signal. The operation principle is numerically analyzed and experimentally validated through successful format conversion of a 640 Gbit/s coherent RZ signal into the equivalent NRZ time-domain data using a simple phase filter implemented by a commercial optical wave-shaper.

3.4.2 Introduction

Future optical networks are likely a hybrid scenario of various technologies owing to the large variety of applications and to their hierarchical structure, which implies diverse specifications for the networks' segments. In this context, a specific network segment employs an adequate modulation format that meets its requirements [102, 103]. Therefore, all-optical format converters are of great importance to transparently and seamlessly interconnect different parts of the networks, avoiding the use of optical-to-electrical (O/E) and electrical-to-optical (E/O) converters, as well as overcoming limitations imposed by electronics in terms of bit rate and frequency bandwidth [103]. In particular, format conversion between RZ and NRZ signals is particularly interesting: both formats are mature and widely used in different parts of the networks, e.g., the RZ format is adopted in time division-multiplexing (OTDM) systems to be able to perform pulse multiplexing, while the NRZ format is preferred in wavelength-division-multiplexing (WDM) systems due to its higher spectral efficiency [71]. In addition, format conversion of an RZ signal to its equivalent NRZ is also desired in de-multiplexing of OTDM signals as NRZ signals improve timing-jitter tolerance in the de-multiplexing process thanks to their flat-top temporal shape [104].

[23] R. Maram, D. Kong, M. Galili, L. K. Oxenløwe and J. Azaña, "640 Gbit/s return-to-zero to non-return-to-zero format conversion based on optical linear spectral phase filtering," Optics Letters, vol. 41, no. 1, pp. 64-67 (2016).

So far, a variety of schemes have been developed to realize RZ-to-NRZ format conversion, mainly using either nonlinear or linear optical signal processing techniques [104, 56, 105, 106, 107, 108, 109, 110]. Schemes based on Kerr nonlinear effects, such as cross-phase modulation (XPM), cross-gain modulation (XGM), and four-wave mixing (FWM), employ different nonlinear media to realize the target format conversion, including highly nonlinear fibers [56], semiconductor optical amplifiers (SOAs) [105] and periodically poled lithium niobate (PPLN) waveguides [106]. On the other hand, format converters based on linear optical signal processing are typically based on linear spectral amplitude filtering to tailor the spectrum of an RZ input signal into the target NRZ signal spectrum, that is the so-called optical spectrum transformation [104, 107, 108, 109]. In particular, linear RZ-to-NRZ format converters rely on the use of a periodic amplitude notch filter with a free spectral range (FSR) fixed to twice the bit rate of the incoming RZ data signal. The required amplitude filters can be implemented using a variety of technologies, such as photonic microring resonators [104, 107, 108], interferometers [109] and fiber Bragg gratings (FBGs) [110]. Though all of the reported nonlinear and linear-based schemes [104, 56, 105, 106, 107, 108, 109, 110] have shown good performances, linear platforms are of greater interest due to their intrinsic simplicity, suitability for high speed operation and stable performance. In addition, unlike nonlinear-based schemes, linear converters do not require any additional optical beam to perform the format conversion while also avoiding the need for high power input signals, as required otherwise to excite optical nonlinear effects.

In this Letter, we propose a novel linear scheme for RZ-to-NRZ format conversion based on optical spectral *phase* filtering. The proposed format converter represents an interesting alternative to the conventional linear amplitude spectrum tailoring method (spectrum transformation), showing, for the first time, how one can generate an NRZ copy of the original RZ optical signal simply by spectral phase-only manipulation of the RZ signal. As such, this approach offers increased energy efficiency since fundamentally no energy is lost in the phase filtering process [233], while generally offering an improved performance for a similar set of filter specifications (e.g., filter line-width). We theoretically study the performance of the proposed format converter using a spectral/temporal evolution analysis. Furthermore, we report a successful proof-of-concept RZ-to-NRZ format conversion experiment at a bit-rate of 640 Gbit/s by manipulating the spectral phase of a coherent RZ signal using a widely available, commercial linear optical wave-shaper. We obtain an excellent agreement between the experimental and numerical results, as well as

provide preliminary bit-error-rate (BER) measurements, validating the performance of the newly proposed format-conversion concept.

3.4.3 Operation principle and simulation results

Optical spectrum transformation method [104, 107, 108, 109] relies on the suppression of the first-order harmonic components in the spectrum of an RZ signal using a periodic amplitude notch filter whose FSR is matched to twice the signal bit rate. The resulting converted NRZ signal after the notch filter yet exhibits relatively large amplitude ripples due to the residual high-frequency components of the spectrum [104, 109]. Therefore, a narrow optical band-pass filter (OBPF) is typically used to eliminate these residual components, leading to a reduction of the amplitude ripples and the associated improvement in the quality of the converted NRZ signal.

Herein, we show that a properly designed optical *phase* filter can also perform the RZ-to-NRZ format conversion by simply phase-shifting the first-order harmonic components in the spectrum of the RZ signal, instead of entirely suppressing them.

The operation principle of the proposed approach is shown in Figure 3.19(a)-(f). To analyze the principle of format conversion, we study progressively the evolution of the RZ signal in the frequency domain and time domain through numerical simulations based on the standard frequency-domain method for linear processes. By definition, the Fourier transform of the input signal is multiplied by the frequency-domain transfer function of the linear filters under test, and the output is inverse-Fourier-transformed to produce the time-domain signal. Figure 3.19(a)–(c) show evolution of the relevant spectra, while Figure 3.19(d)‑(f) are the corresponding time-domain eye diagrams.

Figure 3.19(a) and (d) show the spectrum and eye diagram of a RZ data signal consisting of 700-fs (FWHM) optical pulses at a bit rate of 640 Gbit/s, coded under a pseudorandom bit sequence (PRBS) of $2^7 - 1$. In Figure 3.19(a), the red curve shows the spectral phase of the used phase filter with a spectral line-width of F_b =10 GHz and a free spectral range (FSR) of 1,280 GHz, which is twice the input signal bit rate. The phase filter π-phase-shifts the first-order harmonic components of the RZ signal with respect to the rest of the signal spectrum.

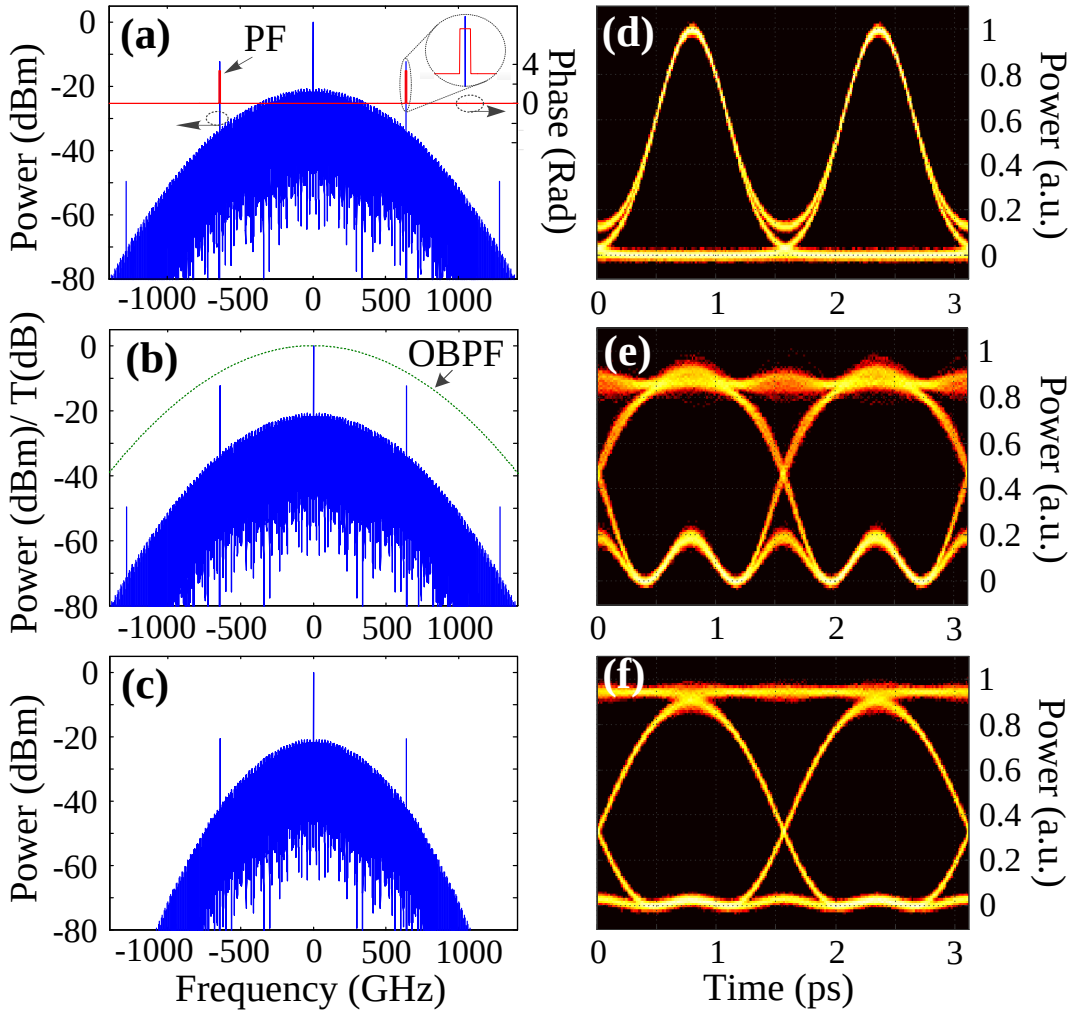

Figure 3.19 – Numerical simulation results. (a)-(f): spectra and eye diagrams evolution of the proposed method for format conversion from RZ to NRZ at 640 Gbit/s. (a) and (d) are the spectrum and eye diagram of the input RZ signal, respectively. (b) and (e) are the spectrum and eye diagram of the RZ signal filtered by a suitable phase filter (PF), respectively. (c) and (f) are the spectrum and eye diagram of the converted NRZ signal, after filtering by an OBPF, respectively.

In Figure 3.19(b), the solid blue curve shows the spectrum of the RZ signal after phase filtering – the filtered spectrum remains unchanged with respect to that of the input signal as the phase-only filtering process does not alter the energy spectrum shape. However, the time-domain eye diagram (shown in Figure 3.19(e)) reveals realization of the target format conversion from RZ to NRZ. It is worth mentioning that the amplitude ripples of the converted NRZ signal after the phase filter are significantly lower than those obtained using the amplitude notch filter approach in

previous reports [104, 109]. The quality of the converted NRZ signal can be further enhanced by an additional OBPF to remove spectral components associated to the fast temporal features of the signal that can be observed in the base-line of the eye diagram shown in Figure 3.19(e). The 3-dB bandwidth of the OBPF used in this example, which is modeled as a Gaussian type filter, is 800GHz, as depicted in Figure 3.19(b). Figure 3.19(c) and (f) show the spectrum and eye diagram of the converted NRZ signal, respectively, after filtering by the OBPF, confirming a clear quality enhancement of the NRZ signal. It is noteworthy that the defined phase filter can be practically implemented using a variety of technologies, such as line-by-line optical pulse shapers (e.g., the wave shaper used in the experiments reported here), Fiber Bragg Gratings (FBG), thin film filters, photonic ring resonators, and photonic crystals, among others [222, 223].

For a good format conversion, both a high *Q*-factor (defined as $Q = (P_1\text{-}P_0) / (\sigma_1+\sigma_0)$, where P_1 and P_0 are the means and σ_1 and σ_0 denote the standard deviations of the logic "one" and "zero" levels, respectively) and low amplitude ripples (defined as the peak-to-peak power deviation of the high level (logic "one" level) rail in the converted NRZ normalized eye diagram) are simultaneously required for the converted NRZ signal [71]. Figure 3.20(a) and (b) show the simulated *Q*-factor and amplitude ripples of the converted NRZ signal as a function of spectral line-width of the phase filter and the OBPF 3-dB bandwidth at a bit-rate of 640 Gbit/s.

One can find optimal regions for bandwidth of the OBPF and spectral line-width of the phase filter, which are denoted by the ellipses in Figure 3.20(a) and (b). A phase filter with a line-width F_b narrower than ~10 GHz and an OBPF with a bandwidth around 800 GHz will result in an optimum RZ-to-NRZ format conversion performance, with high *Q*-factor and low amplitude ripples. In the presented numerical example, shown in Fig. 1, the *Q*-factor and amplitude ripple of the converted NRZ data signal are 27.7 and 0.073, respectively, for a phase filter spectral line-width of 10GHz and an OBPF 3-dB bandwidth of 800GHz. Recall that these values are feasible with present filter technologies. It is worth restating that the results presented in Figure 3.20 are obtained for an input data signal with a PRBS length of $2^7 - 1$ and a bit-rate of 640Gbit/s. By changing the PRBS length and/or the bit-rate, the required filtering specifications will change accordingly. In particular, by increasing the PRBS length and/or reducing the bit-rate, a narrower line-width is required for the phase filter.

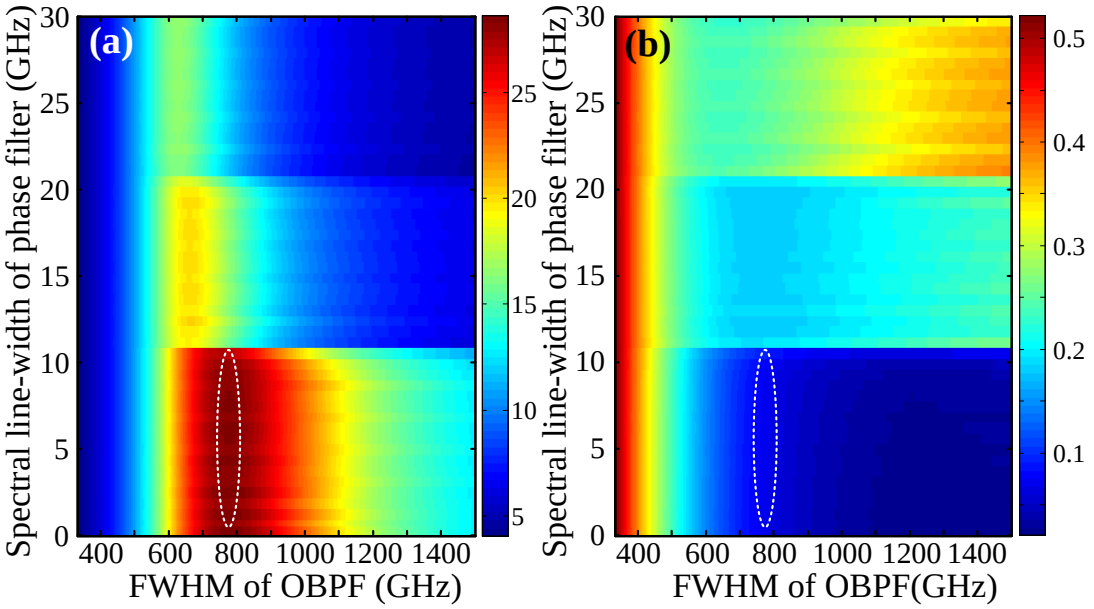

Figure 3.20 – Calculated (a) *Q*-factor and (b) amplitude ripple of the converted NRZ versus spectral line-width and bandwidth of the OBPF for 640 Gbit/s RZ-to-NRZ format conversion.

3.4.4 Experimental results

We furthermore report on a proof-of-concept experiment to validate the proposed concept by performing the RZ-to-NRZ format conversion at a bit rate of 640 Gbit/s. Figure 3.21 represents the experimental setup for the target format conversion. The setup consists of three main blocks: 1- the transmitter, to generate a 640 Gbit/s phase-coherent RZ signal, 2- the spectral phase and band-pass filters, to convert the RZ data format into its equivalent NRZ, and 3- the receiver, to measure the temporal waveform and spectrum of the converted NRZ data signal.

In the transmitter, optical pulses are generated by an erbium-glass oscillating pulse generating laser (ERGO-PGL) at 1542 nm with pulsewidth of 1.5 ps and 10-GHz repetition-rate. Subsequently, the pulses are compressed down to 720 fs by self-phase modulation in a 400-m long Section of dispersion-flattened highly nonlinear fiber (DF-HNLF) and filtered with an optical band-pass filter (OBPF) at 1537 nm with a 3-dB bandwidth of 16 nm.

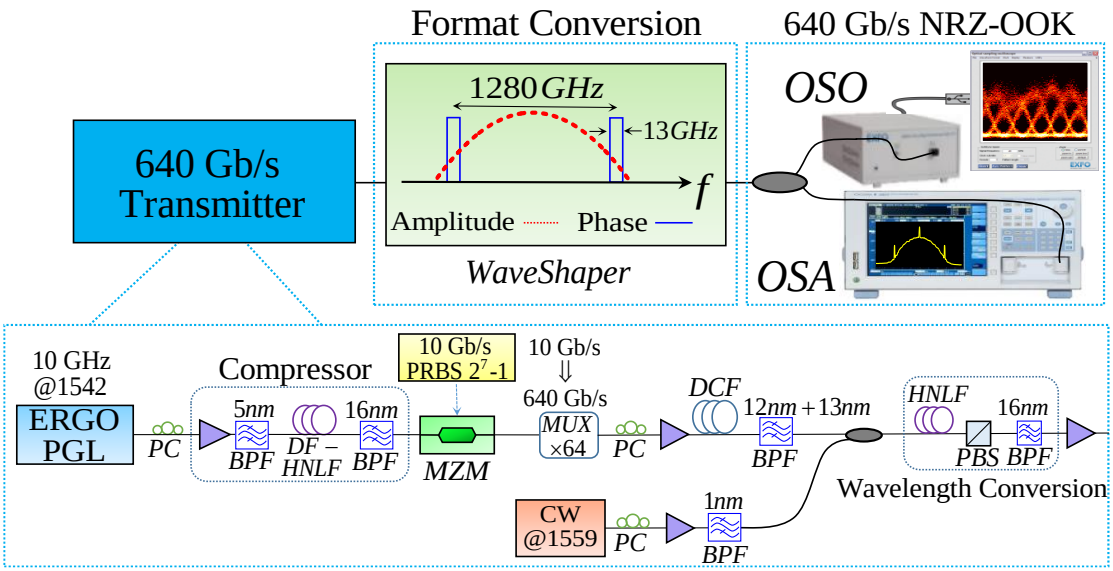

Figure 3.21 – Experimental setup of the 640 Gbit/s all-optical RZ-to-NRZ format conversion using a phase filter with Fb=13GHz and OBPF with FWHM = 500GHz, both implemented by a Waveshaper.

The pulses are then intensity modulated at the 10 Gbit/s base rate with a 2^7 -1 PRBS sequence. The modulated pulses are time-multiplexed in a passive fiber-based split-and-delay multiplexer (MUX) to constitute the 640 Gbit/s RZ OTDM signal. In the OTDM signal, the phases of the different tributary channels are uncorrelated, making the OTDM signal pulse-to-pulse incoherent. To perform the format conversion successfully, a phase-coherent RZ OTDM signal is however required, which can be obtained by wavelength converting the original incoherent OTDM signal. Hence, the 640 Gbit/s RZ OTDM signal is subsequently wavelength converted using a polarization-rotating Kerr switch [71, 104]. For this purpose, the signal is first amplified using an erbium-doped fiber amplifier (EDFA) and coupled together with an amplified CW probe at 1559 nm in a 200-m HNLF (nonlinear coefficient: 10 W^{-1}·km^{-1}; zero dispersion wavelength: λ_0 =1552 nm; dispersion slope: 0.011 ps/(nm^2·km)). At the fiber output, a polarizer is placed with its axis orthogonal to the CW light. Briefly, the polarization of the data is 45º with respect to the polarizer. The CW light is blocked by the polarizer when the data signal is a "0" level bit. When the data signal is a "1" bit, the Kerr effect in the fiber generates birefringence between the polarization direction of the data signal and its orthogonal direction. Therefore, in this case, the state of polarization of the CW light will rotate due to the induced birefringence thus passing through the polarizer. As a result, the phase-uncorrelated OTDM data signal switches the CW light and a pulse-

to-pulse phase-correlated signal is generated at the CW light wavelength. Before wavelength conversion, OBPFs with bandwidths of 12 and 13 nm (data signal) and 1 nm (CW) are used to filter out the amplified spontaneous emission (ASE) introduced by the EDFAs. The converted RZ signal is then amplified before being input to the phase filter.

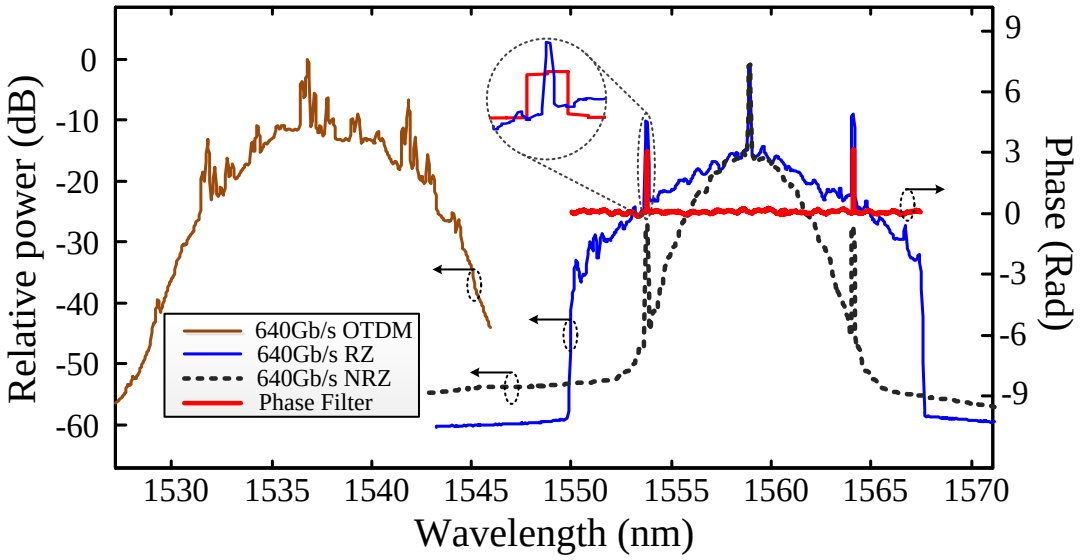

Figure 3.22 – Spectra of the original OTDM (brown), wavelength-converted coherent RZ (blue) and format converted NRZ (dashed black) signals, as well as spectral phase profile of the used phase filter (red).

The coherent RZ signal is then delivered to the format conversion sub-system, comprising the proposed phase filter and OBPF. A line-by-line pulse shaper (Finisar WaveShaper 4000S) has been programmed to produce the needed filtering specifications, i.e., Gaussian amplitude filter with 500 GHz FWHM and a spectral phase filter with periodic π phase shifts with a FSR of 1,280 GHz and F_b = 13GHz. The spectral line-width of the employed filter is determined by the minimum bandwidth (frequency resolution) of the utilized line-by-line pulse shaper, $F_b \approx$ 13GHz. The spectra of the 640 Gbit/s incoherent and coherent input RZ and the output NRZ signals, captured by a standard optical spectrum analyzer (OSA), together with the spectral phase profile of the filter are depicted in Figure 3.22. The spectral phase response of the phase filter is measured with an Optical Vector Analyzer (Luna Technologies).

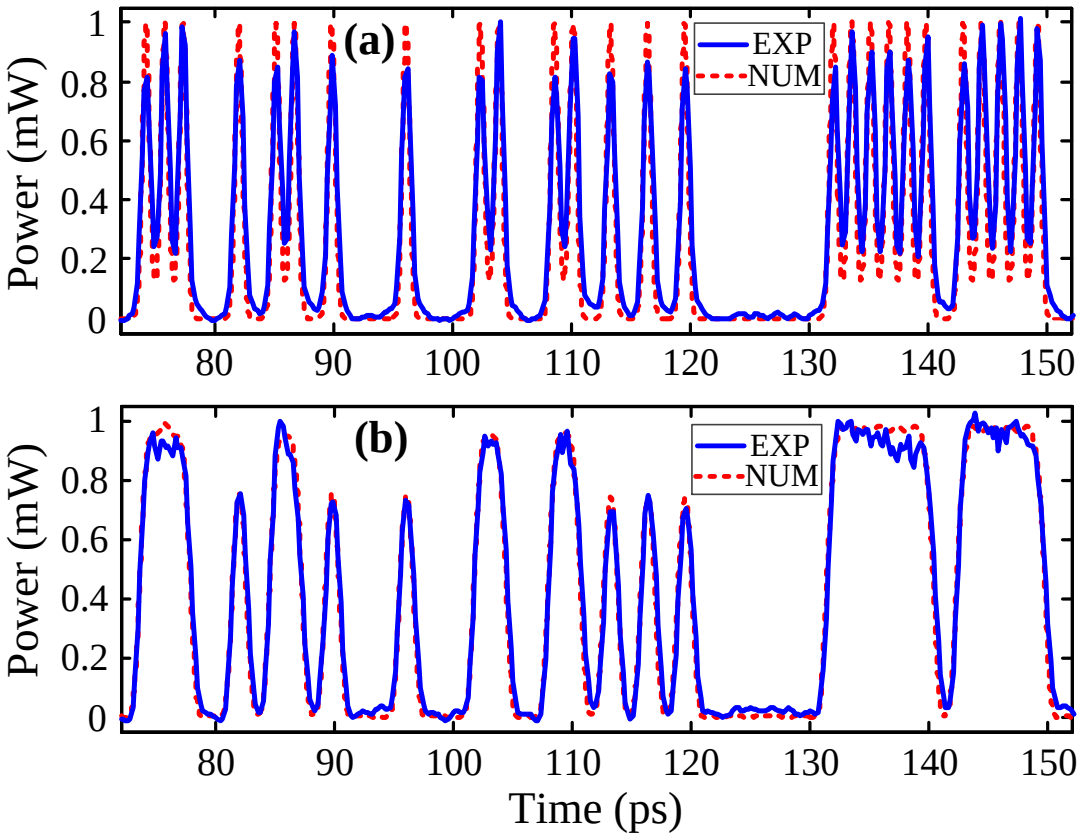

Figure 3.23 – Temporal traces of the 640 Gbit/s coherent input data signal and the extracted clock signal.

Owing to the lack of pulse-to-pulse phase correlation between the tributary channels of the original 640 Gbit/s OTDM signal, one can notice that the OTDM spectrum (brown) does not contain strong clock components at frequencies corresponding to multiples of the bit rate. However, the 640 Gbit/s wavelength-converted RZ spectrum (blue) displays clear and strong clock components and is thus suitable for the proposed format conversion by optical phase filtering. For this purpose, the spectral clock components of the 640 Gbit/s wavelength-converted RZ spectrum are phase-shifted by π with respect to the rest of the signal spectrum by the phase filter (red), as shown in Figure 3.22. As mentioned above, the spectrum of output signal (dashed black) is identical to that of the input signal, except for the fact that the output signal's spectrum is narrower due to the OPBF.

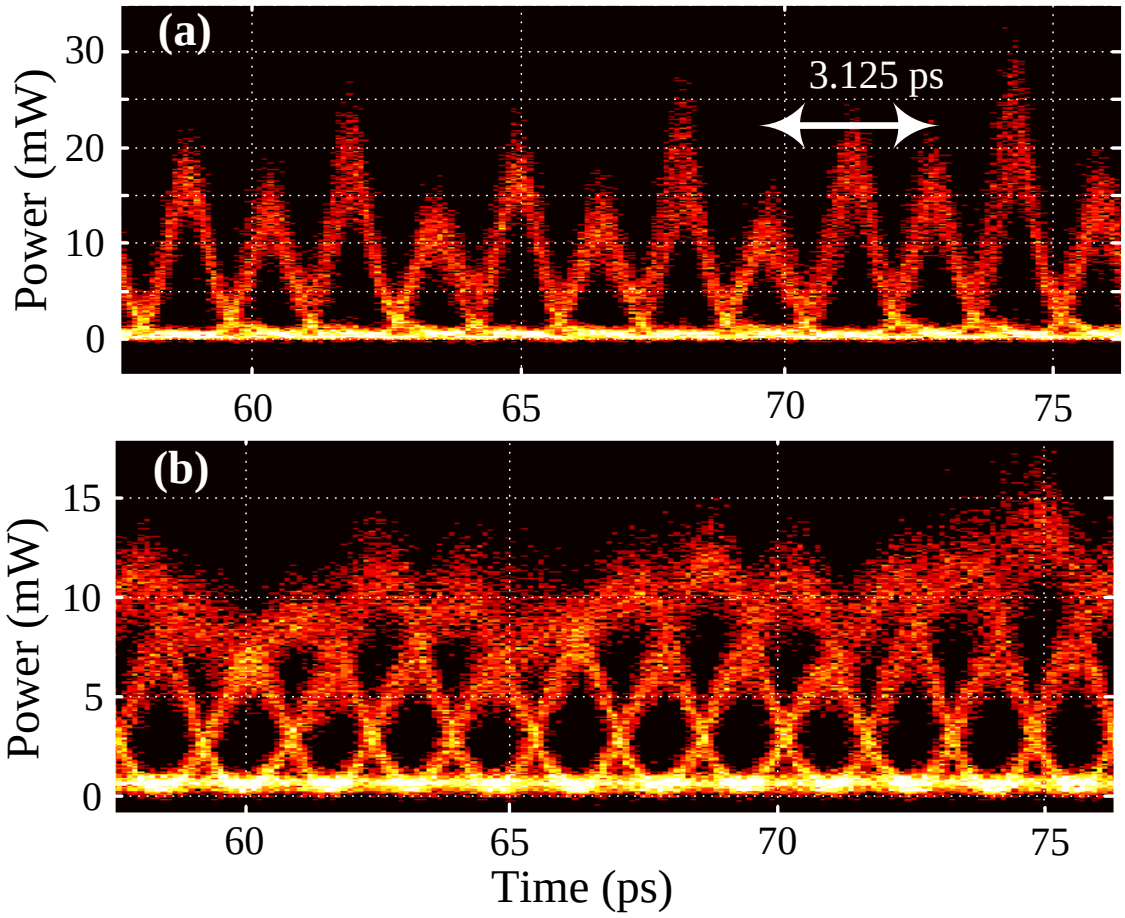

Figure 3.24 – Corresponding (a) eye diagram of the input data and (b) and format converted NRZ signals shown in Fig. 5.

Figure 3.23 illustrates the temporal intensity traces of (a) the 640 Gbit/s input coherent RZ data signal and (b) the converted NRZ signal at the output, measured by a 500-GHz bandwidth optical sampling scope (Exfo PSO-101) in averaging mode. For comparison purposes, the numerical results (dashed red) are also plotted together with the experimental results. Figure 3.24 shows the corresponding eye-diagram of the 640 Gbit/s input RZ signal (Figure 3.22(a)) and the converted NRZ signal (Figure 3.22(b)), respectively. As can be clearly seen, the proposed concept has successfully implemented the target RZ-to-NRZ format conversion. It should be noticed that the imperfect format conversion of the input signal shown in Figure 3.23Figure 3.24 is due to the fact that the chosen OBPF bandwidth and the spectral line-width of the phase filter are relatively far from the predicted optimal regions shown in Figure 3.20(a) and (b), as imposed by the specifications of the filtering method (waveshaper) used for our proof-of-concept demonstrations.

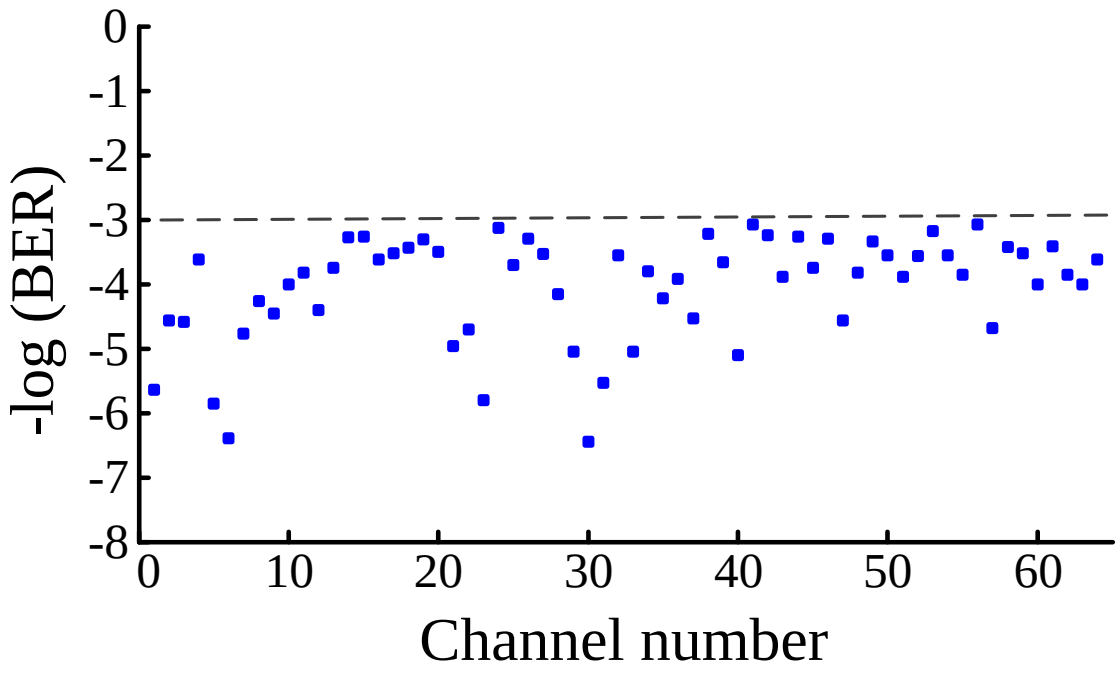

Figure 3.25 – BER measurement of all 64 OTDM tributaries demultiplexed from the 640 Gbit/s NRZ signal at a receiver power of -33 dBm.

Finally, Figure 3.25 shows the bit error rate (BER) measurement obtained for the 64 OTDM tributaries demultiplexed from the 640 Gbit/s NRZ signal at a receiver power of -33 dBm. The measured BER of the 640 Gbit/s input RZ signal is around 10^{-7} at the same receiver power. The data signal is converted with a BER performance below 10^{-3} forward error correction (FEC) limit [234] for all the 64 OTDM channels at a receiver power of -33 dBm. We anticipate that a BER lower than 10^{-3} could be obtained using a higher receiver power. Whereas these results further validate the proper operation of the proposed RZ-to-NRZ conversion method, BER measurements of the individual channels of the converted signal versus receiver power could not be performed at the time of realization of the reported experiments.

3.4.5 Conclusion

In summary, we have proposed and experimentally demonstrated a novel, simple and practical all-optical RZ-to-NRZ format conversion concept based on linear spectral phase filtering of an RZ data signal. Proof-of-concept experiments at 640 Gbit/s have validated the proposed concept and predicted advantages.

Chapter 4

Conclusions and Perspectives

4.1 Conclusions of the Thesis

Energy consumption is a key consideration in the development of practical circuits for optical signal processing. From an energy consumption point of view, optical signal processing is presently much more inefficient than electronic signal processing, which is a potentially significant barrier to the practical use of optical circuits. Therefore, more attention needs to be paid to energy consumption issues in the research and development of new optical technologies.

In this dissertation, we have directly addressed energy consumption issues by developing novel signal-processing scheme to realize energy-efficient optical signal processors at high bit rates and with energy consumption significantly lower than present optical counterparts. The demonstrated schemes are based on the use of purely linear processes to manipulate the temporal and spectral profiles of the signal under test, namely linear temporal modulation and/or linear spectral filtering, respectively, to realize the target processing. The energy consumption is significantly reduced in the desired functionalities due to the fact that the input signal energy can be fully preserved if only the signal phase is manipulated in the time and spectral domains. In the newly proposed processors, the incoming signal's energy is effectively redistributed to build up the target output signal without using any additional external optical power.

In **Chapter 2**, we use the combination of temporal and spectral Talbot effects, i.e., temporal phase modulation and spectral phase filtering, to control and program the repetition rate of an input pulse laser source. In particular, we have proposed a pulse repetition-rate multiplier that is simpler, and far more flexible, and energy efficient than current approaches. For this proposed scheme, we have provided a full analytical methodology to design and determine the system specifications. In particular, we have derived an analytical equation for the temporal phase modulation profile that

is required to achieve a desired multiplication factor. The key feature of the proposed design is that the dispersive medium is fixed and the multiplication factor can be programmed by simply modifying the temporal phase modulation profile according to the derived formulation; the repetition rate of the output signal can be tuned to be any integer multiple of the input repetition rate. An experimental proof-of-concept has been successfully carried out by constructing a programmable and stable fiber-optics source that can be tuned to operate at rates that are integer multiples of ~ 10GHz (input pulse repetition-rate) up to 40GHz. This all-fiber rate-multiplier can be a simple and reliable source for fiber optics communications, optical computing, material processing, frequency combs and nonlinear optics.

As the next step in **Chapter 2**, we have proposed and experimentally demonstrated, for the first time to our knowledge, a lossless "fractional" pulse repetition-rate multiplication technique. Using this proposed method, the output pulse train repetition rate can ideally be designed to be any fractional multiple of the input repetition rate. This offers an unprecedented degree of flexibility compared with previously reported PRRM approaches, which are generally limited to integer repetition-rate multiplication factors. As an example, we experimentally demonstrated multiplication factors of 1.25, 1.33, 1.5, 1.6, 1.75, 2.25, 2.33, and 2.5 with high fidelity from a mode-locked laser with an input repetition rate between 10 and 20 GHz.

As the last step in **Chapter 2**, a new feature of the temporal Talbot effect, referred to as "inverse" temporal Talbot effect, has been reported to demonstrate a passive amplification technique for repetitive optical signals, where the energy of input repetitive pulses is coherently accumulated to fewer replica pulses to build up an output signal with a reduced repetition rate and intensity-amplified pulses. We have shown experimentally intensity amplification of repetitive optical pulse waveforms with a gain from 2 to ~20, with the corresponding repetition-rate division. This was, to my knowledge, the first report of a passive amplification method that does not amplify or inject noise in the output signal and even enhances the extinction ratio and reduces noise fluctuation of the input waveform train through its real-time averaging attribute. These noise-mitigating effects allowed us to show in a side-by-side comparison in one of our experiments how Talbot amplification can extract a weak noisy signal nearly buried beneath a noisy background, whereas a typical active amplifier buries the signal further beneath the noise. Perhaps another, greater significance of this work is how passive amplification using our method can be readily

applied to other spectral regions or wave systems, such as acoustic, electronic, and quantum. This passive amplification technique is applicable to any wave system in which the temporal and dispersive spectral phase can be controlled. Such control is not only available throughout the entire electromagnetic spectrum, but also for many other wave systems, such as acoustic and matter waves for which active gain mechanisms are extremely challenging to implement or simply not available. For example, passive probability amplification of matter-waves could provide another tool for atom optics to control and manipulate quantum states of matter as well as single photon pulses.

In **Chapter 3**, we have developed novel approaches for base-rate and sub-harmonic clock recovery of on-off-keying (OOK) data signals. In particular, the base-rate clock recovery technique is based on spectral phase-only (all-pass) optical filtering. Besides its intrinsic implementation simplicity, this technique significantly enhances both the recovered optical clock quality and energy efficiency in comparison with conventional amplitude optical filtering approaches using a Fabry–Perot filter. The proposed concept and predicted advantages were validated through recovery of the optical clock from a 640 Gbit/s RZ-OOK data signal using a commercial linear optical waveshaper. Furthermore, we proposed and experimentally demonstrated the realization of a reconfigurable subharmonic clock recovery technique based on the inverse temporal Talbot effect, involving temporal phase modulation and dispersive spectral filtering of the input data signal. The scheme can be easily reconfigured to achieve base-rate clock recovery by simply bypassing the temporal phase-modulation step. The proposed scheme has been validated through experimental demonstrations, and in particular, we have reported successful extraction of 4.85-GHz and 3.23-GHz sub-harmonic clock signals as well as the 9.7-GHz base-rate clock signal from a 9.7-Gbit/s RZ-OOK data signal.

Finally, in **Chapter 3**, we have introduced a novel energy-efficient approach for all-optical return-to-zero (RZ) to non-return-to-zero (NRZ) telecommunication data format conversion based on linear spectral phase manipulation of an RZ data signal. The proposed format converter represents an interesting alternative to the conventional linear amplitude spectrum tailoring method (spectrum transformation), showing, for the first time, to my knowledge, how one can generate an NRZ copy of the original RZ optical signal simply by spectral phase-only manipulation of the RZ signal. The operation principle is numerically analyzed and experimentally validated through

successful format conversion of a 640 Gbit/s coherent RZ signal into the equivalent NRZ time-domain data using a simple phase filter implemented by a commercial optical waveshaper. An excellent agreement between the experimental and numerical results was achieved.

This research line to create energy-efficient optical functionalities may open new, important perspectives for implementing other critical optical signal processors with unprecedented energy efficiency, overcoming the energy-consumption limitations of present optical technologies without trading their processing speed advantage.

4.2 Future perspectives

Next, we briefly discuss several potential lines of future research considered as of higher relevance by the author:

1. In **Chapter 1**, we have proposed an implementation of a programmable fiber-optics pulse repetition-rate multiplication approach. The dispersive medium is fixed to satisfy an integer Talbot condition. However, in this approach, the maximum demonstrated multiplication factor is still limited by two main problems. First, the needed amount of dispersion is generally very high, e.g., requiring the use of long fiber-optics dispersive lines, such that distortions induced by high-order dispersion terms on picosecond-long pulses may not be negligible. Second, the ultimate multiplication factor is additionally limited by the available electrical bandwidth of the arbitrary waveform generator used to generate the multi-level phase modulation profile, which becomes more complex (larger number of discrete phase levels) for higher multiplication factors. To alleviate these problems, it should be possible to employ a more practical design using the fractional Talbot condition for the dispersive medium. As such, this new design could be used to electrically tune the repetition-rate of the output pulse train to higher multiplication factors with lower amount of dispersion and a notably simpler phase modulation profile than that of the scheme presented in this Thesis.

2. In **Chapter 2**, we used the combination of the temporal and spectral Talbot effect, i.e., temporal phase modulation and spectral phase filtering, to control and program the repetition-rate of a low-rate laser source. We particularly derived specific formulations for the temporal phase modulation profile and spectral filter to be able to generate uniform pulse trains at the output. However, for many applications, including ultrahigh-speed optical communications and

photonically assisted generation of millimeter-wave and microwave electromagnetic waveforms, it is desirable to generate high repetition-rate pulse trains with additional control on the amplitude of each pulse. An extension of our work on programmable repetition-rate multiplication can be investigated to design a programmable pulse repetition-rate multiplication with additional control on the relative peak power of the output pulses. Using this envisioned scheme, the amplitude of each single pulse in a period could be arbitrarily tailored by simply changing the temporal phase modulation profile.

3. As mentioned in **Chapter 2**, one of the distinct characteristics of the Talbot-based passive waveform amplification method is that it improves noise present on the input temporal signal, effectively implementing a real-time averaging process. We have already demonstrated experimentally this averaging effect for random (white) intensity noise (i.e. ASE-like noise). We also predict that Talbot amplification can improve other important forms of noise, such as pulse-to-pulse intensity fluctuation and timing-jitter, present on the input signal. A comprehensive theoretical and experimental study needs to be conducted to examine these predictions.

4. The phase-only filtering technique used in **Chapter 3** can also be applied for other crucial signal processors, including logic gates. Logic gates are fundamental building blocks in digital signal processing (DSP) circuits. In the last decade, a vast surge of research has been undertaken to build optical logic gates. Though many optical logic gates have been demonstrated with speeds thousands of times faster than the best electronics, the power required for most proposals is approximately one thousand times higher than their electronic counterparts. As it is, the solutions proposed for optical logic gates are much more inefficient from an energy consumption viewpoint than current state-of-the-art electronics. General thermodynamic arguments show that fundamentally, one should be able to design a logic gate that can consume arbitrarily low energy (no lower limit), so-called "zero-energy" logic gates. In particular, several researchers recently have proposed that a "zero-energy" gate could be designed with optics. In spite of many attempts, the practical realization of a high-speed "zero energy" logic-gate has remained elusive. As an extension of proposed optical functionalities proposed in this Thesis for processing optical data signals, we envision the design and demonstration of zero-switching-energy logic gates using a purely passive and phase-only linear process, a process that inherently preserves the entire input signal energy, thus approaching the predicted "zero-energy" paradigm. The result of this follow-

up research may represent a new paradigm shift in gate design to implement optical logic with significantly reduced energy consumption at ultrahigh speeds.

Chapitre 4

Conclusions ET Perspectives (en français)

4.1 Conclusions de la Thèse

La consommation de l'énergie est un facteur clé dans le développement de circuits pratiques pour le traitement du signal optique. En matière de consommation d'énergie, le traitement du signal optique est actuellement beaucoup plus inefficace que le traitement de signal électronique, qui est un obstacle important pour l'utilisation pratique des circuits optiques. Par conséquent, une plus grande attention doit être accordée aux questions de consommation d'énergie dans la recherche et le développement de nouvelles technologies optiques.

Dans cette thèse, nous avons abordé les problèmes de consommation d'énergie en développant un nouveau système de traitement de signaux pour la réalisation des processeurs de signaux optiques à haute efficacité énergétique travaillant à des débits élevés et avec une consommation d'énergie nettement plus faible que celle des solutions optiques existantes actuellement. Ces systèmes proposés sont basés sur l'utilisation de procédés purement linéaires pour manipuler les profils temporels et spectraux du signal sous test, à savoir, la modulation temporelle linéaire et/ou le filtrage spectral linéaire, respectivement, pour réaliser le traitement visé. La consommation d'énergie est considérablement réduite dans les fonctionnalités souhaitées car l'énergie du signal d'entrée peut être entièrement préservée si seule la phase du signal est manipulée dans les domaines temporel et spectral. Dans les processeurs nouvellement proposés, l'énergie du signal entrant est efficacement redistribuée pour construire le signal de sortie ciblé sans l'utilisation d'une puissance optique externe supplémentaire.

Dans le **Chapitre 2**, nous avons utilisé la combinaison de l'effet Talbot temporel et spectral, à savoir la modulation de phase temporelle et le filtrage de phase spectrale, pour contrôler et programmer le taux de répétition et l'énergie par impulsion associée d'une source laser impulsionnelle à faible taux de répétition. En particulier, nous avons proposé un multiplicateur de taux de répétition d'impulsions qui est plus simple et beaucoup plus flexible et économe en énergie que les approches actuelles. Pour ce système proposé, nous avons fourni une méthodologie analytique complète pour concevoir et déterminer les exigences du système. En particulier, nous avons établi une équation analytique pour le profil de modulation de phase temporelle requis pour atteindre un facteur de multiplication souhaité. La principale caractéristique de la conception proposée est que le milieu dispersif est fixé et le facteur de multiplication peut être programmé en modifiant simplement le profil de la modulation de phase temporelle selon la formulation dérivée; le taux de répétition du signal de sortie peut être réglé pour être un multiple entier quelconque du taux répétition d'entrée. Une démonstration de faisabilité expérimentale a été réalisée avec succès en construisant une source à fibre optique programmable et stable qui peut être réglé pour fonctionner à des taux qui sont des multiples entiers de ~ 10GHz (taux de répétition d'entrée) jusqu'à 40GHz. Ce multiplicateur de taux de répétition tout-fibre peut être une source simple et fiable pour les communications par fibres optiques, l'informatique optique, le traitement des matériaux, les peignes de fréquences et l'optique non linéaire.

Dans l'étape suivante dans le **Chapitre 2**, nous avons proposé et démontré expérimentalement, pour la première fois à notre connaissance, une technique de multiplication sans perte et fractionnaire du taux de répétition des impulsions. En utilisant cette méthode, le taux de répétition du train d'impulsion de sortie peut être idéalement conçu pour être un multiple fractionnaire du taux de répétition d'entrée, offrant un degré de flexibilité sans précédent par rapport aux approches de multiplication rapportées précédemment, qui sont généralement limités à des facteurs de multiplication entiers. A titre d'exemple, nous avons démontré expérimentalement des facteurs de multiplication de 1,25, 1,33, 1,5, 1,6, 1,75, 2,25, 2,33 et 2,5 avec une haute fidélité à partir d'un laser à verrouillage de mode et un taux de répétition d'entrée entre 10 et 20 GHz.

Dans la dernière étape du **Chapitre 2**, une nouvelle propriété de l'effet Talbot temporel appelée 'effet Talbot temporel inverse', a été étudiée pour démontrer une technique d'amplification passive des signaux optiques répétitifs, où l'énergie d'entrée des impulsions est

additionnée de manière cohérente pour construire un signal de sortie avec un taux de répétition réduit et une intensité d'impulsions amplifiée. Nous avons montré expérimentalement l'amplification de l'intensité de trains d'impulsions avec un gain de 2 à ~ 20, avec les divisions de taux de répétition correspondantes. Ce fut, à notre connaissance, la première démonstration d'une méthode d'amplification passive qui n'amplifie et n'introduit pas de bruit dans le signal de sortie, et améliore même, le taux d'extinction et réduit le bruit de fluctuation du train de forme d'onde d'entrée grâce à sa propriété de moyenne en temps réel. Ces effets d'atténuation du bruit ont permis de montrer dans une comparaison côte à côte dans une de nos expériences comment l'amplification par effet Talbot inverse permet d'extraire un signal faible et bruité presque enterré sous un fond bruyant, alors qu'un amplificateur actif typique enfouit plus le signal sous le bruit. Une autre signification possible plus grande de ce travail peut être de savoir comment appliquer facilement l'amplification passive développée dans ce travail à d'autres régions spectrales ou des systèmes d'ondes, comme l'acoustique, L'électronique et le domaine quantique. Cette technique d'amplification passive est applicable à tout système d'onde dans lequel la phase temporelle et la phase spectrale dispersive peuvent être contrôlées. Un tel contrôle est non seulement disponible dans l'ensemble du spectre électromagnétique, mais aussi dans de nombreux autres systèmes d'ondes, comme l'acoustique et les ondes de matière pour lesquels les mécanismes de gain actifs sont extrêmement difficiles à mettre en œuvre ou tout simplement inexistants. Par exemple, l'amplification passive de la probabilité des ondes de matière pourrait fournir un autre outil pour l'optique atomique pour contrôler et manipuler les états quantiques de la matière ainsi que des impulsions de photons uniques.

Dans le chapitre 3 nous avons développé des approches pour la récupération des signaux d'horloge de base et sous-harmonique dans les signaux de données de type tout-ou-rien (OOK for on-off-keying en anglais). En particulier, la technique de récupération des signaux d'horloge de base est basée sur le filtrage optique (passe-tout) de la phase-seule dans le domaine spectral. Outre sa simplicité intrinsèque de mise en œuvre, cette technique améliore considérablement la qualité de l'horloge optique récupérée et l'efficacité énergétique par rapport aux approches classiques de filtrage optique d'amplitude utilisant un filtre Fabry-Perot. Le concept proposé et ces avantages prévus ont été validés par la récupération de l'horloge optique à partir d'un signal de données RZ OOK à 640 Gbit/s en utilisant un façonneur d'onde (waveshaper) optique linéaire commercial.

En outre, nous avons proposé et démontré expérimentalement la réalisation d'une technique reconfigurable de récupération d'horloge sub-harmonique basée sur l'effet Talbot inverse, impliquant une modulation de phase temporelle et un filtrage spectral dispersif du signal de données d'entrée. Ce système peut être facilement reconfiguré pour réaliser la récupération du signal d'horloge de base en omettant l'étape de modulation de phase temporelle. Le système proposé a été validé par des démonstrations expérimentales, en particulier, nous avons démontré l'extraction avec succès des signaux d'horloge sous-harmoniques de 4.85 GHz et 3.23 GHz ainsi qu'un signal d'horloge de base de 9.7 GHz à partir d'un signal de données RZ-OOK à 9.7 Gbit/s.

Enfin, dans le **Chapitre 3**, nous avons introduit une nouvelle approche efficace énergétiquement pour la conversion tout-optique de format de données de télécommunication : retour-à-zéro (RZ) au non-retour-à-zéro (NRZ), basée sur la manipulation linéaire de la phase spectrale du signal de données RZ. Le convertisseur de format proposé représente une alternative intéressante à la méthode linéaire classique d'adaptation du spectre d'amplitude (transformation du spectre), montrant pour la première fois, à notre connaissance, comment on peut générer une copie NRZ du signal optique RZ d'origine simplement par la manipulation de la phase spectrale-seule du signal RZ d'origine. Le principe de fonctionnement est analysé numériquement et validé expérimentalement par une conversion de format d'un signal RZ cohérent de 640 Gbit/s vers son équivalent NRZ en utilisant un filtre de phase simple mis en œuvre à l'aide d'un façonneur d'onde (waveshaper) optique commercial. Un excellent accord entre les résultats expérimentaux et numériques a été atteint.

Cette ligne de recherche visant à créer des fonctionnalités optiques efficace énergétiquement peut ouvrir de nouvelles perspectives, importantes pour la mise en œuvre d'autres processeurs de signaux optiques critiques avec une efficacité énergétique sans précédent, surmontant ainsi les problèmes de consommation d'énergie des technologies optiques actuelles sans compromis sur leur avantage en matière de vitesse de traitement.

4.2 Perspectives

Dans ce qui suit, nous discutons brièvement plusieurs futures lignes de recherches potentielles considérées comme hautement pertinentes par l'auteur:

1. Dans le **Chapitre 1**, nous avons proposé une mise en œuvre d'une approche programmable de multiplication du taux de répétition d'impulsions impulsion basée sur des fibres optique. Le milieu dispersif est fixé pour satisfaire la condition de l'effet Talbot entier. Cependant, dans cette approche, le facteur de multiplication maximal démontré est limité par deux problèmes principaux. Tout d'abord, la quantité nécessaire de dispersion est généralement très élevée, par exemple, nécessitant l'utilisation de longues lignes dispersives à fibres optiques, de façon que les distorsions induites par les termes de dispersion d'ordre élevé sur des longues impulsions picosecondes ne puissent plus être négligées. Ensuite, le facteur de multiplication ultime est limité également par la bande passante électrique disponible du générateur de forme d'onde arbitraire utilisé pour générer le profil de modulation de phase multi-niveau, qui devient plus complexe (plus grand nombre de niveaux de phase discrets) pour les facteurs de multiplication élevés. Pour pallier à ces problèmes, on pourrait utiliser une conception plus pratique en se servant de la condition Talbot fractionnaire pour le milieu dispersif. Ce nouveau design pourrait être utilisé pour régler électriquement le taux de répétition du train d'impulsions de sortie à des facteurs de multiplication plus élevés avec une dispersion plus faible et un profil de modulation de phase plus simple que celui du système présenté dans cette thèse.

2. Dans le **Chapitre 2**, nous avons utilisé la combinaison de l'effet Talbot temporel et spectral, c.-à-d. la modulation de phase temporelle et le filtrage de phase spectrale, pour contrôler et programmer le taux de répétition d'une source laser impulsionnelle à faible taux répétition. Nous avons en particulier établi des formulations spécifiques pour le profil de modulation de la phase temporelle et le filtre spectral pour être en mesure de générer des trains d'impulsions uniformes à la sortie. Cependant, pour de nombreuses applications, y compris les communications optiques ultra-rapides et la génération des formes d'ondes électromagnétiques millimétriques et micro-ondes assistée par la photonique, il est souhaitable de générer des trains d'impulsions à un taux de répétition élevé avec un contrôle supplémentaire sur l'amplitude de chaque impulsion. Une extension de notre travail sur la multiplication programmable du taux de répétition peut être étudiée pour concevoir une multiplication avec un contrôle supplémentaire sur la puissance de crête relative des impulsions de sortie. En utilisant ce système, l'amplitude de chaque impulsion dans une période pourrait être arbitrairement contrôlée simplement en changeant le profil de la modulation de phase temporelle.

3. Comme mentionné dans le **Chapitre 2**, l'une des caractéristiques distinctes de la méthode d'amplification passive à base d'effet Talbot, est qu'elle améliore le bruit présent sur le signal temporel d'entrée, en réalisant une moyenne temporelle de manière efficace en temps réel. Nous avons déjà démontré expérimentalement cet effet de moyenne pour le bruit aléatoire (blanc) d'intensité (comme celui de l'ESA: émission spontanée amplifiée). Nous prévoyant également que l'amplification-Talbot peut améliorer d'autres types de bruits présents dans le signal d'entrée, tels que les fluctuations d'intensité d'impulsion à impulsion et la gigue temporelle. Une étude théorique et expérimentale approfondie doit être menée pour examiner ces perspectives.

4. La technique de filtrage de phase-seule utilisée dans le **Chapitre 3** peut également être appliquée à d'autres processeurs de signaux cruciaux, y compris des portes logiques. Les portes logiques sont des éléments fondamentaux dans les circuits de traitement numérique du signal. Dans la dernière décennie, un effort de recherche considérable a été investi pour construire des portes logiques optiques. Bien que beaucoup de portes optiques logiques aient été démontrées avec des vitesses des milliers de fois plus rapide que les meilleurs circuits électroniques, la puissance nécessaire pour la plupart des dispositifs proposés est d'environ un millier de fois plus élevée que leurs homologues électroniques. Les solutions proposées pour les portes logiques optiques sont beaucoup moins efficaces en matière de consommation d'énergie que les dispositifs électronique à l'état de l'art actuel. Des arguments généraux de la thermodynamique montrent que fondamentalement, on devrait être en mesure de concevoir une porte logique qui consomme une quantité d'énergie arbitrairement faible dite portes logiques "zéro-énergie". En particulier, plusieurs chercheurs ont récemment proposé qu'une porte "zéro énergie" pourrait être conçu à l'aide de l'optique. Malgré de nombreuses tentatives, la réalisation pratique d'une porte logique grande vitesse " zéro- énergie" est restée inaccessible. Dans le prolongement des fonctionnalités optiques pour le traitement des signaux de données optiques proposées dans cette thèse, nous envisageons la conception et la démonstration de portes logiques à zéro-énergie de commutation en utilisant un processus linéaire purement passif et agissant sur la phase-seule, un tel processus préserve intrinsèquement L'entière énergie du signal à l'entrée, se rapprochant ainsi du paradigme "zéro énergie". Le résultat de cette recherche de suivi pourrait représenter un nouveau changement de paradigme dans la conception de porte logiques pour mettre en œuvre des portes logiques optiques avec une consommation d'énergie considérablement réduite à des vitesses ultrahautes.

References

[1] C. Kao and G. Hockham, "Dielectric-fibre surface waveguides for optical frequencies," *Proc. IEE*, vol. 113, p. 1151–1158, 1966.

[2] L. N. Binh, Digital processing optical transmission and coherent receiving techniques, Boca Raton, FL: CRC Press, 2014.

[3] T. Richter, E. Palushani, C. Schmidt-Langhorst, M. Nölle, R. Ludwig and C. Schubert, "Single wavelength channel 10.2 Tb/s TDM-data capacity using 16-QAM and coherent detection," in *Optical Fiber Communication (OFC)*, Los Angeles, 2011.

[4] D. Hillerkuss, R. Schmogrow, T. Schellinger, M. Jordan, M. Winter, G. Huber, T. Vallaitis, R. Bonk, P. Kleinow, F. Frey, M. Roeger, A. L. S. Koenig, A. Marculescu, J. Li, M. Hoh, M. Dreschmann, J. Meyer, S. B. Ezra, N. Narkiss and B. Nebendahl, "26 Tbit/s line-rate super-channel transmission utilizing all-optical fast Fourier transform processing," *Nat. Photonics*, vol. 5, pp. 364–371, 2011.

[5] A. Sano, H. Masuda, Y. Kisaka, S. Aisawa, E. Yoshida, Y. Miyamoto, M. Koga, K. Hagimoto, T. Yamada, T. Furuta and H. Fukuyama, "14-Tb/s (140 × 111-Gb/s PDM/WDM) CSRZ-DQPSK transmission over 160 km using 7 THz bandwidth extended L-band EDFAs,"," in *Proceedings of European Conference on Optical Communications (ECOC)*, Cannes, France, 2006.

[6] Cisco, "Cisco Visual Networking Index: Forecast and Methodology, 2014–2019," [Online]. Available: http://www.cisco.com/c/en/us/solutions/collateral/service-provider/visual-networking-index-vni/VNI_Hyperconnectivity_WP.html. [Accessed 01 06 2016].

[7] R. Ramaswami and K. Sivarajan, Optical networks: A practical perspective, London: Morgan Kaufmann Publishers, 1998.

[8] R. Tucker and K. Hinton, "Energy consumption and energy density in optical and electronic signal processing," *IEEE Photonics J.*, vol. 3, pp. 821–833, 2011.

[9] P. Stavroulakis, Reliability, survivability and quality of large scale telecommunication systems: case study: olympic games, West Sussex, England: Wiley, 2003.

[10] K. Tatas, K. Siozios, A. Bartzas, C. Kyriacou and D. Soudris, "A novel prototyping and evaluation framework for NoC-based MPSoC," *Int. J. Adapt. Resilient Auto. Syst.*, vol. 4, pp. 1-24, 2013.

[11] S. Wabnitz and B. J. Eggleton, All-optical signal processing data communication and storage applications, New York, US: Springer, 2015, pp. 157-183.

[12] E. Desurvire, " Capacity demand and technology challenges for lightwave systems in the next two decades," *J. Lightwave Technol.*, vol. 24, pp. 4697–4710, 2006.

[13] K. Samdanis, P. Rost, A. Maeder, M. Meo and C. Verikoukis, Green Communications: Principles, Concepts and Practice, Sussex: Wiley, 2015.

[14] L. LeBlond, "Models Show That Internet Produces Vast Amounts Of Greenhouse Gas," Red Orbit, [Online]. Available: http://www.redorbit.com/news/science/1112756793/internet-produces-greenhouse-gas-010313/. [Accessed 05 08 2016].

[15] "SMART 2020: Enabling the low carbon," Global engagement studies institute (GeSi), [Online]. Available: http://gesi.org/article/43. [Accessed 05 08 2016].

[16] J. Baliga, R. Ayre, K. Hinton and R. S. Tucker, "Photonic switching and the energy bottleneck," in *Photonics in Switching*, San Francisco, US, 2007.

[17] L. Oxenløwe, M. Galili, H. H. Mulvad, H. Hu, J. L. Areal, E. Palushani, H. Ji, A. Clausen and P. Jeppesen, "Nonlinear optical signal processing for Tbit/s Ethernet applications," *Int. J. Opt.*, vol. 11, pp. 573843(1-14), 2012.

[18] S. J. B. Yoo, "Optical packet and burst switching technologies for the future photonic internet," *IEEE J. lightwave technol. let.*, vol. 24, pp. 4468–4492, 2006.

[19] Y. Paquot, *Novel linear and nonlinear optical signal processing for ultra-high bandwidth communications*, Sydney: University of Sydney, 2014.

[20] K. Hinton, P. M. Farrell and R. S. Tucker, "The photonic bottleneck," in *Optical Fiber Communication (OFC)*, Anaheim, US, 2007.

[21] K. Hinton, G. Raskutti, P. M. Farrell and R. S. Tucker, "Switching energy and device size limits on digital photonic signal processing technologies," *IEEE J. Sel. Top. Quantum Electron.*, vol. 14, pp. 938-945, 2008.

[22] D. A. B. Miller, "Are optical transistors the logical next step?," *Nat. Photonics*, vol. 4, pp. 3-5, 2010.

[23] R. S. Tucker, "Energy consumption and energy density in optical and electronic signal processing," *IEEE Photonics J.*, vol. 3, pp. 821-833, 2011.

[24] D. Solli and B. Jalali, "Analog optical computing," *Nat. Photonics*, vol. 9, pp. 704-706 , 2015.

[25] H. J. Caulfield and S. Dolev, "Why future supercomputing requires optics," *Nat. Photonics*, vol. 4, pp. 261-263, 2010.

[26] H. J. Caulfield, A. Zavalin and L. Qian, "Zero-energy optical logic: can it be practical?," *Supercomput.*, vol. 62, pp. 681–688, 2012.

[27] P. Del'Haye, A. Schliesser, O. Arcizet, T. Wilken, R. Holzwarth and T. J. Kippenberg, "Optical frequency comb generation from a monolithic microresonator," *Nature*, vol. 450, pp. 1214–1217, 2007.

[28] A. Turner, M. Foster, A. Gaeta and M. Lipson, "Ultra-low power parametric frequency conversion in a silicon microring resonator," *Opt. Express*, vol. 16, pp. 4881–4887 , 2008.

[29] F. Li, T. Vo, C. Husko, M. Pelusi, D.-X. Xu, A. Densmore, R. Ma, S. Janz, B. Eggleton and D. Moss, "All-optical XOR logic gate for 40 Gb/s DPSK signals via FWM in a silicon nanowire," *Opt. Express*, vol. 19, pp. 20364–20371, 2011.

[30] B. Corcoran, C. Monat, M. Pelusi, C. Grillet, T. P. White, L. O'Faolain, T. F. Krauss, B. J. Eggleton and D. J. Moss, "Optical signal processing on a silicon chip at 640Gb/s using slow-light," *Opt. Express*, vol. 18, pp. 7770-7781, 2010.

[31] L. K. Oxenlowe, M. Pu, Y. Ding, H. Hu, F. D. Ros, D. Vukovic, A. S. Jensen, H. Ji, M. Galili, C. Peucheret and K. Yvind, "All-optical signal processing using silicon devices," in *The European Conference on Optical Communication (ECOC)*, Cannes, France, 2014.

[32] H. Ji, H. Hu, M. Pu, Y. Ding, A. S. Jensen, M. Galili, K. Yvind and L. K. Oxenløwe, "Silicon nanowires for ultra-fast and ultrabroadband optical signal processing," in *Opto-Electronics and Communications Conference (OECC)*, Shanghai, China, 2015.

[33] A. R. Motamedi, A. H. Nejadmalayeri, A. Khilo, F. X. Kartner and E. P. Ippen, "Ultrafast nonlinear optical studies of silicon nanowaveguides," *Opt. Express*, vol. 20, pp. 4085–4101, 2012.

[34] S. Y. R. J. R. W. Loh and P. W. Juodawlkis, "A nonlinear optoelectronic filter for electronic signal processing," *Sci. Rep.*, vol. 4, pp. 3613(1-5), 2014.

[35] M. Kuschnerov, T. Bex and P. Kainzmaier, "Energy efficient digital signal processing," in *Optical Fiber Communications (OFC)*, Los Angeles, US, 2014.

[36] R. Stabile, A. Albores-Mejia, A. Rohit and K. A. Williams, "Integrated optical switch matrices for packet data networks," *Nat. Microsys. & Nanoengin.*, vol. 2, pp. 15042(1-10), 2016.

[37] M. R. Fernández-Ruiz, A. Carballar and J. Azaña, "Design of ultrafast all-optical signal processing devices based on fiber Bragg gratings in transmission," *IEEE J. Lightwave Technol.*, vol. 31, pp. 1593-1600, 2013.

[38] R. Ashrafi, M. Li and a. J. Azaña, "Coupling-strength-independent long-period grating designs for THz-bandwidth optical differentiators," *IEEE Photonics J.*, vol. 5, pp. 7100311(1-11), 2013.

[39] X. Fang, K. F. MacDonald and N. I. Zheludev, "Controlling light with light using coherent metadevices: all-optical transistor, summator and invertor," *Nat. Light Sci. Appl.*, vol. 4, pp. e292(1-7), 2015.

[40] J. Azana, "Ultrafast analog all-optical signal processors based on fiber-grating devices," *IEEE Photon. J*, vol. 2, pp. 359-386, 2010.

[41] J. Azaña and M. A. Muriel, "Temporal self-imaging effects: theory and application for multiplying pulse repetition rates," *IEEE J. Sel. Top. Quant. Electron.*, vol. 7, pp. 728–744, 2001.

[42] G. P. Agrawal, Nonlinear fiber optics, Burlington, US: Elsevier, 2006.

[43] J. Gong, J. Xu, M. Luo, X. Li, Y. Qiu, Q. Yang, X. Zhang and S. Yu, "All-optical wavelength conversion for mode division multiplexed superchannels," *Opt. Express,* vol. 24, pp. 8926-8939, 2016.

[44] N. Andriolli, S. Faralli, X. J. M. Leijtens, J. Bolk and G. Contestabile, "Monolithically integrated all-optical regenerator for constant envelope WDM signals," *Opt. Express,* vol. 31, pp. 322-327, 2013.

[45] A. Pasquazi, L. Caspani, M. Peccianti, M. Clerici, M. Ferrera, L. Razzari, D. Duchesne, B. E. Little, S. T. Chu, D. J. Moss and R. Morandotti, "Self-locked optical parametric oscillation in a CMOS compatible microring resonator: a route to robust optical frequency comb generation on a chip," *Opt. Express,* vol. 21, pp. 13333-13341, 2013.

[46] T. Von-Lerber, S. Honkanen, A. Tervonen, H. Ludvigsen and F. Küppers, "Optical clock recovery methods: Review," *Opt. Fiber Technol.,* vol. 15, pp. 363–372, 2009.

[47] J. Azaña and M. A. Muriel, "Temporal self-imaging effects: theory and application for multiplying pulse repetition rates," *IEEE J. Sel. Top. Quant. Electron.,* vol. 7, pp. 728–744, 2001.

[48] R. Gutiérrez-Castrejón, "Turbo-switched Mach-Zehnder interferometer performance as all-optical signal processing element at 160 Gb/s," *Opt. Commun.,* vol. 282, pp. 4345–4352, 2009.

[49] T. Yang, J. Dong, L. Lu, L. Zhou, A. Zheng, X. Zhang and J. Chen, "All-optical differential equation solver with constant-coefficient tunable based on a single microring resonator," *Sci. Rep.,* vol. 4, pp. 5581(1-6), 2014.

[50] G. New, Introduction to Nonlinear Optics, Cambridge : University Press, 2011.

[51] R. W. Boyd, Nonlinear optics, Cambridge: Academic Press, 2008.

[52] A. Rostami, H. Baghban and R. Maram, Nanostructure semiconductor optical amplifiers: building blocks for all-optical processing, Berlin, Genmany: Springer-Verlag, 2011.

[53] X. Zhao, C. Lou and Y. Feng, "Optical signal processing based on semiconductor optical amplifier and tunable delay interferometer," *Front. Optoelectron. China,* vol. 4, pp. 308–314, 2011.

[54] J. Qiu, K. Sun, M. Rochette and L. R. Chen, "Reconfigurable all-optical multilogic gate (XOR,AND, and or) based on cross-phase modulation in a highly nonlinear fiber," *IEEE Photonics Technol. Lett.,* vol. 22, pp. 1199–1201, 2010.

[55] L. Li, J. Wu, J. Qiu, B. Wu, K. Xu, X. Hong, Y. Li and J. Lin, "Reconfigurable all-optical logic gate using four-wave mixing (FWM) in HNLF for NRZ-PolSK signal," *Opt. Commun.,* vol. 283, pp. 3608–3612, 2010.

[56] A. L. Yi, L. S. Yan, B. L. W. Pan, J. Ye, Z. Y. Chen and J. H. Lee, "Simultaneous all-optical RZ-to-NRZ format conversion for two tributaries in PDM signal using a single section of highly nonlinear fiber," *Opt. Express* , vol. 20, pp. 9890-9896, 2012.

[57] A. E. Willner, S. Khaleghi, M. R. Chitgarha and O. F. Yilmaz, "All-optical signal processing," *IEEE J. Lightwave Technol.*, vol. 32, pp. 660-680, 2014.

[58] R. Neo, J. Schröder, Y. Paquot, D. Choi, S. Madden, B. Luther-Davies and B. J. Eggleton, "Phase-sensitive amplification of light in a χ(3) photonic chip using a dispersion engineered chalcogenide ridge waveguide," *Opt. Express*, vol. 21, pp. 7926-7933, 2013.

[59] A. Hussain, F. Adeel, J. Ahmed and M. Y. Siyal, Optical signal processing by silicon photonics, Singapore: Springer , 2013.

[60] O. Wada, "Advances in III–V semiconductor photonics: Nanostructures and integrated chips," in *International Conference on Indium Phosphide and Related Materials (IPRM)*, Kobe, South Korea, 2013.

[61] M. Hopkinson, T. Martin and P. Smowton, "III–V semiconductor devices integrated with silicon," *Semicond. Sci. Technol.*, vol. 28, pp. 090301, 2013.

[62] A. Bogoni, X. Wu, Z. Bakhtiari, S. Nuccio and A. E. Willner, "640 Gbits/s photonic logic gates," *Opt. Lett.*, vol. 35, pp. 3955–3957, 2010.

[63] A. Malacarne, G. Meloni, G. Berrettini, N. Sambo, L. Potì and A. Bogoni, "Optical multicasting of 16QAM signals in periodically-poled lithium niobate waveguide," *J. Lightwave Technol.*, vol. 31, pp. 1797-1803, 2013.

[64] A. Yang, L. Zuo, J. Zhou, Y. Qiao and Y. Sun, "Periodically poled lithium niobate based ultra-wide bandwidth optical sampling oscilloscope," in *International Conference on Optical Instruments and Technology: Optoelectronic Devices and Optical Signal Processing*, Beijing, China, 2013.

[65] K. Hinton, G. Raskutti, P. M. Farrell and R. S. Tucker, "Switching energy and device size limits on digital photonic signal processing technologies," *IEEE J. Sel. Topics Quantum Electron.*, vol. 14, pp. 938-945, 2008.

[66] J. Azaña, N. K. Berger, B. Levit and B. Fischer, "Spectral Fraunhofer regime: time-to-frequency conversion by the action of a single time lens on an optical pulse," *Appl. Opt.*, vol. 43, pp. 483–490 , 2004.

[67] B. E. A. Saleh and M. C. Teich, Fundamentals of Photonics, New York, US: Wiley, 2007.

[68] A. V. Oppenheim, S. W. A and S. Hamid, Signals and systems, Essex, England: Pearson, 1996.

[69] R. Salem, M. A. Foster and A. L. Gaeta, "Application of space–time duality to ultrahigh-speed optical signal processing," *Adv. Opt. Photonics*, vol. 5, pp. 274–317, 2013.

[70] W. S. Fegadolli, L. Feng, M. Mujeeb-U-Rahman, J. E. B. Oliveira, V. R. Almeida and A. Scherer, "Experimental demonstration of a reconfigurable silicon thermo-optical device based on spectral tuning of ring resonators for optical signal processing," *Opt. Express*, vol. 22, pp. 3425–3431, 2014.

[71] H. Hu, P. Münster, E. Palushani, M. Galili, H. C. H. Mulvad, P. Jeppesen and L. K. Oxenløwe, "640 GBd phase-correlated OTDM NRZ-OOK generation and field trial transmission," *IEEE Photon. Technol. Lett.*, vol. 31, pp. 696-701, 2013.

[72] M. Kondrat, M. Szustakowski, N. Pałka, W. Ciurapiński and M. Życzkowski, "A Sagnac-Michelson fibre optic interferometer: Signal processing for disturbance localization," *Opto-Electron. Rev.*, vol. 15, pp. 127-132, 2007.

[73] M. J. Strain and M. Sorel, "Integrated III-V Bragg gratings for arbitrary control over chirp and coupling coefficient," *IEEE Photonics Technol. Lett.*, vol. 20, pp. 1863–1865, 2008.

[74] R. Kashyap, Fiber Bragg gratings, Burlington, US: Academy press, 2010.

[75] J. Caraquitena, M. Beltrán, R. Llorente, J. Martí and M. A. Muriel, "Spectral self-imaging effect by time-domain multilevel phase modulation of a periodic pulse train," *Opt. Lett.*, vol. 36, pp. 858–860, 2011.

[76] R. Maram and J. Azaña, "Spectral self-imaging of time-periodic coherent frequency combs by parabolic cross-phase modulation," *Opt. Express*, vol. 21, pp. 28824–28835, 2013.

[77] P. Dong, S. Liao, D. Feng, H. Liang, D. Zheng, R. Shafiiha, C.-C. Kung, W. Qian, G. Li, X. Zheng, A. V. Krishnamoorthy and M. Asghari, "Low Vpp, ultralow-energy, compact, high-speed silicon electro-optic modulator," *Opt. Express*, vol. 17, pp. 22484-22490, 2009.

[78] L. K. Oxenløwe, F. Gómez-Agis, C. Ware, S. Kurimura, H. C. H. Mulvad, M. Galili, H. Nakajima, J. Ichikawa, D. Erasme, A. T. Clausen and P. Jeppesen, "640-Gbit/s data transmission and clock recovery using an ultrafast periodically poled lithium niobate device," *J. Lightw. Technol.*, vol. 27, pp. 205-213, 2009.

[79] I. Kim, C. Kim, G. Li, P. LiKamWa and J. Hong, "180- GHz clock recovery using a multisection gain-coupled distributed feedback laser," *IEEE Photon. Technol. Lett.*, vol. 17, pp. 1295-1297, 2005.

[80] J. S. Vardakas and K. E. Zoiros, "Performance investigation of all-optical clock recovery circuit based on Fabry-Pérot filter and semiconductor optical amplifier assisted Sagnac switch," *Opt. Eng.*, vol. 46, pp. 085005(1-21), 2007.

[81] R. Maldonado-Basilio, J. Parra-Cetina, S. Latkowski, N. Calabretta and P. Landais, "Experimental investigation of the optical injection locking dynamics in single-section quantum-dash Fabry-Pérot laser diode for packet-based clock recovery applications," *J. Lightwave Technol.*, vol. 31, pp. 860-865, 2013.

[82] J. Zou, Y. Yu, W. Yang, Z. Wu, M. Ye, G. Chen and X. Zhang, "An SOI based polarization insensitive filter for all-optical clock recovery," in *Optical Fiber Communications (OFC)*, San Francisco, US, 2014.

[83] Y. El-Sayed, A. Wageeh, T. Ismail and H. Mostafa, "All-optical clock and data recovery using self-pulsating lasers for high-speed optical networks," in *International Conference on Energy Aware Computing Systems & Applications (ICEAC)*, Cairo, Egypt, 2015 .

[84] J. P. Cetina, J. Luo, N. Calabretta and P. Landais, "All optical clock recovery of 40 GHz quantum dash mode-locked laser to return-to-zero 160 Gb/s data stream," in *Lasers and Electro-Optics Europe (CLEO EUROPE)* , Munich, Germany, 2013.

[85] T. Huanga, S. Fua, J. Sunb, J. Lic and L. R. Chen, "Comparison of nonlinear fiber-based approaches for all-optical clock recovery at 40 Gb/s," *Opt. Commun.,* vol. 298, pp. 213–221, 2013.

[86] F. G. Agis, C. Ware, D. Erasme, R. Ricken, V. Quiring and W. Sohler, "10 GHz clock recovery using an opto-electronic phase-locked loop based on three-wave mixing in periodically-poled lithium niobate," in *Quantum Electronics and Laser Science Conference*, Long Beach, US, 2006.

[87] L. K. Oxenløwe, F. Gómez-Agis, C. Ware, S. Kurimura, H. C. H. Mulvad, M. Galili, H. Nakajima, J. Ichikawa, D. Erasme, A. T. Clausen and P. Jeppesen, "640-Gbit/s data transmission and clock recovery using an ultrafast periodically poled lithium niobate device," *J. Lightwave Technol.,* vol. 27, pp. 205-213, 2009.

[88] C. Ware, L. K. Oxenløwe, F. G. Agis, H. C. Mulvad, M. Galili, S. Kurimura, H. Nakajima, J. Ichikawa, D. Erasme, A. T. Clausen and P. Jeppesen, "320 Gbps to 10 GHz sub-clock recovery using a PPLN-based opto-electronic phase-locked loop," *Opt. Express,* vol. 7, pp. 5007-5012, 2008.

[89] F. Gomez-Agis, S. K. L. K. Oxenløwe, C. Ware, H. C. H. Mulvad, M. Galili and D. Erasme, "Ultrafast phase comparator for phase-locked loop-based optoelectronic clock recovery systems," *J. Lightwave Technol.,* vol. 27, pp. 2439-2448, 2009.

[90] D. Zibar, J. Mørk, L. Oxenløwe and A. Clausen, "Phase noise analysis of clock recovery based on an optoelectronic phase-locked loop,," *J. Lightwave Technol.,* vol. 25, pp. 901–914, 2007.

[91] M. Saruwatari, "All-optical signal processing for terabit/second optical transmission," *IEEE J. Sel. Top. Quantum Electron.,* vol. 6, pp. 1363–1374, 2000.

[92] F. G. Agis, C. Ware, D. Erasme, R. Ricken, V. Quiring and W. Sohler, "10-GHz clock recovery using an optoelectronic phase-locked loop based on three-wave mixing in periodically poled lithium niobate," *IEEE Photon. Technol. Lett.* , vol. 18, pp. 1460–1462, 2006.

[93] D. Kim, S. Kim, J. Jo and S. Choi, "Ultrahigh-speed clock recovery with optical phase lock loop based on four-wave-mixing in a semiconductor optical amplifier," *Opt. Commun.,* vol. 182 , pp. 329–334, 2000.

[94] C. Ware, L. K. Oxenløwe, F. G. Agis, H. C. H. Mulvad, M. Galili, S. Kurimura, H. Nakajima, J. Ichikawa, D. Erasme, A. T. Clausen and P. Jeppesen, "320 Gbps to 10 GHz sub-clock recovery using a PPLN-based opto-electronic phase-locked loop," *Opt. Express*, vol. 16, pp. 5007-5012, 2008.

[95] R. Salem, A. Ahmadi, G. Tudury, G. Carter and T. Murphy, "Two-photon absorption for optical clock recovery in OTDM networks," *J. Lightwave Technol.*, vol. 24, pp. 3353-3362, 2006.

[96] F. Wang, Y. Yu, Y. Zhang and X. Zhang, "All-optical clock recovery using a single Fabry–Perot semiconductor optical amplifier," *J. Lightwave Technol.*, vol. 30, pp. 1632-1637, 2012.

[97] X. Zhou, C. Lu, P. Shum, H. Shalaby, T. Cheng and P. Ye, "A performance analysis of an all-optical clock extraction circuit based on Fabry–Perot filter," *J. Lightwave Technol.*, vol. 19, pp. 603–613, 2001.

[98] C. R. Fernández-Pousa, F. Mateos, L. Chantada, M. T. Flores-Arias, C. Bao, M. V. Pérez and C. Gómez-Reino, "Broadband noise filtering in random sequences of coherent pulses using the temporal Talbot effect," *J. Opt. Soc. Am. B*, vol. 21, pp. 914-922, 2004.

[99] D. Pudo, M. Depa and L. R. Chen, "All-optical clock recovery using the temporal Talbot effect," in *Optical Fiber Communication (OFC) Conference*, Anaheim, USA, 2007.

[100] D. Pudo, M. Depa and L. Chen, "Single and multiwavelength all-optical clock recovery in single-mode fiber using the temporal Talbot effect," *J. Lightw. Technol.*, vol. 25, pp. 2898-2903, 2007.

[101] M. Oiwa, S. Minami, K. Tsuji, N. Onodera and M. Saruwatari, "Study of all-optical clock recovery performance by the primary and the secondary temporal Talbot effects in a second-order dispersive medium," *Opt. Fiber Technol.*, vol. 16, pp. 192–204, 2010.

[102] P. J. Winzer and R. Essiambre, "Advanced modulation formats for high-capacity optical transport networks," *IEEE Photon. Technol. Lett. ,* vol. 24, pp. 4711-4728, 2006.

[103] E. Lazzeri, A. T. Nguyen, G. Serafino, N. Kataoka, N. Wada, L. Ascari, A. Bogoni and L. Potì, "All-optical NRZ-DPSK to RZ-OOK format conversion using optical delay line interferometer and semiconductor optical amplifier," in *Photonics in Switching Conference*, Monterey, US, 2010.

[104] Y. Ding, H. Hu, M. Galili, J. Xu, L. Liu, M. Pu, H. C. H. Mulvad, L. K. Oxenløwe, C. Peucheret, P. Jeppesen, X. Zhang, D. Huang and H. Ou, "Generation of a 640 Gbit/s NRZ OTDM signal using a silicon microring resonator," *Opt. Express,* vol. 19, pp. 6471-6477, 2011.

[105] A. Rostami, H. Baghban and R. Maram, Nanostructure semiconductor optical amplifiers: building blocks for all-optical processing, Berlin, Genmany: Springer-Verlag, 2011.

[106] J. Wang, J. Sun, X. Zhang, D. Huang and M. M. Fejer, "Optical phase erasure and its application to format conversion through cascaded second-order processes in periodically poled lithium niobate," *Opt. Lett.*, vol. 33, pp. 1804-1806, 2008.

[107] Y. Ding, C. Peucheret, M. Pu, B. Zsigri, J. Seoane, L. Liu, J. Xu, H. Ou, X. Zhang and D. Huang, "Multi-channel WDM RZ-to-NRZ format conversion at 50 Gbit/s based on single silicon microring resonator," *Opt. Express* , vol. 18, pp. 21121-21130, 2010.

[108] Y. Zhang, E. Xu, D. Huang and X. Zhang, "All-optical format conversion from RZ to NRZ utilizing microfiber resonator," *IEEE Photon. Technol. Lett.*, vol. 21, pp. 1202-1204, 2009.

[109] X. Zhang, Y. Yu, H. Dexiu, L. Lijun and F. Wei, "20-Gb/s all-optical format conversions from RZ signals with different duty cycles to NRZ signals," *IEEE Photon. Technol. Lett.*, vol. 19, pp. 1027-1029, 2007.

[110] H. Cao, X. Shu, J. Atai, A. Gbadebo, B. Xiong, T. Fan, H. Tang, W. Yang and Y. Yu, "Optimally-designed single fiber Bragg grating filter scheme for RZ-OOK/DPSK/DQPSK to NRZ-OOK/DPSK/DQPSK format conversion," *Opt. Express*, vol. 22, pp. 30442-30460, 2014.

[111] Z. Y. Zhang, A. E. H. Oehler, B. Resan, S. Kurmulis, K. J. Zhou, Q. Wang, M. Mangold, T. Süedmeyer, U. Keller, K. J. Weingarten and R. A. Hogg, "1.55 mm InAs/GaAs quantum dots and high repetition rate quantum dot SESAM mode-locked laser," *Sci. Rep.*, vol. 2, pp. 477.1-447.5, 2012.

[112] S. Ma, H. S. Z. Chen and N. K. Dutta, "High speed all optical logic gates based on quantum dot semiconductor optical amplifiers," *Opt. Express*, vol. 18, pp. 6417–6422, 2010.

[113] F. Ferdous, H. Miao, D. E. Leaird, K. Srinivasan, J. Wang, L. Chen, L. T. Varghese and A. M. Weiner, "Spectral line-by-line pulse shaping of on-chip microresonator frequency combs," *Nat. Photonics*, vol. 5, pp. 770–776, 2011.

[114] R. R. Gattass and E. Mazur, "Femtosecond laser micromachining in transparent materials," *Nat. Photonics*, vol. 2, pp. 219–225, 2008.

[115] S. A. Diddams, L. Hollberg and V. Mbele, "Molecular fingerprinting with the resolved modes of a femtosecond laser frequency comb," *Nature*, vol. 445, pp. 627–630, 2007.

[116] P. Grelu and N. Akhmediev, "Dissipative solitons for mode-locked lasers," *Nat. Photonics*, vol. 6, pp. 84–92, 2012.

[117] W. Ng, R. Stephens, O. Persechini and K. V. Reddy, "Ultra-Iow jitter modelocking of Er-fibre laser at 10 GHz and its application in photonic sampling for analogue-to-digital conversion," *Electron. Lett.* , vol. 37, pp. 113-115, 2001.

[118] L. N. Binh and N. Q. Ngo, Ultra-fast fiber lasers, principles and applications with MATLAB Models, Boca Raton, FL, USA: CRC Press, 2011.

[119] K. Yiannopoulos, K. Vyrsokinos, E. Kehayas, N. Pleros, K. Vlachos, H. Avramopoulos and G. Guekos, "Rate multiplication by double-passing Fabry–Pérot filtering," *IEEE Photon. Technol. Lett.*, vol. 15, pp. 1294–1296, 2003.

[120] J. Magn, J. Bolger, M. Rochette, S. LaRochelle, L. R. Chen, B. J. Eggleton and J. Azaña, "Generation of a 4 × 100 GHz Pulse-Train From a Single-Wavelength 10-GHz Mode-Locked Laser Using Superimposed Fiber Bragg Gratings and Nonlinear Conversion," *IEEE J. Lightwave Technol.*, vol. 24, pp. 2091-2099, 2006.

[121] H. Tsuda, Y. Tanaka, T. Shioda and T. Kurokawa, "Analog and digital optical pulse synthesizers using arrayed-waveguide gratings for high-speed optical signal processing," *IEEE J. Lightwave Technol.,* vol. 26, pp. 670–677, 2008.

[122] A. Haboucha, W. Zhang, T. Li, M. Lours, A. N. Luiten, Y. L. Coq and G. Santarelli, "Optical-fiber pulse rate multiplier for ultralow phase-noise signal generation," *Opt. Lett.,* vol. 36, pp. 3654-3656, 2011.

[123] I. Kim, H. Sung and D. Seo, "High-speed optical pulse train generation by line-by-line spectral intensity and phase coding," in *Opto-Electronics and Communications Conference (OECC)*, Busan, Korea, 2012.

[124] D. Kielpinski and O. Gat, "Phase-coherent repetition rate multiplication of a mode-locked laser from 40 MHz to 1 GHz by injection locking," *Opt. Express,* vol. 20, pp. 2717–2724, 2012.

[125] M. Pu, H. Ji, L. H. Frandsen, M. Galili, L. K. Oxenlowe and J. M. Hvam, "High-Q microring resonator with narrow free spectral range for pulse repetition rate multiplication," in *Conference on Lasers and Electro-Optics (CLEO)*, Baltimore, US, 2009.

[126] D. E. Leaird, A. M. Weiner, S. Kamei, M. Ishii, A. Sugita and K. Okamoto, "Generation of flat-topped 500 GHz pulse bursts using loss engineered arrayed waveguide gratings," *IEEE Photon. Technol. Lett.,* vol. 14, pp. 816–818, 2002.

[127] A. Haboucha, W. Zhang, T. Li, M. Lours, A. N. Luiten, Y. L. Coq and G. Santarelli, "Optical-fiber pulse rate multiplier for ultralow phase-noise signal generation," *Opt. Lett.,* vol. 36, pp. 3654-3656, 2011.

[128] P. D. Heyn, J. Luo, S. D. Lucente, N. Calabretta, H. J. S. Dorren and D. Van-Thourhout, "In-band label extractor based on cascaded si ring resonators enabling 160Gb/s optical packet switching modules," *J. Lightwave Technol.,* vol. 32, pp. 1647-1653, 2014.

[129] H. Teimoori, J. D.Topomondzo, C. Ware and D. Erasme, "Optical packet header processing using time-to-wavelength mapping in semiconductor optical amplifiers," *J. Lightwave Technol.,* vol. 25, pp. 2149-2158, 2007.

[130] M. F. Chiang, Z. Ghassemlooy, H. L. Minh and W. P. Ng, "All-optical packet-switched routing based on pulse-position-modulated header," in *7th IASTED International Conferences on Wireless and Optical Communications (WOC 2007)*, Montreal, Canada, 2007.

[131] H. F. Talbot, "Facts relating to optical science," *Philos. Mag.,* vol. 9, pp. 401–407, 1836.

[132] T. Jannson and J. Jannson, "Temporal self-imaging effect in single-mode fibers," *J. Opt. Soc. Am.,* vol. 71, pp. 1373–1376, 1981.

[133] F. Mitschke and U. Morgner, "The temporal Talbot effect," *Opt. Photon. News,* vol. 9, pp. 45–47, 1998.

[134] J. Azaña and M. A. Muriel, "Technique for multiplying the repetition rates of periodic trains of pulses by means of a temporal self-imaging effect in chirped fiber gratings," *Opt. Lett.*, vol. 24, pp. 1672–1674, 1999.

[135] J. Azaña and M. A. Muriel, "Temporal Talbot effect in fiber gratings and its applications," *Appl. Opt.*, vol. 38, pp. 6700–6704, 1999.

[136] J. A. Bolger, P. Hu, J. T. Mok, J. L. Blows and B. J. Eggleton, "Talbot self-imaging and cross-phase modulation for generation of tunable high repetition rate pulse trains," *Opt. Commun.*, vol. 249, pp. 431–439, 2005.

[137] P. A. Andrekson, "Linear propagation of optical picosecond pulse trains over oceanic distances," *Opt. Lett.*, vol. 18, pp. 1621-1623 , 1993.

[138] J. J. O'Connor and E. F. Robertson, "William Henry Fox Talbot," MacTutor History of Mathematics , 2005. [Online]. Available: http://www-groups.dcs.st-and.ac.uk/history/Biographies/Talbot.html. [Accessed 10 05 2016].

[139] L. Rayleigh, "On copying diffraction-gratings, and on some phenomenon connected therewith," *Phil. Mag.*, vol. 11, pp. 196–205 , 1881.

[140] A. Winkelmann, "Ubereinige erscheinungen, die bei der beugung des lichtesdurch gitter auftreten," *Ann. Phys. (Leipzig)*, vol. 332, pp. 905–954, 1908.

[141] H. Weisel, "Uber die nach Fresnelscher art beobachteten beugungser-scheninungen der gitter," *Ann. Phys. (Leipzig)*, vol. 338, pp. 995–1031, 1910.

[142] M. Wolfke, "Uber die abbidung eines gitters a erhald der einstellebene," *Ann. Phys. (Leipzig)*, vol. 345, pp. 194–200, 1913.

[143] J. M. Cowley and A. F. Moodie, "Fourier images II. The out-of-focus patterns," *Proc. Phys. Soc. (London)*, vol. B 70, pp. 497–504, 1957.

[144] W. D. Montgomery, "Self-imaging objects of infinite aperture," *J. Opt. Soc. Am.*, vol. 57, pp. 772–778, 1967.

[145] T. Young, "On the theory of light and colours," *Philos. Trans. R. Soc. London*, vol. 92, pp. 12-48, 1802.

[146] J. W. Goodman, Introduction to Fourier optics, 2nd ed., New York: McGraw-Hill, 1996.

[147] F. Träger, Springer handbook of lasers and optics, London: Springer, 2012.

[148] J. T. Winthrop and C. R. Worthington, "Theory of Fresnel images. I. Plane periodic objects in monochromatic light," *J. Opt. Soc. Am.*, vol. 55, pp. 373–381, 1965.

[149] J. Wen, Y. Zhang and M. Xiao, "The Talbot effect: recent advances in classical optics, nonlinear optics, and quantum optics," *Adv. Opt. Photonics*, vol. 5, pp. 83-130, 2013.

[150] K. Patorski, "The self-imaging phenomenon and its applications," in *Progress in Optics, vol. 27*, Amsterdam, North-Holland, 1989, pp. 1–108.

[151] J. M. Cowley, Diffraction Physics, Amsterdam: North-Holland, 1995.

[152] S. A. Akhmanov, A. S. Chirkin, K. N. Drabovich, A. I. Kovrigin, R. V. Khokhlov and A. P. Sukhorukov, "Nonstationary nonlinear optical effects and ultrashort light pulse formation," *IEEE J. Quantum Electron.*, Vols. QE-4, pp. 598-605, 1968.

[153] S. A. Akhmanov, A. P. Sukhorukov and A. S. Chirkin, "Nonstationary phenomena and space-time analogy in nonlinear optics," *SOU. Phys.-JETP* , vol. 28, pp. 748-757, 1969.

[154] B. E. A. Saleh and M. I. Irshid, "Collet–Wolf equivalence theorem and propagation of a pulse in a single-mode optical fiber," *Opt. Lett.*, vol. 7, pp. 342–343, 1982.

[155] B. H. Kolner, "Space-time duality and the theory of temporal imaging," *IEEE J. Quantum Electron.*, vol. 30, pp. 1951-1963, 1994.

[156] S. Longhi, M. Marano, P. Laporta, O. Svelto, M. Belmonte, B. Agogliati, L. Arcangeli, V. Pruneri, M. N. Zervas and M. Ibsen, "40-GHz pulse train generation at 1.5 m with a chirped fiber grating as a frequency multiplier," *Opt. Lett.*, vol. 25, pp. 1481–1483, 2000.

[157] S. Arahira, S. Kutsuzawa, Y. Matsui, D. Kunimatsu and a. Y. Ogawa, "Repetition-frequency multiplication of mode-locked pulses using fiber dispersion," *IEEE J. Lightwave Technol.*, vol. 16, p. 405–409, 1998.

[158] J. Caraquitena, Z. Jiang, D. E. Leaird and A. M. Weiner, "Tunable pulse repetition-rate multiplication using phase-only line-by-line pulse shaping," *Opt. Lett.*, vol. 32, pp. 716–718, 2007.

[159] J. Azaña, "Spectral Talbot phenomena of frequency combs induced by cross-phase modulation in optical fibers," *Opt. Lett.*, vol. 30, pp. 227–229, 2005.

[160] J. M. Lukens, D. E. Leaird and A. M. Weiner, "A temporal cloak at telecommunication data rate," *Nature*, vol. 498, pp. 205–208, 2013.

[161] B. Fischer, B. Vodonos, S. Atkins and A. Bekker, "Dispersion-mode pulsed laser," *Opt. Lett.*, vol. 25, pp. 728–730, 2000.

[162] J. Lukens, O. Odele, C. Langrock, M. Fejer, D. Leaird and A. Weiner, "Generation of biphoton correlation trains through spectral filtering," *Opt. Express*, vol. 22, pp. 9585-9596, 2014.

[163] G. Meloni, G. Berrettini, M. Scaffardi and A. Bogoni, "250-times repetition frequency multiplication for 2.5 THz clock signal generation," *IEEE Electron. Lett.*, vol. 41, pp. 1294 - 1295, 2005.

[164] J. Magné, J. Bolger, M. Rochette, S. LaRochelle, L. R. Chen, B. J. Eggleton and J. Azaña, "Generation of a 4 × 100 GHz pulse-train from a single-wavelength 10-GHz mode-locked laser using superimposed fiber Bragg gratings and nonlinear conversion," *IEEE J. Lightwave Technol.*, vol. 24, pp. 2091 - 2099, 2006.

[165] J. Magne, J. Bolger, M. Rochette, S. LaRochelle, L. Chen, B. Eggleton and J. Azana, "Generation of a 4 × 100 GHz pulse-train from a single-wavelength 10-GHz mode-locked laser using superimposed fiber Bragg gratings and nonlinear conversion," *IEEE J. Lightwave Technol.*, vol. 24, pp. 2091-2099, 2006.

[166] J. A. Boiger, P. Hu, J. T. Mok, J. L. Blows and B. J. Eggleton, "Talbot self-imaging and cross-phase modulation for generation of tunable high repetition rate pulse trains," *Opt. Commun.,* vol. 249, pp. 431-439, 2005.

[167] D. Pudo and L. R. Chen, "Tunable passive all-optical pulse repetition rate multiplier using fiber Bragg gratings," *J. Lightw. Technol.,* vol. 23, pp. 1729–1733, 2005.

[168] J. H. Lee, Y. Chang, Y. G. Han, S. Kim and S. Lee, "2~5 times tunable repetition-rate multiplication of a 10 GHz pulse source using a linearly tunable, chirped fiber Bragg grating," *Opt. Express,* vol. 12, pp. 3900–3905, 2004.

[169] P. J. Delfyett, S. Gee, S. Ozharar, F. Quinlan, K. Kim, S. Lee and W. Lee, "Ultrafast modelocked semiconductor laser - techniques and applications in networking, instrumentation and signal processing," in *18th Lasers and Electro-Optics Society Annual Meeting*, 2005.

[170] L. A. Jiang, M. E. Grein, H. A. Haus, E. P. Ippen and H. Yokoyama, "Timing jitter eater for optical pulse trains," *Opt. Lett.,* vol. 28, pp. 78-80, 2003.

[171] H. A. Haus and A. Mecozzi, "Noise of mode-locked lasers," *IEEE J. Quantum Electron.,* vol. 29, pp. 983-996, 1993.

[172] M. E. Grein, H. A. Haus, Y. Chen and E. P. Ippen, "Quantum-limited timing jitter in actively modelocked lasers," *IEEE J. Quantum Electron.,* vol. 40, pp. 1458-1470, 2004.

[173] T. Yilmaz, C. M. Depriest, A. Braun, J. H. Abeles and P. J. Delfyett, "Noise in fundamental and harmonic modelocked semiconductor lasers: experiments and simulations," *IEEE J. Quantum Electron.,* vol. 39, pp. 838-849, 2003.

[174] S. Gee, F. Quinlan, S. Ozharar and P. J. Delfyett, "Simultaneous optical comb frequency stabilization and super-mode noise suppression of harmonically mode-locked semiconductor ring laser using an intracavity etalon," *IEEE Photon. Technol. Lett.,* vol. 17, pp. 199-201, 2005.

[175] S. Gee, S. Ozharar, F. Quinlan, J. J. Plant, P. W. Juodawlkis and P. J. Delfyett, "Self-stabilization of an actively mode-locked semiconductor-based fiber-ring laser for ultralow jitter," *IEEE Photon. Technol. Lett.,* vol. 19, pp. 498-500, 2007.

[176] F. Quinlan, S. Gee, S. Ozharar and P. J. Delfyett, "Greater than 20-dB supermode noise suppression and timing Jitter reduction via CW injection of a harmonically mode-locked laser," *IEEE Photon. Technol. Lett.,* vol. 19, pp. 1221-1223, 2007.

[177] M. Mangold, S. M. Link, A. Klenner, C. A. Zaugg, M. Golling, B. W. Tilma and U. Keller, "Amplitude noise and timing jitter characterization of a high-power mode-locked integrated external-cavity surface emitting laser," *IEEE Photonics J.,* vol. 6, pp. 1500309(1-9), 2014.

[178] D. Pudo and L. R. Chen, "Simple estimation of pulse amplitude noise and timing jitter evolution through the temporal Talbot effect," *Opt. Express,* vol. 15, pp. 6351–6357, 2007.

[179] C. R. Fernandez-Pousa, F. Mateos, L. Chantada, M. T. Flores-Arias, C. Bao, M. V. Pérez and C. Gómez-Reino, "Timing jitter smoothing by Talbot effect. I. Variance," *J. Opt. Soc. Am. B,* vol. 21, pp. 1170-1177, 2004.

[180] M. Oiwa, J. Kim, K. Tsuji, N. Onodera and M. Saruwatari, "Experimental demonstration of timing jitter reduction based on the temporal Talbot effect using LCFBGs," in *Conference on Lasers and Electro-Optics and Conference on Quantum Electronics and Laser Science (CLEO/QELS)*, 2008.

[181] H. G. d. Chatellus, E. Lacot, O. Hugon, O. Jacquin, N. Khebbache and J. Azaña, "Phases of Talbot patterns in angular self-imaging," *J. Opt. Soc. Am. A,* vol. 32, pp. 1132-1139, 2015.

[182] L. R. Cortés, H. G. d. Chatellus and J. Azaña, "On the generality of the Talbot condition for inducing self-imaging effects on periodic objects," *Opt. Lett.*, vol. 41, pp. 340-343, 2016.

[183] H. A. Haus and W. S. Wong, "Solitons in optical communications," *Rev. Mod. Phys.*, vol. 68, pp. 423–444, 1996.

[184] D. R. Solli, C. Ropers, P. Koonath and B. Jalali, "Optical rogue waves," *Nature,* vol. 450, pp. 1054–1057, 2007.

[185] D. Pudo and L. R. Chen, "Tunable passive all-optical pulse repetition rate multiplier using fiber Bragg gratings," *J. Lightw. Technol.*, vol. 23, pp. 1729–1733, 2005.

[186] R. Maram, D. Kong, M. Galili, L. K. Oxenløwe and J. Azaña, "Ultrafast all-optical clock recovery based on phase-only linear optical filtering," *Opt. Lett.*, vol. 39, pp. 2815–2818, 2014.

[187] S. Tainta, M. Erro, W. Amaya, M. J. Garde, S. Sales and M. A. Muriel, "Periodic time-domain modulation for the electrically tunable control of optical pulse train envelope and repetition rate multiplication," *J. Sel. Top. Quantum.*, vol. 18, pp. 377-383, 2012.

[188] R. Maram, J. V. Howe, M. Li and J. Azaña, "Noiseless intensity amplification of repetitive signals by coherent addition using the temporal Talbot effect," *Nat. Commun.*, vol. 5, pp. 4827(1-10), 2014.

[189] A. Malacarne and J. Azaña, "Discretely tunable comb spacing of a frequency comb by multilevel phase modulation of a periodic pulse train," *Opt. Express,* vol. 21, pp. 4139–4144, 2013.

[190] R. J. Essiambre, G. Kramer, P. J. Winzer, G. J. Foschini and B. Goebel, "Capacity limits of optical fibre networks," *J. Lightwave Technol.,* vol. 28, pp. 662-701, 2010.

[191] F. Ferdous, H. Miao, D. E. Leaird, K. Srinivasan, J. Wang, L. Chen, L. T. Varghese and A. M. Weiner, "Spectral line-by-line pulse shaping of on-chip microresonator frequency combs," *Nat. Photonics,* vol. 5, pp. 770-776, 2011.

[192] A. Haboucha, W. Zhang, T. Li, M. Lours, A. N. Luiten, Y. Le Coq and G. Santarelli, "Optical-fiber pulse rate multiplier for ultralow phase-noise signal generation," *Opt. Lett.*, vol. 36, pp. 3654-3656, 2011.

[193] F. Helmchen and W. Denk, "Deep tissue two-photon microscopy," *Nat. Methods,* vol. 2, pp. 932-940, 2005.

[194] J. Cheng, C. Liua, S. Shangb, D. Liub, W. Perrieb, G. Deardenb and K. Watkinsb, "A review of ultrafast laser materials micromachining," *Opt. & Laser Technol.,* vol. 46, pp. 88-102, 2013.

[195] G. A. Mourou, T. Tajima and S. V. Bulanov, "Optics in the relativistic regime," *Rev. Mod. Phys.* , vol. 78, pp. 309-371, 2006.

[196] L. Yan, A. E. Willner, X. Wu, A. Yi, A. Bogoni, Z.-Y. Chen and H.-Y. Jiang, "All-optical signal processing for ultrahigh speed optical systems and networks," *J. Lightwave Technol.,* vol. 30, pp. 3760-3770, 2012.

[197] R. S. Tucker, "Green optical communications—Part I: Energy limitations in transport," *IEEE J. Sel. Top. Quant. Electron.,* vol. 17, pp. 245-260, 2011.

[198] B. Jalali and S. Fathpour, "Silicon photonics," *J. Lightwave Technol.,* vol. 24, pp. 4600-4615, 2006.

[199] L. De Forest, "The audion-detector and amplifier," *Proc. of the IEEE,* vol. 2, pp. 19-25, 1914.

[200] J. Bardeen and W. H. Brattain, "The transistor, a semi-conductor triode," *Phys. Rev. Lett.*, vol. 74, pp. 230-231, 1948.

[201] R. J. Mears, L. Reekie, M. Jauncey and D. N. Payne, "Low-noise erbium-doped fiber amplifier operating at 1.54 μm," *Electron. Lett.*, vol. 26, pp. 1026-1028, 1987.

[202] M. Kozuma, Y. Suzuki, Y. Torii, T. Sugiura, T. Kuga, E. W. Hagley and L. Deng, "Phase-coherent amplification of matter waves," *Science* , vol. 286, pp. 2309-2312, 1999.

[203] C. Joachim, J. K. Gimzewski and A. Aviram, "Electronics using hybrid-molecular and mono-molecular devices," *Nature* , vol. 408, pp. 541-548, 2000.

[204] M. A. Foster, A. C. Turner, J. E. Sharping, B. S. Schmidt, M. Lipson and A. L. Gaeta, "Broad-band optical parametric gain on a silicon photonic chip," *Nature* , vol. 441, pp. 960-963, 2006.

[205] R. P. Beardsley, A. V. Akimov, M. Henini and A. J. Kent, "Coherent terahertz sound amplification and spectral line narrowing in a Stark ladder superlattice," *Phys. Rev. Lett.*, vol. 104, pp. 085501(1-4), 2010.

[206] Z. Tong, C. Lundström, P. A. Andrekson, C. J. McKinstrie, M. Karlsson, D. J. Blessing, E. Tipsuwannakul, B. J. Puttnam, H. Toda and L. Grüner-Nielsen, "Towards ultrasensitive optical links enabled by low-noise phase-sensitive amplifiers," *Nat. Photonics,* vol. 5, pp. 430-436, 2011.

[207] T. Eidam, J. Rothhardt, F. Stutzki, F. Jansen, S. Hädrich, H. Carstens, C. Jauregui, J. Limpert and A. Tünnermann, "Fiber chirped-pulse amplification system emitting 3.8 GW peak power," *Opt. Express,* vol. 19, pp. 255-260, 2011.

[208] J. Tümmler, R. Jung, H. Stiel, P. V. Nickles and W. Sandner, "High-repetition-rate chirped-pulse-amplification thin-disk laser system with joule-level pulse energy," *Opt. Lett.,* vol. 34, pp. 1378-1380, 2009.

[209] Y. Vidne, M. Rosenbluh and T. W. Hansch, "Pulse picking by phase-coherent additive pulse generation in an external cavity," *Opt. Lett.,* vol. 28, pp. 2396-2398, 2003.

[210] H. A. Haus, "The proper definition of noise figure of optical amplifiers," in *Optical Amplifiers and Their Applications, OSA/OAA*, Québec, Canada, 2000.

[211] J. R. Jones and J. Ye, "Femtosecond pulse amplification by coherent addition in a passive optical cavity," *Opt. Lett.,* vol. 27, pp. 1848-1850, 2002.

[212] R. Maram, J. Van Howe and J. Azaña, "Noise-eating amplifier for repetitive signals," in *IEEE photonic conference (IPC)*, San Diego, USA, 2014.

[213] P. AB, "http://www.proximion.com/Products/DCM-HDC," 2014.

[214] J. P. Heritage and A. M. Weiner, "Advances in spectral code-division multiple access communications," *IEEE J. Sel. Top. Quantum Electron.,* vol. 13, pp. 1351-1369, 2007.

[215] J. D. Jackson, Classical Electrodynamics, New York, US: Wiley, 1998.

[216] W. M. Robertson, C. Baker and C. B. Bennett, "Slow group velocity propagation of sound via defect coupling in a one-dimensional acoustic band gap array," *Am. J. Phys.,* vol. 72, pp. 255-257, 2004.

[217] A. D. Cronin, J. Schmiedmayer and D. E. Pritchard, "Optics and interferometry with atoms and molecules," *Rev. Mod. Phys.,* vol. 81, pp. 1051-1129, 2009.

[218] L. Deng, E. W. Hagley, J. Denschlag, J. E. Simsarian, M. Edwards, C. W. Clark, K. Helmerson, S. L. Rolston and W. D. Phillips, "Temporal, matter-wave-dispersion Talbot effect," *Phys. Rev. Lett.,* vol. 83, pp. 5407-5411, 1999.

[219] M. J. Madou, From MEMS to Bio-MEMS and Bio-NEMS: manufacturing techniques and applications, Boca Raton, FL, USA: CRC Press, 2011.

[220] P. Kolchin, C. Belthangady, S. Du, G. Y. Yin and S. E. Harris, "Electro-optic modulation of single photons," *Phys. Rev. Lett.,* vol. 101, pp. 103601(1-4), 2008.

[221] J. Luo, N. Calabretta, J. Parra-Cetina, S. Latkowski, R. Maldonado-Basilio, P. Landais and H. J. S. Dorren, "320 Gb/s all-optical clock recovery and time de-multiplexing after transmission enabled bysingle quantum dash mode-locked laser," *Opt. Lett.,* vol. 38, pp. 4805-4808, 2013.

[222] Z. Wang and S. Fan, "Compact all-pass filters in photonic crystals as the building block for high-capacity optical delay lines," *Phys. Rev.,* vol. 68, pp. 066616 , 2003.

[223] J. T. Willits, A. M. Weiner and S. T. Cundiff, "Line-by-line pulse shaping with spectral resolution below 890 MHz," *Opt. Express,* vol. 20, pp. 3110-3117, 2012.

[224] L. K. Oxenløwe, R. Slavık, M. Galili, H. C. H. Mulvad, A. T. Clausen, Y. Park, J. Azana and P. Jeppesen, "640 Gb/s timing jitter-tolerant data processing using a long-period fiber-Grating-based flat-top pulse shaper," *IEEE J. Sel. Top. Quant. Electron.,* vol. 14, pp. 566-572, 2008.

[225] J. H. Lee, Y. Chang, Y.-G. Han, S. Kim and S. Lee, "2~5 times tunable repetition-rate multiplication of a 10 GHz pulse source using a linearly tunable, chirped fiber Bragg grating," *Opt. Express,* vol. 12, pp. 3900–3905, 2004.

[226] C. J. S. de-Matos and J. R. Taylor, "Tunable repetition-rate multiplication of a 10 GHz pulse train using linear and nonlinear fiber propagation," *Appl. Phys. Lett.,* vol. 38, pp. 5356–5358, 2003.

[227] J. Caraquitena and J. Martí, "High-rate pulse-train generation by phase-only filtering of an electrooptic frequency comb: analysis and optimization," *Opt. Commun.*, vol. 282, pp. 3686–3692, 2009.

[228] H. Hu, H. C. H. Mulvad, M. Galili, E. Palushani, J. Xu, A. T. Clausen, L. K. Oxenlowe and P. Jeppesen, "Polarization- insensitive 640Gb/s demultiplexing based on four wave mixing in a polarization-maintaining fibre loop," *J. Lightw. Technol.*, vol. 28, pp. 1789-1795, 2010.

[229] A. M. de-Melo, S. Randel and K. Petermann, "Mach–Zehnder interferometer-based high-speed OTDM add–drop multiplexing," *J. Lightw. Technol.,* vol. 25, pp. 1017–1026, 2007.

[230] J. Parra-Cetina, J. Luo, N. Calabretta, S. Latkowski, H. J. S. Dorren and P. Landais, "Subharmonic all-optical clock recovery of up to 320 Gb/s signal using a quantum dash Fabry–Perot mode-locked laser," *Electron. Lett.*, vol. 31, pp. 3127–3134, 2013.

[231] M. Oiwa, S. Minami, K. Tsuji, N. Onodera and M. Saruwatari, "Temporal-Talbot-effect-based preprocessing for pattern-effect reduction in all-optical clock recovery using a semiconductor-optical-amplifier-based fiber ring laser," *Optical Fiber Technol.,* vol. 16, pp. 63-71, 2010.

[232] R. Maram and J. Azaña, "Spectral self-imaging of time-periodic coherent frequency combs by parabolic cross-phase modulation," *Opt. Express,* vol. 21, pp. 28824–28835, 2013.

[233] R. Maram, D. Kong, M. Galili, L. K. Oxenløwe and J. Azaña, "Ultrafast all-optical cock recovery based on phase-only linear optical filtering," *Opt. Lett.,* vol. 39, pp. 2815-2818, 2014.

[234] I. P. Kaminow, T. Li and A. E. Willner, Optical fiber telecommunications VB: systems and networks, San Diego, US: Academic press, 2010.